MECHANISMS AND MODELLING OF ENVIRONMENT-DEPENDENT FATIGUE CRACK GROWTH IN A NICKEL BASED SUPERALLOY

(FINAL REPORT)

by

H. Ghonem and D. Zheng

Mechanics of Solids Laboratory
Department of Mechanical Engineering
University of Rhode Island
Kingston, R.I. 02881

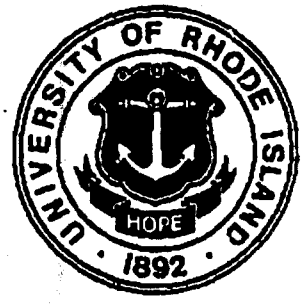

Prepared for

Department of Air Force
Air Force Office of Scientific Research
Bolling Air Force Base, Washington D.C. 20332

(Contract AF-89-0285)

March 1992

MECHANISMS AND MODELLING OF ENVIRONMENT-DEPENDENT FATIGUE CRACK GROWTH IN A NICKEL BASED SUPERALLOY

(FINAL REPORT)

by

H. Ghonem and D. Zheng

Mechanics of Solids Laboratory
Department of Mechanical Engineering
University of Rhode Island
Kingston, R.I. 02881

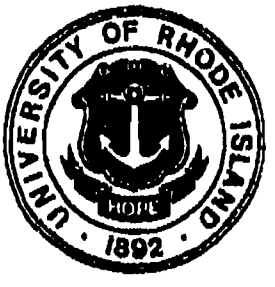

Prepared for

Department of Air Force
Air Force Office of Scientific Research
Bolling Air Force Base, Washington D.C. 20332

(Contract AF-89-0285)

March 1992

(U)

SECURITY CLASSIFICATION OF THIS PAGE

REPORT DOCUMENTATION PAGE

Form Approved OMB No. 0704-0188

1a. REPORT SECURITY CLASSIFICATION: UNCLASSIFIED	1b. RESTRICTIVE MARKINGS
2a. SECURITY CLASSIFICATION AUTHORITY	3. DISTRIBUTION/AVAILABILITY OF REPORT: APPROVED FOR PUBLIC RELEASE DISTRIBUTION IS UNLIMITED
2b. DECLASSIFICATION/DOWNGRADING SCHEDULE	
4. PERFORMING ORGANIZATION REPORT NUMBER(S): URI-MSL-921	5. MONITORING ORGANIZATION REPORT NUMBER(S)
6a. NAME OF PERFORMING ORGANIZATION: UNIVERSITY OF RHODE ISLAND; 6b. OFFICE SYMBOL (If applicable)	7a. NAME OF MONITORING ORGANIZATION: AFOSR/NA
6c. ADDRESS (City, State, and ZIP Code): MECHANICS OF SOLIDS LABORATORY, WALES HALL, KINGSTON, RI 02881	7b. ADDRESS (City, State, and ZIP Code): BUILDING 410, BOLLING AFB, WASHINGTON, DC 20332-6448
8a. NAME OF FUNDING/SPONSORING ORGANIZATION: AFOSR/NA; 8b. OFFICE SYMBOL (If applicable): NA	9. PROCUREMENT INSTRUMENT IDENTIFICATION NUMBER: AFOSR-89-0285
8c. ADDRESS (City, State, and ZIP Code): BUILDING 410, BOLLING AFB, WASHINGTON, DC 20332-6448	10. SOURCE OF FUNDING NUMBERS: PROGRAM ELEMENT NO. 61102F; PROJECT NO. 2302; TASK NO. BS; WORK UNIT ACCESSION NO.

11. TITLE (Include Security Classification): MECHANISMS AND MODELLING OF ENVIRONMENT-DEPENDENT FATIGUE CRACK GROWTH IN SUPERALLOYS (U)

12. PERSONAL AUTHOR(S): H. GHONEM and D. ZHENG

13a. TYPE OF REPORT	13b. TIME COVERED	14. DATE OF REPORT (Year, Month, Day)	15. PAGE COUNT
FINAL	FROM 1989 TO 1991	1991/12/12	

16. SUPPLEMENTARY NOTATION

17. COSATI CODES			18. SUBJECT TERMS (Continue on reverse if necessary and identify by block number)
FIELD	GROUP	SUB-GROUP	GROWTH RATE, GRAIN BOUNDARY DUCTILITY, OXIDATION DIFFUSIVITY, INTERGRANULAR, HOLD TIME, SLIP, HOMOGENEITY

19. ABSTRACT (Continue on reverse if necessary and identify by block number)

At loading frequencies below that of the transitional frequency level, which is typical of mission cycles of jet engines, the elevated temperature fatigue crack growth process in Alloy 718 is viewed to be fully environment-dependent. Of all the crack growth stages, this process, while is the most critical in high temperature application due to its highly accelerated crack growth rate, is the least studied or understood. The objective of this research program is to focus on the understanding of the mechanism controlling this oxidation-dependent stage in order to develop the ability to predict its associated crack growth performance under different environment conditions. For this purpose, three major studies have been carried out; the first was to provide evidence of the existence of the fully environment-dependent stage in which the crack growth rate would be equal to the oxygen penetration rate at the crack tip, the second study was to establish a crack tip oxidation mechanism on the basis of material, environmental and loading parameters interactions in the crack tip region. The last objective of this program is to establish a micromechnical based quantitative model to predict the environmentally-dominated crack growth stage.

20. DISTRIBUTION/AVAILABILITY OF ABSTRACT: ☒ UNCLASSIFIED/UNLIMITED ☐ SAME AS RPT. ☒ DTIC USERS	21. ABSTRACT SECURITY CLASSIFICATION: UNCLASSIFIED	
22a. NAME OF RESPONSIBLE INDIVIDUAL: DR. WALTER JONES	22b. TELEPHONE (Include Area Code): 202-767-0470	22c. OFFICE SYMBOL: NA

DD Form 1473, JUN 86 — Previous editions are obsolete. — SECURITY CLASSIFICATION OF THIS PAGE

(U)

ABSTRACT

At cyclic loading frequencies below that of the transitional frequency level, the elevated temperature fatigue crack growth process in Alloy 718 is viewed to be fully environment-dependent. Of all the crack growth stages, this stage, while is the most critical in high temperature applications due to its highly accelerated crack growth rate, is the least studied or understood. The objective of this study is to focus on the understanding of the controlling mechanisms of this environment-dependent crack growth stage in Alloy 718 in order to develop the ability to predict the crack growth performance under different loading and environment conditions. For this purpose, two major studies have been carried out here. The first was to provide evidence of the existence of the fully environment-dependent stage in which the crack growth rate is viewed to be equal to the oxygen penetration rate at the crack tip. This has been achieved by indirectly estimating the depth of oxygen diffusion at the crack tip of compact tension specimens tested at 650°C under cyclic loadings with and without hold time durations at minimum load level. As a result, the relationship between the intergranular oxygen diffusion rate and the value of the stress intensity factor has been established. This relationship, when integrated over the cycle effective oxidation time, results in a closed form solution describing the environment-dependent fatigue crack growth rate. A good agreement was obtained when a comparison was made between the results of this solution and the corresponding experimental results.

The second study was to establish a micromechanical based quantitative model to predict the environmentally-dominated crack growth performance. This model was based on the concept of the intergranular two-stage crack-tip oxidation mechanism. According to this mechanism, the oxygen partial pressure controls the preferential formation of the oxide layers at the crack tip, and it suggests that intergranular oxidation under air environment occurs in two stages with the formation of a Ni-Fe rich oxide followed by that of the more protective film formed by Cr_2O_3 oxide. Thus, the reduction of the grain boundary ductility along the grain boundary fracture path depends on the rate of formation of the chromia layer in relation to the build-up of other oxide types at the crack tip. The determination of the amount of Cr_2O_3 depends on the amount of both oxygen diffused along the affected grain boundary and chromium transported via a mobile dislocation network. The reduction in grain boundary ductility due to oxidation is balanced by considering the effective strain at the crack tip resulting from the external loading. This balance defines the fracture criterion of the model and permits the calculation of the crack advance per cycle. The model was then used to predict the crack growth rate in Alloy 718 at 650 °C for two different loading conditions, and a good agreement was achieved when the results obtained from the model compared with those obtained experimentally.

The significant contribution of this three-year study is that it provides the jet engine manufactures with a mechanical approach, parallel to alloying, by which the intrinsic resistance of jet engine components to environment-dependent crack growth process can be controlled.

ACKNOWLEDGEMENTS

The authors are grateful to Dr. T. Nicholas of Materials Directorate, Wright Patterson Air Force Base, Professor A. Pineau of Ecole des Mines de Paris, France, and Mr. Jeff Hill and Mr. D. Szafir of United Technologies Corporation, Pratt & Whitney Group for their ideas, time and their interest in this work.

The authors also acknowledge the contribution of Mr. A. Madsen, a research assistant of Mechanics of Solids Laboratory in URI, in performing all the vacuum tests required in this work, Mr. Ray MacLaughlin and Mr. Manuel Merrill of the Department of Mechanical Engineering, URI for their continue assistance in maintaining the electronic equipment and machining all the test specimens and the mechanical parts required in this project.

This study was supported by US Air Force Office of Scientific Research under contract AFOSR-89-0285 monitored by Dr. G. Haritos (1989-1990) and Dr. W. Jones (1990-1992) of USAF.

TABLE OF CONTENTS

LIST OF TABLES

LIST OF FIGURES

CHAPTER 1

INTRODUCTION

Alloy 718[1] is a precipitation strengthened nickel-base superalloy with a excellent resistance to creep and stress rupture up to 650°C. Because of its good mechanical properties, weldability, fabricability and cost effectiveness, Alloy 718 is widely used in aircraft engines, nuclear structures, oil fields and gas production industries. Damage tolerance methodologies needed in some of these applications require accurate predictions of the crack growth behavior under typical service conditions. For this reason, and as part of material characterization, extensive studies [1-31,37,47,49,50,69,82] have been carried out in the past three decades investigating the influence of various operating parameters on the crack growth mechanisms under different loading and environment conditions. In order to recognize the role of each of these parameters and to establish the objectives of this research program, an attempt will be made in this chapter to review several related studies. The parameters which will be analyzed in this review are temperature, frequency, wave shape, hold time, microstructure and environment.

Effects of Temperature

A comprehensive evaluation of the effect of temperature on the crack growth in Alloy 718 is that of Weerasooriya et al [1]. Constant ΔK tests at R=0.1 were conducted

[1] Alloy 718 is a generic name of Inconel 718 which is the trademark of Huntington Alloys Inc..

at K_{max} = 27.8 and 40.0 MPa$\sqrt{m}$ for frequencies ranging from 0.001 to 1.0 Hz. Results of the tests at K_{max} = 40 MPa$\sqrt{m}$ in the form of the fatigue crack growth rate versus reciprocal absolute temperature are shown in Fig. 1.1. The frequency effects are discussed in the next section. For temperatures between room temperature and 650°C, the growth rate increases with increase in temperature. The rate of increase in the lower temperature regime (c) is limited and is attributed to a combination of the change in modulus and plastic deformation characteristics of the material with temperature. The fracture mode is transgranular and the behavior is characterized as cycle dependent. At some transition temperature, depending upon frequency, the growth rate increases significantly with further increase in temperature. In this region (b) the fracture is a combination of transgranular and intergranular and the behavior is characterized as mixed mode. As can be observed in Fig. 1.1, the temperature at which this transition occurs is higher for higher frequencies. At the highest temperatures, the behavior of this material becomes purely intergranular, the mode is characterized as time dependent, and the rate of change of growth rate with temperature is maximum. This region is denoted by (a) in Fig. 1.1. The transition temperature from mixed mode to time dependent, denoted in this figure as T_{tm}, again, depends on test frequency and has a higher value for higher frequencies. Similar observations of the fatigue crack growth rate behavior as a function of frequency where the mode of fracture and the rate of crack growth can be correlated are presented in the next section.

The effects of temperature on the fatigue crack growth rate can also be observed when Alloy 718 is tested in vacuum environment. However, the fatigue crack growth rate

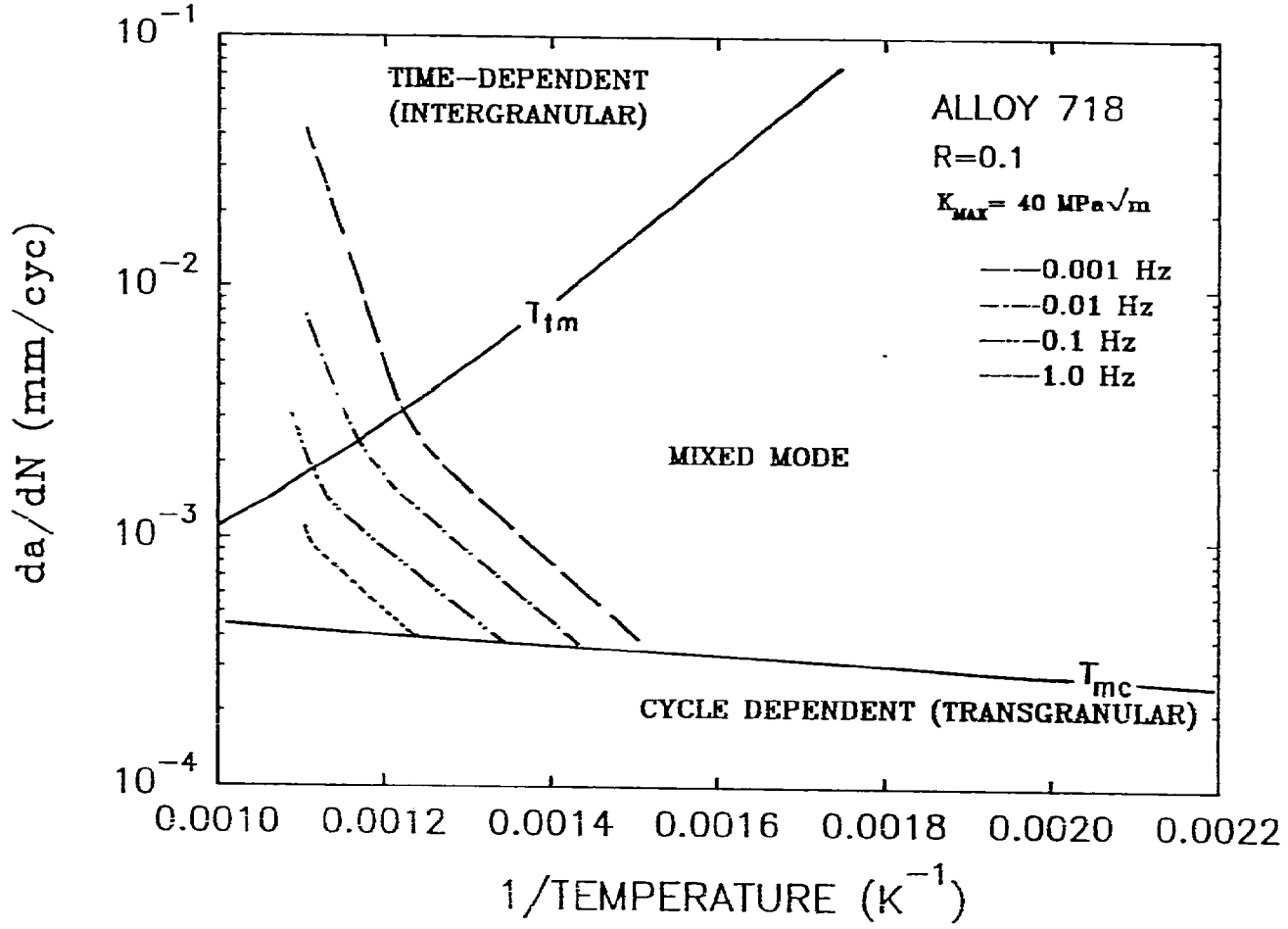

Fig. 1.1 The effects of temperature on crack growth rate at K_{max} = 40 MPa$\sqrt{m}$.

only increases slightly with increase in temperatures compared to the changes observed in air [2].

Effects of Frequency

The effects of cyclic frequency on the fatigue crack growth behavior of Alloy 718 has been the subject of many researches [3,4,5-8]. James [3] studied the frequency effects for Alloy 718 at 538°C over the range of 1.39×10^{-3} Hz to 6.67 Hz, the results are shown in Fig. 1.2. It can be seen from this figure that the fatigue crack growth rates increase as cyclic frequencies decrease. This trend was also noted by Clavel and Pineau [4] in their work at 550°C over the range of 5×10^{-3} Hz to 20 Hz. Crack growth rates in laboratory air at a temperature of 650°C are also found to depend strongly on frequency. Increasing the frequency generally results in a decrease in crack growth rate per cycle. For example, Weerasooriya [6,7] has shown that at two constant ΔK conditions the behavior ranges from purely time dependent at frequencies below 0.01 Hz to purely cycle dependent at frequencies in excess of 10 Hz. His work also show that different mechanisms of crack growth are activated in each regime: striation formation is generally observed in the cycle-dependent regime, intergranular crack growth is dominant in the time-dependent regime, and a mixed transgranular-intergranular mode of crack extension is observed in the mixed regime. Similar observations of the frequency dependence have been documented by Floreen and Kane [5] and Pedron and Pineau [9]. Although the magnitude of the change in growth rate with decrease in frequency varies depending on the alloy microstructure, temperature, and frequency, the pattern of behavior is widely

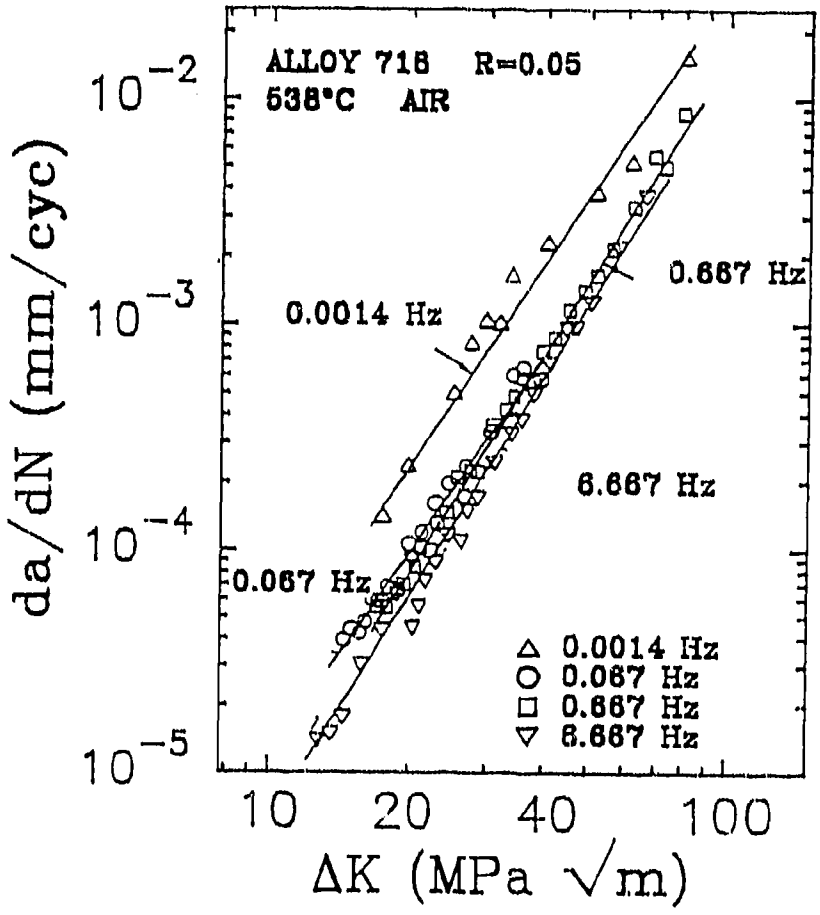

Fig. 1.2 The effects of cyclic frequency on crack growth rate at 538°C in air.

noted in all Nickel-based superalloys and is generally attributed to decreasing environmental resistance with increasing exposure time as cyclic frequency decreases.

While most of frequency studies were conducted in air environment, Floreen and Kane [5] studied the fatigue crack growth behavior of Alloy 718 at 650°C over the range of 0.01 Hz to 1 Hz in air and helium (99.995% purity) as well. In helium environment, as the frequency decreased, the fatigue crack growth rate only slightly increased, while in air environment, the fatigue crack growth rate increased substantially as frequency decreased.

Similar to other high strength superalloys, the frequency effects for Alloy 718 are only observed at elevated temperatures and not at room temperature [8]. Further, the cycle dependent (high frequency) growth rate at high temperature corresponds closely with the rate observed at room temperature as well as those observed in vacuum, indicating a lack of environmental contributions to the growth rate process when the transgranular fatigue mode dominates [7].

Effects of Wave Shape

Although the behavior of crack growth in Alloy 718 as a function of frequency is widely noted and accepted, this behavior when more complex wave shapes are involved is not as well understood nor are the results consistent among the various investigators. There are a number of observations involving other wave shapes which illustrate the variable nature of the elevated temperature crack growth behavior. James [10] found that the crack growth rate at 538°C in Alloy 718 is significantly faster for a square wave

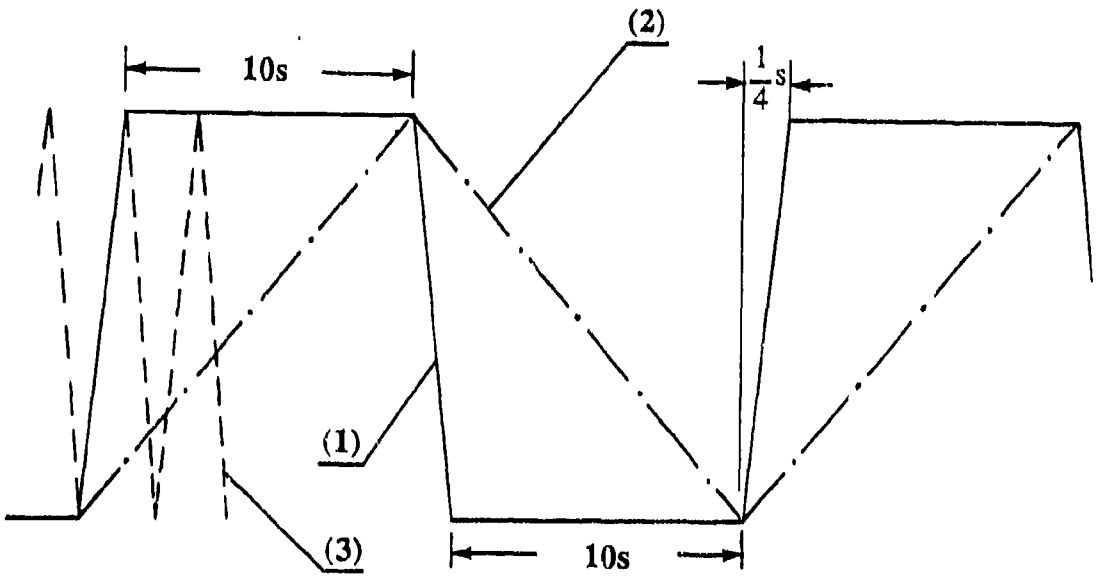

Fig. 1.3 Various wave shape configurations used at 560°C for frequency 0.05 Hz.

form than for a sawtooth wave form of the same cyclic duration when the loading frequency was much lower than the unloading frequency. In these experiments, the hold time contribution in the square wave appears to dominate the cyclic contribution, even for a low loading frequency in the sawtooth wave. Somewhat conflicting results were obtained by Clavel and Pineau [4] who examined the wave-shape effects on the fatigue crack growth rate using square and triangular wave shapes at 550°C. Three cyclic wave shapes were chosen (shown in Fig. 1.3) for differentiating the effect of loading and unloading rate as well as the effect of hold time at maximum and minimum load. Wave-shape 3 corresponds to a frequency of 2 Hz, whereas wave-shape 2 leads to a frequency of 0.05 Hz. Wave-shape 1 has the same loading and unloading rate as wave-shape 3 but superposes a 10 s hold time at the maximum load level and at the minimum load level, and its cyclic duration is the same as that of wave-shape 2. Their results showed that the fatigue crack growth rate of wave-shape 2 is higher than those of the other two wave shapes, and the fatigue crack growth rate of wave-shape 1 is only slightly higher than that of wave-shape 3. They inferred that a hold-time of 10 s both at the maximum and at the minimum load has no significant effect on the fatigue crack growth rate, and that the main parameter is not the frequency *per se* but the loading and the unloading rate. As already pointed out by Bathias and Pelloux [11] the slip character strongly affects the aspect of the fracture surfaces. In fact, their fractographic examination showed that, at 550°C, the cracks propagate by a transgranular mode when the frequency is higher than 0.5 Hz, while at lower frequency (0.05 Hz) the crack growth occurs by a mixture of transgranular and intergranular fracture. The well known fact for this material

is that homogeneity in plastic deformation promotes transgranular fracture mode while inhomogeneity in plastic deformation favors intergranular fracture mode [12,13-17]. This subject will be discussed in more detail later. Obviously, for wave-shape 1 the loading and unloading rates promoted the homogeneity in plastic deformation which generally has less time-dependent sensitivity, thus the hold times after the loading and unloading portions are not expected to produce a large influence on the fatigue crack growth rate which is why the fatigue crack growth rate of wave-shape 1 is only slightly higher than that of wave-shape 3. For wave-shape 2, the loading and unloading rates produced the inhomogeneity in plastic deformation near crack tip which, in turn, favors the occurrence of intergranular fracture, and certainly the fatigue crack growth rate is much higher than that of wave-shape 1.

Ashbaugh [18] conducted a series of tests at 649°C using triangular wave shapes on CT specimens and R=0.1. In addition to symmetric wave shapes with frequencies covering the range from 0.01 Hz to 10 Hz, asymmetric wave shapes were used in which the rise and fall times had different values corresponding to the baseline frequencies of the symmetric wave form tests. For various combinations of rising and falling frequencies from 1 Hz to 0.01 Hz, growth rates per cycle were essentially equivalent to those obtained using symmetric wave shapes where the frequency was that of the rising portion of the asymmetric wave. This observation implies that the fatigue damage occurs almost exclusively during the rising load portion of the fatigue cycle. At the temperature and frequencies at which these experiments were conducted, the fracture mode is a mixed mode combination of intergranular and transgranular [7].

Effects of Hold Time

It is widely reported that the addition of a hold time at maximum load to a fatigue cycle tends to increase the crack growth rate per cycle in Alloy 718 as well as in a number of other nickel-base superalloys [4,19-28]. Fig. 1.4 shows, for example, results from the work of Pedron and Pineau [24] involving Alloy 718 at 650°C where hold times are added to baseline fatigue cycles. This results in an increase in growth rate per cycle. In all three cases it can be seen that the behavior at long hold times is essentially purely time dependent, that is, growth rate increases linearly with increase in hold time. There are, however, a number of observations which do not show this same trend. Shahanian and Sadananda [20] show that at 760°C, the addition of hold times of 0.1, 1, or 10 min. does not increase the crack growth rate in Alloy 718. The results of this investigation also showed that growth rates obtained under constant load range (increasing ΔK) conditions depend on load amplitude, thereby demonstrating the inadequacy of ΔK as a correlating parameter at this temperature. At 593°C, VanStone et al. [28] showed that Alloy 718 still exhibits an increase in growth rate with increase in hold time, but the effect is not as pronounced as at 650°C.

There are several instances where hold times retard crack growth instead of accelerating it and even contribute to total crack arrest. This has been observed when hold times occur at other than maximum load [22]. In these cases, either significant creep occurs at the test temperature, thereby blunting the crack tip, or the stress intensity during hold is generally less than the creep crack growth threshold.

Several observations have been made in Alloy 718 at 649°C of the effect of a hold

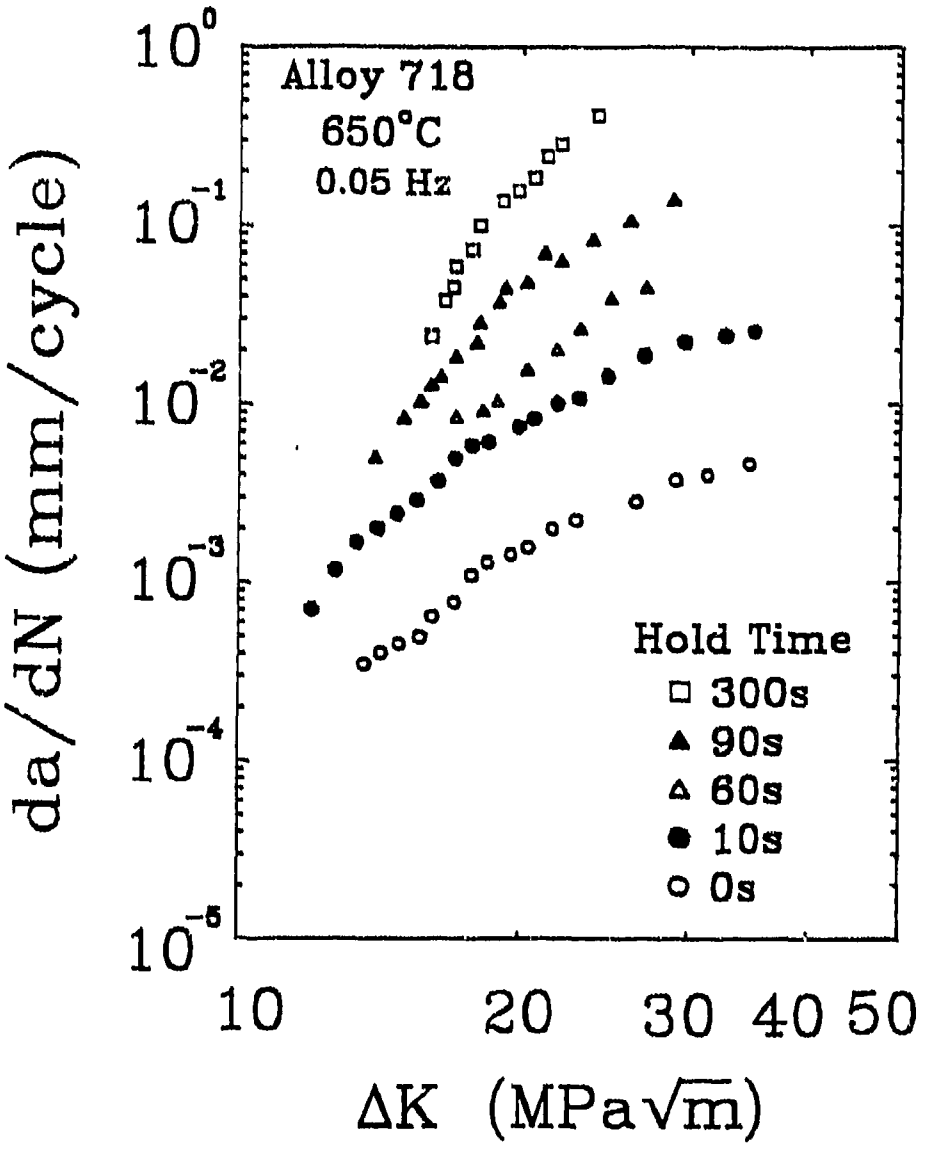

Fig. 1.4 The effects of hold time on crack growth rate at 650°C in air.

time at minimum load on the crack growth rate. In these studies, the minimum load has been below the threshold for crack growth under sustained load, thereby producing no contribution in a linear summation model prediction. Nicholas and Weerasooriya [23] found no effect of hold times between 50 and 500 s under constant K conditions. Shahinian and Sadananda [22] and Sadananda and Shahinian [26], on the other hand, observed a definite increase in growth rate due to the addition of a hold time at minimum load. They attributed this acceleration of growth rate to the additional time available for oxidation. Similar observations have been made by Diboine and Pineau [25] where hold times at minimum load between 3 and 3000 s showed an increase in growth rate compared to that obtained under continuous cycling. In comparing these apparently contradictory results, Ghonem et al. [17] have noted that the frequency of the cyclic loading was different in the three cases cited. In the work of Nicholas and Weerasooriya [23], the cyclic frequency was 1 Hz which produces transgranular crack growth. In [22] and [25], the frequencies were 0.1 and 0.05 Hz, respectively, both of which produce intergranular crack growth. Thus, the effect of frequency is important in this situation because of the differences in mechanisms resulting from different rates of diffusion of oxygen into the grain boundaries. As discussed previously, the strain rate for the 1 Hz cycle must promote homogeneity in plastic deformation near the crack tip, and this kind of deformation mode has less time-dependent sensitivity, thus the hold-time effect does not appear. However, strain rates for 0.17 Hz and 0.05 Hz certainly favor the inhomogeneity in plastic deformation near the crack tip, which will enhance time-dependent behavior and thus will show strong hold-time effects.

Saturation effects of the hold time at minimum load level on the fatigue crack growth rate have been noted by both Sadananda and Shahinian [26] and Diboine and Pineau [25]. The former observed the saturation effect appears for hold times about 1 minute, the latter reported that a saturation effect seems to occur for hold times longer than about 1000s.

If the test temperature is not sufficiently high, the hold-time effect may disappear. For example, Sadananda and Shahinian [19] showed that at 425°C the 1-min. hold time period has a negligible effect on the crack growth process. Furthermore, they found that, at 425°C, hold-times up to 10 minutes still produced purely cycle-dependent behavior. Clearly, the effects of temperature and hold time are synergistic.

Very few studies [2,5,9,21,27-30] have dealt with the effects of hold time on fatigue crack growth rate in an environment other than in air. Ghonem and Zheng [30] have examined the effects of hold time in vacuum by conducting tests of continuous cycling at a frequency of 0.05 Hz and cycling with a hold time of 300 s at maximum load level. They found that the fatigue crack growth rate for a hold time test is higher than that for a continuous cycling test. Similar results have been reported by Smith and Michel [21], Sadananda and Shahinian [29] and VanStone et al. [28].

Effects of Microstructure

Large amount of observations have revealed that the fatigue crack growth properties of Alloy 718 at elevated temperatures are strongly dependent on their

microstructure. In air environment, microstructural parameters, particularly grain size, grain boundary morphology and precipitate particle size, can be altered to produce order of magnitude changes in high temperature crack growth behavior [9,10,13,33-43]. Thamburaj et al [36] observed that high temperature fatigue crack growth rate was much faster in fine-grained structure than in coarse-grained structure for Alloy 718 at 650°C, thus they deduced that more severe grain boundary oxidation can occur in relatively fine grained Alloy 718 due to the greater grain boundary area available along which rapid, stress assisted diffusion of oxygen can occur. The work done by James [10], Smith and Michel [37], Pedron and Pineau [9] also showed that the coarse-grained structure improves crack growth resistance, and the necklace microstructure renders the highest fatigue crack growth resistance. Again, they attributed this grain size effect on crack growth rate to the larger grain boundary area exposed to oxygen penetration in the fined-grained structure comparing with that in the coarse-grained structure.

Grain boundary morphology is another important microstructural factor that controls the high temperature crack growth behavior. Thamburaj et al [36] have pointed out that an irregular grain boundary morphology developed by grain boundary δ phase precipitates will enhance creep ductility and resistance of high temperature fatigue crack growth rate. Andrieu [35] observed that the presence of δ precipitates along the grain boundaries leads to an improvement in creep crack growth resistance. Apart from the factor of irregular grain boundary morphology created by δ phase particles, he suggested that this beneficial influence of δ phase might be related to grain boundary oxidation behavior either because of the intrinsic oxidation resistance of Ni_3Nb phase or because

of the existence of oxygen traps formed along the δ phase interfaces.

While the effects of grain size and grain boundary morphology are important, there have been a number of investigations [10,39,41,42] in which indirect evidence of an inverse relationship between matrix γ' and γ'' particle size and the sensitivity to environmental embrittlement has been demonstrated. When the matrix precipitate is very fine, dislocations cut the precipitate particles instead of bypassing them and are confined to move in coplanar arrays, causing planar pile-ups and consequently, intense stress concentrations at grain boundaries and other obstacles to their motion. If at the same time, the grain boundary cohesive strengths have been weakened as a result of oxidation effect, intergranular cracking would be promoted. Besides, it is also thought that in materials exhibiting predominantly planar slip character, oxygen diffusion [43,44] into the material can occur quite rapidly along planes of intense deformation at elevated temperatures and be swept to the grain boundaries as a result of a solute-dislocation interaction. In the presence of more homogeneous slip, the number of dislocations arriving at a grain boundary would be reduced and consequently, the stress concentrations and oxygen transport to the grain boundaries occurring due to a dislocation "sweep-in" mechanism will be reduced as well. Examined thin foils prepared from regions immediately below fracture surfaces by means of transmission electronic microscope, Thamburaj et al [36] observed that planar deformation was predominant in the case of existing the finest γ'' particle size distributions, and the poor resistance of fatigue crack growth in this case is consistence with the mechanism discussed above.

It has been reported that the overaging heat treatment or the modified heat

treatment (higher solutioning temperature and longer aging time) for Alloy 718 appears to improve crack growth resistance significantly in air environment [5,12,45]. Sadananda and Shahinian [45] observed that the prolonged aging increases the tensile ductility of the alloy by nearly fifty percent, they believed that this increased ductility causes the crack tip to blunt readily and indirectly decreases the environmental sensitivity to the crack growth [46]. Floreen and Kane [5] have noticed that the fracture surface of overaging heat treatment specimen seems to reduce the amount of intergranular crack growth compared to that of conventional heat treatment specimen. They then speculated that homogenization of slip and consequently minimization of localized stress concentrations at the grain boundaries through changes in precipitate morphology at the grain boundaries is a way in which overaging heat treatment could increase the resistance to crack growth. Smith and Michel [12] suggested that the improvement in crack growth resistance produced by the modified heat treatment is likely to be a result of the alteration of dislocation interactions with γ'' particles and grain boundaries. Comparison of the slip line appearance for the conventional and modified heat treatments at 427°C in vacuum revealed that the modified heat treatment produced a microstructural condition conducive to homogeneous deformation which has been found by Fournier and Pineau [15] to result in significant decrease in crack growth rate.

In sum, one can conclude that the types of microstructure that would be most susceptible to environmental embrittlement would be those are fine grained, have very few grain boundary strengthening agents, and/or exhibit pronounced planar deformation characteristics at elevated temperatures. Incidently, it has been reported by several

investigators [5,34,36] that crack growth rate in vacuum environment was almost independent of microstructure.

Effects of Environment

As reviewed previously, the high temperature fatigue crack growth in Alloy 718 is influenced by thermally-activated and time-dependent processes. These processes are generally ascribed to the phenomena including creep and/or oxidation degradation processes. The relative importance of these two processes depends on a number of factors such as the aggressiveness of the environment, the strengthening characteristics of the material, the operating temperature, the duration of exposure time and the applied load level. Nickel base superalloys, in particular Alloy 718, are a class of high strength alloys that have been designed as highly creep resistant materials. Brooks and Bridges [47], for example, have shown that Alloy 718 is microstructurally stable after 10,000 hours exposure at temperatures up to 600°C. Nicholas et al [23] and Pineau [48] have estimated the Riedel-Rice characteristic time for transition from small scale yielding to extensive creep in Alloy 718 at 650°C to be in the range of 20 hours to 3 years. This time period is much larger than the possible cyclic periods and hold time durations in practical applications of this material in gas turbine engines, for example, but the material may be insufficient for applications in the power industry where lifetimes are measured in tens of years.

When examining the relationship between load and load line displacement during creep-fatigue tests in Alloy 718 at 650°C, Pedron and Pineau [33] found that the specimen

behavior is predominantly elastic, thus they suggested that the creep-fatigue crack growth behavior of Alloy 718 at 650°C can be described in terms of linear elastic fracture mechanics, in other words, the stress intensity factor K is the controlling parameter in this case. Sadananda and Shahinian [45] also concluded similarly that when there is a significant contribution from environmental interactions, creep effects are minimized because of the rapid growth of cracks and under these conditions the stress intensity factor K can adequately characterize the crack growth rates. In addition, fractographic observations of Alloy 718 [5,6,25] showed that there was no evidence of any creep cavitation along grain boundaries in cycling tests. All these observations demonstrated that the time-dependent effects in Alloy 718 are principally due to the environmental degradation process.

Besides other environments, air environment has received more attentions and is commonly considered as an aggressive environment for the resistance of high temperature crack growth [5,21,26,30,33,34,38,49,50]. In general, the air environmental effects on crack growth behavior are studied by comparing the crack growth rates in both air and vacuum, and under the certain loading conditions where the environmental effects can be shown up, it has been found that crack growth rates in air are several orders higher than their counterpart in vacuum [12,26,49].

One of the major issue of studying the influences of air environment on fatigue life or fatigue crack growth behavior is to identify which constituents in air actually cause the reduction in the fatigue life or the resistance of the fatigue crack growth rate [26,51,52]. After studying the fatigue properties of pure lead in air at various reduced

pressures and in separate gas atmospheres, Snowden [51,53,54] found that oxygen is the element in air environment responsible for the fatigue life reduction, while environments of nitrogen, hydrogen or water vapor had much less effect. Same conclusion has been reached by Sadananda and Shahinian [26]. Moreover, in static load tests carried out on Alloy 718 at 650°C, in which the environment was alternated from air to vacuum to air [26], the history of environment was found to be of no importance and the environmental effect was found to be limited to the crack tip region. This localized oxidation around crack-tip region was also observed by Andrieu et al [35,55].

It has been realized that mechanical loading conditions can considerably influence the environmental degradation process [56-68]. Coffin [56] is probably the earliest to recognize the effect of mechanical loading on oxidation. His work documented the observation of highly localized regions of surface oxidation in certain high-temperature alloys when subjected to cyclic plastic strain at elevated temperatures. The explanation of the observed effects was based on localized and reversed grain boundary deformation, leading to repeated rupture of the protective oxide film, and accelerated oxidation in the region of deformation. In order to determine if oxygen had been transported into the material during fatigue crack propagation, Swanson and Marcus [63] have analyzed the fracture surfaces of specimens by comparing fatigue crack growth rate in vacuum with that in isotope oxygen-18 environment. Their results indicated that fatigue process enhances the oxygen penetration. Remy and associates [66,67] studied fatigue oxidation interaction in a cobalt-base superalloy MAR-M509 and a nickel-base superalloy IN100 by quantitative metallography, they found that low cycle fatigue at high temperature can

strongly enhance matrix oxidation kinetics in these superalloys, and the enhancement of matrix oxidation is by cyclic stress for MAR-M509 but is by cyclic straining for IN100. The work done by Ward et al [62] in a low carbon steel and by Bucklow and Skelton [58] in a Cr-Mo-V steel has also shown that cyclic stress has a strong influence on oxidation kinetics. Balsone and Nicholas [68] examined the effect of stress on the magnitude of oxidation in Rene'80, their results demonstrated that oxidation is significantly greater under an applied stress than in the unstressed condition, and the depth of oxidation penetration increases as the stress level increases.

So far, several parameters which influences the fatigue crack growth rate in Alloy 718 have been reviewed, and the factors that can alter the fatigue crack growth rate in this material are shown to be complex, many of these variables may interact synergistically to produce a variety of fatigue crack growth behaviors. The above review, however, can lead to the following conclusions:

1) The high temperature fatigue crack growth behavior is related to the cyclic loading frequency. In this regard, three crack growth stages can be identified: cyclic-dependent stage (at high frequency), cyclic- plus time-dependent stage (around transitional frequency) and time-dependent stage (at low frequency).

2) The time-dependent crack growth behavior is primarily due to the environmental influence.

3) Oxygen is the element responsible for the oxidation degradation process.

4) Mechanical loading conditions can strongly influence the oxidation process.

It should be noticed that the time-dependent crack growth stage is the most critical in high temperature applications due to its highly accelerated crack growth rate, it is, however, the least studied or understood in all of the high temperature crack growth stages. This time-dependent crack growth stage is the focus of the present study with the objective of understanding the crack tip controlling mechanism in order to develop the ability to predict its fatigue crack growth performance under different loading conditions. Thus, following this introductory chapter, the subject of Chapter 2 is to analyze the nature of the time-dependent crack growth process by studying the depth of intergranular oxygen diffusion in the crack tip region. Chapter 3 focuses on the intergranular crack-tip oxidation mechanism and outline experimental studies carried out to verify the proposed mechanism. A quantitative crack growth model based on the knowledge of grain boundary oxidation mechanism and localized stress and strain analyses will be detailed in Chapter 4. Chapter 5 describes the numerical simulation of this model and examines its predictive capability by comparing the results generated from the model with corresponding experimental data. Chapter 6 summarizes the results and presents the conclusions of this research program.

CHAPTER 2

ENVIRONMENT-DEPENDENT FATIGUE CRACK GROWTH STAGE

In this chapter attentions will be made to establish the fact that the environment-dependent crack growth stage in Alloy 718 is fully controlled by the depth of oxygen penetration at the crack tip along an intergranular fracture path. This notion will be derived mathematically and supported by experimental results as well.

2.1 High-temperature Fatigue Crack Growth Stages in Alloy 718

As discussed in the previous chapter, attempts to predict elevated temperature fatigue crack growth behavior in Alloy 718 have been considered as the combined effects of the cyclic and the oxidation damage in the crack tip region. In this regard, the damage process ranges from purely cyclic dependent at high frequency levels to fully environment-dependent at very low frequency levels. The relationship between loading frequency and environmental effects on the acceleration of the fatigue crack growth rate in Alloy 718 can be explained in terms of the intergranular oxygen diffusion process in the crack tip region. One of the governing factors of this process is the grain boundary diffusivity of oxygen — a subject that has not been extensively studied particularly in the case of Alloy 718. It is recognized, as discussed in last chapter, that intergranular oxygen diffusion depends on the stress and strain states along affected grain boundaries, thus the diffusivity of a stressed grain boundary, D_g, is proposed to be:

$$D_g = D\exp\left(-\frac{Q_g'}{RT}\right) \tag{2.1}$$

where D is a diffusivity constant, R is the gas constant, T is the temperature in Kelvin, and Q_g' is the effective activation energy of the grain boundary diffusion which could be expressed as:

$$Q_g' = Q_g - f(W_p) \tag{2.2}$$

where Q_g is the activation energy of the grain boundary diffusion in the stress-frees state and W_p is the inelastic strain energy density. Through this definition the influence of loading frequency and the associated deformation mode on the magnitude of D_g and $f(W_p)$ also consequently on the crack growth response can be interpreted qualitatively as follows. High frequency loading, which is generally characterized by high slip density and a homogeneous form of deformation, would result in both strain accommodation as well as stress relief along affected grain boundaries in the crack tip region. Hence variations in $f(W_p)$, and consequently D_g, tend to be minimal. In addition, the increase in slip density, generally, leads to an increase in the lateral matrix diffusion across the affected grain boundaries. These two combined effects would result in limited or no acceleration of intergranular oxygen diffusion rate. In this situation, the influence of crack tip oxidation is minimal and crack tip damage becomes generally dominated by cycle-dependent effects, giving rise to transgranular fracture mode. On the other hand, low frequency loading accompanied by low slip density would promote grain boundary stress concentration resulting in an increase in the magnitude of both $f(W_p)$ and D_g. This

is magnified, particularly, if stress relieve by grain boundary sliding is not permitted, as in the case of the highly creep resistant Alloy 718. Furthermore, the decrease in slip density would limit the grain boundary lateral matrix diffusion process. Here, the expected increase in the grain boundary diffusivity and associated increase in depth of grain boundary oxidation results in an increase in the crack tip damage due to environment effects giving rise to intergranular fracture process.

The relationship between slip line homogeneity and fracture mode characteristics, as described above, has been investigated in the work of Ghonem et al [7] using compact tension specimens made of Alloy 718 with large grain size (50-120 μm) tested at 650°C in air. In this work, fatigue fracture mode as well as slip line density were compared for loading frequency of 30 Hz versus that of 0.05 Hz which includes 300 seconds hold time at maximum load level. Slip line traces at and below the fracture surface of the test specimens were obtained using the decoration technique described in [69]. These traces for different ΔK levels in both test conditions are shown in Figs. 2.1 and 2.2. In Fig. 2.1, which corresponds to a fully transgranular fracture mode, the degree of homogeneous deformation is evident by the high slip line density and the confinement of the reversed plastic zone to a narrow band near the fracture surface. This could be compared with Fig. 2.2(b) which corresponds to a fully intergranular fracture and displays a lower slip line density as well as larger plastic zone size. One should also observe that in the three intergranular locations in Fig. 2.2, the degree of slip homogeneity, measured as the inverse of the slip line interspacing, increases as ΔK increases.

On the basis of above argument the crack growth response of Alloy 718 with respect

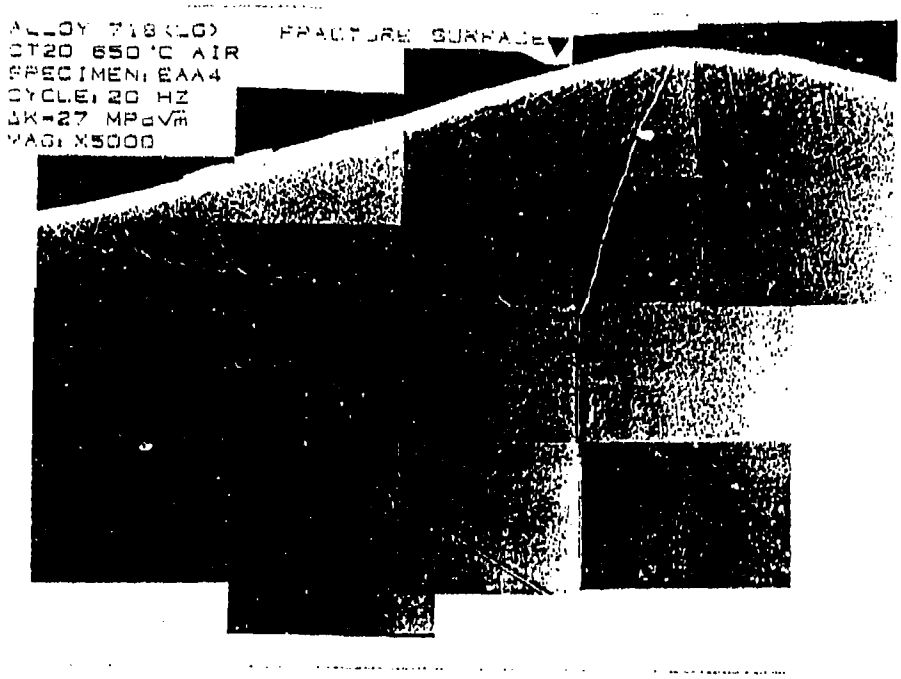

Fig.2.1 Slip line traces along the crack edge for frequency 30 Hz and $\Delta K = 27$ MPa$\sqrt{m}$.

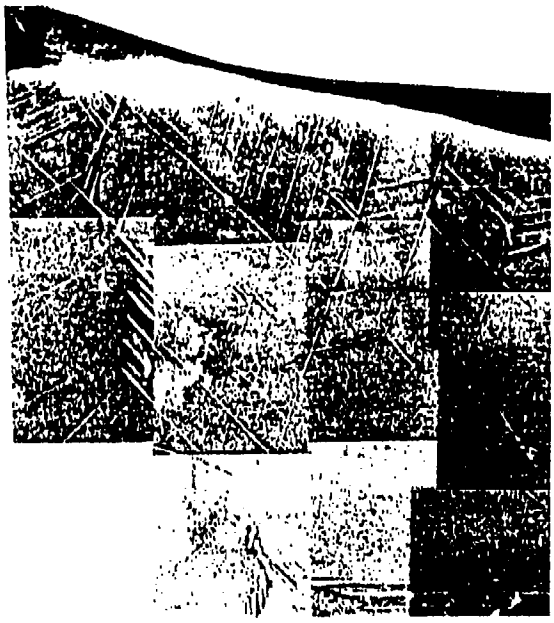

(a)

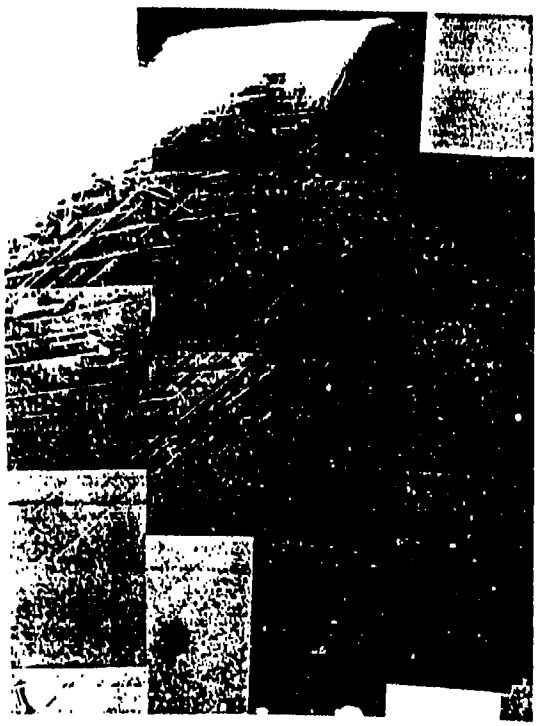

(b)

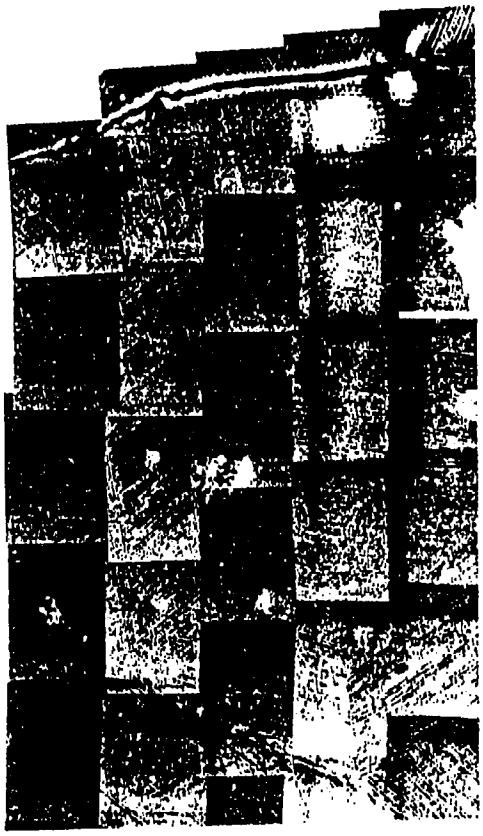

(c)

Fig. 2.2 Slip line traces along the crack edge for low frequency test at different ΔK levels (a) 21 MPa$\sqrt{m}$, (b) 27 MPa$\sqrt{m}$, (c) 38 MPa$\sqrt{m}$

to loading frequency, f, has been divided, following the work of Pineau [48] and Nicholas and co-workers [6,7], into three distinctive types as shown in Figs. 2.3 and 2.4. The first type is associated with high frequency loading in which the deformation mode is governed by a high degree of slip homogeneity. Cracking proceeds primarily in the matrix material (in contrast to the grain boundary), resulting in a predominantly transgranular fracture mode. The value of the frequency, f, required to produce this type of environment-independent behavior, decreases as the magnitude of ΔK increases. This type of crack growth behavior is generally, predicted by the use of a Paris-type equation.

As loading rate decreases, the degree of slip line homogeneity in the crack tip zone is lowered, resulting in a relative increase of the intergranular oxygen diffusion. Under this condition, the crack tip damage becomes a combination of oxidation and cycle-dependent components. In this type of response, the total crack tip damage has been described by many authors [20,66,70-73] using various models which are generally reduced to a form of the linear summation rule and can be expressed as:

$$\left(\frac{da}{dN}\right)_{total} = \left(\frac{da}{dN}\right)_{cycle} + \left(\frac{da}{dN}\right)_{time-dependent} \qquad (2.3)$$

where, in the absence of sustained loading effects (hold times), the time-dependent term represents the contribution of oxidation to crack tip damage and could be written as a time integral in the form:

$$\left(\frac{da}{dN}\right)_{time-dependent} = \int_{t_{ox}} \left(\frac{da}{dt}\right) dt \qquad (2.4)$$

where t_{ox} represents the time period of the cycle during which the oxidation process is an

active damaging component. As shown in Figs. 2.3 and 2.4, this oxidation enhanced process is characterized by a mixed transgranular/intergranular fracture mode. The degree of contribution of each of the cycle- and time-dependent terms in the above equation depends on both the frequency and ΔK values. For the same frequency, as ΔK increases the contribution of the cycle-dependent damage also increases, since increasing ΔK leads to an increase in the degree of slip line homogeneity, see Fig. 2.1. The increase in the cycle-dependent damage is measured by the increase in percentage of the transgranular features along the fracture surface. For the same ΔK value, however, the influence of the time-dependent damage increases as frequency decreases.

The third type of response mentioned above occurs for loading frequencies below a transitional level, f_c, where the crack tip damage becomes mainly an environment-dependent process in which crack growth is largely intergranular. The value of the transitional frequency, for a particular ΔK, in Alloy 718 was found to depend on both temperature and microstructure [7,17,48]. As shown in Fig. 2.4, for a grain size around 100 μm at 650°C and ΔK=40 MPa$\sqrt{m}$, the value of f_c is on the order of 0.1 Hz. The influence of air environment on fatigue crack growth behavior, where the test frequency is in the environment-dependent regime ($f < f_c$), is depicted in Fig. 2.5 by comparing the fatigue crack growth rates tested in air and vacuum (10^{-8} torr) conditions. It clearly shows that the fatigue crack growth rate in vacuum is about 5 to 10 times slower than that in air. Furthermore, the fracture surfaces in both cases are shown in Figs. 2.6(a) and 2.6(b) where they exhibit fully intergranular fracture in the case of air testing and fully transgranular fracture in the case of vacuum testing.

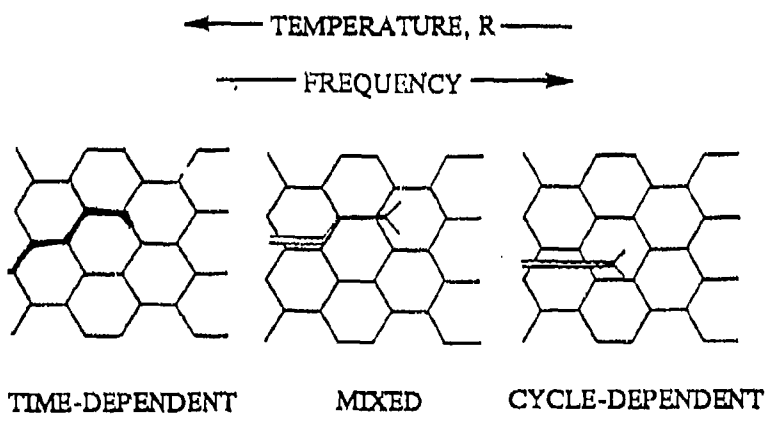

Fig. 2.3 Schematic of high temperature fatigue crack growth stages.

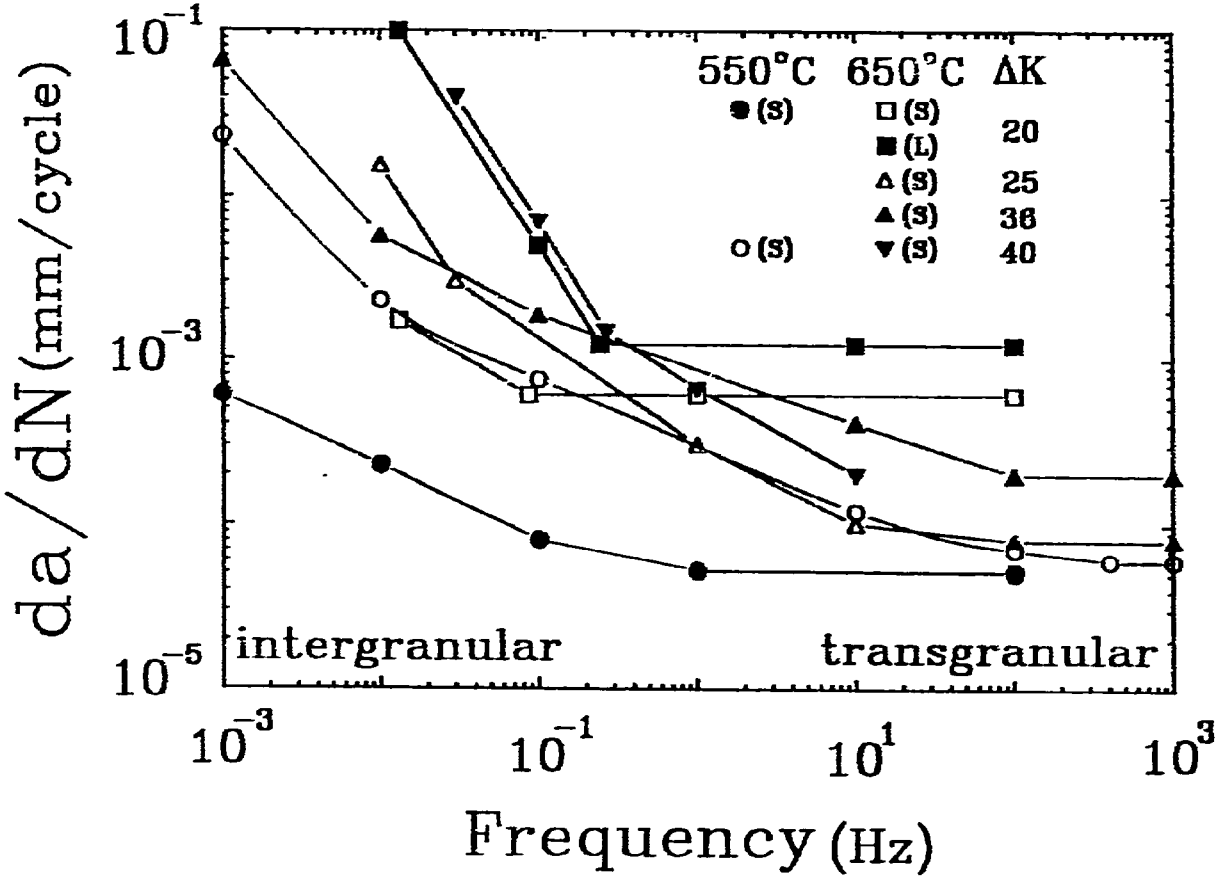

Fig. 2.4 Effect of frequency on fatigue crack growth rate of Alloy 718 at R = 0.1 for different temperatures, grain sizes (S≈20.50μm, L≈150μm) and ΔK levels.

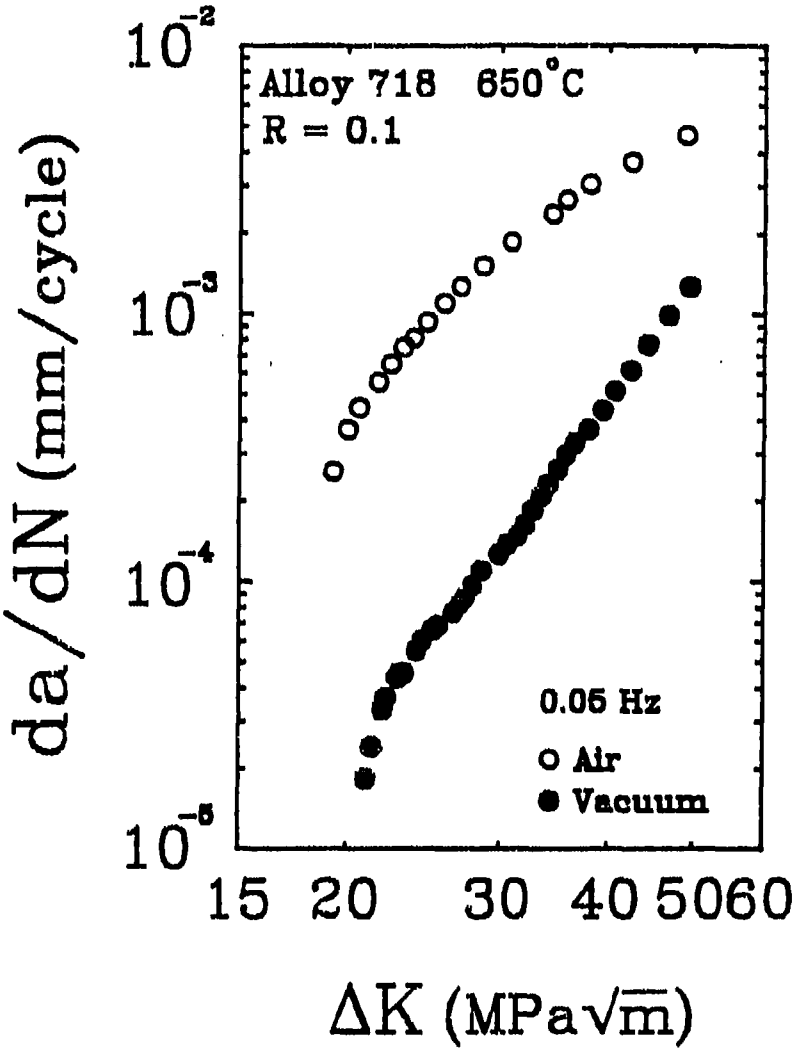

Fig. 2.5 Comparison of fatigue crack growth rate in air and vacuum (frequency 0.05 Hz, temperature 650°C).

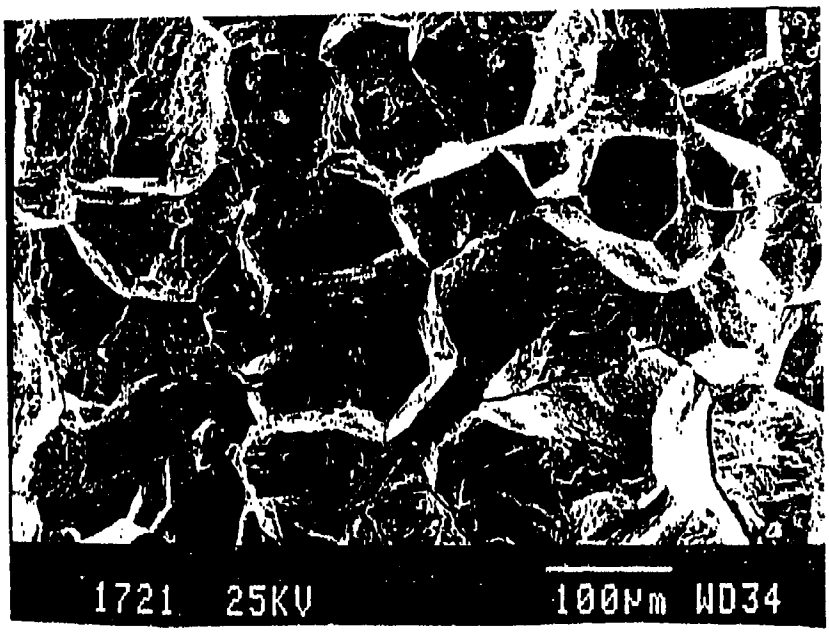

(a)

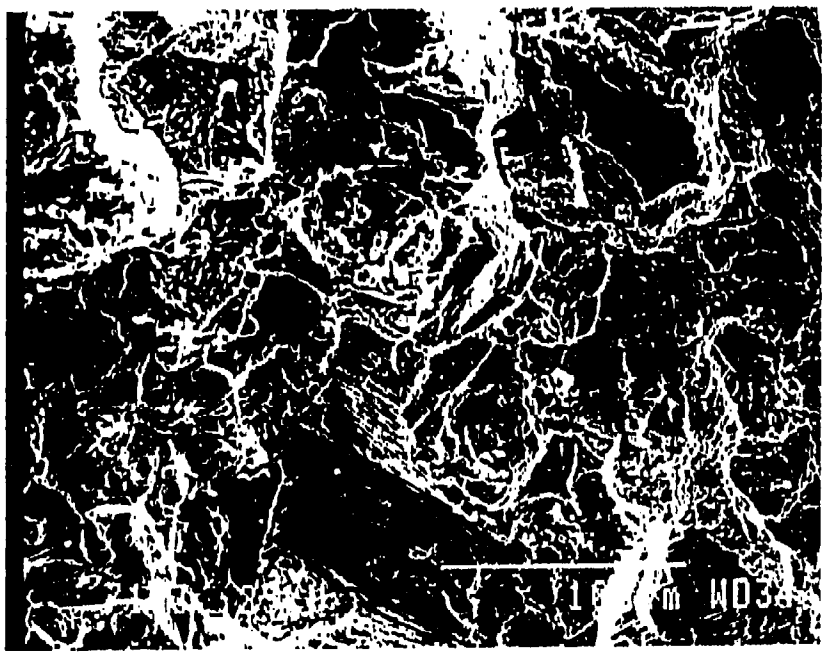

(b)

Fig. 2.6 Scanning electron micrographs of fracture surfaces of Alloy 718 tested with 0.05 Hz at 650°C in (a) air and (b) vacuum.

2.2 Environment-Dependent Fatigue Crack Growth Stage

2.2.1 Intergranular Depth of Oxygen Diffusion

If one makes the assumption that in the environment-dependent stage the crack growth increment per cycle is equal to the intergranular depth of oxygen diffusion, X, occurring during the cycle effective oxidation time, t_{ox}, then the fatigue crack growth rate can be expressed as:

$$\left(\frac{da}{dN}\right)_{total} = \int_{t_{ox}}\left(\frac{da}{dt}\right)dt = \int_{t_{ox}}\dot{X}(\Delta K,t)\,dt \qquad (2.5)$$

where $\dot{X}$ is the oxygen intergranular diffusion rate, generally it varies with time. The recognition that oxygen diffusion is an energy activated process, it could then be treated as a function of the stress intensity factor range, ΔK, acting on the crack tip during the cycle effective oxidation time. Testing the validity of this assumption (i.e. the ability of the above equation to describe the environment-dependent stage), requires the knowledge of both t_{ox} as well as the relationship between $\dot{X}$ and ΔK. These two requirements are not readily available in literature and therefore an attempt will be made here to determine these requirements experimentally.

2.2.2 Cycle Effective Oxidation Time

The cycle effective time, t_{ox}, is defined here as being the period of the cycle during which the oxidation effects take place. Several authors have assigned different measures to t_{ox}. For example, Achter et al [74] in their study of the effect of oxygen partial

pressure on crack growth rate in Type 316 stainless steel at elevated temperature, proposed a calculation method which was based on the assumption that the time required for adsorbing a gas atom monolayer at the crack tip is equal to half of the tensile part of the cycle or a quarter of the whole cycle period. Wei and associates [75,76] in their attempt to predict environment assisted crack growth behavior in AISI 4340 steel, assumed that the value of the maximum load is the controlling factor for crack surface reaction rate. The cycle oxidation time in their work was assumed to be equal to half of the loading period plus half of the unloading period. Nicholas et al [23,71], in their work on Alloy 718, developed a model to predict purely time-dependent fatigue crack growth behavior by integrating the sustained load growth rate. They argued that the loading part of the cycle is the part responsible for the environment-assisted effects. Similar conclusions were made by Floreen [52] in his work on grain boundary diffusion in nickel-base superalloys. Other investigators, specially Liu an McGowan [77], Rechet et al [66], Antolovich [78], Romanoski [79] and Saxena [73] employed, for different materials, different cycle period to represent t_{ox}. In the face of these different definitions of t_{ox}, an experimental attempt was made here to determine the effective oxidation time for Alloy 718 at temperature level of 650°C and for loading frequencies less than f_c.The fatigue crack growth tests were conducted under constant load range, ΔP, and R=0.1 where R is the load ratio. These tests involved triangular wave forms with different cycle durations, all satisfying the condition that $f < f_c$. These durations include 27.5 seconds (25s-2.5s), 50 seconds (25s-25s), 100 seconds (25s-75), and 100 seconds (90s-10s); labelled here as cases A, B, C and D, respectively. Fracture surfaces corresponding to all tests exhibited

fully intergranular fracture features (confirming that $f < f_o$), as seen in Fig. 2.7. Results in the form of fatigue crack growth rate, da/dN versus ΔK are plotted in Fig. 2.8. They show the fatigue crack growth rate for case C to be identical to that of case D indicating that for the same frequency, varying the ratio of loading and unloading portions of the cycle will not influence the fatigue crack growth behavior. This result is contrary to results obtained, for example, by Coffin [80] in his work on fatigue crack initiation in OFHC copper at 400°C and on 304 stainless steel at 650°C. His results showed that in an asymmetric loading cycle, slow-fast loading is more damaging than fast-slow loading. Similar results have been obtained by Ghonem et al for crack growth behavior in various ductile materials [81]. However, their results have been interpreted as time-dependent crack growth caused by grain boundary cavitation. In this, cracking mechanism, cavity growth and consequently crack growth is aided by slow rate loading while unloading results in cavity healing with no contribution to the crack growth process. This cavity growth related mechanism is not operative in the highly creep resistant Alloy 718. In this alloy, for time-dependent environmental effects which are governed by temperature and load levels, both segments of the loading cycle should exert the same damage effects at the crack tip. Furthermore, cases of A, B and C, which are of different frequencies but identical loading times, did not result in similar crack growth behavior so that an increase in the total cycle duration yields, as expected, an increase in the crack growth rate. The conclusion, based on these observations, is that for loading frequencies lower than the transitional frequency, the cycle effective oxidation time is equal to the total time of the loading cycle.

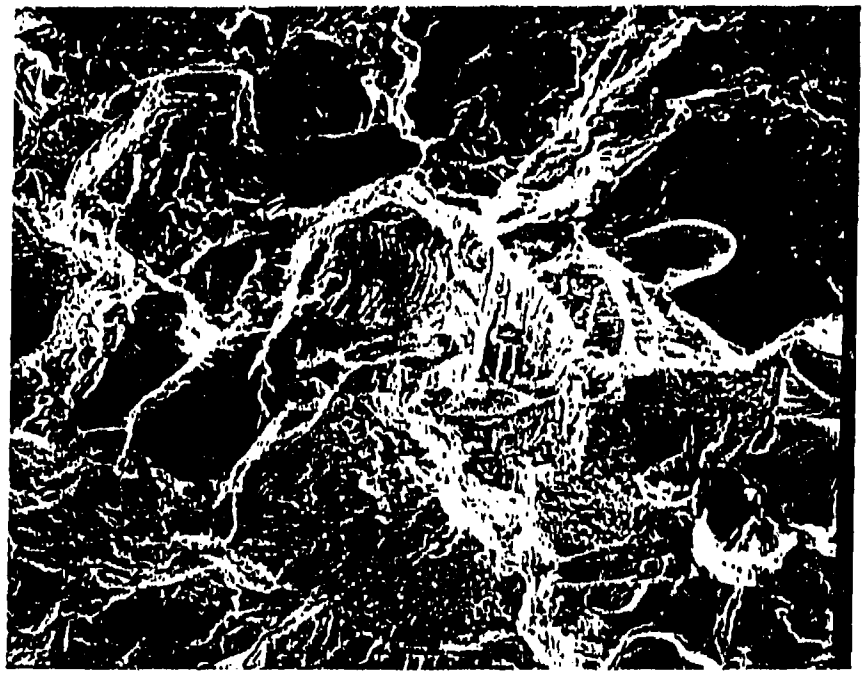

(a)

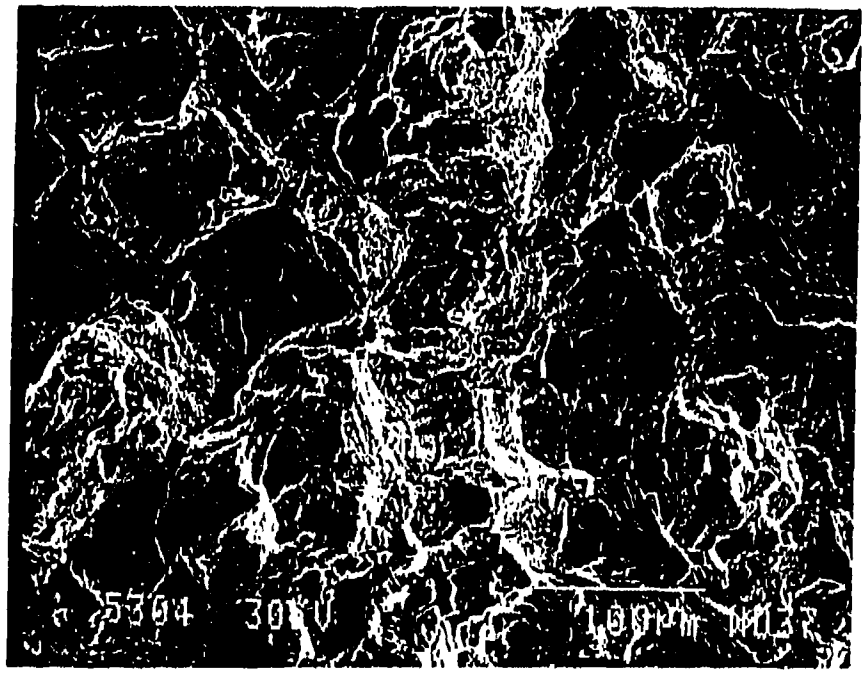

(b)

Fig. 2.7a Scanning electron micrographs of fracture surfaces of Alloy 718 tested at 0.05 Hz and 650°C for (a) 25s-2.5s (b) 25s-25s.

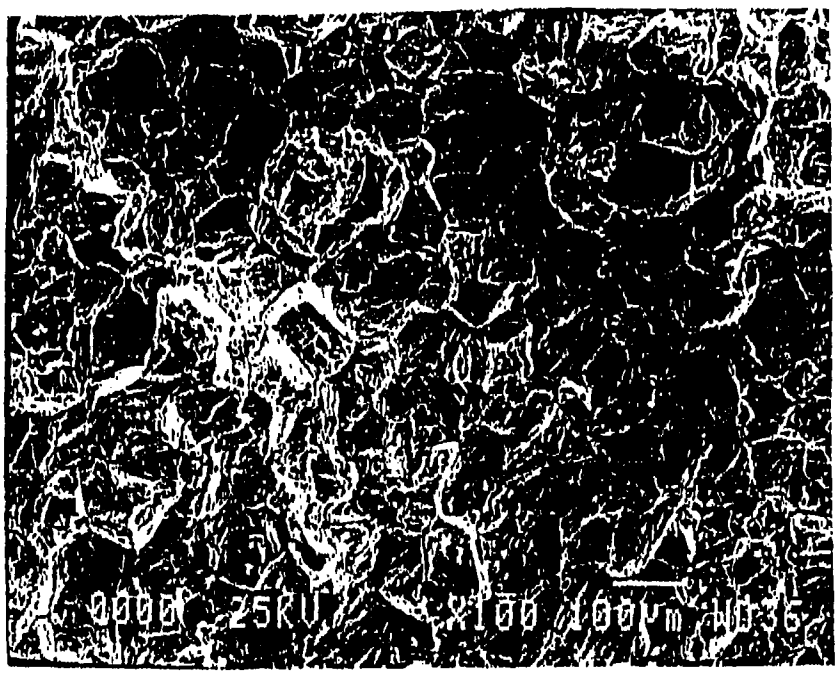

Fig. 2.7b Scanning electron micrographs of fracture surface of Alloy 718 tested at 0.05 Hz and 650°C for 90s-10s.

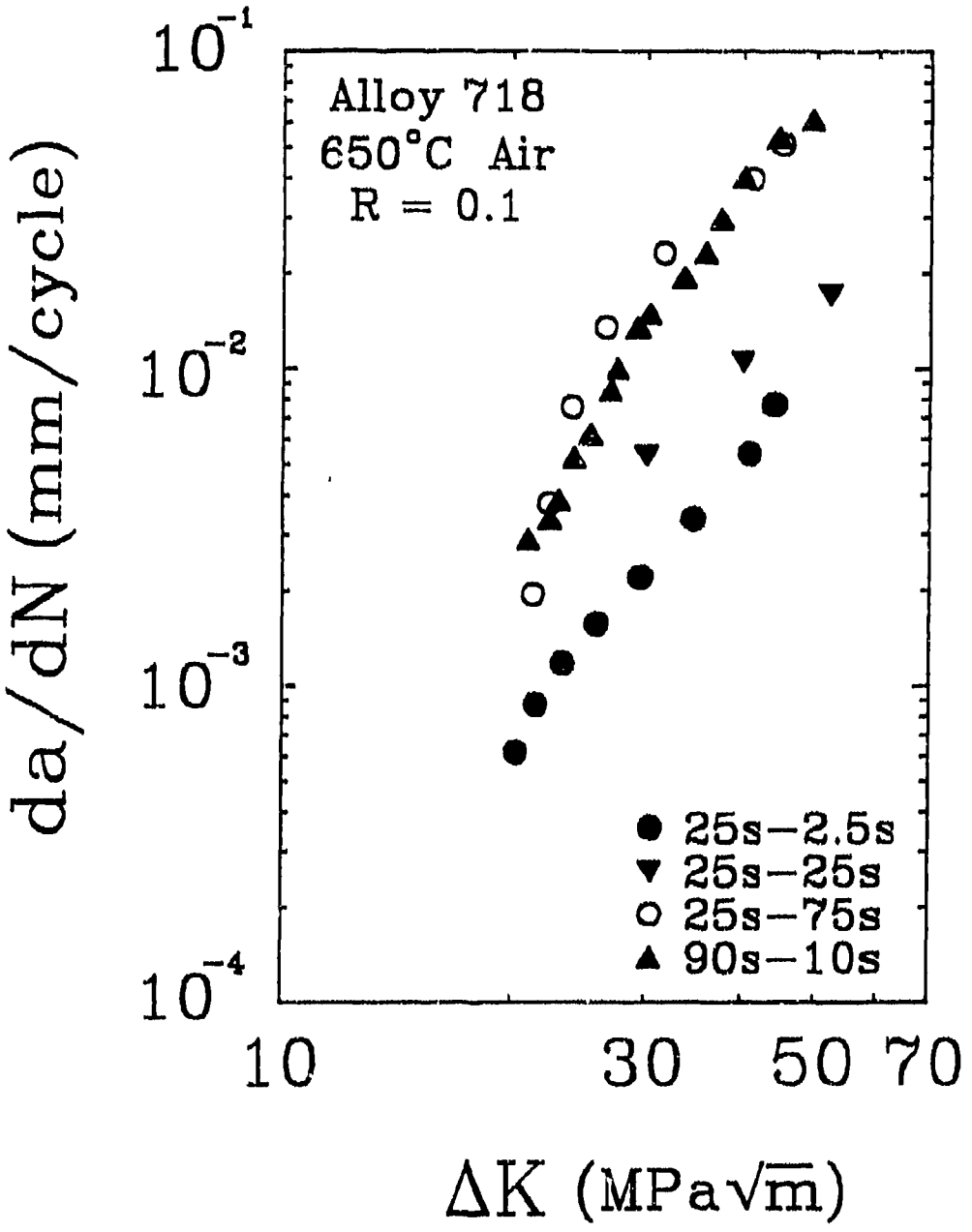

Fig. 2.8 da/dN versus ΔK for different frequencies with different loading and unloading rates.

In comparing these results with those of Ashbaugh [18], it should be noted that the variation in loading frequency between case D and the other three is less than a factor of 4 whereas Ashbaugh investigated the effect using frequencies which differed by either one or two orders of magnitude. Further, the crack growth rates differ by much less than an order of magnitude at low ΔK values in the results of the present work, whereas Ashbaugh reported that the growth rates were "comparable." Although the loading frequency in the asymmetric wave produced growth rates in Ashbaugh's study which were nearly identical to those from symmetric wave forms of the same frequency at high values of ΔK in excess of 30 MPa$\sqrt{m}$, differences appeared at lower ΔK. In particular, the slow-fast (50s-5s) wave had a lower fatigue crack growth rate than the symmetric 0.01 Hz (50s-50s) while the fast-slow (5s-50s) had a considerably higher fatigue crack growth rate than the (5s-5s) symmetric wave. This demonstrates that total cycle time as well as loading frequency can influence growth rate, depending on the particular conditions.

These results indicate that as long as the inhomogeneity in plastic deformation near the crack tip has been produced by slow strain rates, the fatigue crack growth rate is dependent on frequency. In general, however, crack growth rates in nickel-base superalloys due to combinations of hold times and cyclic loading involve a complex interaction which can be attributed to a variety of mechanisms including fatigue, creep or stress relaxation, environmental degradation, and crack tip blunting or crack branching. Further, the ΔK value can influence the results because of the differing contributions of cycle dependent and time dependent mechanisms.

2.2.3. Relationship between $\dot{X}$ and Stress Intensity Factor Range ΔK

2.2.3.1 Concept

Work of Nicholas and Weerasooriya [23], has demonstrated that subjecting Alloy 718 to elevated temperature fatigue testing with a loading cycle having a frequency $f > f_c$, and an imposed hold time at the minimum load level for periods up to 1000 seconds did not result in any measurable acceleration in the crack growth rate when compared to the crack growth rate due to the base cycle without the hold time periods. By lowering the loading frequency to levels below the transitional frequency of the alloy, an accelerated intergranular crack growth was detected when addition of hold times at minimum load level were imposed for periods as small as 30 seconds, see Diboine et al [25]. This observed increase in the crack growth rate is interpreted in the work of Ghonem et al [17], as being a result of further intergranular oxidation taking place at the crack tip during the hold time period, provided that the minimum load level does not contribute to the mechanical driving force of the crack tip. The crack growth rate under this type of loading calculated using a damage summation form similar to that of eq. (2.3) can be:

$$\left(\frac{da}{dN}\right)_{cyc+h} = \left(\frac{da}{dN}\right)_{cyc} + \left(\frac{da}{dN}\right)_{h} \qquad (2.6)$$

where the first term of the right hand side of the above equation represents the contribution to the crack growth rate due to the reversed part of the cycle and the second term is the contribution due to the hold time period. The above equation can be expressed in terms of (da/dt) as:

$$\left(\frac{da}{dN}\right)_{cyc+h} = \int_{t_{cyc}}\left(\frac{da}{dt}\right)dt + \int_{t_h}\left(\frac{da}{dt}\right)dt \qquad (2.7)$$

The term (da/dt) is viewed as being equal to the intergranular oxygen diffusion rate $\dot{X}$ which, as mentioned before, is assumed to be a function of the stress intensity factor range, ΔK. Therefore, eq. (2.7) could be rewritten as:

$$\left(\frac{da}{dN}\right)_{cyc+h} = \left(\frac{da}{dN}\right)_{cyc} + \int_t \dot{X}(\Delta K, t)\,dt \qquad (2.8)$$

The intergranular depth of oxygen diffusion, X, could then be written as:

$$X = \left(\frac{da}{dN}\right)_{cyc+h} - \left(\frac{da}{dN}\right)_{cyc} \qquad (2.9)$$

The differential form of this equation is expressed as:

$$\dot{X} = \lim_{\Delta t \to 0}\frac{\Delta X}{\Delta t} \approx \frac{\left(\frac{da}{dN}\right)_{cyc+h} - \left(\frac{da}{dN}\right)_{cyc}}{\Delta t} \qquad (2.10)$$

Where Δt, in this case, is the hold time duration t_h. Therefore

$$\dot{X} \approx \frac{\left(\frac{da}{dN}\right)_{cyc+h} - \left(\frac{da}{dN}\right)_{cyc}}{t_h} \qquad (2.11)$$

The determination of $\dot{X}$ could thus be achieved through the knowledge of the hold time period t_h and the crack growth rates, $(da/dN)_{cyc+h}$ and $(da/dN)_{cyc}$ which correspond to the total loading cycle and the reversed part of the cycle; respectively. In order to solve this equation an experimental program was carried out to provide these data for different of

K and t_h values. This experimental program as well as its results and analysis will be described in the following section.

2.2.3.2 Experiments, Results and Analysis

In this program, a set of crack growth experiments were performed on compact tension specimens made of the Ailoy 718 previously described at temperature level of 650°C and a stress ratio of 0.1. This set of experiments consisted of constant ΔK tests with and without hold time periods imposed at the minimum load level. Three different values of ΔK were selected; 30, 40, and 50 MPa$\sqrt{m}$. For each level of ΔK four different hold time periods were investigated, these are 50, 100, 680 and 3600 seconds. The load level during the hold time period was determined such that the hold time period would produce, at the longest expected crack length, a stress intensity factor with a value lower than that of the fatigue threshold stress intensity factor for this material which was estimated to be 12 MPa$\sqrt{m}$. Under this condition, an observed increase in the crack length would be purely correlated with the oxygen influence at the crack tip. Results of these tests in the form of the ratio $(da/dN)_{cyc+h}/(da/dN)_{cyc}$ versus t_h for different values of ΔK are shown in Fig. 2.9. They indicate that the influence of the hold time at minimum load level on the crack growth rate is measurable for hold time periods as small as 50 seconds. This observation confirms similar findings reported by Diboine and Pineau [25]. The influence of the hold time reaches a saturated level at t_h values that increases as ΔK decreases. These results in the form of $(da/dN)_{cyc+h}/(da/dN)_{cyc}$ when substituted in eq.(2.11) yield values of X calculated as a function of t_h and ΔK. This type of

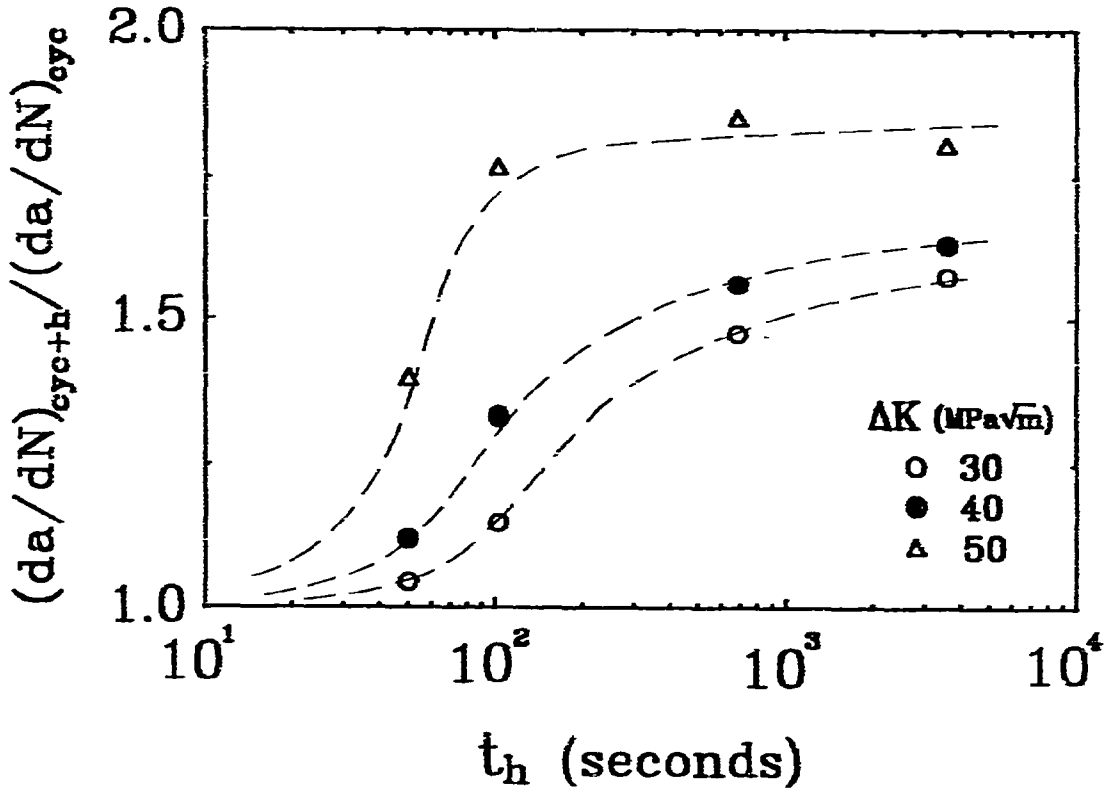

Fig. 2.9 Effect of hold time at minimum load level on $(da/dN)_{cyc+h}/(da/dN)_{cyc}$ for different K_h levels.

relationship is illustrated in Fig. 2.10. It shows that, for all values of ΔK, $\dot{X}$ decreases as t_h increases. This relationship between $\dot{X}$ and t_h could be interpreted on the basis of the two-stage oxidation mechanism, see [82]. At the onset of the oxidation process, the oxygen diffusion rate reaches its peak since no barrier to diffusion exits. As the oxidation time increases thus permitting the formation of the dense chromia (Cr_2O_3) layer, the oxygen penetration rate decreases. When the formation of Cr_2O_3 is completed after a certain transition oxidation time which is microstructure dependent [50], $\dot{X}$ would approach zero. The relationship between $\dot{X}$ and both t_h and ΔK, as illustrated in Fig. 2.10, is fitted into the following mathematical form

$$\dot{X} = G_1(t)\,\Delta K^m \tag{2.12}$$

where m is a constant with the value of 3.144, and $G_1(t)$ assumes the following polynomial form:

$$G_1(t) = A\,t^{-a_1}\,e^{-\frac{a_2}{t}}\left(1 - a_1 + \frac{a_2}{t}\right) \tag{2.13}$$

A, a_1 and a_2 are coefficients having the values of 1.787×10^{-8}, 0.632 and 28.67, respectively. One should observe that in the above equation when time t approaches infinity, both $G_1(t)$, and consequently $\dot{X}$, approaches zero.

The validity of eq. (2.12) can not be tested through direct measurements of $\dot{X}$, it could, however, be verified through the use of $\dot{X}$ to derive a fatigue crack growth rate expression, which can be tested by comparing its predictive results to those

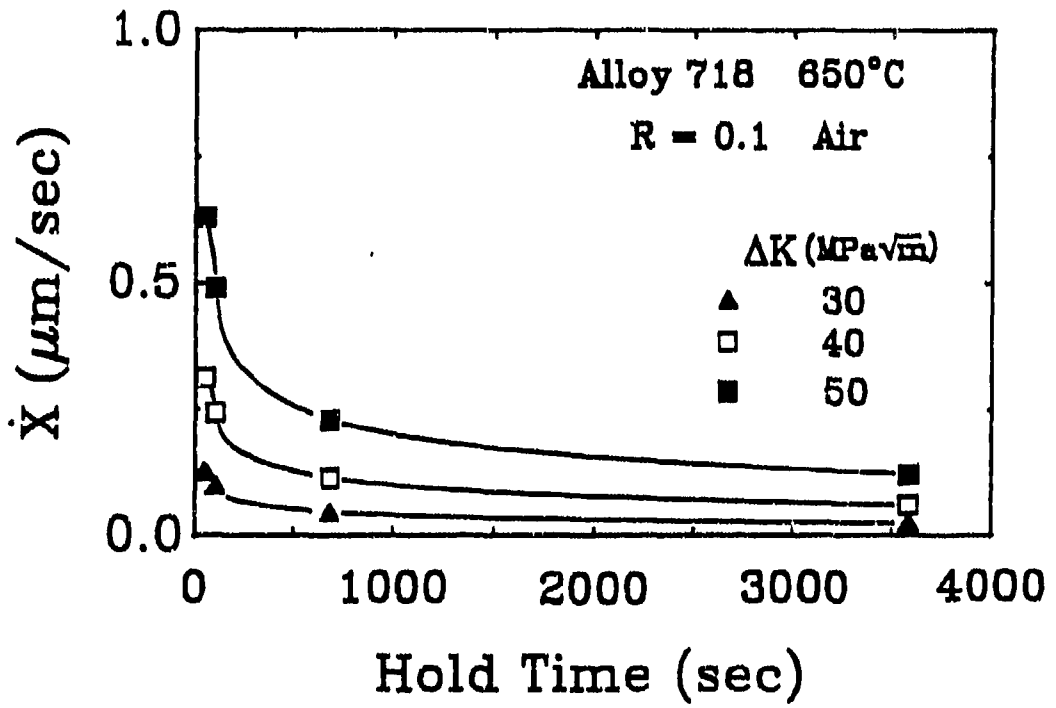

Fig. 2.10 Oxygen intergranular diffusion rate, $\dot{X}$, vs hold time, t_h, imposed at minimum load for different ΔK levels.

experimentally generated. This is achieved as follows. One can write the crack growth rate equation as:

$$\frac{da}{dN} = \int_0^{t_{ox}} \dot{X}\, dt \qquad (2.14)$$

where t_{ox} is the effective oxidation time during a loading cycle. Substituting eq. (2.12) into eq. (2.14) and considering the oxidation time of a loading cycle to be, as previously discussed, equal to the total cycle time, the fatigue crack growth rate can then be derived as:

$$\dot{X} = \frac{da}{dN} = G_2(f)\, \Delta K^m \qquad (2.15)$$

where

$$G_2(f) = A\, f^{-a_1} e^{-a_2 f}$$

f is the loading frequency while A, a_1 and a_2 are constants having the same numerical values as those in eq. (2.12). Eq. (2.15) could now be tested by comparing its predictive results with those experimentally obtained for the same loading frequency. The degree of matching between these two sets of results can then determine the validity of eq.(2.12). Eq. (2.15) was applied for three different frequencies, i.e. 0.01, 0.02 and 0.05 Hz all of which are below f_o for the alloy 718 used in this study. Results of this application are shown in Fig. 2.11. It is observed that a reasonable agreement exists in the full range of ΔK between the values and trends of the three experimentally obtained data sets and those theoretically predicted through the use of eq. (2.15). This result is taken in support of eq.(2.12) as being a valid expression for estimating the oxygen diffusion rate in Alloy 718

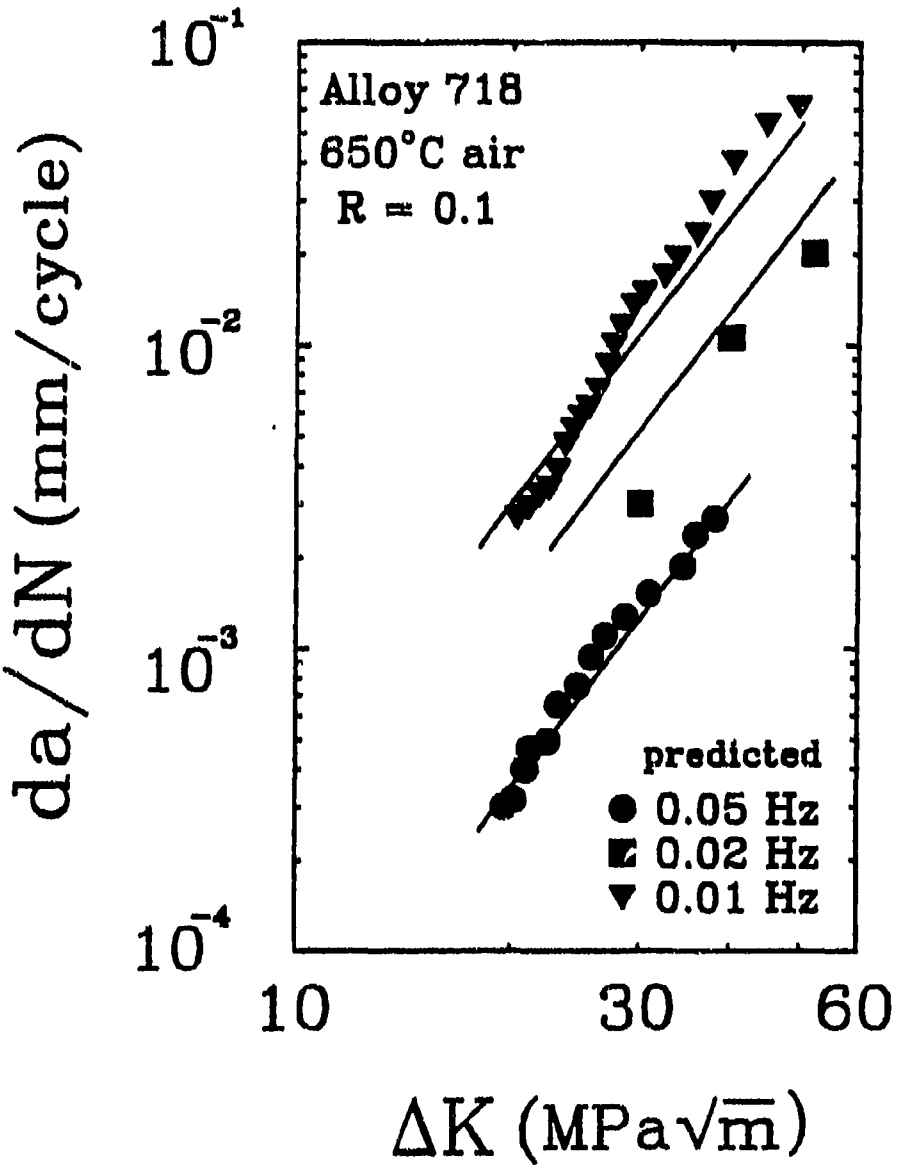

Fig. 2.11 da/dN vs ΔK for both experimental and theoretically predicted results.

and also as an indirect support to the notion that the growth process governed by eq. (2.15) is a fully environment-dependent process.

An important feature of eq. (2.12) is in its use to directly calculate the oxygen diffusivity of grain boundaries, D_g, a parameter required for the physical understanding and the quantitative modelling of the crack tip oxidation mechanism in Alloy 718, see [83]. This could be achieved as follows: a parabolic diffusion law when applied to estimate the intergranular depth of oxygen diffusion, X, during a time interval t could be written as:

$$X = \alpha\sqrt{D_g t} \tag{2.16}$$

where α is a geometrical constant, D_g is the oxygen diffusivity of grain boundaries. The intergranular depth of oxygen diffusion, X, during the time interval corresponding to one loading cycle, could thus be calculated as:

$$X = \alpha\sqrt{\frac{D_g}{f}} \tag{2.17}$$

where f is the loading frequency. Another identification of X is that described in eq. (2.15). By equating these two X-expressions, i.e. eqs. (2.15) and (2.17), an explicit relationship linking the oxygen diffusivity of grain boundaries, D_g, with both ΔK and frequency f can be derived. This relationship is obtained here as

$$D_g = G_3(f)\,\Delta K^{2m} \quad ; \quad \Delta K>0 \tag{2.18}$$

where

$$G_3(f) = \left(\frac{A}{\alpha}\right)^2 f^{-(2a_1+1)} e^{-2a_2 f}$$

This relationship between D_g, ΔK and f as illustrated in Fig. 2.12 shows that, for the same ΔK range, the diffusivity D_g is inversely proportional to the loading frequency. This can be explained, as qualitatively discussed in eq. (2.1), by considering the influence of frequency on the local stress field near the grain boundary regions. For example, the decrease in the loading frequency is expected to result in an inhomogeneous form of plastic deformation which consequently leads to the increase of stress concentration across the affected grain boundary paths near the crack tip. This would then result in the decrease of the effective diffusional activation energy, Q_g', of these affected boundaries. The decrease in Q_g' is expressed in eq. (2.1) through the introduction of an inelastic strain energy function $f(W_p)$ which could now be shown, through the comparison between eqs. (2.1) and (2.18), to be a ΔK- and f-dependent function. Furthermore, Fig. 2.12 shows that, for the same loading frequency, the diffusivity D_g increases as ΔK increases. This, again, can be explained in terms of the direct influence of the crack tip stress field on the diffusional characteristic of the grain boundary path. Now, if one make the assumptions that the ratio of matrix diffusivity, D_m, to grain boundary diffusivity, D_g, is maintained at 10^4 [84] and, furthermore, D_m is a frequency-independent parameter, one could thus establish profiles of D_m for different ΔK values. These profiles are shown as dashed lines in Fig. 2.12. The point of intersection between two corresponding D_m and D_g lines would then identify the transitional frequency, f_c, for a particular ΔK level. Below f_c, D_g dominates giving rise to intergranular crack growth mode, while above f_c, D_m dominates

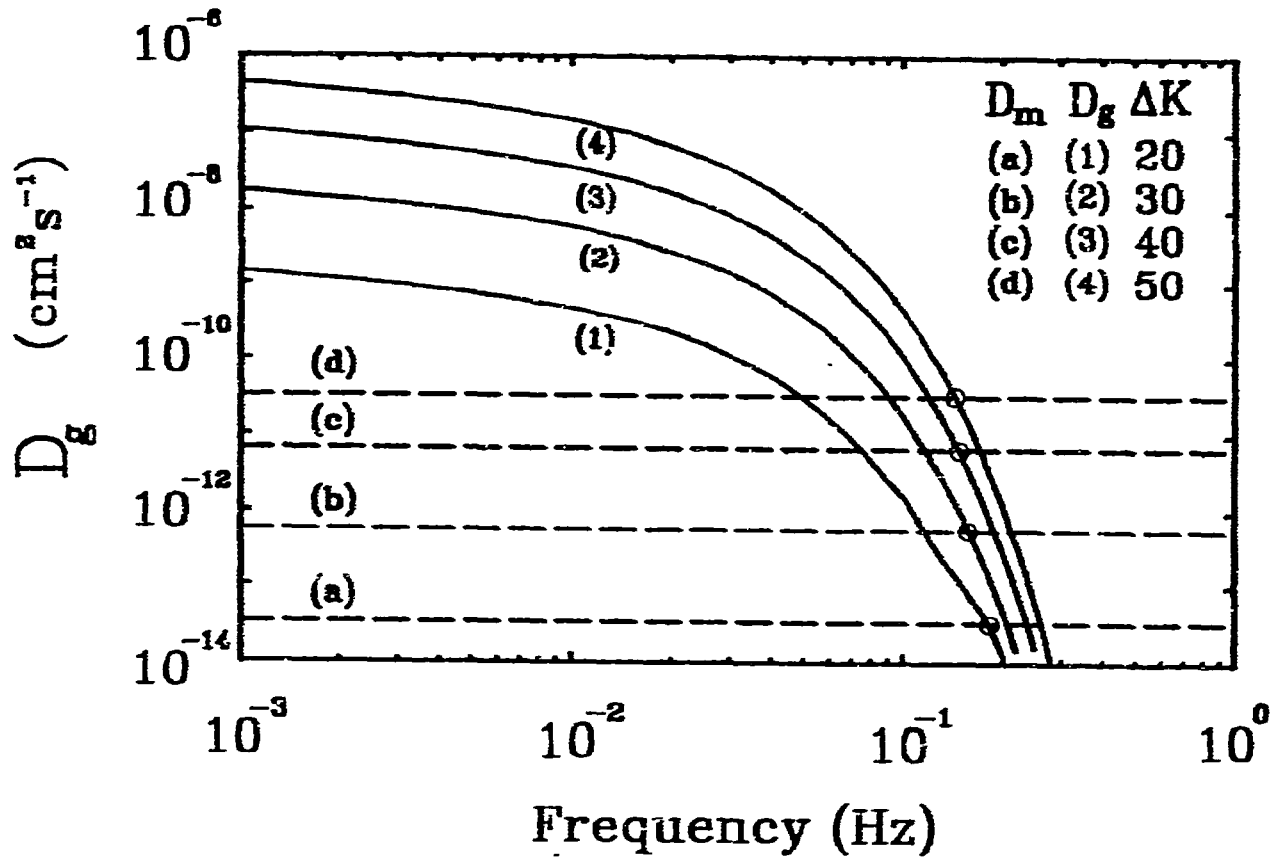

Fig. 2.12 Variations of th oxygen diffusivity of grain boundaries, D_g, with loading frequency f and ΔK.

resulting in transgranular crack growth path. In this case, while f_c decreases as ΔK increases, the variation of f_c is, as described by Weerasooriya et al [6,7], to the narrow range between 0.1 to 0.2 Hz.

CHAPTER 3

INTERGRANULAR CRACK-TIP OXIDATION MECHANISM

In the previous chapter it is established that the environment-dependent crack growth stage in Alloy 718 is fully linked to the crack tip oxygen diffusion process. In this chapter, the crack tip oxidation process will be detailed and will be then used in chapter 4 in a quantitative approach to predict the crack growth behavior in this alloy.

3.1 Crack Tip Oxidation Mechanisms

As mentioned before, extensive evidence exists in literature showing that the time dependency of high temperature crack initiation and propagation is the result of the aggressive effect of environment. The early work of Smith et al [85] has clearly demonstrated that environmental degradation effect is a result of oxygen penetration at the crack tip. Efforts have been made in the last two decade to detail the crack tip oxidation mechanism and provide correlations between these mechanisms and both material and loading parameters. When not considering simple adsorption of oxygen at the crack tip, oxidation mechanisms could be identified, in general, in terms of oxygen short and long range diffusion processes. In the short range diffusion process, oxygen forms an oxide layer at the crack tip with a depth that depends on many operating and materials parameters. The formation of this layer, under the restricted concave crack tip geometry, results in high stresses that could easily be transmitted to the substrate. The

important aspect of this oxidation mechanism, however, is the possible formation of wedge-shaped oxide intrusions along the crack front. The rupture of these wedges at grain boundary intersections, could result in an accelerated, intergranular crack-growth rate, see Bricknell and Woodford [86] McMahon and Coffin [87], Coffin [88] and McMahon [89]. In the long range diffusion process, oxygen penetrates the crack-tip material along rapid diffusion paths, such as, slip planes and grain boundaries. The internal oxidation process taking place along these path could occur in the form of internal oxide sites, cavity formations, and/or solute segregation. As pointed out by Woodford and Bricknell [90], it is also possible for oxygen to take part in chemical reactions releasing known embrittlement agents onto grain boundaries. Each, or all, of these may be operative in any particular alloy under a given set of conditions. These processes, in particular, along grain boundaries result in the inhibition of the sliding and migration of these boundaries and thus reduce their ability to relieve local stresses built up during deformation.

While it is recognized that the oxidation mechanisms associated with the short and long range diffusion are not completely separated, experimental observations indicate that, for Alloy 718, at an intermediate temperature range and at lower cyclic loading frequencies, the short-range oxygen diffusion contributes primarily to the occurrence of an intergranular fracture mode. Recognizing that oxygen partial pressure plays an important role in the development of this oxidation process, Andrieu [50] has suggested a qualitative model which depends on the type, and sequence, of oxide layers formation at the crack tip. This model will be termed as the two-stage crack-tip oxidation

mechanism in the following chapters of this report.

3.2 Two-stage crack-tip oxidation mechanism

The damage process associated with short-range oxygen diffusion at the crack tip has been studied by several authors [34,58,91]. Important factors to be considered in this process are those related to temperature, frequency, alloy chemistry and oxygen partial pressure, PO_2. The first clear demonstration of the effect of PO_2 was exhibited in the work of Smith et al [85]. They observed that reducing the oxygen partial pressure during fatigue crack propagation in 316 stainless steel at both 500 and 800°C led to a lower crack-growth rate. Transition to higher crack growth rates, as PO_2 increased, was also observed, among others, by Smith and Michel [92] in their work on a Co-base alloy at 427°C, by Stegmann and Shahinian [93] on nickel alloy at 500°C and by Smith and Shahinian [94] on Silver at 20, 150 and 350°C. This transition was interpreted by Achter [95] in terms of the impingement rate of oxygen molecules on successive rows of freshly exposed metal atoms at the crack tip. As discussed by Ericsson [96], the geometry of the impingement concepts has, in general, been described in vague terms facing the difficulty of providing an explanation for the severity of damage that a monolayer of oxide could cause at the crack tip. These concepts, furthermore, cannot support the experimental observations made, for example, by Smith and Shahinain [94]. They reported that the effect of oxygen partial pressure on fatigue life of Silver at 350°C is small compared to the effect of that at 20°C and 150°C. An increase in the initial rate of oxygen adsorption has, however, been observed with increased temperature at the range of 20°C to 350°C.

Another interpretation of the influence of PO_2 on crack growth, is related to the ability of oxygen at different pressures to control the preferential formation of certain oxides that may shield or contribute to the crack tip damage through the passivation or the enhancement of the oxidation process, respectively. It is known that oxidation of some elements, e.g. chromium, can produce protective oxide layers, and chromia (Cr_2O_3) is such oxide. While oxides of less noble elements, e.g. the iron and nickel oxides and their spinel type oxides, are less protective [87]. If chromium diffusion in the alloy is too low to sustain the supply of chromium at the scale/metal interface, less noble elements of the alloy will be oxidized at the scale/metal interface. This will result in an increased reaction rate [95]. In this regard, Andrieu [50] has experimentally examined the influences of PO_2 on the formation of selective oxides. In his work, small discs, with a thickness of 3 mm and diameter of 20 mm, were machined from Alloy 718 with an average grain size of 150 μm. These electro- and mechanically polished discs were subjected to different PO_2 levels ranging from 3×10^{-1} to 10^{-5} torr for periods of 480 seconds at 650°C using a high-vacuum devise equipped with a mass spectrometer. An Auger spectrometry analysis was subsequently used to identify the oxide type formed on the free surfaces of these discs as a function of the operating PO_2 level. Sputter profiles of the formed oxides are summarized in Fig. 3.1. It is interesting to observe that oxygen partial pressure as high as 10^{-4} torr promotes selective oxidation of chromium and that, under the pressure from 10^{-1} to 10^{-2} torr, the first oxides to appear are nickel and iron oxides. The relationship between time required to form the chromium oxide as a function of oxygen partial pressure is schematically shown in Fig. 3.2; at atmospheric pressure this

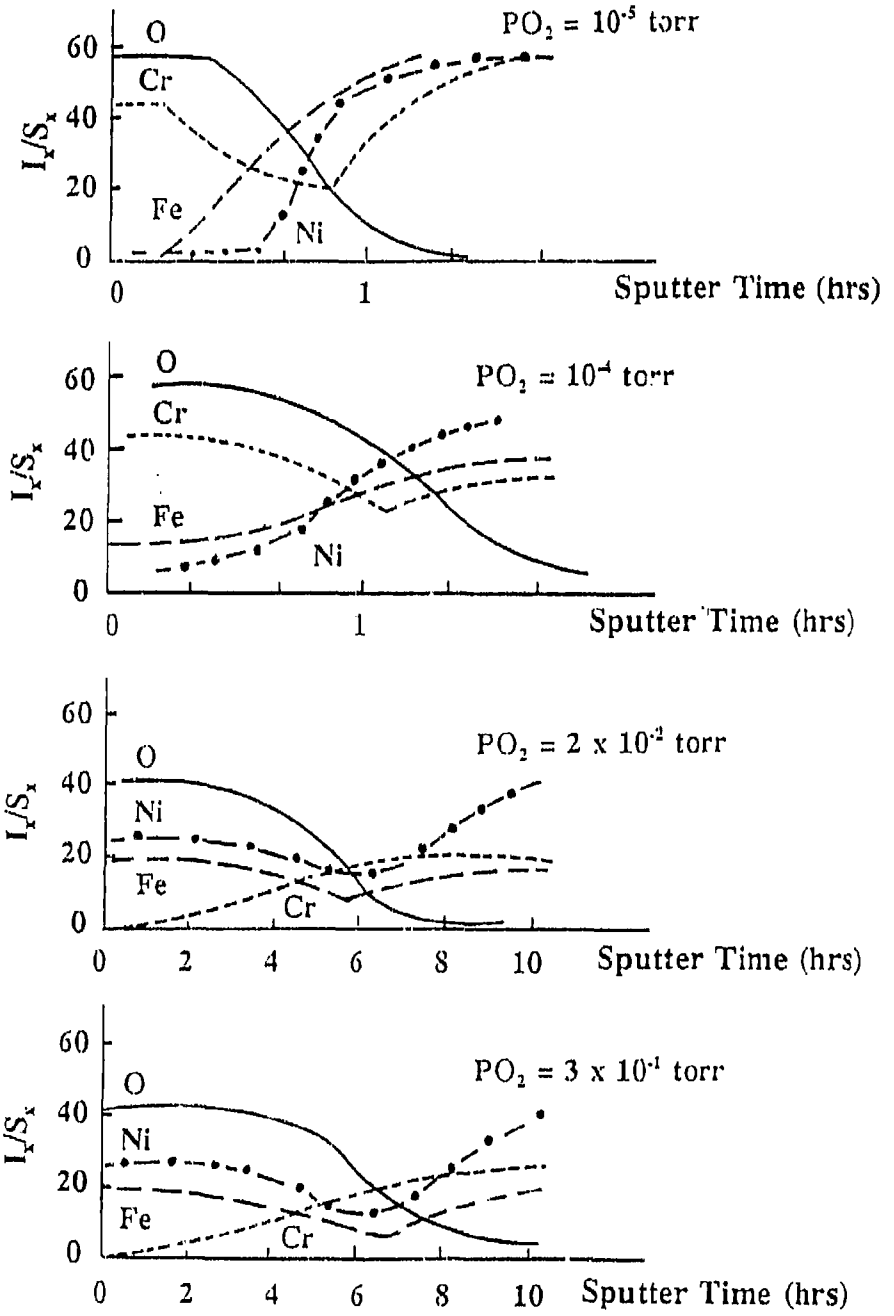

Fig. 3.1 Sputter-depth profiles of the surface oxides (oxidation time 8 min, temperature 650°C).

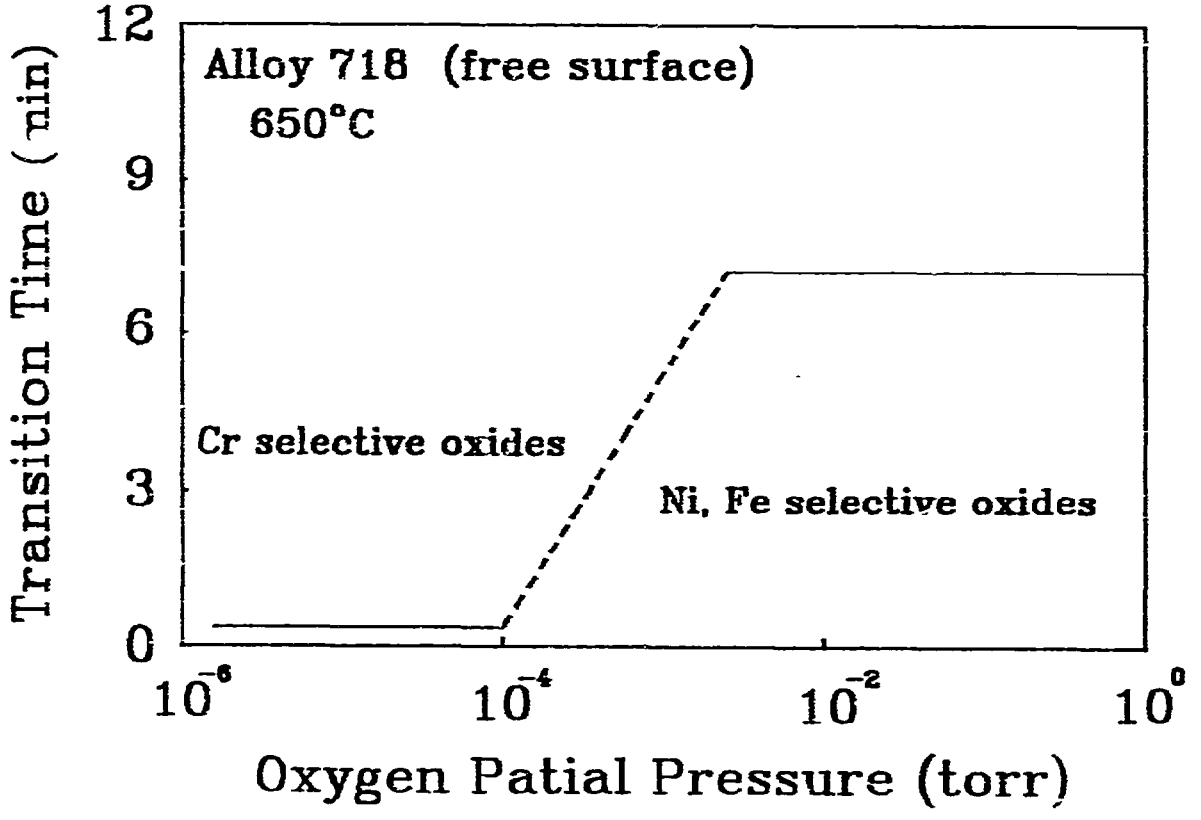

Fig. 3.2 Types of oxides as a function of transition time t_p and oxygen partial pressure.

passivation time is estimated to be in the range of 5-8 minutes. Throughout this study it was difficult to distinguish whether the surface being analysis was of a matrix or of a gain-boundary interface. Transmission Electron Microscopy work was, therefore, carried out on a foil made of the same material in which grain boundary was identified. This foil was subjected to a temperature of 650°C for 240 seconds in room environment. Results of this TEM work are shown in Fig. 3.3. They indicated that, under atmospheric pressure, microcrystallized oxides of nickel and iron developed rapidly along grain boundaries.

Furthermore, attempts have been made to identify the role of PO_2 in determining the cracking mode. This was achieved by carrying out a series of slow strain-rate, tensile tests on axisymmetrically precracked fatigue round bars made of the same alloy. These tests were performed at 650°C in an ultra high vacuum apparatus detailed in Ref. [50]. Using a mapping technique employed on the resulted fracture surfaces, examples of which are shown in Fig. 3.4, the percentage of transgranular fracture area, with respect to the total fracture surface area, was measured. These percentages in terms of oxygen partial pressure are reported in Fig. 3.5. They indicate that the intergranular fracture ratio increases at the PO_2 increases and under atmospheric pressure, 60% of the fracture surface of the test specimens was found to be intergranular. Also, a transition exists between 10^{-2} and 1 torr, below which the failure mode is fully transgranular. This range of transitional pressure is consistent with observations made on different alloys [92-94].

These results, when linked to those in Fig. 3.1 showing the influence of PO_2 in determining the type and sequence of selective oxides, could provide a qualitative view

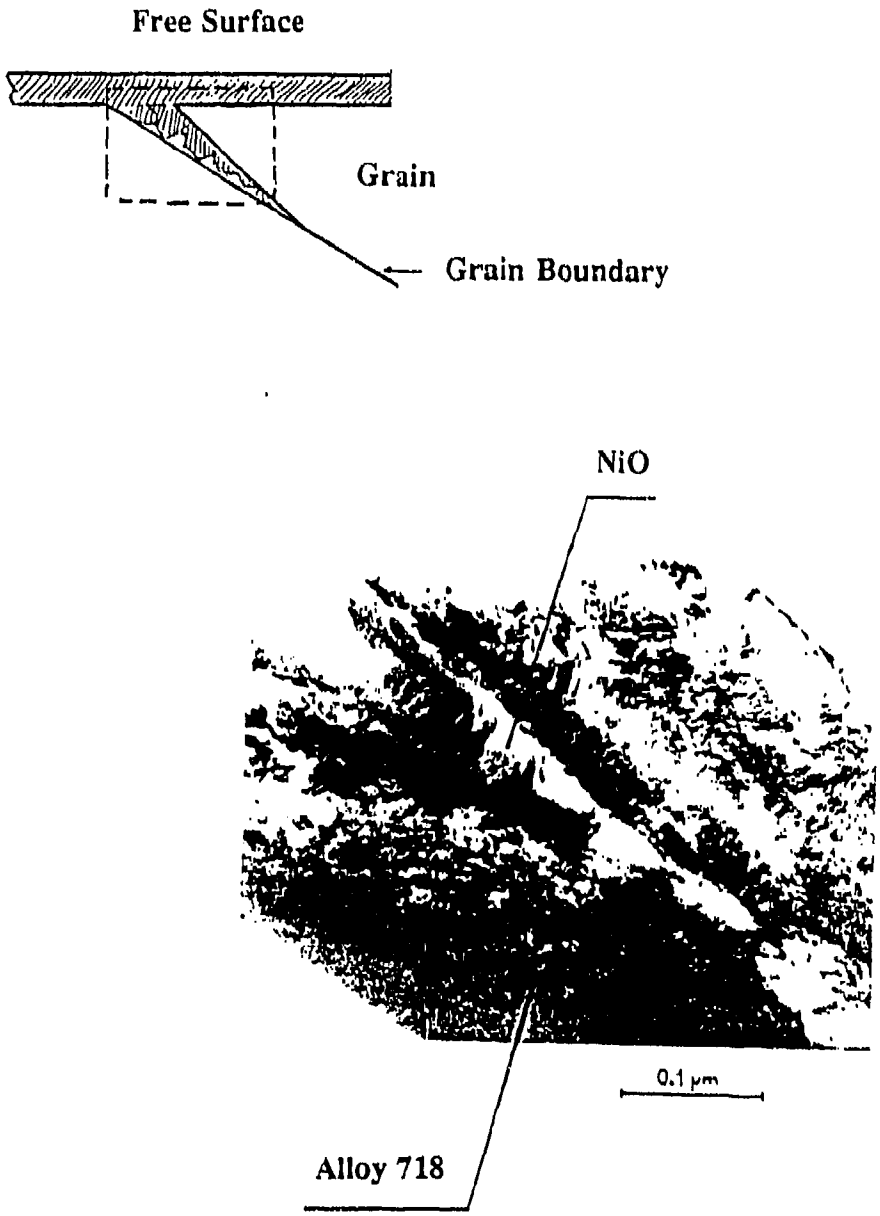

Fig. 3.3 Static oxidation of a grain boundary at 650°C (exposure time 4 min).

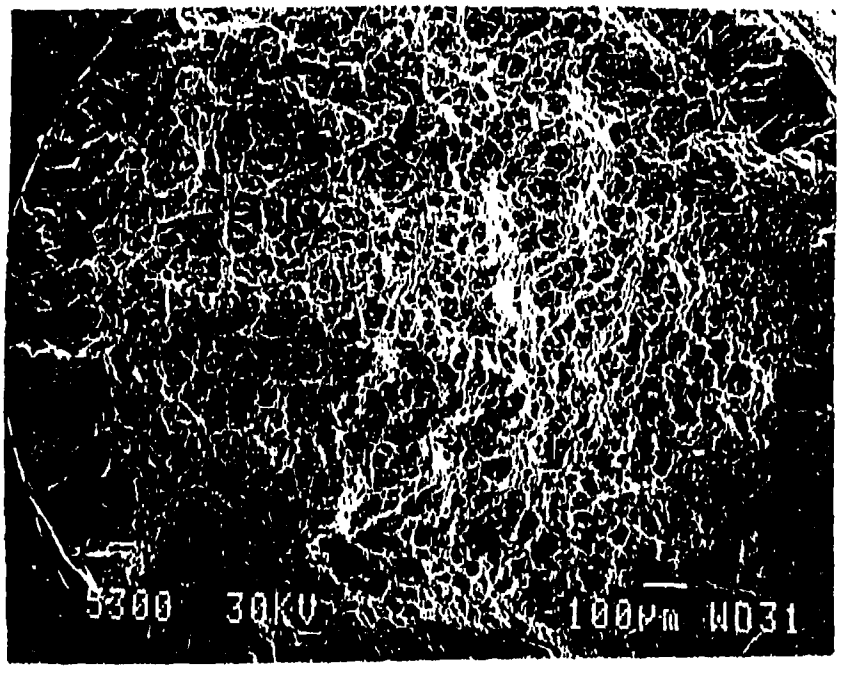

(a)

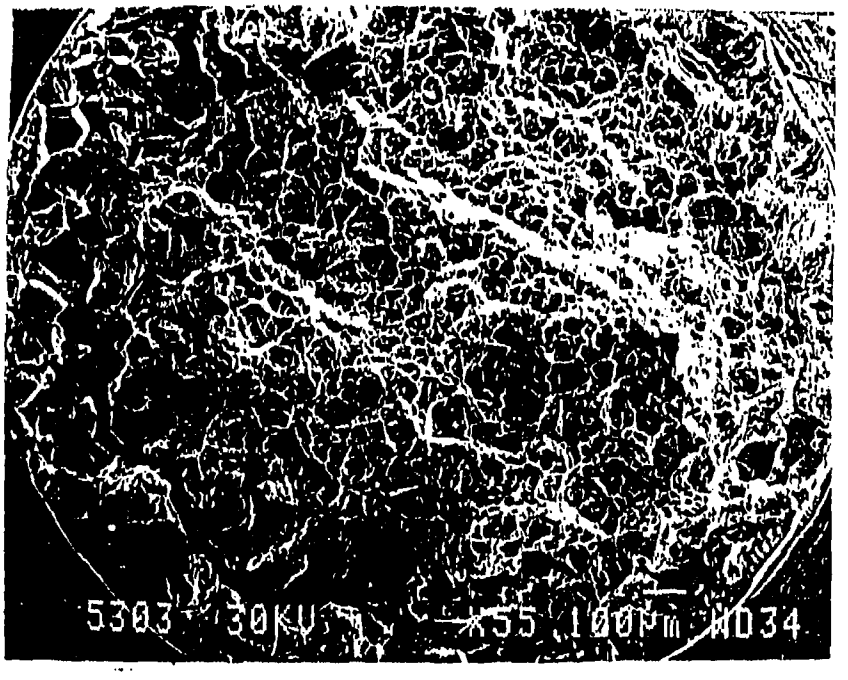

(b)

Fig. 3.4a Fracture surfaces corresponding to different oxygen partial pressures (a) 10^{-4} torr and (b) 1 torr.

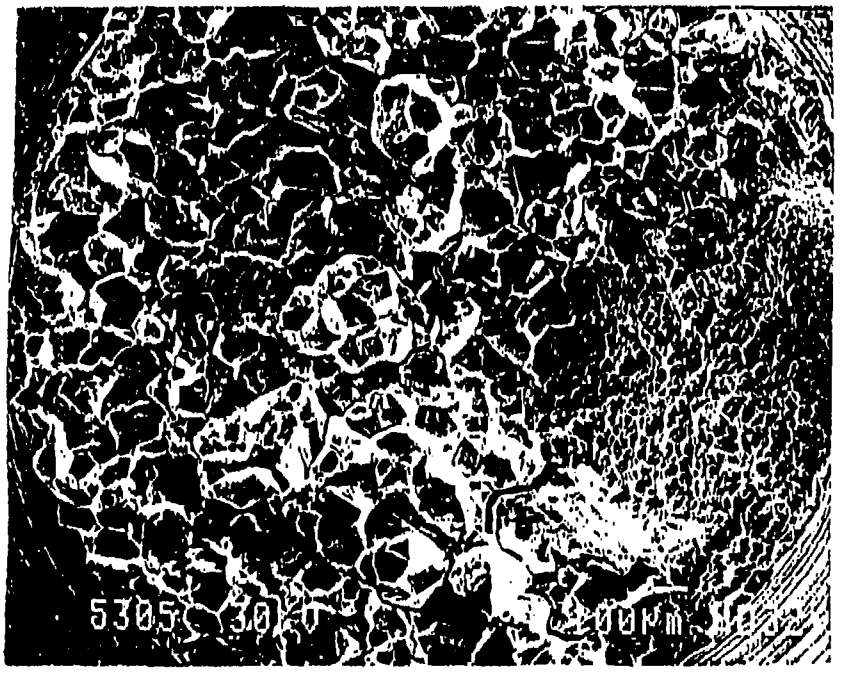

Fig. 3.4b Fracture surface corresponding to the oxygen partial pressure of 4 torr.

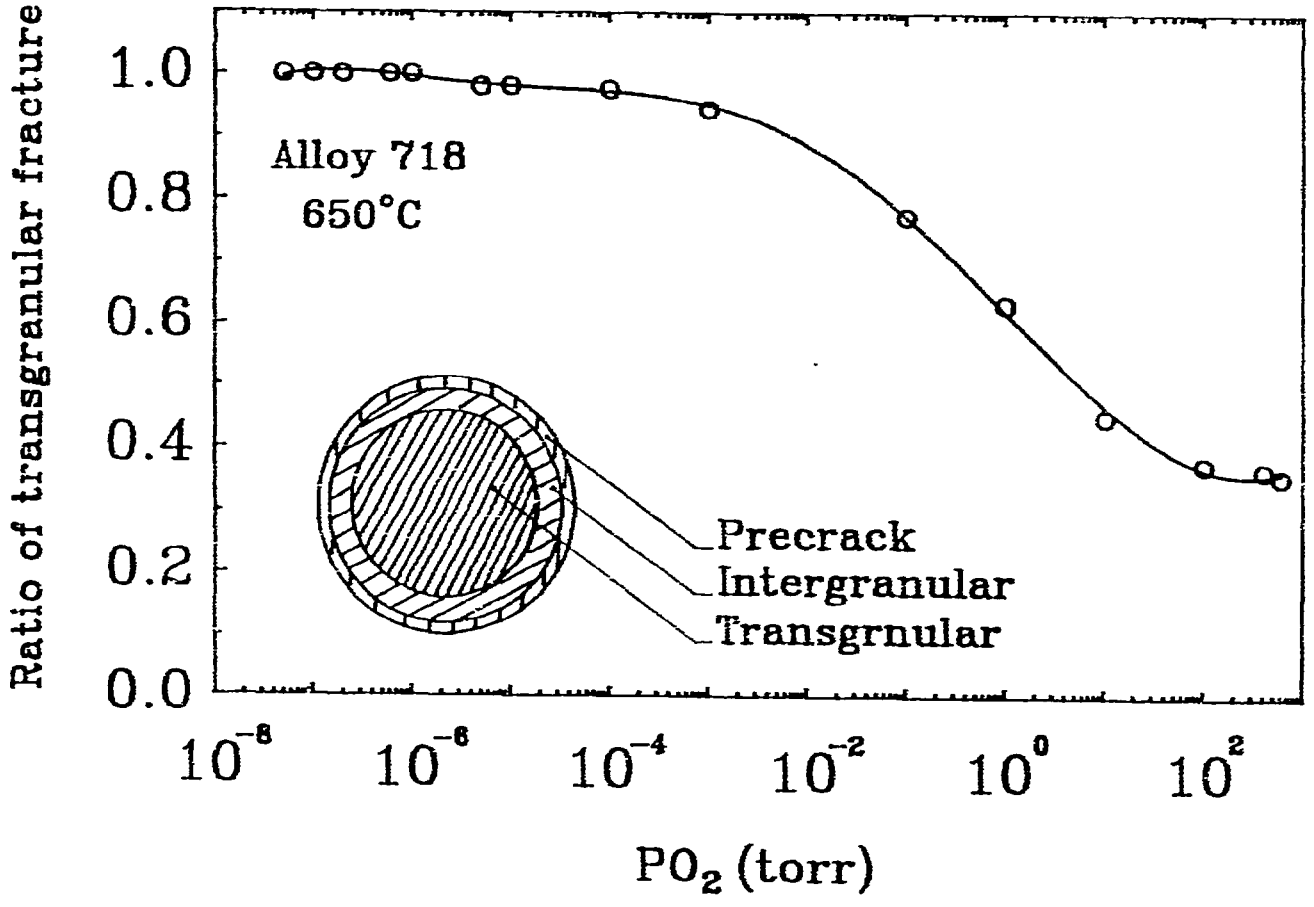

Fig. 3.5 Ratio of transgranular fracture versus oxygen partial pressure.

of the crack-tip oxidation along a preferred grain boundary path. This view suggests that oxidation occurs in two stages, schematically depicted in Fig. 3.6. The first stage, influenced by atmospheric level of oxygen partial pressure, would result in the formation of FeO and NiO and their spinels. For these oxides which are permeable to oxygen, the gas diffusion through the pores plays an important role in determining the reaction rate as a function of time. The build-up of these oxide products would result in, at the oxide/metal interface, lowering the oxygen partial pressure. This, consistent with the Ellingham/Richardson diagram, would provide the reaction kinetics required for the formation of a dense Cr_2O_3 oxide sub-layer. This dense layer is considered protective in the sense that it limits oxygen diffusion to the grain boundary material and thus decreases the metal/oxygen reaction rate [25]. The complete formation of this layer along the crack front is regarded as an attainment of oxide depth saturation. The time required to reach this stage is identified as the transition time, t_p, which is a function of temperature, PO_2 and localized stress ad strain fields. When this time is reached, an assumption is made that the condition for oxygen passivation is met and no further oxygen penetration can take place along the effected grain boundary paths. One should observe that the passivation effect is not assumed here to be a discrete process, it is a continuous gradual decrease in the oxide depth formation rate as the ratio of the Cr_2O_3 to the total oxide weight increases.

3.3 Experimental Verification

This two stage crack-tip oxidation mechanism was verified by Andrieu et al [82].

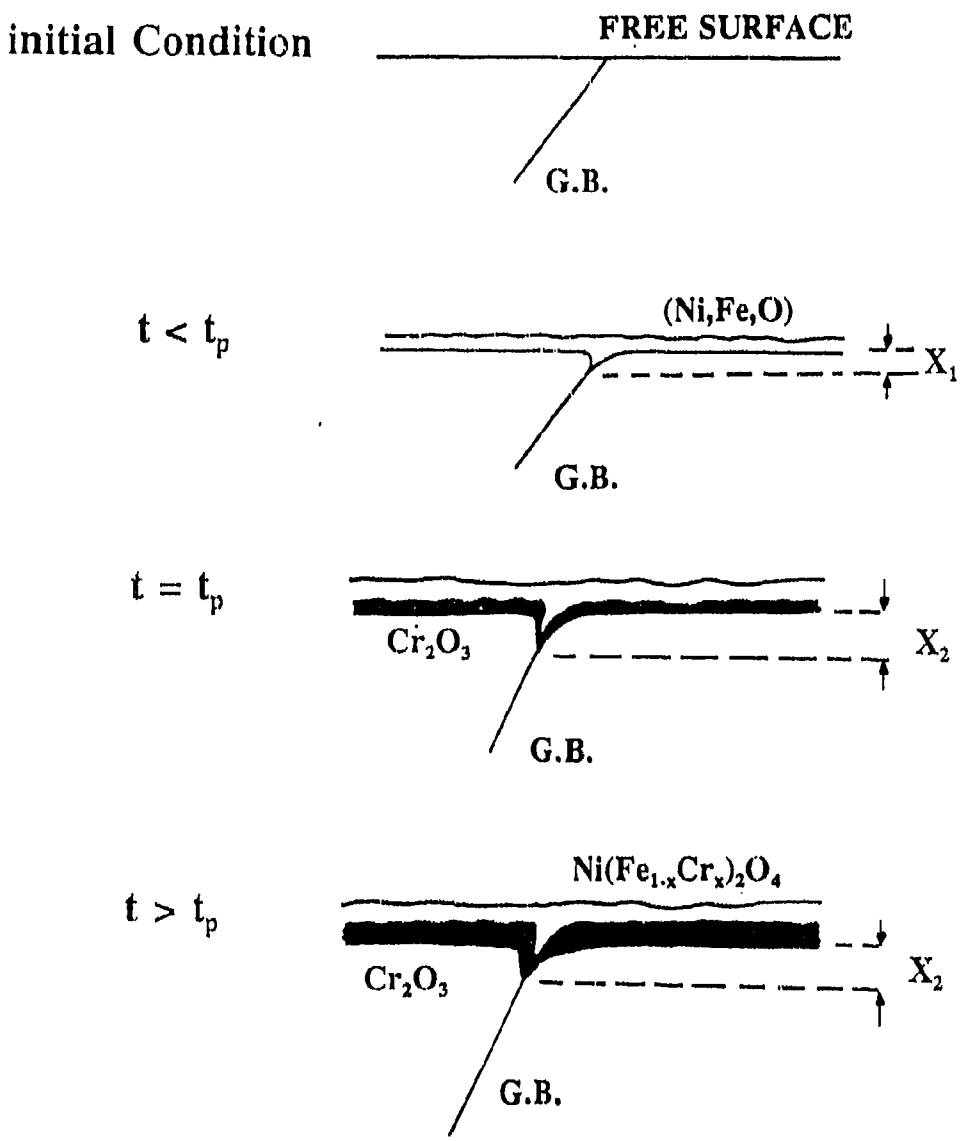

Fig. 3.6 Suggested mechanism of grain boundary oxidation.

In their work, two sets of high temperature fatigue crack growth tests were carried out. These experiments utilized compact tension type specimens made of Alloy 718 with grain size of about 20-50μm. The objective of the first set of experiments was to investigate the influence of crack-tip oxidation during a time duration equal to transition time, t_p, on the subsequent fatigue crack growth rate. This was accomplished by comparing the crack growth rate of continuous cycling (labeled case A) with that of cycling imposed a hold time at minimum load level (labeled case B). The duration of this hold time was selected to be 600 seconds which is in the order of the transition time, t_p, of this alloy [25,49]. In order to insure intergranular fracture mode, the frequency used in the study was 0.05 Hz which is below the transitional frequency of this material. Results of these tests are shown in Fig. 3.7. They show a distinct increase in the crack growth rate as a result of imposing a hold time at minimum load during which crack-tip oxidation is assumed to be the only active process. These results could be explained on the basis that the hold time has permitted uninterruped metal/oxygen reaction leading to the formation of the protective chromia layer. Upon applying a loading cycle with a frequency that induces intergranular cracking, the depth of ruptured oxides along the intergranular fracture path would represent an additional jump of the crack tip. Furthermore, the type of oxides formed on the fracture surface of the air tested specimen was identified by analytical transmission electron microscopy on a thin foil of a fracture surface edge. Fig. 3.8 indicates the existence of two oxide layers - the inner layer (A) at the metal/oxide interface is identified as a Cr_2O_3 while the outer layer (B) has been identified as a spinel oxide $Ni(Fe\ Cr)_2O_4$ in the same order as suggested in the proposed model.

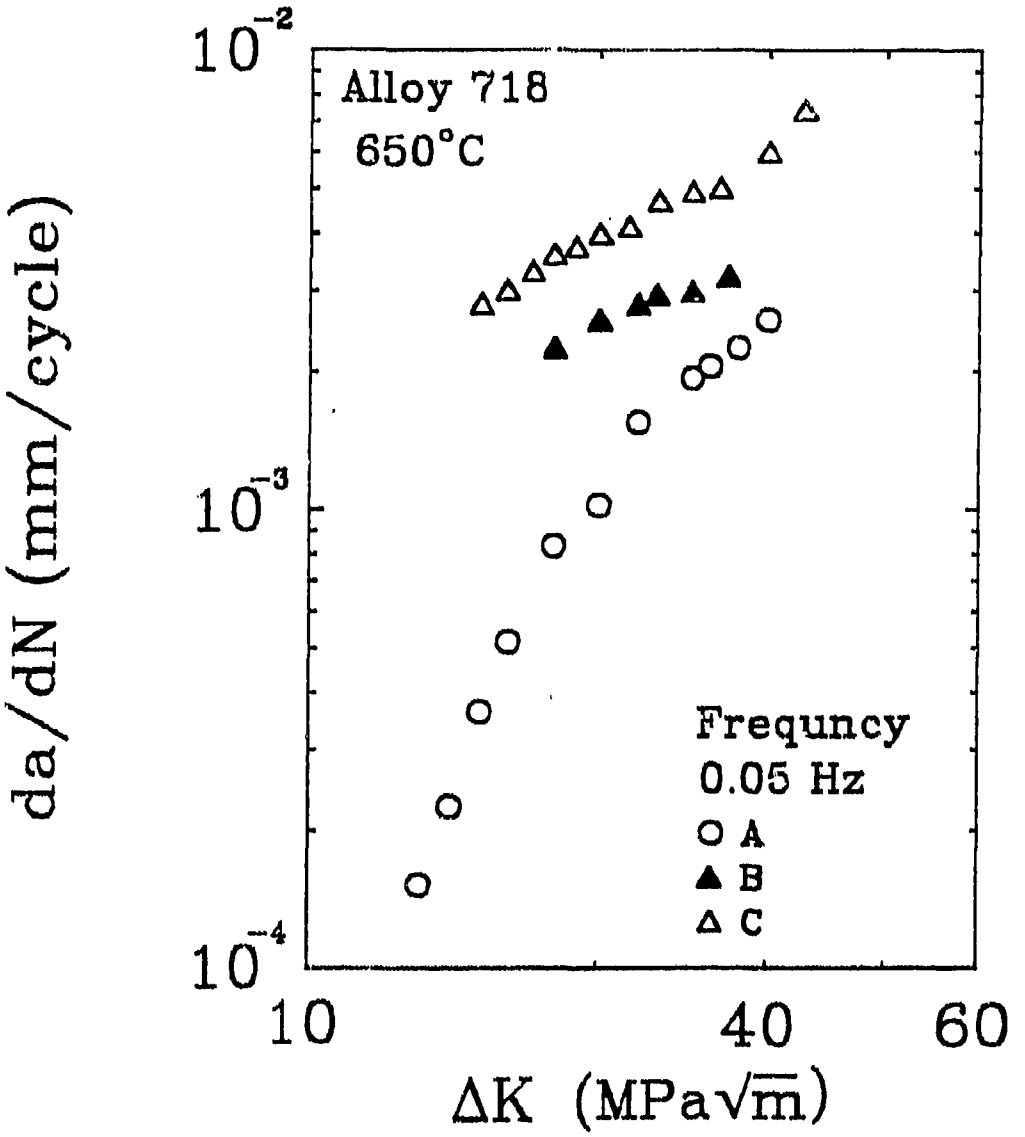

Fig. 3.7 Effect of hold-time at minimum load as well as effect of minor cycle superimposed on hold-time at minimum on crack growth rate.

Fig. 3.8 TEM observation and microanalysis of oxides types developed on fracture surface.

Ghonem et al pointed out that the depth of oxide layer under the hold time tests condition would correspond to a saturated depth since the hold time is of the order of the transition time. However, if a high frequency minor cycle is imposed on the hold time period in case B, then the metal/oxygen reaction processes will be disturbed by continuously rupturing the rapid formation of nickel and iron oxides. This would continuously alter the oxygen partial pressure on the metal/oxides interface, consequently, the oxygen/metal reaction rate will keep high which, in turn, prolongs the duration of the transition time, t_p, and delays the formation of protective chromia layer. As a result, the oxide depth along the intergranular path will be deeper. This idea was examined experimentally by repeating case B with a high frequency (1 Hz) minor cycle imposed on the hold time duration (illustrated in Fig. 3.9), labeled case C, and the corresponding results in terms of da/dN versus ΔK are shown also in Fig. 3.7. These results, which clearly indicate an increase in the crack growth rate when compared with those results of tests A and B, are seen here as an indirect support of the two stage crack-tip oxidation concept.

The two stage crack-tip oxidation concept was then applied in the present study to develop a quantitative model to predict the high temperature fatigue crack growth rate for Alloy 718, this will be the subject of Chapter 4.

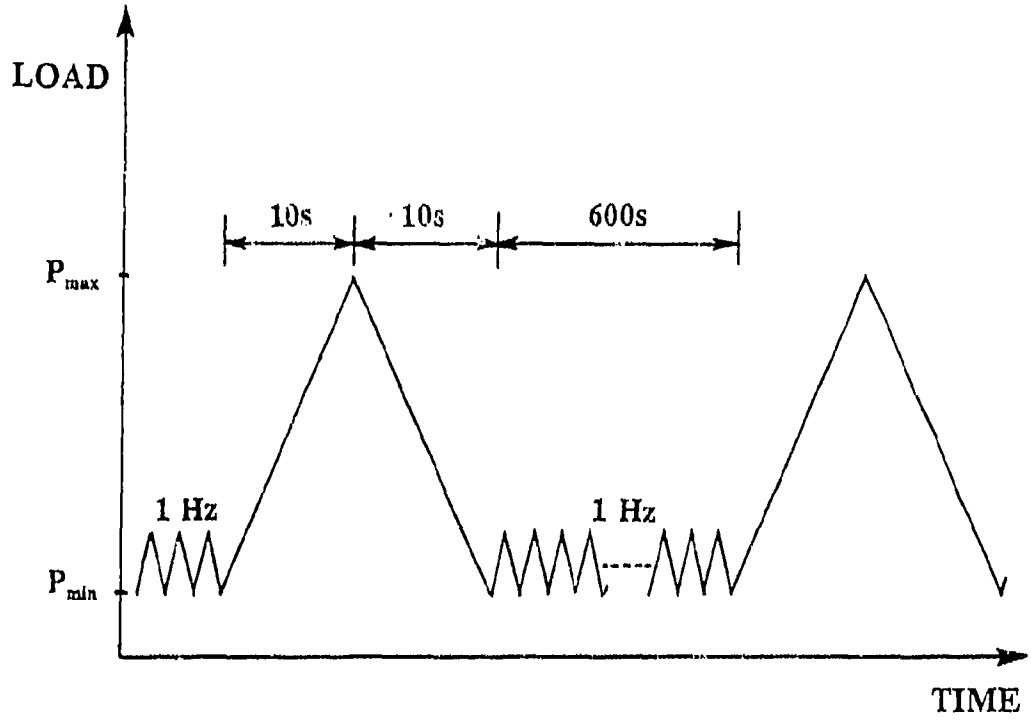

Fig. 3.9 Load spectrum including a minor cycle with high frequency imposed on hold time at minimum load level.

CHAPTER 4

MATHEMATICAL MODELLING OF INTERGRANULAR FATIGUE CRACK GROWTH BEHAVIOR AT 650°C

In this chapter, a mathematical model employing the basic concepts of the two-stage crack-tip oxidation mechanism will be developed. As a first step towards this objective, an attempt will be made in the following section to review the existing fatigue-oxidation crack growth models.

4.1 Review of Existing Fatigue-Oxidation Crack Growth Models

As mentioned in the previous chapter, one of the objective of understanding the crack tip oxidation mechanism, particular in the high temperature alloys, is to provide basis for the development of quantitative models that predict crack growth for these alloys under different temperatures and loading conditions. As a result, a wide spectrum of prediction models have been developed for different materials based on different views of the fatigue-oxidation interaction process. One of the earlier models to quantitatively describe the high temperature fatigue crack growth behavior is that proposed by Haigh et al [98]. Their model can be written as:

$$\frac{da}{dN} = C(f)\Delta K^{n} \qquad (4.1)$$

where n is a constant and C(f) is a frequency dependent term which reflects the time

dependency or the oxidation effects. This Paris type model was applied to Cr-Mo-V steel in both air and vacuum at 550°C but was not extended to other materials or different ranges of temperature.

Liu and McGowan [77] made the assumption that within the environmental effect region, the fatigue crack growth rate is controlled by the rate of the transport of detrimental chemical species. They correlated the fatigue crack growth rate with the Arrhenius relation in the following form:

$$\frac{da}{dN} = B\left(\frac{f_0}{f}\right)^m \exp\left(-\frac{Q}{R}\left(\frac{1}{T}-\frac{1}{T_0}\right)\right)\Delta K^n \qquad (4.2)$$

where f_0 and T_0 are frequency and temperature at a reference state, respectively, B, m and n are constants, Q is the activation energy and R is the gas constant. The data of IN100 and 304 stainless steel supported the analysis based on this empirical model, the data of Waspalloy was not, however, sufficient to draw any conclusion.

Several other models [58,60,61,66] have built their argument on the assumption that the high temperature fatigue crack growth per cycle in air environment can be expressed as a linear summation of the following damage components:

$$\frac{da}{dN} = \left(\frac{da}{dN}\right)_{vac} + \left(\frac{da}{dN}\right)_{ox} \qquad (4.3)$$

where the first term represents the pure time-independent mechanical damage, while the second term represents the oxidation influences on the crack growth behavior. In Skelton and Bucklow's work on Cr-Mo-V steel at 550°C [58] the oxidation term was written as:

$$\left(\frac{da}{dN}\right)_{ox} = K\frac{\alpha\Delta\varepsilon_t^3}{PBR} \tag{4.4}$$

where α is a constant, $\Delta\varepsilon$ is the total strain range and K is a magnification factor which depends on the strain range, Pilling-Bedworth Ratio (PBR) and current crack length. If oxygen penetration becomes more significant, Marshall [61] suggested that the above equation can be replaced by

$$\left(\frac{da}{dN}\right)_{ox} = 2\sqrt{Dt} \tag{4.5}$$

where D is the fatigue-enhanced diffusion coefficient and t is the cycle period.

To account for oxidation damage, Strangeman [60] introduced the term "metal recession rate by oxidation per cycle" MRR which only be calculated from experimental data. Again, based on the linear summation damage concept, his equation is written as:

$$\frac{da}{dN} = A(\Delta K_\varepsilon)^B + MRR \tag{4.6}$$

where A and B are material constants and ΔK_ε is the strain intensity factor range. The dependency of the model on the term ΔK_ε limits its application to the condition of very low-strain-intensity factor values at which the crack tip strains are insufficient to fracture the oxide scale, a condition which is incompatible with the strain state in gas turbine components, for example.

Remy [66,99] also applied the linear summation rule to model the fatigue-oxidation interaction process, but more sophisticated metallurgical method was used in his work to evaluated the oxidation damage. He represented the "pure" fatigue damage

based on the work of Tomkin [100], while the oxidation effects was derived from his metallurgical observations on partly fatigue specimens, i.e.

$$\left(\frac{da}{dN}\right)_{ox} = (1-f_c)\alpha_m(1+K_m\Delta\varepsilon_p)\Delta t\sqrt{2} + f_c\alpha_c g(\Delta\varepsilon_p)\Delta t^{\frac{1}{4}} \qquad (4.7)$$

where f_c is the effective volume of carbides on the crack path, K_m is a constant, Δt is the cycle period, $g(\Delta\varepsilon_p)$ is a function of plastic strain range, $\Delta\varepsilon_p$, α_m and α_c are the oxidation constants of the matrix and the carbides under zero stress, respectively. This equation was applied successfully to model the behavior of MAR M509 under various temperature and loading conditions.

Based on the concept of decohesive strength of grain boundary, Ramanoski et al [79] postulated a fatigue crack growth model which depends on the effective stress range $\Delta\sigma_{eff}$:

$$\frac{da}{dN} = A\Delta\sigma_{eff}^{m} \qquad (4.8)$$

where A and m are constants. If expressing the effective stress range in a form which incorporates a threshold stress for microcrack extension σ_T, the above equation can then be written as:

$$\frac{da}{dN} = A(\sigma_{max} - \sigma_T) \qquad (4.9)$$

This model represents a balance between the mechanical driving force and the resistance of the material to this force. The relationship between the cohesive strength of the grain boundary and environmental factors was not, however, considered. In addition, while the

oxidation process is time dependent, neither time nor test frequency is apparent in eq.(4.9).

Attempts also have been made to model hold time effects, during which the influence of oxidation and/or creep might be activated [101-104]. Utah [103] developed the MSE model which is based on the following equation:

$$\frac{da}{dN} = \exp(B)\left(\log\left(\frac{\Delta K}{\Delta K_o}\right)\right)^P\left(\log\left(\frac{\Delta K_e}{\Delta K}\right)\right)^D \qquad (4.10)$$

where ΔK is the stress intensity factor range, ΔK_o and ΔK_e represent the threshold and the maximum values of ΔK, respectively, B, P and D are constants for a given set of experimental conditions. Annis et al [104] have also proposed a SINH model as follows

$$\log\left(\frac{da}{dN}\right) = C_1 \mathrm{Sinh}(C_2(\log\Delta K + C_3)) + C_4 \qquad (4.11)$$

where C_1, C_2, C_3 and C_4 are constants which can be expressed as functions of frequency, temperature, hold time and stress ratio. Predictions of both MSE model and SINH model were made of the fatigue crack growth rate in alloy AF115 over a temperature range from 538°C to 760°C, stress ratios from 0.1 to 0.9, frequencies from 0.0025 Hz to 2.5 Hz, and hold times up to 5 minutes. In general, these two models could represent the data set, from which the constants of the model are derived, reasonably well. Here one should realized that while both MSE model and SINH model are, in principle, regression models and are not based on any physical mechanisms, they are useful for fitting to a particular data set.

Based on the linear summation rule, Nicholas et al [69] have developed an

empirical relationship for complex wave shapes as follows

$$\frac{da}{dN} = f(K,R)\left\{C_1 + C_2(T)\nu_L^{-\gamma(T)} + C_3(T)\left[\int_{\tau_L} \dot{a}dt + \beta \int_{\tau_u} \dot{a}dt\right]\right\} \qquad (4.12)$$

where C_1 is a constant, ν_L and ν_u are frequencies of loading portion and unloading portion, respectively, $\tau_L = 1/(2\nu_L)$ and $\tau_u = 1/(2\nu_u)+\tau_h$, where τ_h is the hold time. The first term of the model represents the purely cycle dependent behavior and is obtainable from low temperature and/or high frequency test. The second term represents the pure cycle dependency. The last two terms represent the time dependent behavior, the integral over the loading portion of the cycle τ_L is always considered, but existence of the integral over the unloading and/or sustained load portion of the cycle τ_u is dependent on β which varies from zero to unity. There is no method for determining the functional variation of β at this stage.

From the above review, it is clear that these models could generally be classified into two main groups. The first one is a phenomenological approach obtained by a regression analysis procedure and carried out on a set (or sets) of experimental data or by modifying the Paris-type law to include parameters such as frequency and temperature to account for the time dependency nature of the high-temperature crack growth process [69,98,103,104]. These models are generally simple in formulation and contain a limited number of constants that are not difficult to determine. However, the absence of physical interpretation of their basic equations makes it difficult to extend their applications to materials or loading conditions different than those used to generate the model. The second approach is based on physical interpretation of metallurgical and mechanical

observations of a specific crack growth mechanism [58,60,66,77,79,99]. These models, while complex, provide good predictions for the same material under all conditions that generate an identical cracking mechanism. Different observations and formulations will, however, be required for a different fracture mechanism.

A general conclusion that could be reached after reviewing all these models is that not one oxidation-assisted crack growth model can be viewed as valid for all materials under different loading conditions. The validity of a particular model must be assessed in relation to a specific material, temperature and cracking mechanism. According to this conclusion, the work described in this chapter was undertaken to quantitatively model the intergranular oxidation enhanced fatigue crack growth process in Alloy 718 at 650°C based on the understanding of the mechanism of intergranular oxidation and the related aspects described in Chapters 2 and 3.

4.2 Model Concept

The concept of the proposed model can be described as follows. At the start of the oxidation process, which is taking place along a preferred grain boundary path in front of the crack tip, a layer of selective oxides will replace the affected grain boundary material. The depth of the oxide layer depends on the degree of oxygen diffusion along the grain boundary. The survival of this layer, as a load-bearing material, is determined from the balance established between the mechanical driving force at the crack tip and the resistance of the layer to this force. This notion is represented in Fig. 4-1 in which the grain boundary material which a ductility, ε_{do}, measured in a high temperature

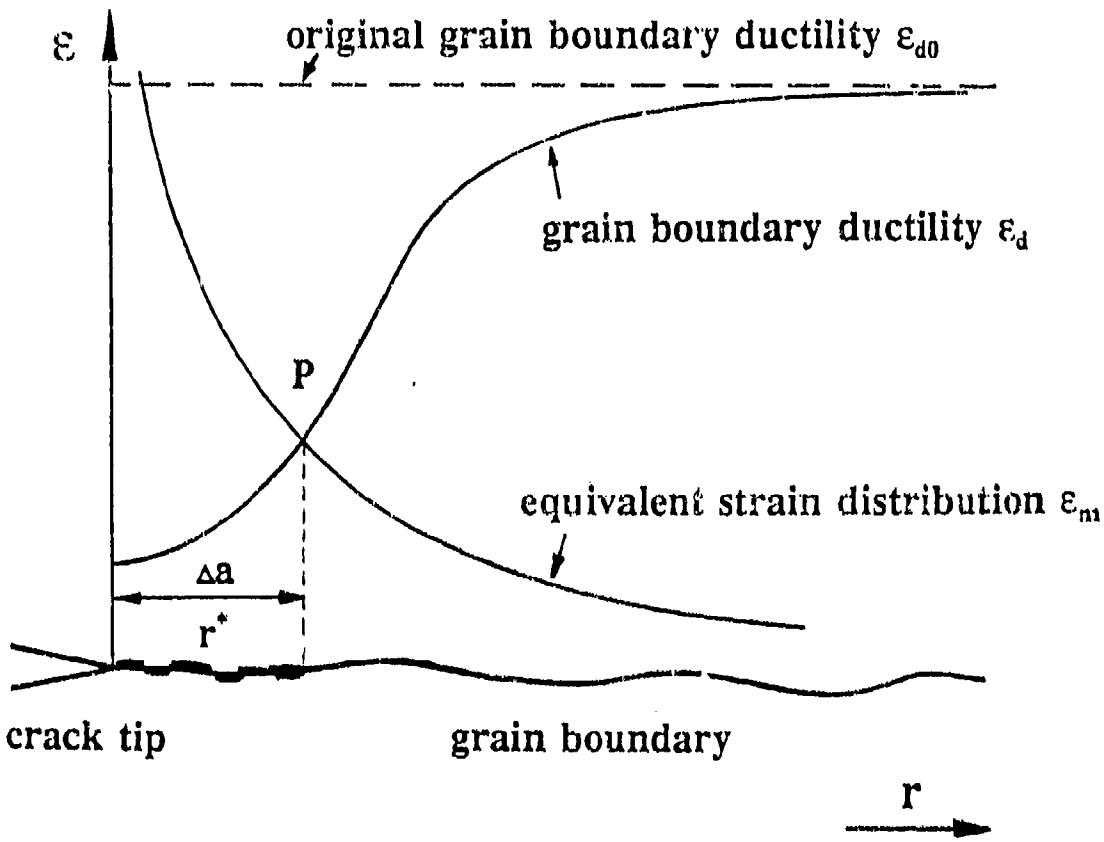

Fig. 4.1 Schematic of the proposed model concept.

vacuum environment, is replaced by material with a variable degree of oxidation and consequent variable amplitude of ductility, ε_d. The distribution of ε_d is influenced by the fact that the closer the grain boundary material is to the crack tip, the higher the degree of oxidation and the higher the degree in reduction of ε_{do}. The changes in ε_d will reach its saturation level when the oxidation time equals or exceeds the transition time, t_p, required to achieve passivation, i.e., time required to complete the formation of Cr_2O_3 layer. Acting in the same zone near the crack tip is the strain distribution, ε_m, produced by the externally applied load. One assumption made here is that the material dealt with here will have elastic-viscoplastic behavior and the imposed loading conditions will only result in small-scale yielding.

The magnitudes of these two competing parameters, ε_d and ε_m, will determine the length of crack tip advancement along the affected grain boundary path. The crack growth rate could therefore be calculated by determining the value of r per cycle where r is the distance measured from the crack tip which corresponds to position P in Fig. 4.1, i.e., when $\varepsilon_m \geq \varepsilon_d$. The present model thus depends on determining the evolution of both the ε_m and ε_d distribution on a cycle-by-cycle basis. Steps to determine these distribution are the subject of the following section.

4.3 Mathematical Derivations

At high temperature and in an air environment, the oxidation of an alloy occurs, in general, through the formation of multiple oxides. For Alloy 718, the possible formation of major oxides and their corresponding spinels are Cr_2O_3, FeO, NiO, $FeCr_2O_4$

and $NiCr_2O_4$. At the beginning of the oxidation process the yield of Cr_2O_3, which is the only protective layer in these various oxides, is small and thus the oxidation effect, in terms of the depth of oxygen penetration and the degree of grain boundary embrittlement, is relatively large. As the oxidation time, t_{ox}, increases, the weight of Cr_2O_3 in relation to the total weight of oxides, increases. When t_{ox} equals t_p the formation of Cr_2O_3 is completed and the condition of passivation is reached. This indicates that no further oxidation can take place and a saturation in the grain boundary ductility level of the oxidized zone has been established. One could thus correlate the amount of Cr_2O_3 the grain boundary ductility by introducing a oxidation parameter, β, which is defined as the ratio between the weight of Cr_2O_3 and the total weight of oxides, i.e.

$$\beta = \frac{m_{Cr_2O_3}}{m_{ox}} \tag{4.13}$$

For Alloy 718 eq. (4.13) was found to take the form (see Appendix III):

$$\beta = \frac{C_1(\gamma)m_{Cr}}{C_2(\gamma)m_{O_2} - C_3(\gamma)m_{Cr}} \tag{4.14}$$

where C_1, C_2, and C_3 are functions of the parameter γ, m_{O2} and m_{Cr} are the amount of oxygen and chromium diffusion along the grain boundary and the dislocation network, respectively. The parameter γ is defined as m_{Fe}/m_{Ni}, where m_{Fe} is the amount of iron required to form FeO, in the grain boundary, and m_{Ni} is the amount of nickel required to form NiO, in the grain boundary. The ratio γ can be experimentally determined by using different experimental techniques.

From the result obtained in Chapter 2, it is clear that the effective oxidation time per cycle can be expressed as:

$$t^* = t_h + \frac{<f_c - f>}{f|f_c - f|} \qquad (4.15)$$

where t_h is the hold time component of the cycle, f is the loading frequency, f_c is the transgranular/intergranular transition frequency and <•> is the MaCauley bracket. If the loading frequency is above the transition frequency, the crack advances along a transgranular path and no oxidation effect will be considered, in this case <•> = 0. The term f_c is temperature and grain size dependent [19,22].

A link could now be established between the oxidation parameter β and the grain boundary ductility. In the early stages of the oxidation process where β is small, a faster degree of reduction in ε_{do} is expected; as β increases the reduction in ε_d should decrease. Upon reaching t_p, β reaches β^* and assumes a saturated value. The relationship between β and ε_d, can be written as:

$$\varepsilon_d = a_1 \operatorname{arctg}(-a_2\beta^2 + a_3) + a_4 \qquad (4.16)$$

where a_1 to a_4 are material, temperature and loading condition dependent.

Turning ones attention to the oxygen diffusion along the grain boundary, one could view it as a short-circuit diffusion process. This process, generally, embraces diffusion of metal or oxygen through extended defects in the oxide scale rather than through the bulk crystal lattice [106]. Most mathematical treatments represent the short-circuit path as an isotropic slab of material with a width of 2δ in which diffusion occurs according

to Fick's law. In this treatment the concentration variation across the slab is neglected and the diffusivity is assumed to be much longer than the diffusion in the surrounding matrix [107-109]. In following this approach the concentration of diffusion species along a grain boundary path as a function of position (x,y) and time t, can be obtained using Whipple's solution [110].

Peterson and Martin [108,111,112] have examined Whipple's solution and pointed out that whilst it is relatively more accurate than other solutions, such as that of Fisher [106], it suffers from certain limitations. For example, it is not appropriate for "wide" grain boundaries since the concentration across the width way may not be uniform. Furthennore it can only be applied to diffusion problems within the Harrison's type B regime [112]. In this paper, the concentration across a grain boundary path in Alloy 718 is considered constant and the matrix diffusion distance is much smaller than that of the grain boundary; Whipple's solution will then be assumed appropriate for our applications. The amount of oxygen diffused along the affected grain boundary within one loading cycle can thus be obtained in the form

$$m_{o_2}(r,0,t^*) = \hat{m}_{o_2}\left\{\operatorname{erfc}\frac{\eta_1}{2} + \frac{\eta_1}{2\sqrt{\pi}}\int_1^{\Delta_1}\frac{du}{u\sqrt{u}}\exp\left(-\frac{\eta_1^2}{4u}\right)\operatorname{erfc}\left[\frac{1}{2}\left(\frac{\Delta_1-1}{\Delta_1-u}\right)\left(\frac{u-1}{\kappa_1}+\xi_1\right)\right]\right\} \tag{4.17}$$

where

$$\eta_1 = \frac{r}{\sqrt{D_{ia}t^*}}\ ,\quad \xi_1 = -\frac{\delta}{\sqrt{D_{in}t^*}}\ ,\quad \kappa_1 = (1-\Delta_1)\xi_1\ ,\quad \Delta_1 = \frac{D_g}{D_{in}}$$

D_g and D_m are diffusivities of oxygen in the grain boundary and the matrix, respectively

whilst r is the distance measured from the crack tip and m_{o2} is the oxygen concentration in an air environment at 650°C.

During the oxidation process an enrichment of chromium was observed along the oxidized grain boundaries [25,102]. This chromium depletion from the interior of the grain structure can be evaluated by considering that chromium is transported to the grain boundaries along edge dislocation lines. By assuming an effective dislocation pipe with a radius d and a effective diffusion distance of chromium, d_{Cr}, similar to eq. (4.17), the amount of chromium transported through the effective dislocation pipe during one loading cycle can be calculated as

$$m_{Cr}(d_{Cr},0,t^*) = \hat{m}_{Cr}\left\{\operatorname{erfc}\frac{\eta_2}{2} + \frac{\eta_2}{2\sqrt{\pi}}\int_1^{\Delta_2}\frac{du}{u\sqrt{u}}\exp\left(-\frac{\eta_2^2}{4u}\right)\operatorname{erfc}\left[\frac{1}{2}\left(\frac{\Delta_2-1}{\Delta_2-u}\right)\left(\frac{u-1}{\kappa_2}+\xi_2\right)\right]\right\} \tag{4.18}$$

where

$$\eta_2 = \frac{d_{Cr}}{\sqrt{D_c t^*}}\ ,\quad \xi_2 = -\frac{d}{\sqrt{D_c t^*}}\ ,\quad \kappa_2 = (1-\Delta_2)\xi_2\ ,\quad \Delta_2 = \frac{D_d}{D_c}$$

Here D_d and D_m are the diffusivities of chromium in the effective dislocation pipe and matrix, respectively while m_{Cr} is the concentration of chromium in the matrix.

An important step, now, is to determine the influence of the stress and strain states on the grain boundary diffusivity. It is recognized that intergranular oxygen diffusion depends on the stress and strain states along affected grain boundaries [22,56-68]. In Chapter 2, for a stressed grain boundary the oxygen diffusivity of grain boundaries, D_g, has been expressed as a function of the inelastic strain energy density, $f(w_p)$, of this

boundary. This is written as an Arrhenius relationship in the following form:

$$D_g = D\exp\left(-\frac{Q_g'}{RT}\right)$$

$$= D\exp\left(-\frac{Q_g - f(W_p)}{RT}\right) \qquad (4.19)$$

where Q_g is the activation energy of grain boundary diffusion in the stress-free state, Q_g' is the effective activation energy of grain boundary diffusion for stressed material, D is a diffusion constant, R is the gas constant and T is the temperature in Kelvin. The function $f(W_p)$ is expressed here as follows:

$$f(W_p) = b + b_2\exp\left(\frac{b_3}{(b_4 W_p + b_5)^2}\right) \qquad (4.20)$$

where b_1 to b_5 are coefficients which depend on temperature and material. An equation similar to eq. (4.20) can be written for the dislocation diffutivity in the stressed state and D_d can be completely determined.

The parameter W_p, in the most general case, for loading conditions which include both cyclic and hold-time components, is expressed as:

$$W_p = W_p^f + W_p^c \qquad (4.21)$$

where W_p^f and W_p^c are the components of W_p corresponding to the contributions of the cyclic process and the hold-time duration, respectively. The cyclic component is

$$W_p^f = \int_0^{\frac{1}{f}} \sigma_m(t)\,\dot{\varepsilon}_m(t)\,dt \tag{4.22}$$

where σ_m and ε_m are the equivalent stress and strain rate near the crack tip region, which are caused by external cyclic loading. The hold-time component, W_p^c, on the other hand, could be written as [113]

$$W_p^c = \frac{1-\mu-2\mu^2}{\pi E}\frac{K_{th}^2}{r} \tag{4.23}$$

where μ is Poisson's ratio, E is Young's modulus, K_{th} is the stress-intensity factor during the hold time duration.

It is obvious from the above two equations that knowledge of stress and viscoplastic strain fields in the crack-tip region is required. A number of authors [114-118] have worked in this field and several finite element codes are available for evaluation stress and strain states under a visco-plastic condition [115-118]. Each of these codes has its merits and limitations. All in general, however, require a complex procedure and a large set of input parameters. In this paper, we will attempt to use the closed-form solution derived by Riedel and Rice [119] with the assumption that we are dealing with a small-scale yielding problem. The stress, σ_{ij}, and strain, ε_{ij}, near the crack tip ($\theta = 0$) could be written as:

$$\sigma_{ij} = A\,t^{-\frac{1}{n+1}}\,\tilde{\sigma}_{ij}(\theta)\,|_{\theta=0} \tag{4.24}$$

and

$$\varepsilon_{ij} = \frac{3}{2} B(n+1) A^n t^{\frac{1}{n+1}} [\tilde{\sigma}'_{ij}(\theta) \tilde{\varepsilon}_e(\theta)^{n-1}] \big|_{\theta=0} \qquad (4.25)$$

where

$$A = \alpha_n \left[\frac{n K_I^2}{\pi (n+1)^2 E B} \right] r^{\frac{1}{n+1}}$$

and

$$\alpha_n = \left[\frac{\pi (1-\mu^2)(n+1)}{n I_n} \right]^{\frac{1}{n+1}}$$

Here B and n are the coefficients and power of Norton's law, respectively, while K_I is the stress intensity factor, I_n is a numerical parameter which depends on n, $\tilde{\sigma}_{ij}(\theta)$, and $\tilde{\varepsilon}_e(\theta)$ are the functions of θ. The term $\tilde{\sigma}'_{ij}(\theta)$ is the deviator of $\tilde{\sigma}_{ij}(\theta)$. Substituting eq. (4.24) for the equivalent stress σ_m, i. e.

$$\sigma_m = \left(\frac{3}{2} \sigma'_{ij} \sigma'_{ij} \right)^{\frac{1}{2}} \qquad (4.26)$$

and noting that the deviatoric stress tensor σ_{ij}' can be written as:

$$\sigma'_{ij} = \sigma_{ij} - \frac{1}{3} \sigma_{kk} \delta_{ij}$$

$$= A t^{-\frac{1}{n+1}} (\tilde{\sigma}'_{ij}(\theta) - \frac{1}{3} \tilde{\sigma}_{kk}(\theta) \delta_{ij})_{\theta=0} \qquad (4.27)$$

eq. (4.26) thus becomes

$$\sigma_m = \sqrt{\frac{3}{2}}\ A t^{-\frac{1}{n+1}} \left[\tilde{\sigma}'_{ij}(\theta) \tilde{\sigma}'_{ij}(\theta) - \frac{1}{3} \tilde{\sigma}_{kk}(\theta) \tilde{\sigma}_{pp}(\theta) \right]_{\theta=0} \qquad (4.28)$$

In the near-tip region the total strain is composed of elastic and inelastic

components

$$\varepsilon_m = \varepsilon_m^e + \varepsilon_m^I \tag{4.29}$$

and since $\varepsilon_m^I >> \varepsilon_m^e$ in the near-tip region, $\varepsilon_m \approx \varepsilon_m^I$. The inelastic strain, ε_m^I, which actually is viscoplastic strain, could consist, in the most general case, of the hold-time and cyclic components, i. e.

$$\varepsilon_m^I = \varepsilon_m^f + \varepsilon_m^c \tag{4.30}$$

The material behavior is described here by Norton's law

$$\dot{\varepsilon}_m^I = B\sigma_m^n \tag{4.31}$$

During the hold time, $\varepsilon_m^I \approx \varepsilon_m^c$, thus by combining eqs. (4.28) and (4.31) then integrating during the hold time duration, one obtains

$$\varepsilon_m^c = \int_0^t B\left(\sqrt{\frac{3}{2}}\,A\right)^n [\sigma_{ij}(\theta)\sigma_{ij}(\theta)]^{\frac{n}{2}}\Big|_{\theta=0}\, t^{-\frac{1}{n+1}}\,dt$$

$$= F\left(\frac{K_{th}^2}{r}\right)^{\frac{n}{n+1}} t^{\frac{1}{n+1}} \tag{4.32}$$

where

$$F = \frac{B}{n+1}\left\{\alpha_n\sqrt{\frac{3}{2}}\left(\frac{n}{\pi(n+1)^2 EB}\right)^{\frac{n}{n+1}} [\sigma_{ij}(\theta)\sigma_{ij}(\theta) - \frac{1}{3}\sigma_{kk}(\theta)\sigma_{pp}(\theta)]^{\frac{n}{2}}\Big|_{\theta=0}\right\}$$

and K_I and t_h are the stress-intensity factor and the hold time, respectively. The cyclic

strain component, ε_m^f, could also be calculated as follows

$$\varepsilon_m^f = \frac{F}{n+1} r^{-\frac{n}{n+1}} \int_t (K_I^{\frac{2n}{n+1}} t^{-\frac{n}{n+1}} + 2nt^{\frac{1}{n+1}} K_I^{\frac{n-1}{n+1}} \dot{K}_I)\, dt \qquad (4.33)$$

which when summed with eq. (4.32) gives the total inelastic strain of the form

$$\varepsilon_m = \begin{cases} \frac{F}{n+1} r^{-\frac{n}{n+1}} \int_0^t (K_I^{\frac{2n}{n+1}} t^{-\frac{n}{n+1}} + 2nt^{\frac{1}{n+1}} K_I^{\frac{n-1}{n+1}} \dot{K}_I)\, dt & 0 \le t \le \frac{1}{f} \\ \frac{F}{n+1} r^{-\frac{n}{n+1}} \int_0^{\frac{1}{f}} (K_I^{\frac{2n}{n+1}} t^{-\frac{n}{n+1}} + 2nt^{\frac{1}{n+1}} K_I^{\frac{n-1}{n+1}} \dot{K}_I)\, dt + F\left(\frac{K_{Ih}^2}{r}\right)^{\frac{n}{n+1}} t^{\frac{1}{n+1}} & \frac{1}{f} \le t \le t_h \end{cases} \qquad (4.34)$$

Noting that $\varepsilon_m \approx \varepsilon_m^I$, one can substitutes eq. (4.34) into Norton's law, then the equivalent stress σ_m is obtained

$$\sigma_m = \begin{cases} \left[\frac{F}{(n+1)B}\right]^{\frac{1}{n}} r^{-\frac{1}{n+1}} (K_I^{\frac{2n}{n+1}} + 2nt^{\frac{1}{n+1}} K_I^{\frac{n-1}{n+1}} \dot{K}_I)^{\frac{1}{n}} & 0 \le t \le \frac{1}{f} \\ \left[\frac{F}{(n+1)B}\right]^{\frac{1}{n}} \left(\frac{K_{Ih}^2}{rt}\right)^{\frac{1}{n+1}} & \frac{1}{f} \le t \le t_h \end{cases} \qquad (4.35)$$

Eqs. (4.34) and (4.35) represent the equivalent strain and stress near the crack tip.

The purpose of model is to generate da/dN versus ΔK, this achieved as follows:

(i) for a desired value of ΔP and an arbitrary distance r measured from the crack tip, ΔK can be calculated;

(ii) the corresponding W_p, ε_m and σ_m are calculated using eqs. (4.21), (4.34) and (4.35);

(iii) from knowledge of W_p, the parameters D_g and D_d are determined using eqs. (4.19) to eq. (4.21);

(iv) values of m_{o2} and m_{Cr} can be obtained using eqs. (4.17) and (4.18);

(v) using an experimentally determined value of γ, the oxidation parameter β can be obtained from eq. (4.14) and the corresponding value of ε_d, at the distance r, is fully determined.

Using an iterative procedure would yield a value of r which satisfies the failure criterion $\varepsilon_m \geq \varepsilon_d$. This distance r is taken as the crack length increment occurring at this specific crack length and this particular cycle. From this procedure the relationship of da/dN versus ΔK can be generated.

In the following chapter, a numerical simulation routine will be conducted for predicting the fatigue crack growth rates under the two different loading conditions. These results then will be compared with the data generated from experiments for the same loading conditions in order to examine the validity of the proposed model.

CHAPTER 5

NUMERICAL SIMULATION OF THE PROPOSED MODEL

In this chapter, the proposed model is numerically applied to predict fatigue crack growth rate for two different loading conditions. The first one is a cyclic load profile including a hold time duration for 300 seconds imposed at the minimum load level, while the second is a continuous cyclic load profile without hold time durations. The frequency of the reversed part of the cycle and the stress ratio of these two tests are 0.05 Hz and 0.1, respectively. A flow chart detailing the application steps is shown in Fig. 5.1. The computer code required to execute this chart is listed in Appendix V. The predicted results using the proposed model are compared with those generated from fatigue crack growth tests under the same loading conditions. Details of the data generation and comparison are given in the following sections.

5.1 Cyclic Loading with Hold Time at Minimum Load

In this application, a hold time duration of 300 seconds is imposed at the minimum load level. The cyclic loading frequency, f, is selected as 0.05 Hz in order to satisfy requirements for obtaining an intergranular fracture mode, see ref. [24]. The stress ratio, R, is 0.1. For this type of loading cycle, the stress-intensity factor can be expressed as

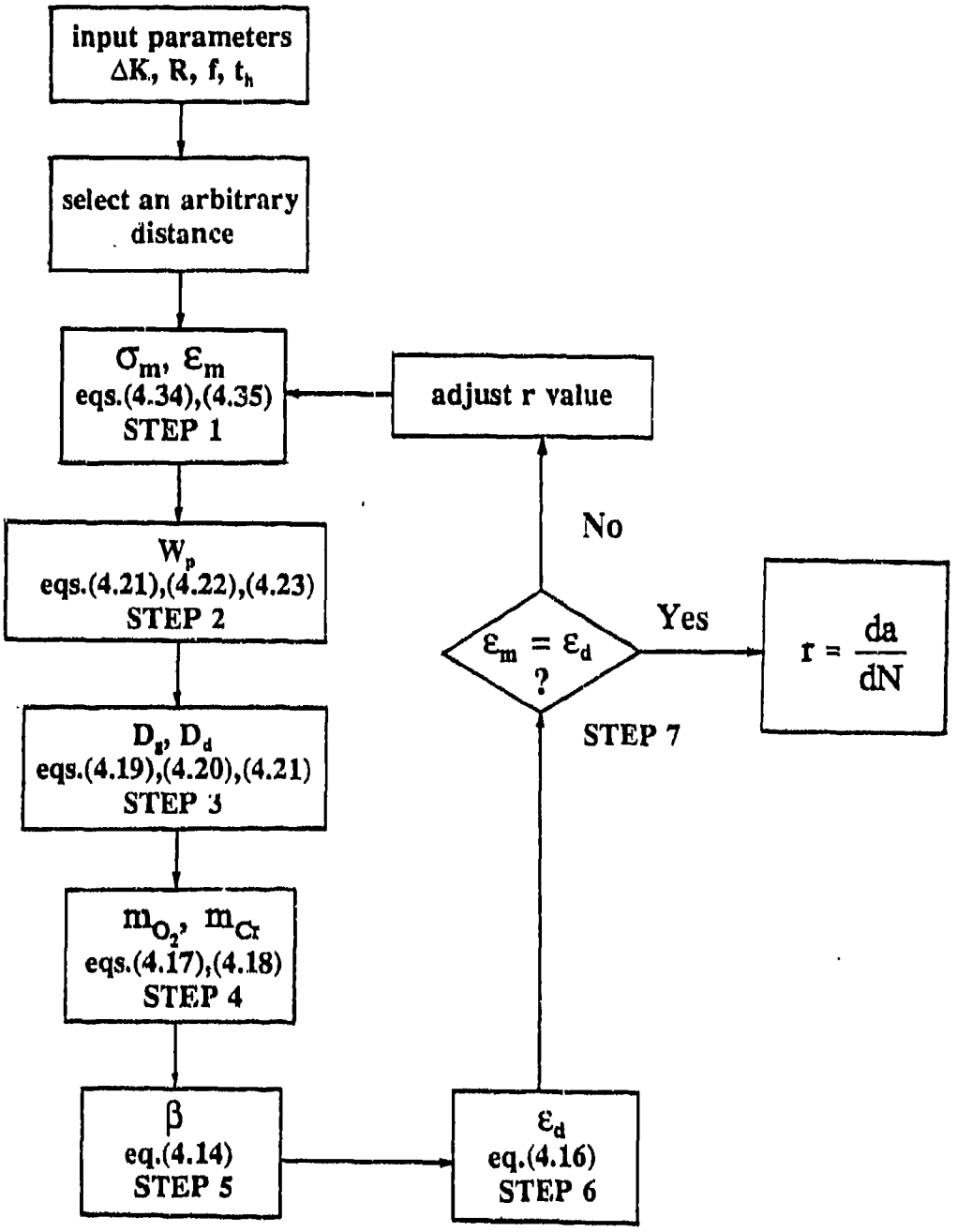

Fig. 5.1 Flow chart showing the calculation procedure involved in performing the proposed model.

$$K_I(t) = \begin{cases} \left(\frac{R}{1-R} + 2ft\right)\Delta K & 0 \le t \le \frac{1}{2f} \\ \left[\frac{R}{1-R} + 2(1-ft)\right]\Delta K & \frac{1}{2f} \le t \le \frac{1}{f} \\ K_{Ih} & \frac{1}{f} \le t \le \left(\frac{1}{f} + t_h\right) \end{cases} \qquad (5.1)$$

where K_{Ih} is the stress-intensity factor during the hold time period; K_{Ih} is equal to K_{min}. In this load profile, the load level, P_{min}, during the hold time period is determined by the condition that, at the longest expected crack length (a/W = 0.7), the corresponding stress-intensity factor would not exceed the threshold value of the test material which is estimated to be 12 MPa$\sqrt{m}$. In this way it is assumed that no "mechanical" crack growth could be produced during the hold time period and any crack advance during this period could thus be entirely attributed to the effect of the environment.

STEP 1:

The first step in the numerical procedure required to determine the crack growth rate is the arbitrary selection of a distance r measured from the crack tip to the point at which the localized equivalent stress, σ_m, and the localized equivalent strain, ε_m, would be calculated. The expression for σ_m and ε_m are:

$$\sigma_m = \left[\frac{2F}{(n+1)B}\right]^{\frac{1}{n}} r^{-\frac{1}{n+1}} \left(K_I^{\frac{2n}{n+1}} t^{-\frac{n}{n+1}} + 2nt^{\frac{1}{n+1}} K_I^{\frac{n-1}{n+1}} \dot{K}_I \right)^{\frac{1}{n}} \qquad 0 \le t \le \frac{1}{f} \qquad (5.2)$$

and

$$\varepsilon_m = \frac{F}{n+1} r^{\frac{-n}{n+1}} \int_0^t (K_I^{\frac{2n}{n+1}} t^{\frac{-n}{n+1}} + 2nt^{\frac{1}{n+1}} K_I^{\frac{n-1}{n+1}} \dot{K}_I) dt + F(\frac{K_{Ih}^2}{r}) r^{\frac{n}{n+1}} t_h^{\frac{1}{n+1}} \quad (5.3)$$

The parameters F, B and n are determined as 8.34 X 10^{-9}, 4.5 X 10^{-33} and n = 10, respectively [25]. When considering that $K_{min} = R\Delta K/(1-R)$, the above two equations could be simplified into:

$$\sigma_m = 1995.52 r^{-0.091} (180.0 K_I^{1.818} t^{-0.909} + K_I^{0.818} t^{0.091} \dot{K}_I)^{0.1} \qquad 0 \le t \le \frac{1}{f} \quad (5.4)$$

and

$$\varepsilon_m = (3.310 + 3.889 t_h^{0.091}) \left(\frac{\Delta K^2}{r} \right)^{0.9091} \times 10^{-8} \quad (5.5)$$

It should be mentioned here that in the present analysis, the residual strain, due to the crack growth history, is neglected. This approximation is justified on the basis that in the small scale yielding condition, the viscoplastic zone size in front of the crack tip is of the same order of magnitude as the distance of the crack advance per cycle [119].

STEP 2:

Once σ_m and ε_m are determined, the inelastic strain energy density, W_p, of the grain boundary at the distance, r, can be evaluated from the expression

$$W_p = W_p^f + W_p^c$$

$$= \int_0^{\frac{1}{f}} \sigma_m(t)\,\dot{\varepsilon}_m(t)\,dt + \frac{1-\mu-2\mu^2}{\pi E}\,\frac{K_{Ih}^2}{r} \qquad (5.6)$$

where μ is Poisson's ratio and E is Young's modulus. The strain rate $\dot{\varepsilon}_m$ can be calculated using Norton's power law:

$$\dot{\varepsilon}_m \approx \dot{\varepsilon}_m^I = B\sigma_m^n \qquad (5.7)$$

Eq. (5.6) can be modified to

$$W_p = \frac{1-\mu-2\mu^2}{\pi E}\,\frac{K_{Ih}^2}{r} + B\int_0^{\frac{1}{f}} \sigma_m^{n+1}\,dt \qquad (5.8)$$

Now, taking E = 165 GPa [25] and μ = 0.283 [120], and setting $K_{Ih} = K_{min}$, W_p can be reduced to

$$W_p \approx 2.976\times10^{-6}\,\frac{\Delta K^2}{r} + 2.882\times10^{-4}\,\frac{K_{Ih}^2}{r}$$

$$= 6.534\times10^{-6}\,\frac{\Delta K^2}{r} \qquad (5.9)$$

STEP 3:

Knowledge of W_p permits the determination of the diffusivities of both the grain boundary path and the effective dislocation pipe, D_g and D_d, respectively. The term D_g

accounts for oxygen diffusion along the grain boundary while D_d accounts for the chromium depletion in the matrix towards the grain boundary. These parameters are expressed as

$$D_g = D \exp\left[-\frac{Q_g}{RT} + f(W_p)\right] \tag{5.10}$$

and

$$D_d = D_1 \exp\left[-\frac{Q_d}{RT} + g(W_p)\right] \tag{5.11}$$

where

$$f(W_p) = 27.6313 - 25.8863 \exp\left(\frac{0.5202}{(5.6114 W_p + 2.1711)^2}\right)$$

and

$$g(W_p) = 32.2362 - 32.0087 \exp\left(\frac{0.3712}{(35.7822 W_p - 37.5720)^2}\right)$$

Other values are $D = 1.477 \times 10^{-6}$ and $D_1 = 1.450 \times 10^{-7}$. The activation energy of the grain boundary, Q_g, and that of the effective dislocation pipe, Q_d, are 115000 J/mol [121] and 128143 J/mol [108], respectively. The gas constant, R, is 8.314 J/mol•K.

STEP 4:

During one loading cycle, the amount of the oxygen diffused along the affected grain boundary, m_{o2}, and those of chromium transported through the effective dislocation

pipe, m_{Cr}, are determined by Whipple's solution as follows

$$m_{o_2}(r,0,t^*) = \hat{m}_{o_2}\left\{\operatorname{erfc}\frac{\eta_1}{2} + \frac{\eta_1}{2\sqrt{\pi}}\int_1^{\Delta_1}\frac{du}{u\sqrt{u}}\exp\left(-\frac{\eta_1^2}{4u}\right)\operatorname{erfc}\left[\frac{1}{2}\left(\frac{\Delta_1-1}{\Delta_1-u}\right)\left(\frac{u-1}{\kappa_1}+\xi_1\right)\right]\right\} \tag{5.12}$$

where

$$\eta_1 = \frac{r}{\sqrt{D_m t^*}}\ ,\quad \xi_1 = -\frac{\delta}{\sqrt{D_m t^*}}\ ,\quad \kappa_1 = (1-\Delta_1)\xi_1\ ,\quad \Delta_1 = \frac{D_g}{D_m}$$

and

$$m_{Cr}(d_{Cr},0,t^*) = \hat{m}_{Cr}\left\{\operatorname{erfc}\frac{\eta_2}{2} + \frac{\eta_2}{2\sqrt{\pi}}\int_1^{\Delta_2}\frac{du}{u\sqrt{u}}\exp\left(-\frac{\eta_2^2}{4u}\right)\operatorname{erfc}\left[\frac{1}{2}\left(\frac{\Delta_2-1}{\Delta_2-u}\right)\left(\frac{u-1}{\kappa_2}+\xi_2\right)\right]\right\} \tag{5.13}$$

where

$$\eta_2 = \frac{d_{Cr}}{\sqrt{D_c t^*}}\ ,\quad \xi_2 = -\frac{d}{\sqrt{D_c t^*}}\ ,\quad \kappa_2 = (1-\Delta_2)\xi_2\ ,\quad \Delta_2 = \frac{D_d}{D_c}$$

The grain boundary width, 2δ, and the diameter of the effective dislocation pipe, d, are taken to be comparable in size and equal approximately to 5 Å [107,108]. Furthermore, the diffusivities of both oxygen and chromium in the matrix are assumed to be the same [108], thus here D_m and D_c are all taken as 1.2×10^{-14} cm^2s^{-1} [102,107]. The term m_{o2} and m_{Cr} are concentrations of oxygen and chromium in air environment and in the matrix at 650°C, respectively. By applying the ideal gas law, m_{O2} can be estimated as 88.73 g/m^3. As for the value of m_{Cr}, since the chromium content in Alloy 718 is about 18.3%(wt), and noting that the density of this alloy is 8.19 g/m^3 [120], m_{Cr} could thus be estimated about

1.4499 x 10^6 g/m^3. The term t^* is the effective oxidation time, which is defined in the previous chapter as follows:

$$t^* = t_h + \frac{< f_c - f >}{f | f_c - f |} \qquad (5.14)$$

where f_c is the transgranular/intergranular transition frequency, which is estimated to be in the order of 10^{-1} Hz, here f_c is selected as 0.2 Hz. The value of t^* in the present application is 320 seconds. Within a first approximation, the effective diffusion distance of chromium, d_{Cr}, is estimated, by using the parabolic rate law, to be about 10 μm.

STEP 5:

The oxidation parameter β, detailed in previous section, is expressed as a function of m_{o2} and m_{Cr}. It can be written as follows

$$\beta = \frac{C_1 m_{Cr}}{C_2 m_{o_2} - C_3 m_{Cr}} \qquad (5.15)$$

where

$$C_1 = 1.462(0.951 + \gamma)$$
$$C_2 = 4.442 + 4.498\gamma$$
$$C_3 = 0.659 + 0.610\gamma$$

and γ is the rate of the amount of iron, m_{Fe}, required to form FeO and the amount of nickel, m_{Ni}, required to form NiO. In the present applications γ is taken as 1.125 [102].

STEP 6:

The grain boundary ductility, ε_d, is related to the degree of oxidation which is

expressed by the oxidation parameter β. The relationship between ε_d and β, as discussed previously, follows a sigmoidal curve which is described by

$$\varepsilon_d = a_1 \operatorname{arctg}(-a_2\beta^2 + a_3) + a_4 \qquad (5.16)$$

where a_1, a_2, a_3, and a_4 are parameters which could vary with material characteristics, service temperature, loading condition and other parameters that may contribute to the grain boundary embrittlement.

Taking $\varepsilon_{do} = 5.37\%$ [102] and using high temperature creep crack test data [22], the relationships between ε_d and β at different ΔK levels are obtained by applying a trial and error curve fitting technique. The normalized $\varepsilon_d / \varepsilon_{do}$ versus β for ΔK values in the range of 18 to 40 MPa$\sqrt{m}$ is presented in Fig. 5.2. The determination of ε_d for any other ΔK level within this range can then be performed by interpolation.

STEP 7:

Steps 1-6 are carried out for different r values. The value of r which results in satisfying the fracture criterion, namely, $\varepsilon_m = \varepsilon_d$, is taken here to be equal to the crack advance per cycle, i.e.,

$$r = \frac{da}{dN} \qquad (5.17)$$

The pattern of the distributions of both the mechanical strain, ε_m, and the grain boundary ductility, ε_d, calculated as functions of the distance r are shown in Fig. 5.3. It can be seen that as r increase, ε_m decreases and ε_d increases approaching the value ε_{do}. The intersection of the ε_m curve and the ε_d curve represents the position of the crack tip

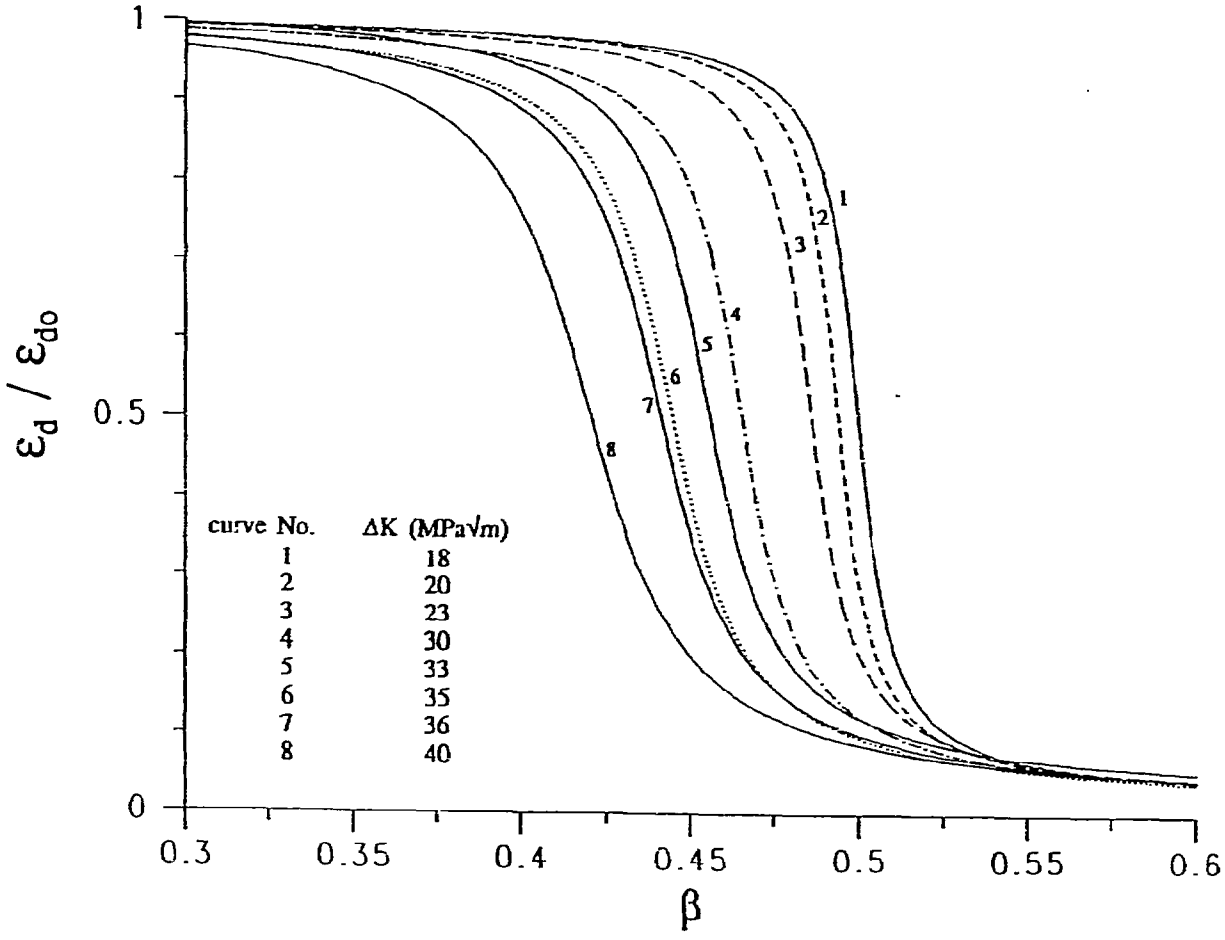

Fig. 5.2 Normalized grain boundary ductility $\varepsilon_d/\varepsilon_{do}$ versus parameter β for the case of cyclic loading with 300 seconds hold time at minimum load level.

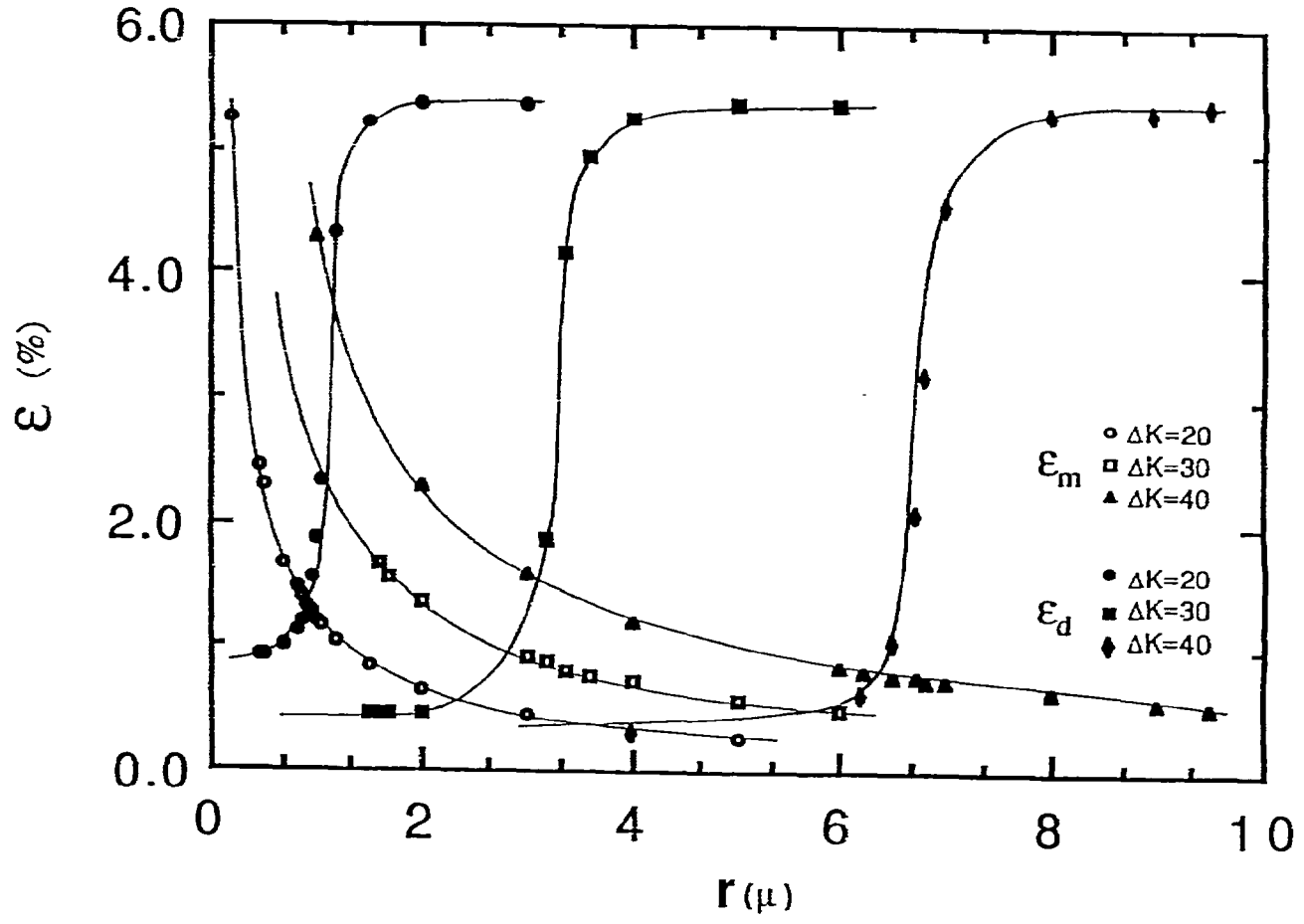

Fig. 5.3 Distributions of ε_m and ε_d as functions of distance r from the crack tip for different levels of ΔK (loading cycle: 10s-300s hold at P_{min}-10s).

at the end of the corresponding cycle.

The calculated results for W_p, m_{o2}/m_{o2}, m_{Cr}/m_{Cr}, β, ε_m and da/dN are listed in Table 5.1, and illustrated in Fig. 5.4 which shows a comparison between the experimental data and the calculated results in terms of da/dN versus ΔK. The predicted results agree very well with the experimental data.

5.2 Cyclic Loading without Hold Time

In this application, all the test material parameters are identical to those used in the previous application except for the hold time, t_h, the effective oxidation time, t^*, and the effective diffusion distance of chromium, d_{Cr}, hence, the calculation steps are the same as in the previous application. Here, the hold time, t_h, and consequently K_{th}, is taken as zero since no hold time duration is included in the loading profile. The effective oxidation time t^* during one cycle is 20 seconds and, the effective diffusion distance of chromium, d_{Cr}, estimated by applying the parabolic rate law, is 2.6 μm. The relationships between ε_d and β at different ΔK levels are obtained, by, again, utilizing a trial and error curve fitting technique. Fig. 5.5 describes the normalized $\varepsilon_d/\varepsilon_{do}$ versus β for ΔK levels in the range of 20 to 40 MPa$\sqrt{m}$. The pattern of the distributions of both ε_m and ε_d in front of the crack tip, for this case, is shown in Fig. 5.6, while the calculated results for W_p, m_{o2}/m_{o2}, m_{Cr}/m_{Cr}, β, ε_m and da/dN are listed in Table 5.2. The comparison between the experimental data and the calculated results in terms of da/dN versus ΔK is also presented in Fig. 5.4. Again in this case, the predicted results agree well with the experimental data.

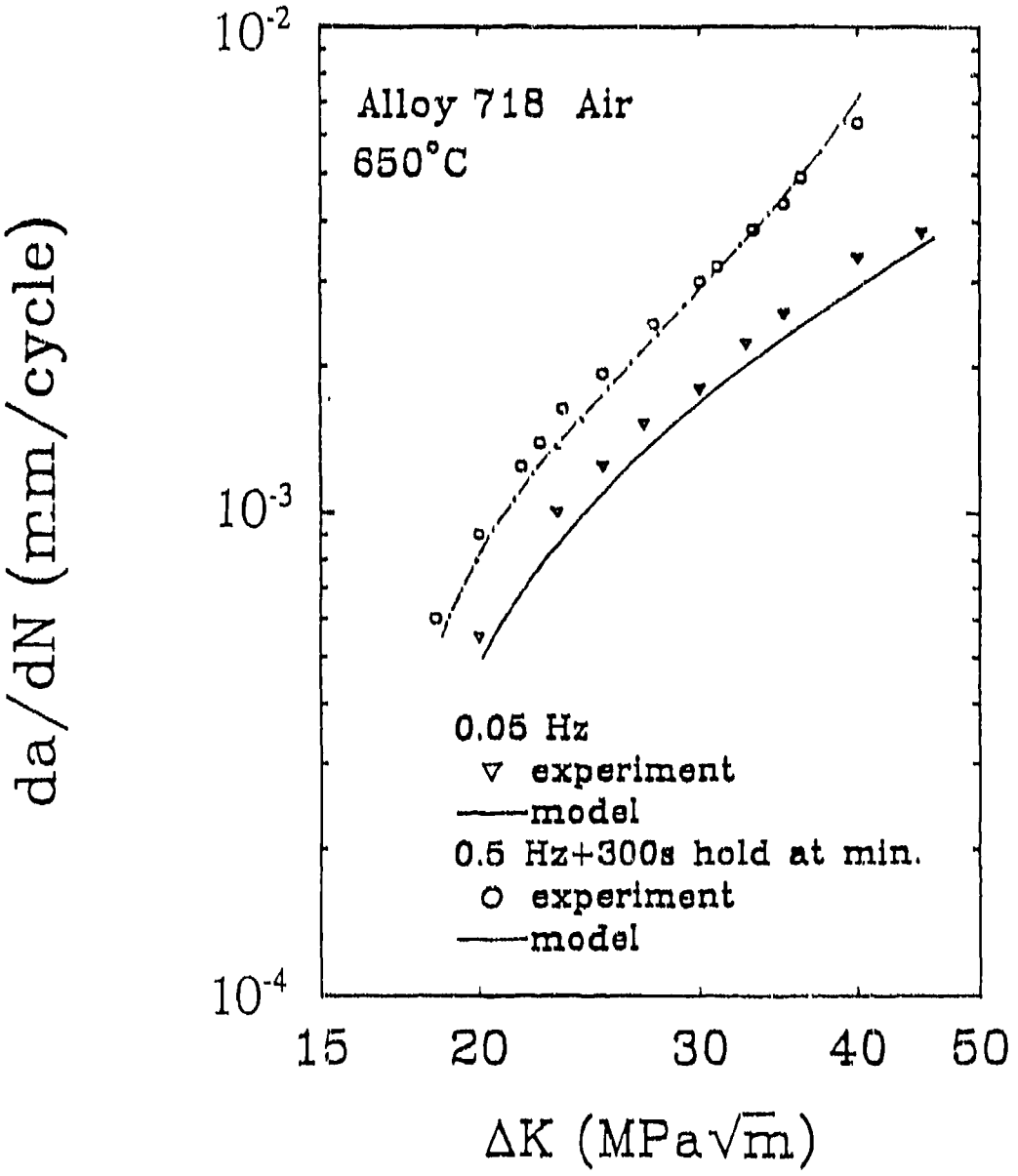

Fig. 5.4 Comparison between experimental and numerical simulated results in terms of da/dN versus ΔK.

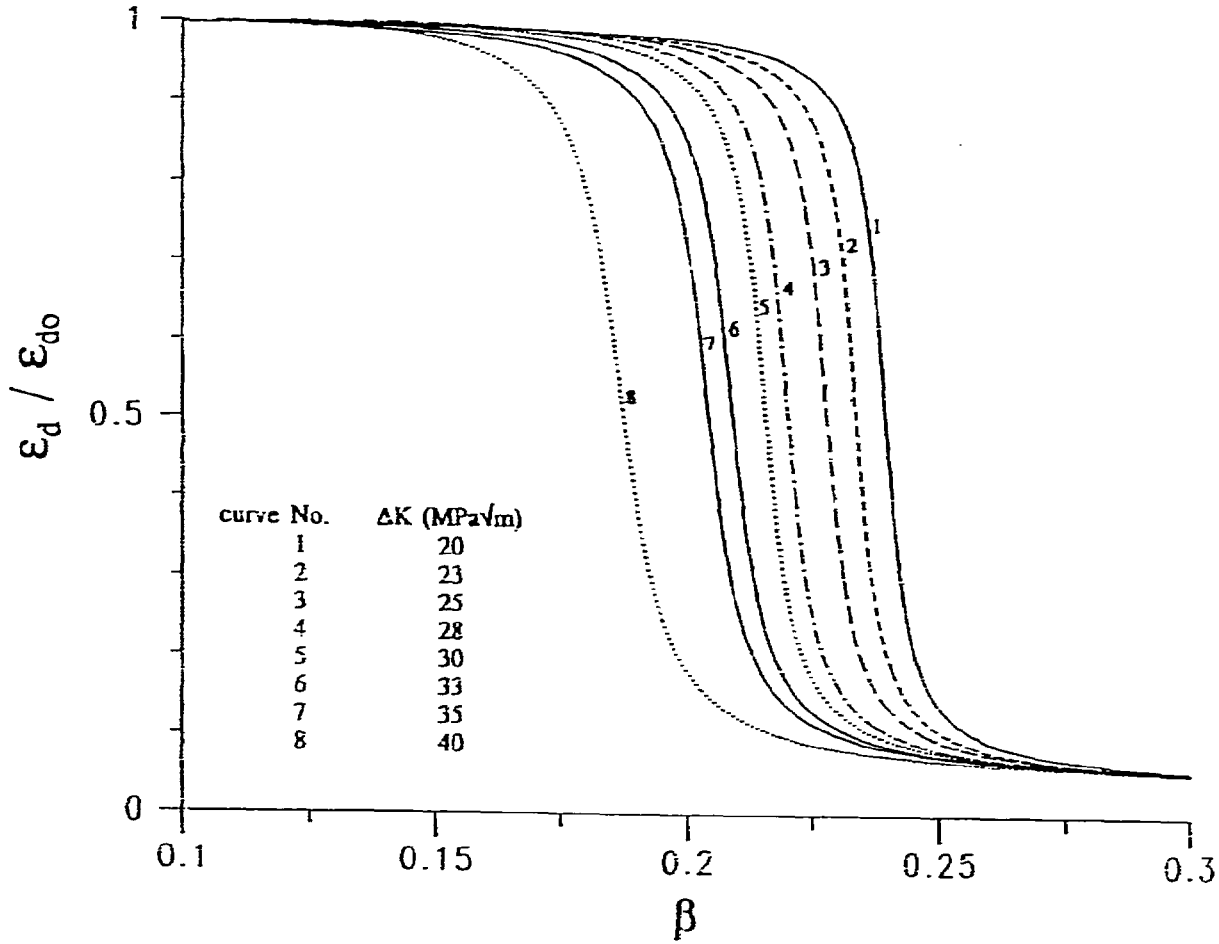

Fig. 5.5 Normalized grain boundary ductility $\varepsilon_d/\varepsilon_{do}$ versus parameter β for the case of cyclic loading without hold time.

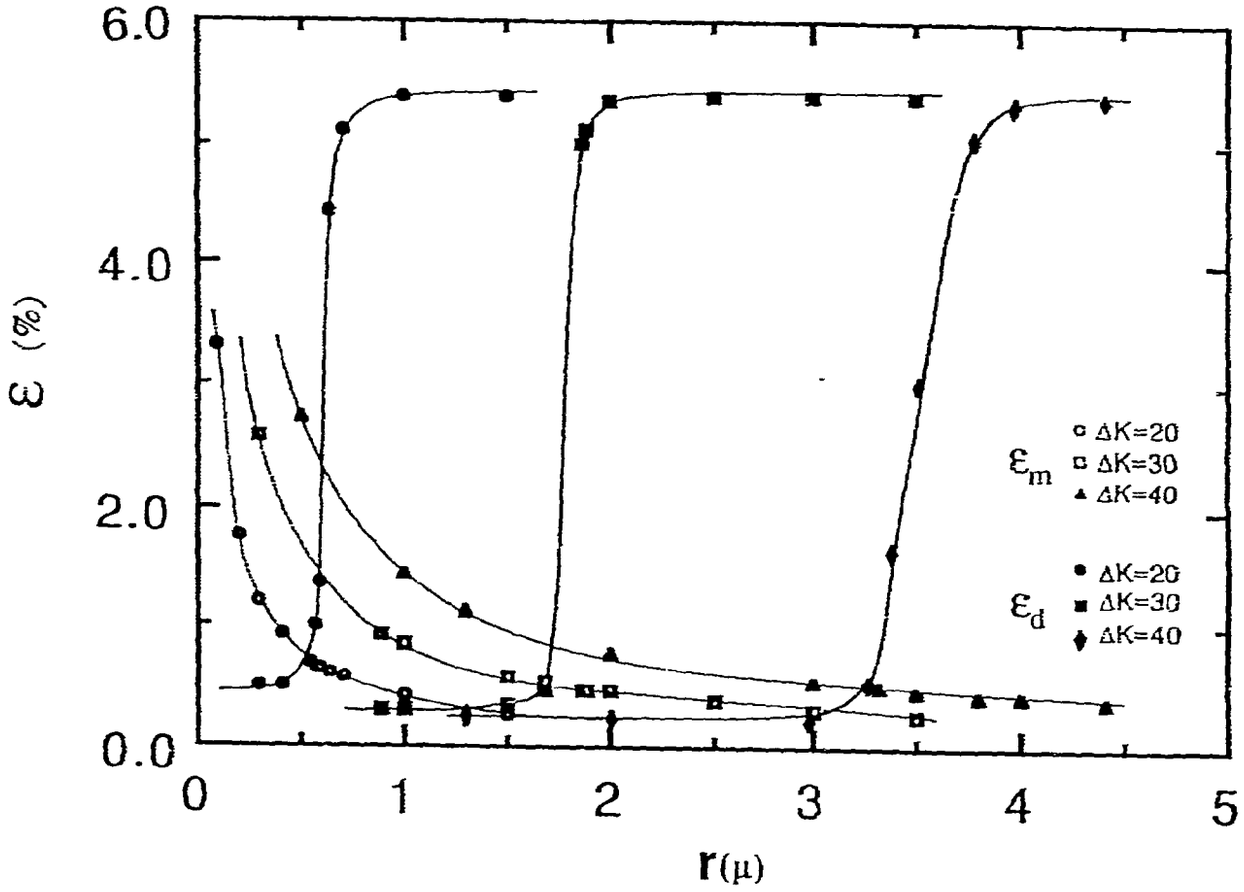

Fig. 5.6 Distributions of ε_m and ε_d as functions of distance r from the crack tip for different levels of ΔK (loading cycle: 10s-10s).

ΔK ($MPa\sqrt{m}$)	W_p (J/mol)	m_{O1}/m_{O2}	m_{Cr}/m_{Cr} $x10^{-5}$	β	ε_m (%)	da/dN (mm/cyc) tested	da/dN (mm/cyc) predicted
18.52	2.7375	0.9883	7.548	0.5049	1.687	$6.0x10^{-4}$	$5.84x10^{-4}$
20.00	2.904	0.9821	7.466	0.5020	1.342	$9.0x10^{-4}$	$8.71x10^{-4}$
23.33	2.592	0.9670	7.187	0.4983	1.029	$1.64x10^{-3}$	$1.61x10^{-3}$
33.09	1.863	0.9221	6.953	0.4970	0.896	$3.84x10^{-3}$	$3.76x10^{-3}$
35.00	1.844	0.9120	6.764	0.4871	0.888	$4.34x10^{-3}$	$4.20x10^{-3}$
36.11	1.739	0.9002	6.487	0.4704	0.842	$4.90x10^{-3}$	$4.29x10^{-3}$
40.00	1.646	0.8704	6.148	0.4592	0.801	$6.35x10^{-3}$	$6.67x10^{-3}$

Table 5.1 Results of the model simulation for load condition 1

ΔK ($MPa\sqrt{m}$)	W_p (J/mol)	m_{O2}/m_{O2}	m_{Cr}/m_{Cr} $x10^{-5}$	β	ε_m (%)	da/dN (mm/cyc) tested	da/dN (mm/cyc) predicted
20.00	2.180	0.9561	3.908	0.2447	0.710	$5.46x10^{-4}$	$5.43x10^{-4}$
23.33	1.574	0.9178	3.080	0.2290	0.528	$1.00x10^{-3}$	$6.26x10^{-4}$
25.00	1.500	0.8977	2.761	0.2099	0.506	$1.24x10^{-3}$	$1.10x10^{-3}$
32.67	1.431	0.8171	2.334	0.1912	0.484	$2.22x10^{-3}$	$2.05x10^{-3}$
35.00	1.424	0.7896	2.283	0.1894	0.482	$2.56x10^{-3}$	$2.38x10^{-3}$
40.00	1.421	0.7270	2.265	0.1818	0.481	$3.35x10^{-3}$	$3.33x10^{-3}$

Table 5.2 Results of the model simulation for load condition 2

5.4 Simplified Approach and Discussion

Applications of proposed model to these two loading profiles showed a good agreement with experimental results. This could be taken as a support for the validity of the proposed model. However, one should realized that, due to the implicit functional form of the model, that an extensive and complex iterative procedure is required for its execution. An attempt is thus made to simplify the model by deriving a closed form equation of da/dN versus ΔK which could prove to be easier to integrate, thus making it possible to include the model into residual life prediction procedures. This was achieved by obtaining semi-empirical equation for both ε_m and ε_d using both eq. (5.3) and Fig. 5.2, respectively. This approach, yielded the following expression

$$\varepsilon_m = G_1(f)\left(\frac{\Delta K^2}{r}\right)^{\frac{n}{n+1}} \tag{5.18}$$

and

$$\varepsilon_d = \varepsilon_{d0} a b r^q \tag{5.19}$$

where $G_1(f)$ is a function of frequency, n has the same meaning as before, and parameters a, b and q are related to the geometrical shape of the grain boundary ductility curve. It was found that parameters a and q are constants with values of 0.9434 and 0.0494 while parameter b depends on both the frequency and ΔK levels, and it could be correlated with frequency and ΔK as follows:

$$b = G_2(f)\Delta K^{-p} \tag{5.20}$$

where $G_2(f)$ is a function of frequency, p is a constant with a value of 1.249. By invoking the fracture criterion previously described and using the above two expressions, one obtains

$$r = \frac{da}{dN} = \left(\frac{G_1(f)}{\varepsilon_{d0} a b} \right)^{\frac{n+1}{n+(n+1)q}} \Delta K^{\frac{2n}{n+(n+1)q}}$$

$$= \left(\frac{G_1(f)}{\varepsilon_{d0} a G_2(f)} \right)^{\frac{n+1}{n+(n+1)q}} \Delta K^{\frac{2n+p(n+1)}{n+(n+1)q}} \tag{5.21}$$

which can be rewritten in the form

$$\frac{da}{dN} = C(f)\Delta K^{m} \tag{5.22}$$

where m is a constant having a value of 3.199, and C is a function of frequency. It should be emphasized the fact that the micromechanistic based model and the approach directly based upon the measurement of intergranular depth of oxygen diffusion lead to the identical results, i.e. the Paris-type law of crack growth expression with a frequency-dependent coefficient. This, again, implies that it is the environmental influences that govern the fatigue crack propagation performance in the environment-dependent crack growth stage.

It must be emphasized here, however, that the model is also limited in use to frequencies smaller than the transitional frequency of Alloy 718 at 650°C. Other constraints of this model lie in the fact that the model is valid only under small-scale

yielding conditions and the assumption that previous damage in the crack-tip region, at the start of each new load cycle, is neglected. These limitations should be recognized when evaluating the degree of validity of the model to conditions different than those described here.

CHAPTER 6

SUMMARY AND CONCLUSIONS

At cyclic loading frequencies below that of the transitional frequency level, the elevated temperature fatigue crack growth process in Alloy 718 is viewed to be fully environment-dependent. Of all the crack growth stages, this stage, while is the most critical in high temperature applications due to its highly accelerated crack growth rate, is the least studied or understood. The objective of this study was to focus on the understanding of the controlling mechanisms of this environment-dependent crack growth stage in order to develop the ability to predict the crack growth performance in Alloy 718 under different loading and environment conditions. For this purpose, two major studies have been carried out here.

The first was to provide evidence of the existence of the fully environment-dependent stage in which the crack growth rate would be equal to the oxygen penetration rate at the crack tip. This has been achieved by measuring the depth of oxygen diffusion at 650°C under the cyclic loading conditions with and without hold time durations at minimum load level. As a result, the relationship between the intergranular oxygen diffusion rate, $\dot{X}$, and the value of the stress intensity factor, ΔK, has been established. This relationship, when integrated over the cycle effective oxidation time, results in a closed form solution describing the environment-dependent fatigue crack growth rate. A good agreement was obtained when a comparison was made between the results of this

solution and the corresponding experimental data. These results were taken in support of the notion that environment-dependent crack growth in fully correlated with the intergranular depth of oxygen penetration at the crack tip. As such, the environment dependent crack growth process is thus viewed as a crack tip oxidation phenomenon.

The second study was to establish a micromechnical based quantitative model to predict the environmentally-dominated crack growth performance. This model was based on the concept of the intergranular two-stage crack-tip oxidation mechanism. According to this mechanism, the oxygen partial pressure controls the preferential formation of the oxide layers at the crack tip, and it suggests that intergranular oxidation under air environment occurs in two stages with the formation of a Ni-Fe rich oxide followed by that of the more protective film formed by Cr_2O_3 oxide. Thus, the reduction of the grain boundary ductility along the grain boundary fracture path depends on the rate of formation of the chromia layer in relation to the build-up of other oxide types at the crack tip. The determination of the amount of Cr_2O_3 depends on the amount of both oxygen diffused along the affected grain boundary and chromium transported via a mobile dislocation network. The reduction in grain boundary ductility due to oxidation is balanced by considering the effective strain at the crack tip resulting from the external loading. This balance defines the fracture criterion of the model and permits the calculation of the crack advance per cycle. The model was then used to predict the crack growth rate in Alloy 718 at 650 °C for two different loading conditions, and a good agreement was observed when the data obtained from the model in the form of da/dN versus ΔK were compared with those obtained experimentally.

From the present study, two major conclusions can be made:

1. The existence of an environment-dependent fatigue crack growth stage in Alloy 718 at elevated temperature conditions is supported on the basis of comparing the results of fatigue crack growth tests in both air and vacuum conditions and also from comparison between the experimental fatigue crack growth results and those obtained from a closed form solution which is directly derived from the knowledge of the intergranular diffusion rate, $\dot{X}$, in the crack tip region over the cycle effective oxidation time, t_{ox}. Two interesting points should be emphasized here, i.e.

   (a) Within the environment-dependent fatigue crack growth stage, the cycle effective oxidation time, t_{ox}, should be taken as the whole cycle duration including both the loading and unloading part of the cycle.

   (b) The oxygen diffusivity of grain boundaries, D_g, is a function of the stress intensity factor range, ΔK, and the loading frequency, f. Through this relationship, the intergranular-transgranular transitional frequency, f_c, can identify as a ΔK-dependent parameter.

2. The quantitative crack growth model developed in this work on the basis of the two-stage crack-tip oxidation mechanism correctly characterizes the environment-dependent fatigue crack growth behavior. Two assumptions, however, were

made in order to simplify the mathematical treatments. The first is that the crack tip zone is subjected only to small-scale yielding and the second is that the initial conditions of the crack tip region at the start of each load cycle are identical. These assumptions limit the applications of this model to conditions which do not consider loadings with a long hold time at the maximum load level. In these types of applications, the spread of crack tip plasticity due to creep associated with hold time durations may not justify the use of ΔK as a crack tip driving force.

REFERENCES

[1] T. Weerasooriya et al., "Research on Mechanical Properties for Engine Life Prediction", AFWAL-TR-88-4062, Wright-Patterson AFB, OH, May 1988

[2] P. Shahinian and K. Sadananda, "Creep-Fatigue-Environment Interaction on Crack Propagation in Alloy 718", in Engineering Aspects of Creep, Institute of Mechanical Engineers, London, **Vol. 2**, 1980, Paper C239/80

[3] L. A. James, "The Effect of Temperature upon the Fatigue-Crack Growth Behavior of Two Nickel-Base Alloy", Journal of Engineering Materials and Technology, **Vol.95**, 1973, pp.254-256

[4] M. Clavel and A. Pineau, " Frequency and Wave-Form Effects on the Fatigue Crack Growth Behavior of Alloy 718 at 298K and 823K", Metallurgical Transactions, **Vol. 9A**, 1978, pp.471-480

[5] S. Floreen and R. H. Kane, "An Investigation of the Creep-Fatigue-Environment Interaction in a Ni-Base Superalloys", Fatigue of Engineering Materials and Structures, **Vol. 2**, 1980, pp.401-412

[6] T. Weerasooriya and S. Venkataraman, "Frequency and Environment Effect on Crack Growth in Inconel 718," in Effects of Load and Thermal Histories, eds. by P. K. Liaw and T. Nicholas, the Metallurgical Society of AIME, Warrendal, PA, 1987, pp.101-108

[7] T. Weerasooriya, "Effect of Frequency on Fatigue Crack Growth Rate of Inconel 718 at High Temperature", in Fracture Mechanics: Nineteenth Symposium, ASTM STP 969, ed. by T. A. Cruse, American Society for Testing and Materials, Philadelphia, PA, 1988, pp.907-923

[8] L. A. James, "Fatigue Crack Propagation in Alloy 718: A review", in Superalloy 718: Metallurgy and Applications, ed. by E. A. Loria, Pittsburgh, PA, American Society for Metals, 1989, pp.499-515

[9] J. P. Pedron and A. Pineau, "The Effect of Microstructure and Environment on the Crack Growth Behavior of Inconel 718 Alloy at 650°C under Fatigue, Creep and Combined Loading", Materials Science and Engineering, **Vol. 56**, 1982, pp.143-156

[10] L. A. James, "The Effect of Grain Size upon the Fatigue-Crack Propagation

Behavior of Alloy 718 under Hold-Time Cycling at Elevated Temperature", Engineering Fracture Mechanics, **Vol. 25**, 1986, pp.305-314

[11] C. Bathias and R. M. Pelloux. "Fatigue Crack Propagation in Martensitic and Austenitic Steels", Metallurgical Transactions, **Vol. 4**, 1973, pp.1265-1273

[12] H. H. Smith and D. J. Michel, "Fatigue Crack Propagation and Deformation Mode in Alloy 718 at Elevated Temperatures", in Ductility and Toughness Considerations in Elevated Temperature Service, MPC-8, ed. by G. V. Smith, American Society of Mechanical Engineering, New York, 1978, pp.225-246

[13] M. Clavel and A. Pineau, "Intergranular Fracture Associated with Heterogeneous Deformation Modes during Low Cycle Fatigue in a Ni-Base Superalloy", Scripta Metallurgy, **Vol. 16**, 1982, pp.361-364

[14] M. Clavel and A. Pineau, "Fatigue Behavior of Two Nickel-Base Alloys, Part I: Experimental Results on Low Cycle Fatigue, Fatigue Crack Propagation and Substructures", Materials Science and Engineering, **Vol. 55**, 1982, pp.157-171

[15] D. Fournier and A. Pineau, "Low Cycle Fatigue Behavior of Inconel 718 at 298K and 823K", Metallurgical Transactions, **Vol. 8A**, 1977, pp.1095-1105

[16] D. J. Wilson, "Relationship of Mechanical Characteristics and Microstructural Features to the Time-Dependent Edge-Notch Sensitivity of Inconel 718 Sheet", Journal of Engineering Materials and Technology, **Vol. 113**, 1973, pp.112-123

[17] H. Ghonem, D. Zheng, E. Andrieu and A. Pineau, "Experimental Observations and Quantitative Modelling of Oxidation-Assisted Crack Growth Behavior in Alloy 718 at 650°C", Annual report, AFOSR-89-0285, 1990

[18] N. E. Ashbaugh, "Waveshape Effects Upon Crack Growth in Inconel 718," presented at 15th National Symposium on Fracture Mechanics, University of Maryland, Clooege Park, MD, July 8, 1982

[19] P. Shahinian and K. Sadananda, "Crack Growth under Creep and Fatigue Conditions", in Creep-Fatigue-Environment Interactions, eds. by R. M. Pelloux and N. S. Stoloff, the Metallurgical Society of AIME, Warrendal, PA, 1981, pp.86-111

[20] P. Shahianian and K. Sadananda, "Crack Growth Behavior under Creep-Fatigue Conditions in Alloy 718," in Creep Fatigue Interaction, MPC3, American Society of Mechanical Engineering, Philadelphia, PA, 1976, pp.365-390

[21] H. H. Smith and D. J. Michel, "Effect of Environment on Fatigue Crack Propagation Behavior of Ally 718 at Elevated Temperatures", Metallurgical

Transactions, **Vol. 17A**, 1986, pp.370-374

[22] P. Shahianian and K. Sadanunda, "Effects of Stress Ratio and Hold-Time on Fatigue Crack Growth in Alloy 718", Journal of Engineering Materials and Technology, **Vol. 101**, 1979, pp.224-230

[23] T. Nicholas and T. Weerasooriya, "Hold-Time Effects in Elevated Temperature Fatigue Crack Propagation," in Fracture Mechanics: Seventeenth Volume, ASTM STP 905, American Society for Testing and Materials, Philadelphia, PA, 1986, pp.155-168

[24] J. P. Pedron and A. Pineau, "Effect of Hold Times on the Elevated Temperature Fatigue Crack Growth Behavior of Inconel 718 Alloy," in Advances in Fracture Research, **Vol. 5**, 1981, pp.2385-2392

[25] A. Diboine and A. Pineau, "Creep Crack Initiation and Growth in Inconel 718 at 650°C," Fatigue and Fracture of Engineering Materials and Structure, **Vol. 10**, 1987, pp.141-151

[26] K. Sadananda and P. Shahinian, "Effects of Environment on High Temperature Crack Growth Behavior of Several Nickel-Base Alloys", in Corrosion of Nickel-Base Alloys, ed. by R. C. Scarberry, ASM Publication, Cincinnati, Ohio, 1985, pp.101-115

[27] P. Shahinian, "Effect of Environment on Creep-Rupture Properties of Some Commercial Alloys", Transactions of the American Society for Metals, **Vol. 49**, 1957, pp.862-882

[28] R. H. VanStone, O. C. Gooden and D. D. Krueger, "Advanced Cumulative Damage Modeling", AFWAL-TR-88-4146, Materials Laboratory, Wright-Patterson AFB, OH, 1988.

[29] K. Sadananda and P. Shahinian, "Crack Growth Behavior in Alloy 718 at 425°C", Journal of Engineering Materials and Technology, **Vol. 100**, 1978, pp.381-387

[30] H. Ghonem and D. Zheng, "Characterization of Environment-Dependent Fatigue Crack Growth in Alloy 718 at 650°C", in Superalloy 718, 625 and Various Derivations, ed. by E. A. Loria, the Minerals, Metals & Materials Society, Warrendal, PA, 1991, pp.477-490

[31] S. Venkataraman and T. Nicholas, "Mechanisms of Elevated Temperature Fatigue Crack Growth in Inconel 718 as a Function of Stress Ratio," in Effects of Load and Thermal Histories, eds. by P. K. Liaw and T. Nicholas, the Metallurgical Society, Inc., 1987, pp.81-99

[32] A. Coles, R. E. Johnson and H. G. Popp, "Utility of Surface-Flawed Tensile Bars in Cyclic Life Studies", Journal of Engineering Materials and Technology, **Vol. 98**, 1976, pp.305-315

[33] H. F. Merrick and S. Floreen, "The Effects of Microstructure on Elevated Temperature Crack Growth in Nickel-Base Alloys", Metallurgical Transactions, **Vol.9A**, 1978, pp.231-236

[34] S. Floreen and R. Raj, "Environmental Effects in Nickel-Base Alloys", in Flow and Fracture at Elevated Temperatures, ed. by R. Raj, American Society for Metals, Metals Park, Ohio, 1985, pp. 383-402

[35] E. Andrieu, R. Cozar and A. Pineau, "Effect of Environment and Microstructure on the High Temperature Behavior of Alloy 718", in Superalloys Metallurgy & Applications, ed. by E. A Loria, Pittsburgh, PA, American Society for Metals, 1989, pp.241-247

[36] R. Thamburaj, T. Terada, A. K. Koul, W. Wallace and M. C. de Malherbe, "The Influence of Microsructure and Environment upon Elevated Temperature Crack Growth Rates in Inconel 718", in Proceedings of the International Conference on Creep, Tokyo, Japan, 1986, pp.275-282

[37] H. H. Smith and D. J. Michel, "Effects of Thermal and Thermomechanical Treatments on the Mechanical Properties of Centrfugally Cast Alloy 718", Materials Science and Engineering, **Vol. 102A**, 1988, pp.161-168

[38] S. Floreen, "High Temperature Crack Growth Structure-Property Relationships in Nickel Base Superalloys", in Creep-Fatigue-Environment Interactions, eds. by R. M. Pelloux and N. S. Stoloff, The Metallurgical Society of AIME, Warrendal, PA, 1982, pp.112-128

[39] R. Thamburaj, W. Wallace, T. L. Prakash and Y. N. Chari, "Influence of Processing Variables on Prior Particle Boundary Precipitation and Mechanical Behavior in PM Superalloy APK1", Powder Metallurgy, **Vol. 27**, 1984, pp.169-180

[40] M. Clavel, C. Levaillant and A. Pineau, "Influence of Micromechanisms of Cyclic Deformation at Elevated Temperature on Fatigue Behavior", in Creep-Fatigue-Environment Interactions, ed by R. M. Pelloux and N. S. Stoloff, AIME Publication, 1980, pp.24-45

[41] S. D. Antolovich and N. Jayaraman, "Metallurgical Instabilities during the High Temperature Low Cycle Fatigue of Nickel-Base Superalloys", Materials Science and Engineering, **Vol. 57**, 1982, L9-L12

[42] R. B. Scarlin, "Some Effects of Microstructure and Environment on Fatigue Crack Propagation", in Fatigue Mechanism, ASTM STP 675, ed. by J. T. Fong, American Society for Testing and Materials, Philadelphia, PA, 1979, pp.396-419

[43] J. M. Davidson and J. K. Tien, "Environmental Effects on the Creep Behavior of a Nickel-Base Superalloy", Metallurgical Transactions, **Vol. 12A**, 1981, pp.865-876

[44] J. Bressers and M. Roth, "The Effect of Time-Dependent Processes on the HTLCF Endurance of PM Astroloy", in Proceedings of International Conference on Advances in Life Prediction Methods, 1983, Albany, NY, American Society of Mechanical Engineering

[45] K. Sadananda and P. Shahinian, "High Temperature Time-Dependent Crack Growth", in Micro and Macro Mechanics of Crack Growth, eds. by K. Sadananda, B. B. Rath and D. J. Michel, The Metallurgical Society of AIME, 1981, pp.119-130

[46] K. Sadananda and P. Shahinian, "Creep Crack Growth behavior and Theoretical Modelling", Metal Science, **Vol. 15**, 1981, pp.425-432

[47] J. W. Brooks and P. J. Bridges, "Long Term Stability of Inconel Alloy 718 for Turbine Disc Applications", in Hihj temperature Alloys for Gas Turbines and Other Applications 1986, eds. by W. Betz, R, Brunetaud, D. Coutsouradis, H. Fischmeister, T. B. Gibbons, I. Kvernes, Y. Lindblom, J. B. Marriott and D. B. Meadowcroft, Reidel Publishing Company, Dordrecht, 1986, pp.1431-1440

[48] A. Pineau, "Intergranular Creep-Fatigue Crack Growth in Ni-Base Alloys", in Flow and Fracture at Elevated Temperature, ed. by R. Raj, American Society for Metals, 1985, pp.317-348

[49] H. Ghonem and D. Zheng, "Intergranular Oxygen Diffusion Depth during Environment-Dependent Fatigue Crack Growth in Alloy 718", to be published in Materials Science and Engineering, 1991

[50] E. Andrieu, "Influence de L'environmnt sur la Propagation des Fissures dans und Superalliage Base Nickel: L'Inconel 718", Ph.D. Thesis, Ecole des Mines de Paris, 1987

[51] K. U. Snowden, "The Effect of Atmosphere on the Fatigue of Lead", Acta Metallurgica, **Vol. 12**, 1964, pp.295-303

[52] S. Floreen, "Effects of Environment on Intermediate Temperature Crack Growth in Superalloys", in Micro and Macro Mechanics of Crack Growth, eds. by K. Sadananda, B. B. Rath and D. J. Michel, The Metallurgical Society of AIME,

1981, pp.177-184

[53] K. U. Snowden and J. N. Greenwood, "Surface Deformation Differences between Lead Fatigue in Air and in Partial Vacuum", Trans. of the Metallurgical Society of AIME, **Vol. 212**, 1958, pp.626-627

[54] K. U. Snowden, "The Distribution of Deformation in Lead Fatigue in Vacuo", Philosophical Magazine, **Vol. 6**, 1961, pp.321-327

[55] J. L. Yueu, P. Roy and W. D. Nix, "Effect of Oxidation Kinetics on the near Threshold Fatigue Crack Growth Behavior of A Nickel Base Superalloy," Metallurgical Transactions, **Vol. 15A**, 1984, pp.1769-1775

[56] L. F. Coffin, Jr., "Cyclic-Strain-Induced Oxidation of high-Temperature Alloys", Trans. of the ASM, **Vol. 56**, 1963, pp.339-350

[57] P. K. Wright, "Oxidation-Fatigue Interactions in a Single-Crystal Superalloy," in Low Cycle Fatigue, ASTM STP 942, eds. by H. D. Solomon, G. R. Halford and B. N. Leis, American Society for Testing and Materials, Philadelphia, PA, 1988, pp.558-575

[58] R. P. Skelton and J. Bucklow, "Cyclic Oxidation and Crack Growth during High Strain Fatigue of Low Alloy Steel", Met. Sci., **Vol. 12**, 1978, pp. 64-70

[59] J. R. Haigh, R. P. Skelton and C. E. Richards, "Oxidation-Assisted Crack Growth during High Cycle Fatigue of A 1%Cr-Mo-V Steel at 550°C," Materals Science and Engineering, **Vol. 26**, 1976, pp.167-174

[60] T. E. Strangman, "Thermal Fatigue Oxidation Resistant Overlay Coatings for Superalloys," Ph.D. Dissertation, University of Connecticut, Storrs, CT, USA, 1978

[61] P. Marshall, "The Influence of Environment on Fatigue and Creep/Fatigue," in Fatigue at High Temperature, International Spring Meeting, Societe Francaise de Metallurgie, Paris, France, 1986, pp.109-145

[62] G. Ward, B. S. Hochkenbull and P. Hancock, "The Effect of Cyclic Stressing on the Oxidation of A Low-Carbon Steel", Matallurgical Transactions, **Vol. 5**, 1974, pp.1451-1455

[63] J. W. Swanson and H. L. Marcus, "Oxygen Transport during Fatigue Crack Growth", Matallurgical Transactions, **Vol. 9A**., 1978, pp.291-293

[64] F. E. Fujita, "Oxidation and Dislocation Mechanisms in Fatigue Crack Formation," in ' acture of Solids, eds. by D. C. Drucker and J. J. Gilman, Interscience

Publisher, New York, 1963, pp.657-670

[65] K. D. Challenger, R. P. Skilton and J. S. Kamen, "The Effect of Oxidation on Fatigue Crack Growth in 2.25Cr-1Mo Steel at 525°C: A Metallographic Examination", Materials Science and Engineering, **Vol. 91**, 1987, pp.1-6

[66] J. Rechet and L. Remy, "Fatigue Oxidation Interaction in a Superalloy — Application to Life Prediction in High Temperature Low Cycle Fatigue," Metallurgical Transactions, **Vol. 14A**, 1983, pp.141-149

[67] M. Reger and L. Remy, "Fatigue Oxidation Interaction in IN100 Superalloy," Metallurgical Transactions, **Vol. 19A**, 1988, pp.2259-2268

[68] S. J. Balsone, T. Nicholas and M. Khobaib, "Effects of Stress History on the Magnitude of the Environmental Attack in Rene' 80," in Environmentally Assisted Cracking: Science and Engineering, ASTM STP 1049, eds. by W. B. Lisagor, T. W. Croofer and B. N. Leis, American Society for Testing and Materials, Philadelphia, PA, 1990, pp.303-318

[69] T. Nicholas, T. Weerasooriya and N. E. Ashbaugh, "A Model for Creep/Fatigue Interaction in Alloy 718", in Fracture Mechanics: Sixteenth Symposium, ASTM STP 868, eds. by M. F. Kannien and A. T. Hopper, American Society for Testing and Materials, Philadelphia, PA, 1985, pp.167-180

[70] R. P. Wei and J. D. Landes, "Correlation between Sustained-Load and Fatigue Crack Growth in High-Strength Steels", Materials Research and Standards, **Vol.9**, 1969, pp.25-28,44 and 46

[71] T. Nicholas, "Fatigue Crack Growth Modeling at Elevated Temperature Using Fracture Mechanics", in Elevated Temperature Crack Growth, eds. by S. Mall and T. Nicholas, American Society of Mechanical Engineers, New York, NY, 1990, pp.107-112

[72] M. R. Winstone, K. M. Nikbin and G. A. Webster, "Modes of Failure under Creep/Fatigue Loading of A Nickel-Based Superalloy", Journal of Materials Science, **Vol. 20**, 1985, pp.2471-2476

[73] A. Saxena, "A Model for Predicting the Environment Enhanced Fatigue Crack Growth Behavior at High Temperature", in Thermal and Environmental Effects in Fatigue: Research-Design Interface, eds. by E. J. Carl, J. H. Stephen, Jr. and E. M. Michael, American Society of Mechanical Engineering, New York, NY, 1983, pp.171-184

[74] M R. Achter, "The Adsorption Model for Environmental Effects in Fatigue Crack

Propagation", Scripta Metallurgica, Vol. 2, 1968, pp.525-528

[75] R. P. Wei, "On Understanding Environment-Enhanced Fatigue Crack Growth —— A Fundamental Approach", in Fatigue Mechanisms, ed. by J. T. Fong, ASTM STP 675, American Society for Testing and Materials, Philadelphia, PA, 1979, pp.816-840

[76] T. W. Weir, G. W. Simmons, R. G. Hart and R. P. Wei, "A Model for Surface Reaction and Transport Controlled Fatigue Crack Growth", Scripta Metallurgica, Vol. 14, 1980, pp.357-364

[77] J. J. McGowan and H. W. Liu, "A Kinetic Model of High Temperature Fatigue Crack Growth", in Fatigue Environment and Temperature Effects, eds. by J. B. Jhon and W. Volker, Plenum Press, New York, NY, 1983, pp.377-390

[78] S. D. Antolovich and E. Rosa, "Low Cycle Fatigue of Rene 77 at Elevated Temperatures", Materials Science Engineering, Vol. 47, 1981, pp.47-57

[79] G. R. Romanoski, S.D. Antolovich and R. M. Pelloux, "A Model for Life Predictions of Nickel-Base Superalloy in High Tmperature Lw Ccle Ftigue", in Low Cycle Fatigue, ASTM STP 942, eds. by H. D. Solomon, G. R. Halford and B. N. Leis, American Society for Testing and Materials, Philadelphia, PA, 1988, pp.456-469

[80] L. F. Coffin, Jr., "Overview of Temperature and Environmental Effects on Fatigue of Structural Metals", in Fatigue: Environment and Temperature Effects, eds. by J. J. Burke and V. Weiss, Plenum Press, New York, NY, 1980, pp.1-40

[81] H. Ghonem and R. Foerch, "Frequency Effects on Fatigue Crack Growth Behavior in A near-α Titanium Alloy", in Elevated Temperature Crack Growth, eds. by S. Mall and T. Nicholas, American Society of Mechanical Engineering, New York, NY, 1990, pp.93-105

[82] E. Andrieu, H. Ghonem and A. Pineau A, "Two Stage Crack Tip Oxidation Mechanism in Alloy 718", in Elevated Temperature Crack Growth, eds. by S. Mall and T. Nicholas, American Society of Mechanical Engineers, New York, NY, 1990, pp.25-29

[83] H. Ghonem and D. Zheng, "Oxidation-Assisted Fatigue Crack Growth Behavior in Alloy 718 —— Part I: Quantitative Modelling", Fatigue & Fracture Engineering Materials & Structures, Vol. 14 , 1991, pp.749-760

[84] P. G. Shewmon, Diffusion in solids, McGraw-Hill Book Company, Inc., New York,1963

[85] H. H. Smith, P. Shahinian and M. R. Achter, "Fatigue Crack Growth Rates in Types 316 Stainless Steel at Elevated Temperature as A Function of Oxygen Pressure", Transactions of the Metallurgical Society of AIME, Vol. 245, 1969, pp. 947-953

[86] R. H. Bricknell and D. A. Woodford, "The Embrittlement of Nickel Following High Temperature Air Exposure", Metallurgical Transactions, Vol. 12A, 1981, pp.425-433

[87] C. J. McMahon and L. F. Coffin, "Mechanisms of Damage and Fracture in High-Temperature Low Cycle Fatigue of A Cast Nickel-Based Superalloy", Metallurgical Transactions, Vol. 1, 1970, pp.3443-3451

[88] L. F. Coffin, "Fatigue at High Temperature", in Fatigue at Elevated Temperatures, ASTM STP 520, American Society of Testing Materials, Philadelphia, PA, 1973, pp.5-34

[89] C. J. McMahon, Jr., "On the Mechanism of Premature in-Service Fallure of Nickel-Base Superalloy Gas Turbine Blades", Materilas Science Engineering, Vol. 13, 1974, pp.295-297

[90] D. A. Woodford and R. H. Bricknell, "Environmental Embrittlement of High Temperature Alloy by Oxygen", in Treatise on Materials Science and Technoloyg, Vol. 25, Academic Press, Inc. 1983, pp.157-199

[91] H. Teranishi and A. J. McEvily, "Effect of Oxidation on Hold Time Fatigue Behavior of 2.25 Cr-1 Mo Steel", Metallurgical Transactions, Vol. 10A, 1979, pp.1806-1808

[92] D. J. Michel and H. H. Smith, "Fatigue Crack Propagation in Neutron Irradiated Type 304 and Type 308 Stainless Steel Plate and Weld Materials", Journal of Nuclear Materials, Vol. 71, 1977, pp.173-177

[93] R. L. Stegman, and P. Shahinian, "Effect of Temperature on the Fatigue of Nickel at Varying Oxygen Pressures", in Fatugue at High Temperature, ASTM STP 459, ASTM, Philadelphia, PA, 1969, pp.42-58

[94] H. H. Smith and P. Shahinian, "Environmental Effects on Fatigue Crack Growth Rates in Silver", J. Int. Metals, Vol. 99, 1971, pp.243-247

[96] T. Ericsson, "Review of Oxidation Effects on Cyclic Life at Elevated Temperature", Canadian Metallurgical Quarterly, Vol. 18, 1979, pp.177-195

[95] M. R. Achter, G. J. Danek and H. H. Smith, "Effect on Fatigue of Gaseous

Environments under Varying Temperature and Pressure", Transactions of the Metallurgical Society of AIME, **Vol. 227**, 1963, pp.1296-1301

[97] P. Kofstad, High Temperature Corrosion, Elsevier Applied Science Publisher LTD, 1988.

[98] J. R. Haigh, R. P. Skelton and C. E. Richards, "Oxidation-Assisted Crack Growth during High Cycle Fatigue of A 1%Cr-Mo-V Steel at 550°C", Materials Science Engineering, **Vol. 26**, 1976, pp.167-174

[99] L. Remy, F. Rezai-Aria, R. Danzer and W. Hoffelner, "Evaluation of Life Prediction Methods in High Temperature Fatigue", in Low Cycle Fatigue, ASTM STP 942, eds. by H. D. Solomon, G. R. Halford and B. N. Leis, American Society for Testing and Materials, Philadelphia, PA, 1988, pp.1115-1132

[100] B. Tomkins, "Fatigue Crack Propagation — An Analysis", Philosophical Magazine, **Vol. 18**, 1968, pp.1041-1066

[101] A. Pineau, "Elevated Temperature Life Prediction Methods", in Advances in Fatigue Science and Technology, eds. by C. M. Brauw and L. G. Rosa, Kluwer Academic Publishers, **Vol. 159**, 1989, pp.314-338

[102] A. Diboine, "Etude de la Propagation des Fissures En Fatigue-Fluage-Oxydation A 650°C Dans un Superalliage Base Nickel L'Inconel 718", Ph.D. dissertation of L'Ecole, Nationale Superieure des Mines de Paris, France, 1986

[103] D. A. Utah, "Crack Growth Modelling in an Advance Powder Metallurgy Alloy", AFWAL-TR-80-4098, Accession No. ADAO 93992, 1980

[104] C. G. Annis, Jr., R. M. Wallace and D. L. Sims, "An Interpolative Model For Elevated Temperature Fatigue Crack Propagation", AFML-TR-76-176, part I, Accession No. ADAO38070, 1976

[105] A. Dboine, "Etude de la Propagation des Fissures en Fatigue-Fluage-oxydation A 650°C Dans un Superalliage Base Nickel L'Inconel 718", Ph.D. Dissertation of L'Ecole Nationale Superieure des Mines de Paris, France, 1986

[106] J. C. Fisher, "Calculation of Diffusion Penetration Curves for Surface And Grain Boundary Diffusion", Journal of Applied Physics, **Vol. 22**, 1951, pp.74-77

[107] N. L. Peterson, "Grain-Boundary Diffusion in Metals", International Metals Review, **Vol. 28**, 1983, pp.65-91

[108] A. Atkinso, "Diffusion Along Grain Boundary and Dislocations in Oxides, Alkali

Halides and Carbides", Solid State Ionics, Vol. 12, 1984, pp.309-320

[109] N. L. Peterson, "Grain-Boundary Diffusion-Structural Effects, Models, and Mechanisms", in Grain-Boundary Structure and Kinetic, ASME Publication, Metals Park, Ohio, 1979, pp.209-238

[110] R. T. P. Whipple, "Concentration Contours in Grain Boundary Diffusion", Philosophical Magazine, Vol. 45, 1954, pp.1225-1236

[111] G. Martin and B. Perraillon, "Measurements of Grain Boundary Diffusion", Transactions of Faraday Society, Vol. 57, 1979, pp.239-295

[112] L. G. Harrison, "Influence of Dislocation on Diffusion Kinetics in Solid with Particular Reference to the Alkali Halides", Transactions Faraday Society, Vol. 57, 1961, pp.1191-1199

[113] G. Glinka, "Relations between the Strain Energy Density Distrabution and Elastic-Plastic Fields near Cracks and Notches and Fatigue Life Calculation", in Fracture Mechanics: Sixteenth Symposium, ASTM STP 868, eds. by M. F. Kannien and A. T. Hopper, American Society for Testing and Materials, Philadelphia, PA, 1988, pp.1022-1047

[114] J. L. Chaboche, "Constitutive Equations in Creep-Fatigue Damage", in Engineering Approches to High Temperature Design, eds. by B. Wilshire and D. R. J. Owen, Vol. 2, Pineridge Press, Swansea, U. K., 1983, pp.177-235,

[115] T. G. Tanaka, "A Unified Numerical Method for Integrating Stiff Time Dependent Constitutive Eequations for Elastic/Visco-Plastic Deformation of Metal and Alloys", Ph.D. Dissertation of Stanford University. USA, 1983

[116] J. L. Chaboche and G. Cailletaud, "On the Calculation of Structures in Cyclic Plasticity or Viscoplasticity", Computer & Structures, Vol. 23, 1986, pp.23-31

[117] V. Moreno and E. H. Jordan, "Prediction of Material Thermo-Mechanical Response with A Unified Viscoplastic Constitutive Model", International Journal of Plasticity, Vol. 2, 1986, pp.233-245

[118] E. Krempl, "The Role of Servocontrolled Testing in the Development of the Theory of Viscoplasticity Based on Total Strain and Overstress", in Mechanical Testing for Deformation Model Development, ASTM STP 765, American Society for Testing and Materials, Philadelphia, PA, 1982, pp.5-28

[119] H. Riedel and J. R. Rice, "Tensile Cracks in Creeping Solids", in Fracture Mechanics: Twelfth Conference, ASTM STP 700, American Society for Testing

and Materials, Philadelphia, PA, 1980, pp.112-130

[120] Source Book on Industrial Alloy and Engineering Data, Compiled by Publications Department, American Society for Metals, Metals Park, Ohio, 1978

[121] D. M. R. Taplin, N. Y. Tang and H. H. E. Leipholz, "On Fatigue-Creep-Environment Interaction and Feasibility of Fatigue Maps", in Advances in Fracture Research, eds. by S. R. Valluri, D. M. R. Taplin, P. R. Rao, J. F. Knott and R. Dubey, Pergaman Press, New York, Vol. 1, pp.127-142, 1986

APPENDIX I

MATERIAL DESCRIPTION

The objective of this appendix is to describe in detail the aspects of physical metallurgy of Alloy 718. This includes the phases of the microstructure, the properties, the strengthening mechanisms and the associated deformation mechanisms in Alloy 718.

As a precipitation-hardenable nickel-chromium alloy developed by Eiselstein [122] in the late 50's, Alloy 718 combines corrosion resistance and high strength with outstanding weldability. This alloy contains significant amount of iron, niobium and molybdenum along with lesser amounts of aluminum and titanium, its nominal composition is given in Table A1.1. The matrix of Alloy 718 is nickel plus iron forming the austenitic γ phase. Elements which partition largely to matrix are chromium and molybdenum. The chromium provides oxidation resistance while both chromium and molybdenum contribute to solid solution strengthening. The niobium, titanium and aluminum govern the phase precipitation characteristics of Alloy 718 while the small additions of carbon and boron are intended to enhance grain boundary strength and ductility. Addition of Nb promotes the γ'' precipitation [123], but the increase in (Ti+Al)/Nb ratio may favor γ' rather than γ'' precipitation [124]. The effects of several elements in nickel-base superalloys are summarized in Table A1.2 [125,126].

I.1 Phases in Alloy 718

Alloy 718 has a large number of phases which either have characteristic

Ni	Cr	Fe	Ti	Mo	Nb+Ta	Al	
50-55	17-21	13.2-22.5	0.65-1.15	2.8-3.3	4.75-5.5	0.2-0.8	
C	S	Si	P	B	Co	Mn	Cu
<0.08	<0.015	<0.35	<0.015	<0.006	<1.0	<0.35	<0.3

Table A1.1 The Nominal Composition of Alloy 718 (wt%)

Effect	Elements	Effect	Elements
Solid-solution Strengtheners	Co,Cr,Mo,W,Ta	Oxidation resistance	Cr
MC carbide former	W,Ta,Ti,Mo,Nb	Sulfidation resistance	Cr
M_7C_3 carbide former	Cr	Increases rupture ductility	Zr,B
$M_{23}C_6$ carbide former	Cr,Mo,W	Causes grain-boundary segregation	B,C,Zr
M_6C carbide former	Mo,W	Raises solvus temperature of γ'	Co
Carbonitrides M(CN) type	C,N	Hardening precipitates	Al,Ti,Nb
Forms γ'	Al,Ti	Forms γ''	Nb

Table A1.2 Role of Elements in Nickel-base Superalloys

morphologies or will form in a specific temperature range. Besides the FCC γ phase matrix, the phases normally found in Alloy 718 are disk-shaped γ'' (Ni_3Nb, Al); spheroidal γ' (Ni_3Al, Ti); a needle/plate-like δ phase, also called β phase in some literature (Ni_3Nb); a round, island-like Laves phase [(Ni, Fe, Cr)$_2$(Mo, Nb, Ti)]; discrete MC carbides; M_6C carbides which may form as a boundary film during service; $M_{23}C_6$ carbides ($Cr_{23}C_6$) were also identified at grain boundaries [124]. The MC phase forms on solidification and remains stable to about 1204°C. The Laves phase forms on solidification in high-niobium interdendritic areas and is stable up to 1177°C, it tends to deplete the matrix of the elements required for precipitation hardening, thereby reducing strength [127]. The δ phase forms on cooling during solidification in high-niobium areas and is stable up to 1010°C in wrought and 1121°C in cast 718, precipitating from 843°C to 982°C. The γ'' phase forms during cooling or heat treatment at 732°C to 900°C. The γ' phase forms on cooling or when heat treatment is in the range of 718°C to 621°C.

It has been shown that in Alloy 718 under the long time (>5000 Hr) thermal exposure (530°C - 718°C) with stress two microstructural grain boundary changes will be produced [47,128,129]. The first change is the precipitation of δ phase along the grain boundaries with the formation of a denuded zone of γ'' precipitates. The second change is the precipitation of blocky particles which were identified as a phase rich in chromium, termed as αCr phase. This phase precipitated along grain boundaries and began to form as low as 593°C. The formation of αCr phase is very dependent on the stress state of the material, it can be formed at much shorted time under creep conditions [47]. Radavich even found σ phase existed during long service conditions at high temperatures. The

long-time structural transitions in Alloy 718 are as follows [130]:

538°C $\gamma'' + \gamma' \rightarrow \gamma'' + \gamma' + \delta$

593°C $\gamma'' + \gamma' \rightarrow \gamma'' + \gamma' + \delta + \alpha Cr$

621°C $\gamma'' + \gamma' \rightarrow \gamma'' + \gamma' \delta + \alpha Cr$

649°C $\gamma'' + \gamma' \rightarrow \gamma'' + \gamma' + \delta + \alpha Cr + \text{Trace}\ \sigma$

704°C $\gamma'' + \gamma' \rightarrow \gamma'' + \gamma' + \delta + \alpha Cr + \sigma$

The time-temperature-transformation (TTT) diagram for Alloy 718 was studied by number of authors [47,131-133] and the typical TTT diagrams are shown in Fig. A1.1. From these TTT diagrams the following phase transforms can be occurred. Over the temperature range of about 649°C to 871°C, precipitation of γ', γ'' and δ phases is shown to follow $\gamma' \rightarrow \gamma'' \rightarrow \delta$ transformation sequence. Solutioning of the γ'' phase begins to occur between 843°C and 871°C. This event is associated with the formation of large amount of δ phase. The γ' solvus is somewhat lower and the solutioning of this phase is complete at 843°C. This TTT diagram also shows that δ phase forms most rapidly at about 941°C and has a solvus temperature near 982°C. Fig. A1.1(b) also shows MC carbides, M_6C carbides, and Laves phase that precipitate in the alloy base metal over the temperature range of about 700°C to 1040°C. All of these phases go into solution around 1065°C. Because the grain-boundary phases are going into solution and are therefore no longer pinning the boundaries, grain growth occurs rapidly at temperature about beyond 1040°C. Based on the knowledge of TTT diagram of Alloy 718, the common used heat treatments of this material are listed in Table A1.3.

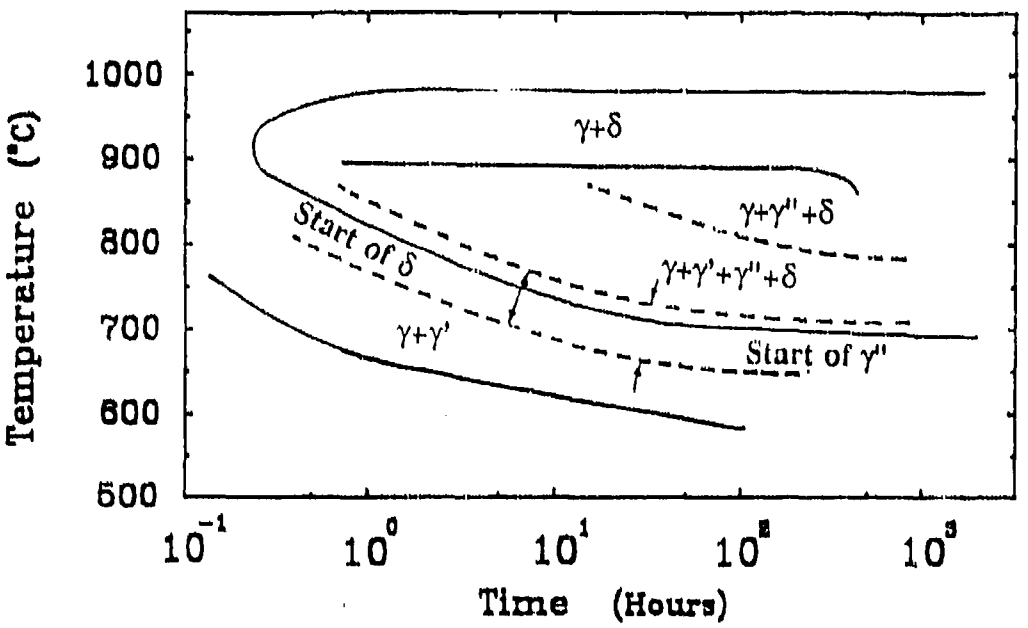

(a)

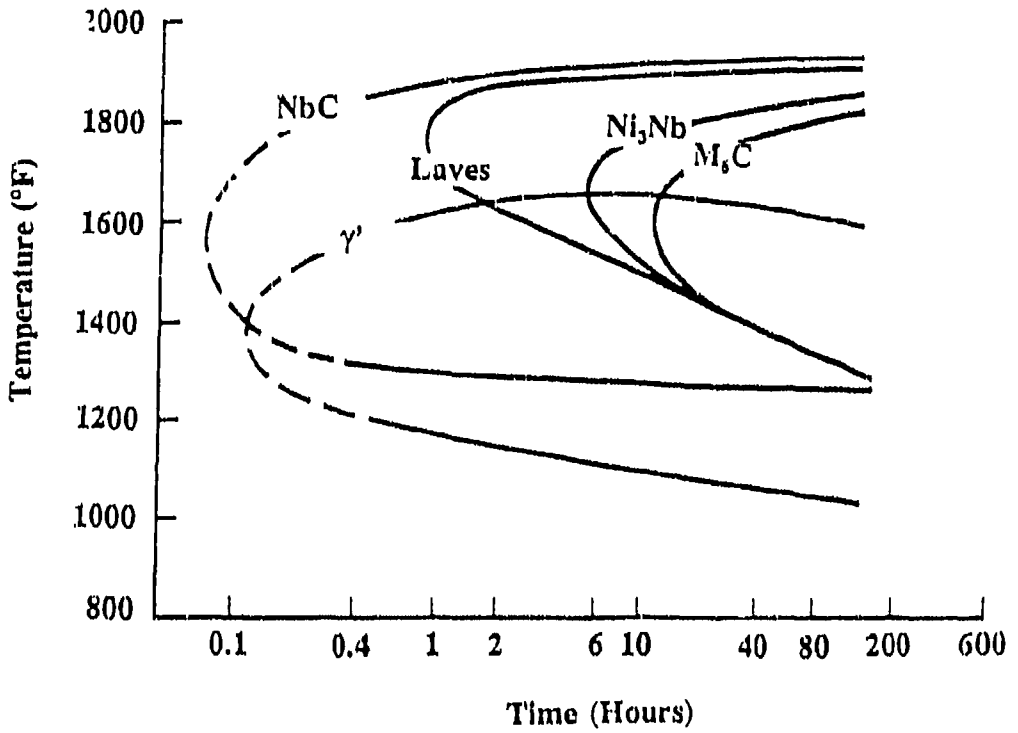

(b)

Fig. A1.1 Time-Temperature-Transformation diagrams for Alloy 718.

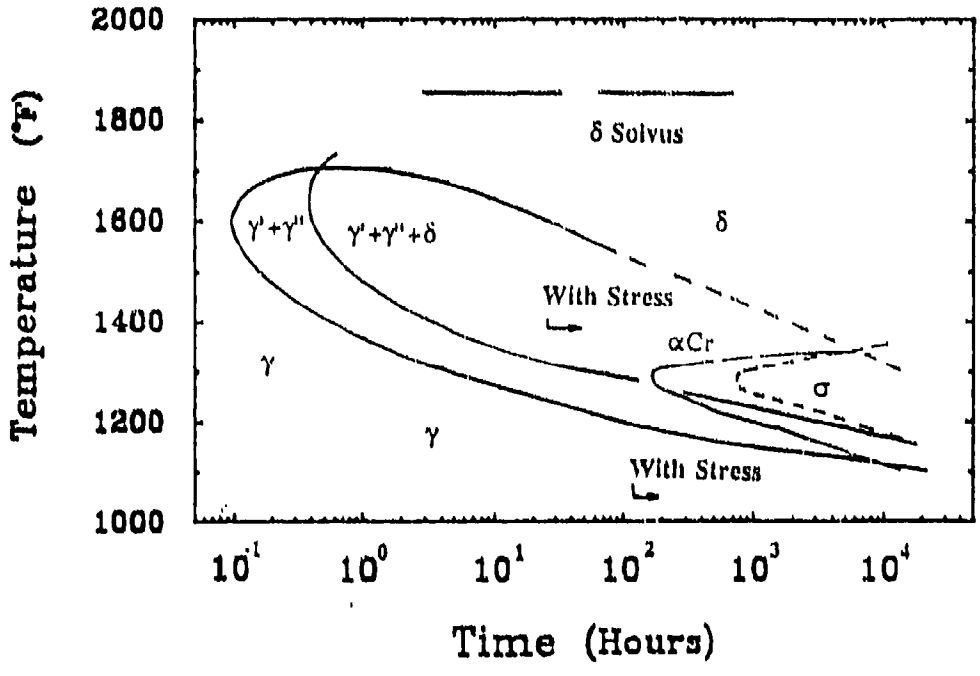

(c)

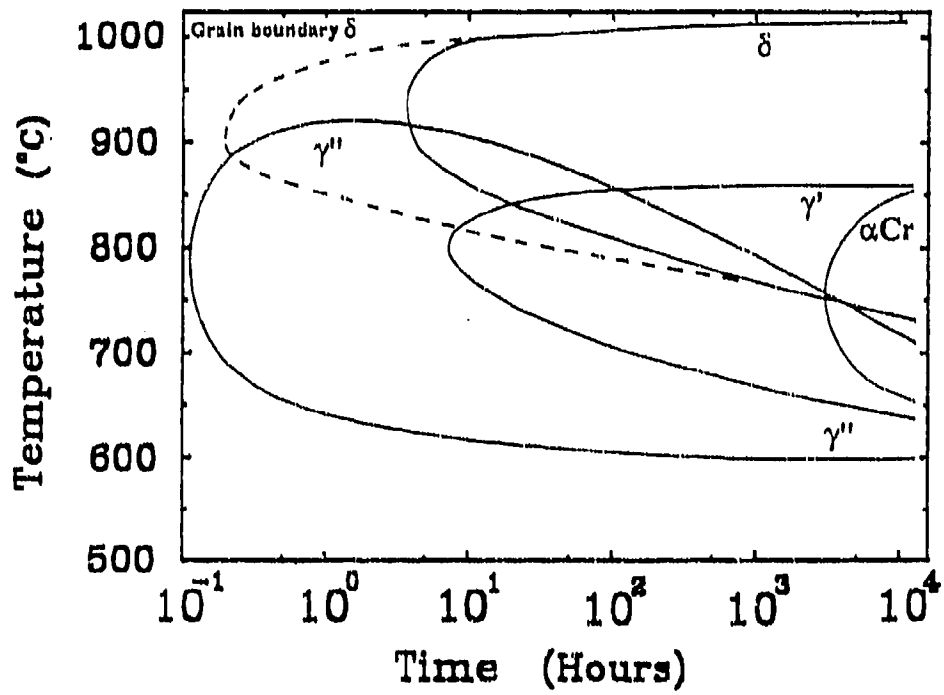

(d)

Fig. A1.1 Time-temperature-transformation diagrams for Alloy 718 (cont.).

Conventional Heat Treatment (CHT)	
Solutioning: (Annealing)	954°C for 1 hr then air cool or faster.
Precipitation Aging: (Duplex Aging)	718.3°C for 8 hrs, furnace cool to 621.1°C at a rate not to exceed 37.8°C/hr, hold at 621°C for 8 hrs and air cool to room temperature.
Modified Heat Treatment (MHT)	
Solutioning:	1093°C for 1 hr, furnace step cooled at 38°C/hr to below 538°C, He cooled to room temperature.
Precipitation Aging:	718.3°C for 4 hr step cooled at 37.8°C/hr to 621°C for 16 hr, then He cooled to room temperature.

Table A1.3 Heat Treatments of Alloy 718

I.1.1 Strengthening Phases

Analysis of the conventionally heat-treated Alloy 718 showed that both γ' and γ'' precipitates enhance the mechanical properties of the alloy, the volume fraction of γ''phase has been observed to be about 15% while that of γ' phase was about 4% [135]. The major strengthening phase in Alloy 718 has been reported to be the γ'' phase [134-136]. γ' phase has a FCC ($L1_2$) structure with spherical shape. Although a small amount of γ' is present, it is believed that any strength contributed by this phase is incidental [134]. The γ'' phase is coherent and has an DO_{22}-ordered body-centered-tetragonal (BCT) structure. The stoichiometry of γ'' is given as Ni_3(Nb, Ti, Al) [137,138]. The lattice parameters for γ'' phase are a_0 = 0.3624 nm and c_0 = 0.7406 nm, and the unit cells for γ' and γ'' are shown in Fig. A1.2. For the conventional heat-treated Alloy 718, the volume fraction of the strengthening phase (primarily γ'') is about 20 % [135]. The γ'' precipitates as disc-shaped particles and with the following orientation relationship:

$$(001)\gamma'' \,||\, (001)\gamma \text{ and } [100]\gamma'' \,||\, \langle 100\rangle\gamma$$

and the c axis is normal to the plane of the disc. Kirman and Warrington [136] have pointed out that the matrix / γ'' precipitate misfit is concentrated in the direction parallel to the c axis, and they estimated that this misfit is about 2.5% whereas that in the plane of the plate is only about 0.8%. It has been observed [124] that the γ'' particles are always seen adjacent to the γ' precipitates, and they believed that γ' particles are potential nucleation sites for γ'' phase. Examination of the two unit cells drawn on Fig. A1.2 shows that the γ'/matrix interfaces can be very favorable nucleation sites for γ'' phase. Except for the measured slight distortion along the a axis and the higher distortion

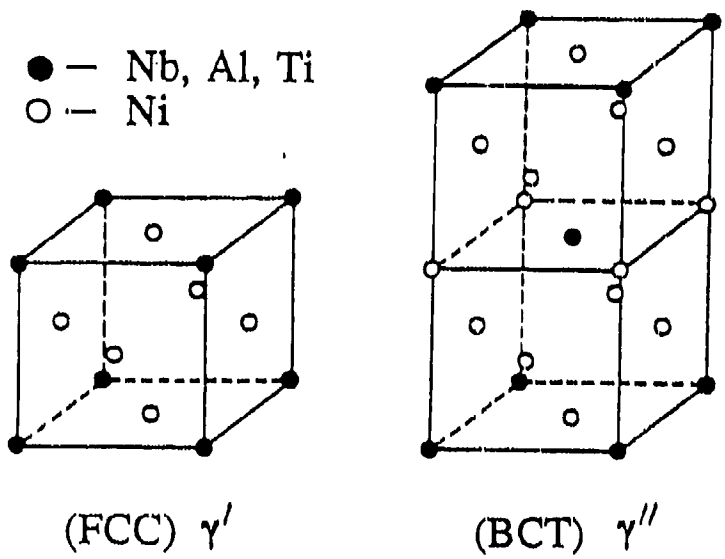

Fig. A1.2 Unit cells showing ordering. (a) FCC ($L1_2$) structure; (b) BCT (DO_{22}) structure.

along the c axis of DO_{22}-ordered structure, the two phases represent ordered variations of the FCC lattice. In the γ' phase, Nb (Al, Ti) atoms are located at the cube corners, while in the γ'' phase, Nb atom occupies the center and the corners of a cell are formed by putting two FCC cells one upon the other. The sizes of γ' and γ'' phases for different heat treatment conditions are listed in Table A1.4 [135]. During prolonged thermal exposure, the growth of γ' and γ'' were observed by several investigators [9,16,135]. Paulonis et al [135], Pedron and Pineau [139] reported that there was no apparent change in volume fraction and only slight coarsening of the γ'' phase (5%-10%) during 100 hr at 649°C. However, considerable coarsening of the γ'' phase occurred during the 100 hr age at 760°C, and the particle volume fraction is sufficiently lower [135].

It worth mentioning that a peculiar precipitation microstructure, compact morphology, has been identified by Cozar and Pineau [124]. It appears to be cube-shaped γ' particles coated with a γ'' shell over their six faces. This morphology has proved to have a very slow rate of coarsening. The condition to achieve this morphology requires a minimum (Ti+Al)/Nb ratio between 0.9 and 1.0. Moreover the ageing temperature has to be chosen in such a way that initially isolated γ' precipitates reach a size of about 200Å before production of γ'' precipitates.

Oblak et al [134] studied the ageing effect on the γ'' phase under stress conditions. They found that the γ'' precipitate forms as ellipsoidal discs lying on {100}. Because the coherent γ'' particles produce a tetragonal distortion of the matrix, the specific variants present can be controlled by application of stress during ageing. For example, only the [001] γ'' variant is formed when a tensile stress is applied along [001]. Reversing the

Heat Treatment	Alloy 718	
	γ' (diameter of sphere)	γ'' (diameter of disc) (thickness: 50-90 Å)
CHT	250 Å	600 Å
CHT+649°C/100 hr	300 Å	725 Å
CHT+760°C/100 hr	600 Å	3000 Å
CHT+843°C/16 hr	750 Å	3500 Å
CHT+871°C/16 hr	—	5500 Å

Table A1.4 Dimension of γ' and γ'' in Alloy 718

stress suppressed the [001] γ'' variant and promotes formation of the [100] and [010] variants. The effect upon strength is significant. The critical resolved shear stress of the former structure is 25% higher than that of standard aged material, while that of the latter is 6% less. This stress-enhanced coarsening of the γ'' precipitates also observed by Radavich [128] and Molins et al [129].

I.1.2 δ Phase

Both γ' and γ'' phases in Alloy 718 are metastable [135], while the γ'' phase is less stable phase than the γ' phase [139]. Upon prolonged thermal exposure the γ'' phase will be replaced by the stable precipitate δ phase. It has an incoherent orthorhombic structure (DO_a) with a stoichiometry of Ni_3Nb [16,140]. The δ phase precipitates as laths (in a Widmenstätten-type morphology) along {111}γ planes with the following orientation relationship:

$$(010)\delta \,||\, \{111\}\gamma \text{ and } [100]\delta \,||\, \langle 110\rangle\gamma$$

The δ phase may also form by a cellular precipitation along grain boundaries [136]. Cozar and Pineau [124] have pointed out that the metastable γ'' particles are dissolved near the δ-Ni_3Nb lathe and only γ' phase remains. Thus, formation of δ phase is detrimental to the strength of the material [139]. Moreover, the γ'' → δ phase transformation is largely accelerated by prior deformation, since it has been shown that planar defects present in the γ'' particles after deformation can be act as efficient nuclei for the precipitation of the stable δ phase [15,141]. This concept has been applied to develop a etching technique for measuring the monotonic zone interface to the fracture

surface [140].

Additional to the amount, Wilkinson [142] found that the morphology of the δ phase is important to the mechanical properties. His work showed that during forging δ phase tends toward spheroidization, which appears to be a preferred morphology. If strain is occurring in a temperature range where δ phase is precipitating, then growth of this phase tends to be discontinues and occurs in short lath type particles within and emanating from the grain boundaries, growing into the grains along crystallographic planes. If material is heated into a temperature range for δ phase precipitation and no deformation or inadequate deformation is carried out, then δ precipitation tends to occur in a more continuous fashion along the grain boundaries and in long needles across the grain width. This morphology has been shown to have an adverse effect on stress rupture ductility and fracture toughness. Brooks and Bridges [47] obtained similar conclusion, and they believed that a microstructure which contains an even distribution of discrete grain boundary δ particles is required to prevent notch sensitive stress rupture behavior.

The effects of δ phase on the mechanical properties are quite subtle. As is just mentioned, deformation of Alloy 718 at elevated temperatures promotes the formation of δ platelet. Presumably the deformed regions in the γ'' phase act as nuclei for δ phase transformation. The local re-ordering of the γ'' lattice along with the similarity of the δ and γ'' compositions should provide for a rapid nucleation event as well as rapid growth since only short range diffusion would be required to convert γ'' phase into δ phase. The formation of deformation-induced δ phase will naturally reduce the strength since Nb is drawn from the principal strengthening phase, γ''. However, the effect of δ phase is not

totally negative, since at grain boundaries it can provide some oxidation resistance or by providing oxygen traps through an increase in the boundary area [35,143]. Such a mechanism would tend to reduce the effective diffusion rate and to require higher effective concentrations of oxygen in order to form deleterious oxides. The ready formation of δ phase by deformation processes at 650°C and above is a major consideration for Alloy 718 in limiting its use to temperature below 650°C. Another use of the δ phase to pin down the boundaries during forging is well known [139]. For wrought Alloy 718 processed below the δ solvus, grain boundary migration is inhibited by the presence of this phase and microstructures retain a fine grain size. Subsequent thermal exposure above this temperature dissolves the δ phase and allow more rapid grain growth.

I.1.3 Laves Phase

Laves phase which is a hexagonal A_2B type intermetallic compound has been identified in Alloy 718. The usual formulae of this phase have been found to be $Fe_2(Nb,Ti,Mo)$, Co_2Ti and $(Ni_{0.5}Fe_{0.25}Cr_{0.25})_2(NbMoSi)$ [144]. The lattice parameter was determined to be $a_0 = 0.47$ nm and $c_0 = 0.75$ nm. Burke et al [144] found that this phase formed either during the solidification process or during the anneal at 1038°C. Investigations [37,139] have shown that the Laves islands are the crack initiation sites. The presence of the Laves phase in wrought materials is a result of incomplete homogenization of the alloy prior to final heat treatments. It has been found that the formation of the Laves phase requires 10-12% Nb, the δ phase requires 6-8% Nb, the γ''

phase needs 4% Nb, while the γ' phase can form with Nb level below 4% [139]. For cast Alloy 718, the γ matrix rejects selectively the large atoms of elements such as Nb, Mo and Ti to the interdendritic regions during solidification. These elements can form MC carbide (NbC) and the Laves phase in the high Nb areas as the metal solidifies from about 1260°C to about 1093°C. In this case, the alloy is heavily segregated and consists of two type of regions: the dendritic regions which are concentrated in Fe, Cr and Ni while the interdendritic areas are very rich in Nb, Mo and Ti. Thus, the Laves phase forms, in general, preferentially in the interdendritic region.

It should be noted that the Laves phase contains about 25% Nb and the formation of this phase depletes the content of Nb in matrix which is needed for γ'' and γ' precipitation, thus the presence of the Laves phase is adverse to mechanical properties. Practically, in order to reduce the presence of the Laves phase and produce a uniform material for forging, the homogenization process is critical. Basically, this homogenization process consists of the Laves phase solutioning and uniform Nb distribution. Solution of the Laves phase is to carefully heat up to the Laves solvus (about 1200°C) and hold there for a period of time (e.g. 2 hrs), then rapidly cooling from solutioning temperature to prevent the reprecipitation of the Laves phase. To uniform the Nb distribution, a duplex aging treatment is usually applied [37]. Current technology of homogenization process includes two types: thermal treatment and thermal-mechanical treatment (hot isostatic pressing or HIP). The work of Smith and Michel [37] showed that both thermal treatment and HIP can improve high temperature fatigue crack growth resistance remarkably.

I.1.4 Carbides

Various carbides are present in Alloy 718 [124,145,146]. The MC carbides (usually (Ti,Nb)C) have a cubic structure with a lattice parameter a_0 = 0.43 - 0.47 nm. They are very stable compounds and are formed during cooling. They exist in blocky or script morphologies and are distributed heterogeneously throughout the alloy, both in intergranular and transgranular positions, often interdendritically. The MC carbides are a major source of carbon for subsequent phase reactions during heat treatment and service. It should be mentioned that carbonitrides ((Ti,Nb)(C,N)) sometimes are also classified into MC type [145,146].

The M_6C carbides have a FCC structure with a lattice parameter a_0 = 1.085 - 1.175 nm. The usual formulae of M_6C are Fe_3Mo_3C, Fe_3Nb_3C and Nb_3Co_3C. They can be formed during heat treatment or service in material containing relatively high molybdenum content and can also be formed from degeneration of MC carbides. They usually have a blocky intergranular morphology.

The $M_{23}C_6$ carbides, with a FCC structure and a lattice parameter a_0 = 1.05 - 1.07 nm, are formed during lower-temperature heat treatment and service (760°C to 980°C) from degeneration of MC carbides and from soluble residual carbon in the alloy matrix. The common compositions of $M_{23}C_6$ are $Cr_{21}Mo_2C_6$, $Cr_{23}C_6$ and $(Cr,Fe,Mo)_{23}C_6$. Although usually seen at grain boundaries as a platelet morphology, they occasionally occur along twin bands.

The M_7C_3 carbides have a hexagonal structure with lattice parameters a_0 = 1.398 nm and c_0 = 0.4523 nm. They typically have blocky intergranular morphology, and the

most common formula of M_7C_3 is Cr_7C_3.

In addition to the γ'' phase strengthening, investigators [47,122,124,137,140,146] have suggested that niobium carbide (NbC) precipitation may also enhance the properties of Alloy 718. Carbide type, distribution and morphology have been shown to affect properties of this alloy, particularly ductility and stress rupture [137].

I.2 Mechanical Properties of Alloy 718

Since Alloy 718 has been used in all kinds of applications which involves static and cyclic loadings and where exposure at elevated temperatures for extended times is required, thus the mechanical properties of this material, including the behaviors of tensile, creep, low cycle fatigue, fracture, crack growth and time-dependent notch sensitivity, has been studied extensively. Also, some important physical properties of Alloy 718 are summarized in Table A1.5 [125] and Fig. A1.3 [125].

I.2.1 Tensile Strength and Ductility

Tensile strength and ductility are the most basic parameters for the design concern. Thus, a large number of research work associated with these properties has been carried out and the results are listed in Table A1.6 [14,15,147,148].

The Young's modulus, E, torsional modulus, G, and Poisson's ratio ν are tabulated in Table A1.7 [120,149].

Fournier et al [150] and Clavel et al [13] also studied the cyclic tensile behavior of Alloy 718 at 25°C and 650°C. They recorded the changes in load during the course

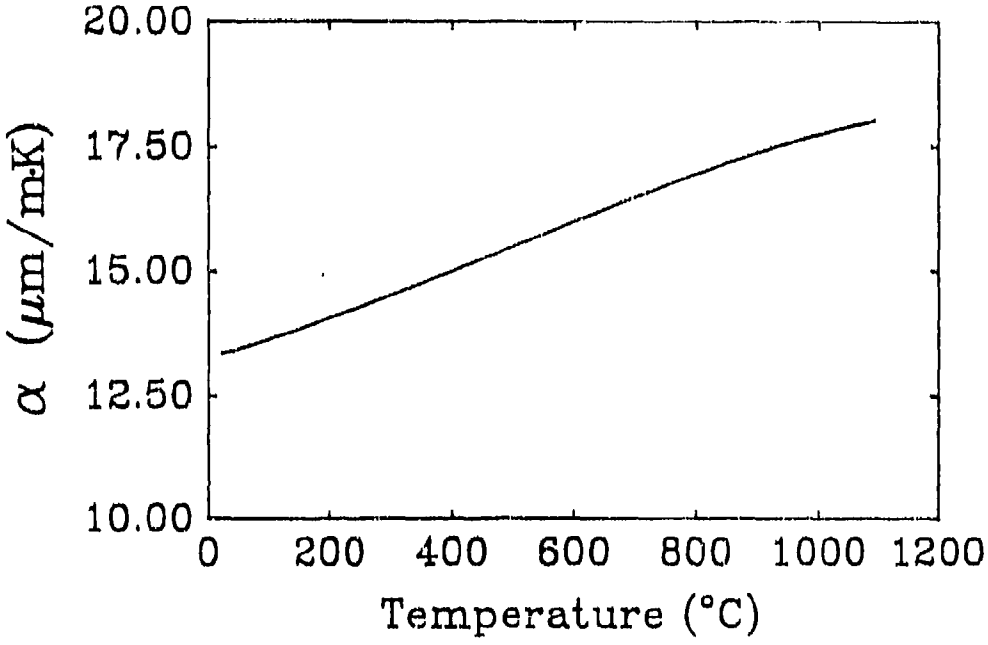

Fig. A1.3 Variations of coefficient of thermal expansion with temperature.

Density (g/cm^3)	Melting Range (°C)
annealed 8.193	1260°C — 1336°C
annealed and aged 8.221	

Table A1.5 Physical Properties of Alloy 718

Heat Treatment	Temperature (°C)	0.2% Yield Strength (MPa)	Ultimate Strength (MPa)	Elongation (%)	Reduction in Area (%)
CHT	24	1150	1420	16	37
CHT	427	1140	1235	20	40
CHT	538	1005	1235	18	41
CHT	550	1000	1200	18	35
CHT	650	975	1160	22	37
MHT	24	1030	1330	19	35
MHT	427	915	1160	17	38
MHT	538	895	1145	18	42

Table A1.6 Tensile Properties of Alloy 718

Temperature (°C)	E GPa	G GPa	ν
21	199.93	77.21	0.294
38	198.55	76.94	0.291
93	195.79	75.83	0.288
149	193.03	75.14	0.280
204	190.27	74.46	0.278
260	186.83	73.08	0.275
316	184.07	72.39	0.272
371	180.62	71.01	0.273
427	177.87	69.63	0.271
482	174.42	68.25	0.272
538	170.97	66.87	0.271
593	166.83	65.49	0.276
649	163.39	63.42	0.283
704	158.56	61.36	0.292
760	153.74	58.60	0.306
816	146.84	55.84	0.321
871	139.26	52.39	0.331
927	129.61	48.95	0.334
982	119.96	44.81	0.341
1038	109.61	33.64	0.366
1093	98.58	26.01	0.402

Table A1.7 Variation of E, G and ν with Temperatures

of the fatigue tests. Fig. A1.4 reported the variation of the cyclic tensile stress with the number of cycles. This figure shows that, at room temperature, Alloy 718 gives rise to a short period of rapid hardening followed by softening. The maximum load is obtained at a certain number of cycles which is smaller for the higher the applied strain amplitude.

At elevated temperature, the evolution of the load with the number of cycles was found to be different from that encountered at room temperature. The period of hardening was absent and the specimens soften from the first cycle. A comparison of the cyclic behavior of specimens tested at various temperatures is plotted in Fig. A1.5.

The comparison of the monotonic and cyclic tensile properties of Alloy 718 can also be made using monotonic and cyclic stress-strain curves, they are shown in Fig. A1.6. These results indicated that, at room temperature, Alloy 718 gives rise to softening when applied plastic strain amplitude is lower than about 1%. Above this value this alloy experiences a slight hardening as compared to the monotonic tensile curve. At 550°C and 650°C, only softening is observed in all the plastic strain range investigated. This softening is quite significant (≈20%) and is larger than that measured at room temperature. The cyclic softening behavior of Alloy 718 is related to its peculiar strengthening mechanism, and this will be discussed later.

Tensile properties of Alloy 718 thermally aged up to 50,000 hours were investigated by Korth and Trybus [150]. The tensile properties of Alloy 718 at room temperature after long term thermal exposure are listed in Table A1.8 [150]. Fig. A1.7 shows the effects of long term aging at 593°C and 649°C on yield and ultimate tensile strength, and Fig. A1.8 illustrates the effects on ductility. The results indicated an

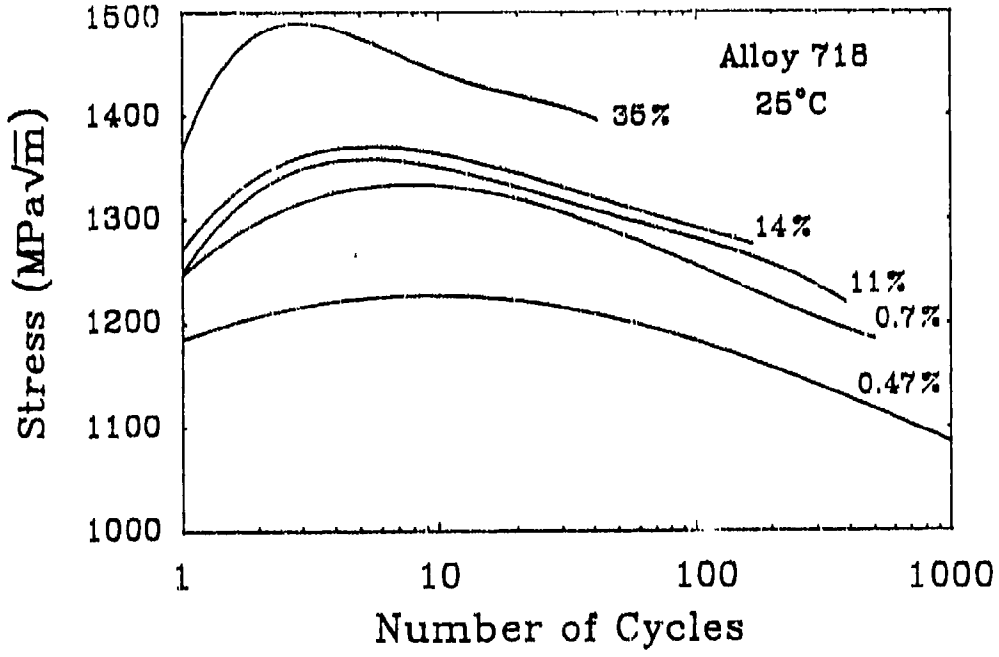

Fig. A1.4 Evolution of the cyclic tensile stress with the number of cycles at 25°C. Numbers denote plastic strain amplitude.

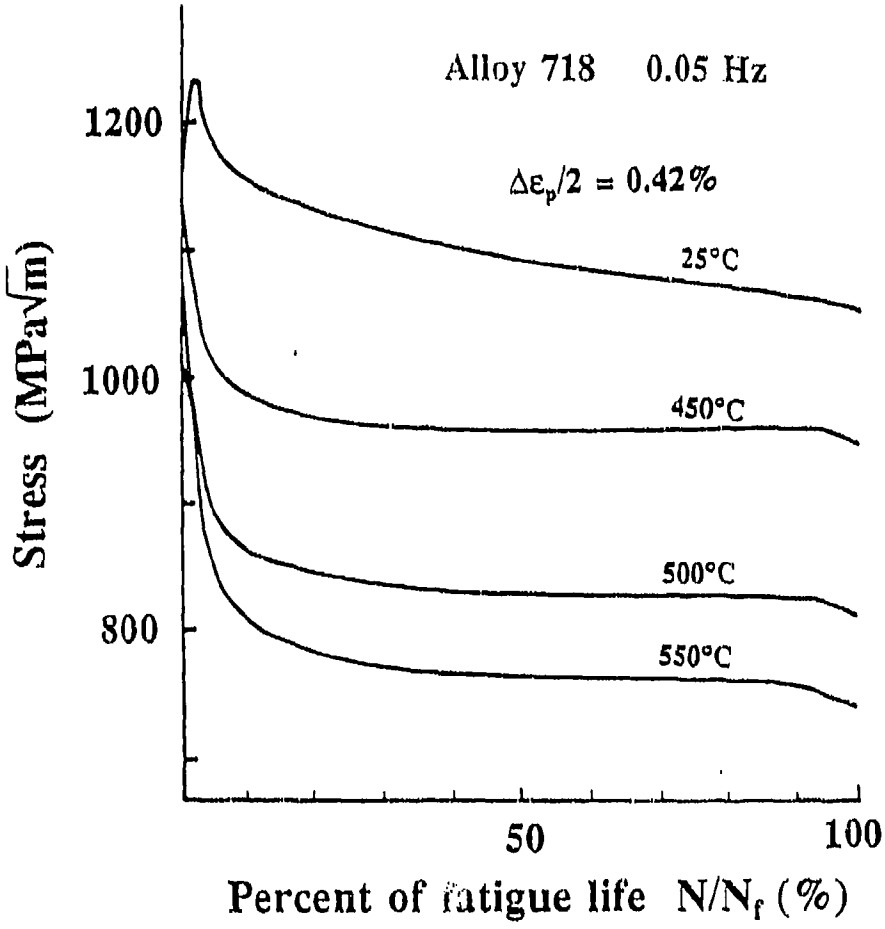

Fig. A1.5 Comparison of the cyclic stress-strain response of Alloy 718 at various temperatures for a plastic strain amplitude of 0.42% and a frequency of 0.05 Hz.

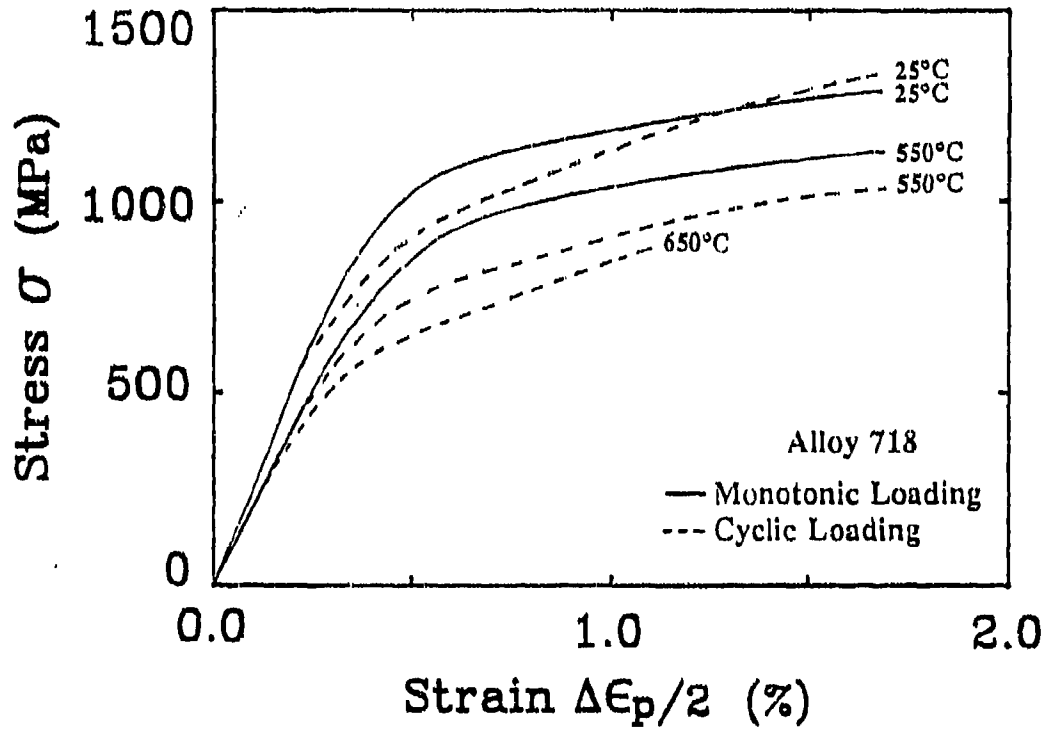

Fig. A1.6 Comparison of the cyclic stress-strain curves and monotonic tensile curves of Alloy 718 at 25°C, 550°C and 650°C.

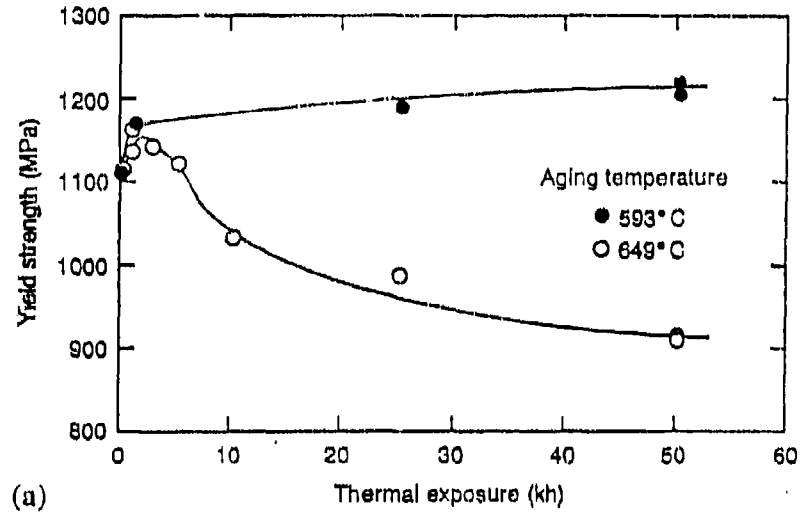

(a)

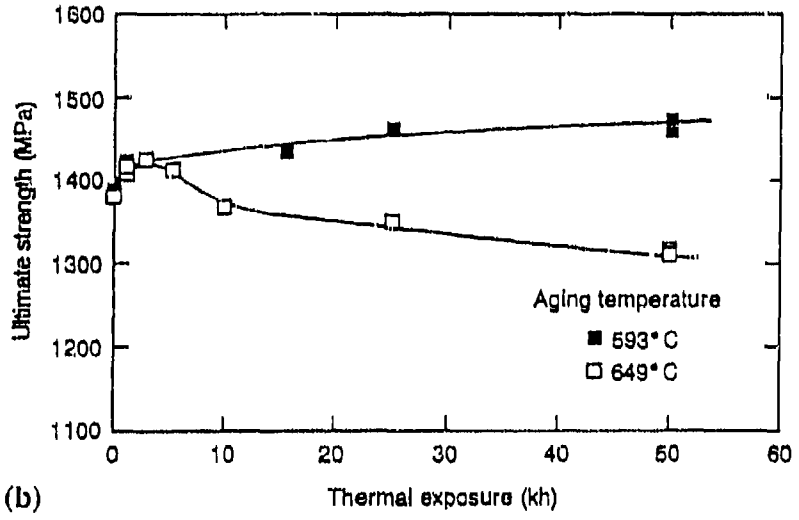

(b)

Fig. A1.7 Effects of long term thermal aging of Alloy 718 on the room temperature (a) yield strength and (b) the ultimate strength.

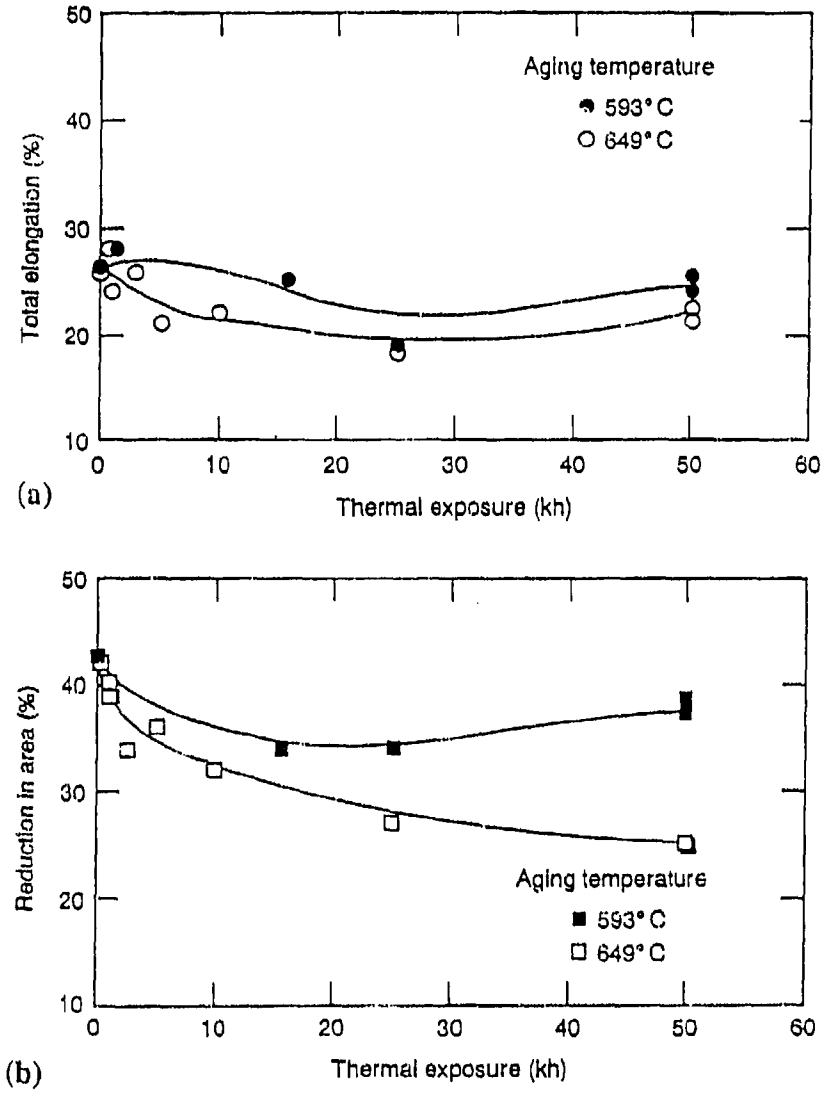

Fig. A1.8 Effects of long thermal aging of Alloy 718 on the room temperature (a) total elongation and (b) reduction in area.

Yield Strength (MPa)	Ultimate Strength (MPa)	Total Elongation (%)	Reduction in Area (%)	Aging History		
				Time (kh)	Temp (°C)	Stress (MPa)
1169	1419	28	39	1.2	593	538
1189	1461	19	34	25	593	0
1142	1426	26	34	2.7	649	338
987	1349	18	27	25	649	0

Table A1.8 Room temperature Tensile Data of Alloy 718

after Long Term Thermal Exposure

increase the hardening after 593°C aging up to 50,000 hr, with most of it occurring in the first few thousand hours. Aging at 649°C results in an increase in strength in the first few thousand hours of aging and then a gradual softening is observed.

I.2.2 Crack Growth Rate

A detailed review on fatigue crack growth rate of Alloy 718 is already given in Chapter 1, so in this section the attention will be focussed on the creep crack growth rate of Alloy 718. The typical creep crack growth rates versus stress intensity factor K for 538°C and 650°C are plotted [151,152] in Figs. A1.9 and A1.10. The grain size effect on creep crack growth in Alloy 718 at 650°C is illustrated by Liu et al [152] and Pedron et al [9] in Figs. A1.11 and A1.12. Research work has indicated that the distribution of the second phase in Alloy 718 could influence the creep crack growth behavior. Pedron et al [9] found that the presence of the δ phase along the grain boundaries leads to an improvement in crack growth resistance (shown in Fig. A1.13),while Liu et al [152] observed that carbide distribution also alters the creep crack growth behavior significantly (see Fig. A1.14). They believed that the carbide distribution determines the local fracture toughness and affects the creep crack growth behavior of Alloy 718 at 650°C via the tearing process.

I.2.3 Fatigue Strength and Life

A particular attractive property of this alloy is its fatigue strength at elevated temperatures. A number of studies [14,148,149] have been conducted on fatigue strength

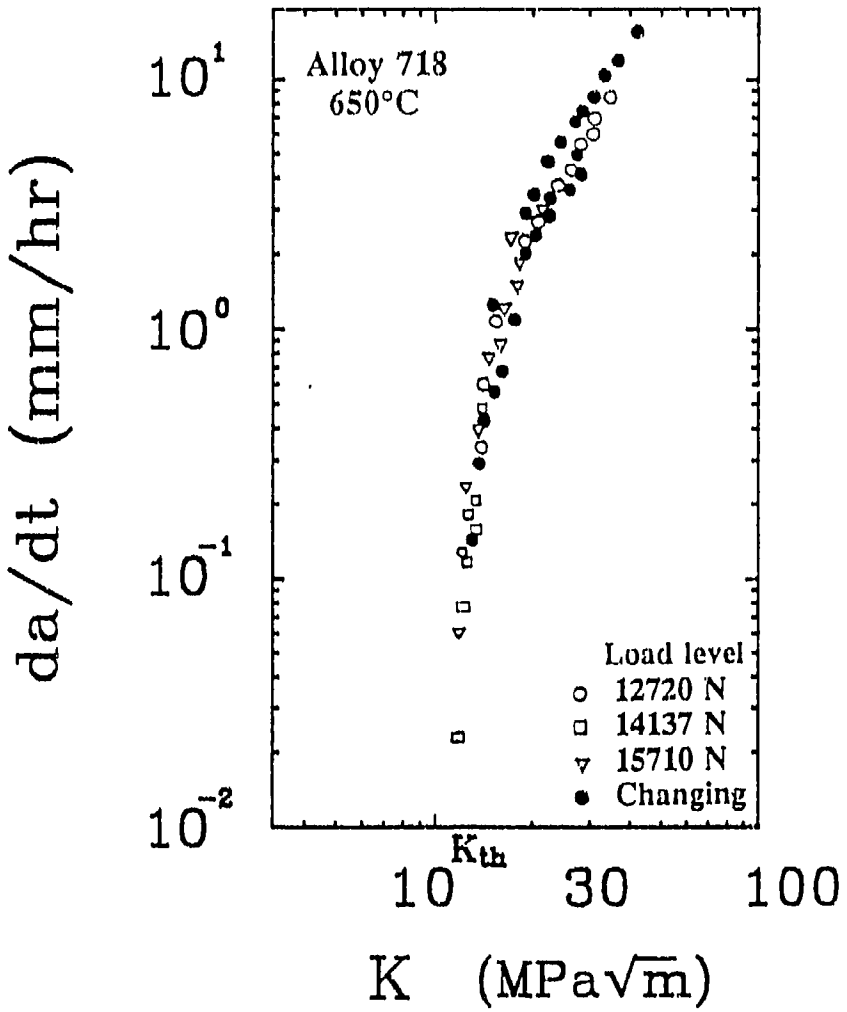

Fig. A1.9 Creep crack growth rate as a function of stress intensity factor K at 650°C.

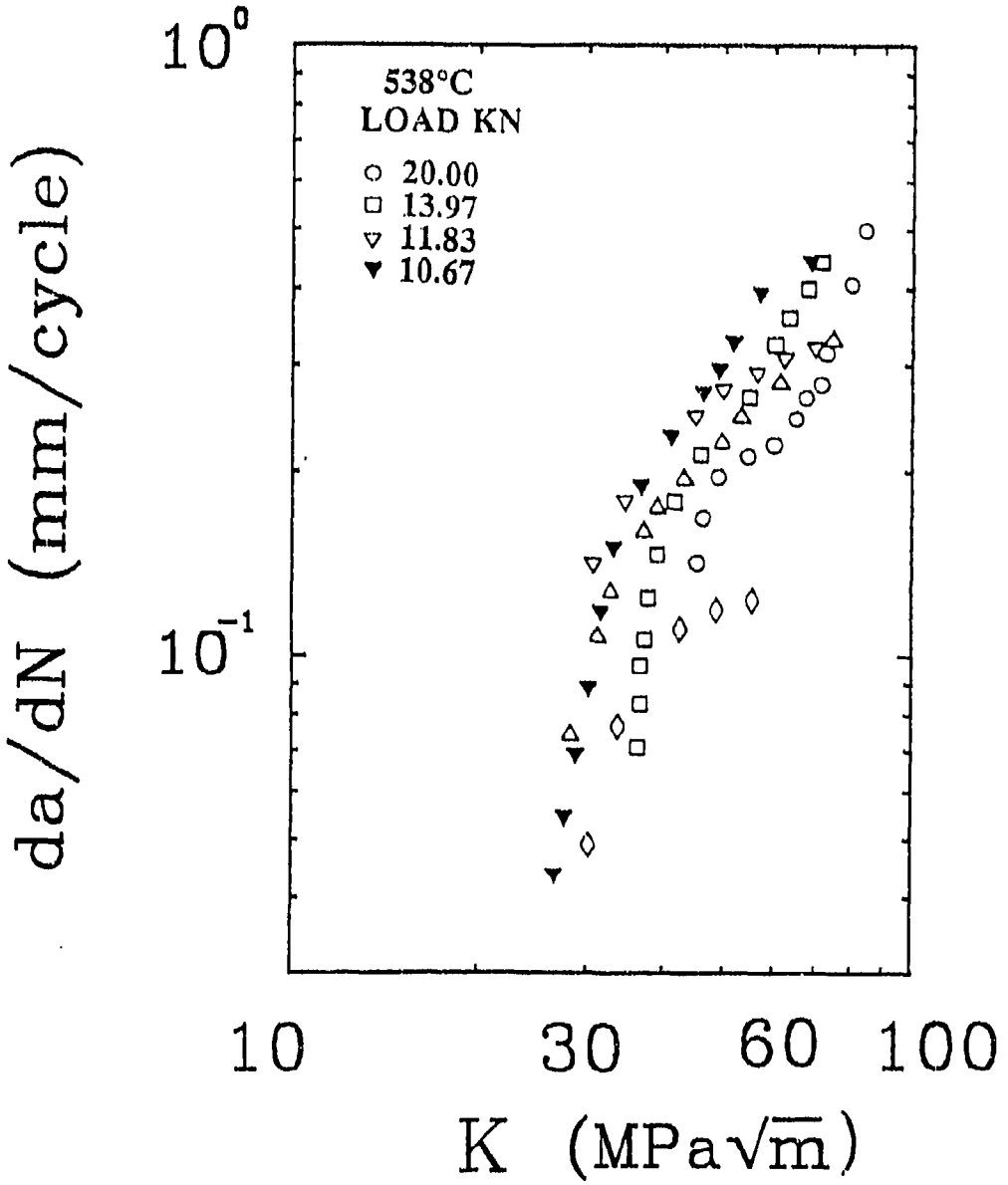

Fig. A1.10 Creep crack growth rate as a function of stress intensity factor K at 538°C.

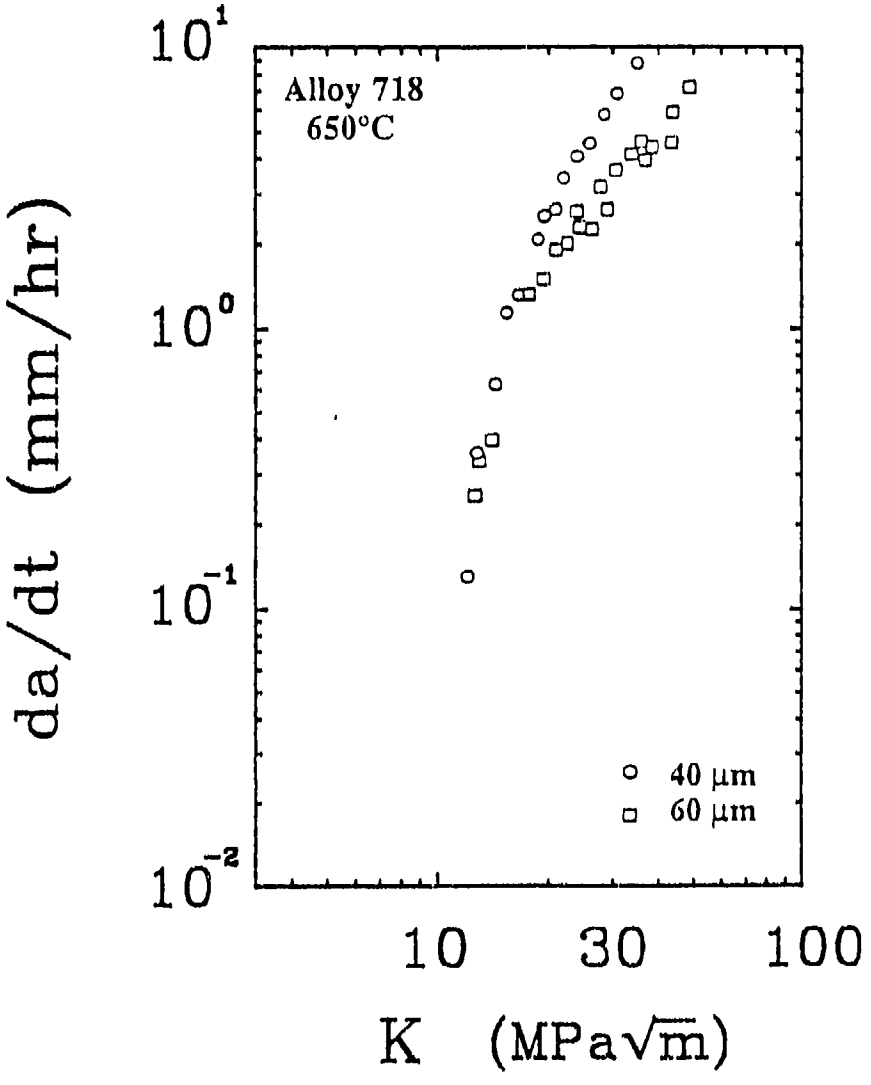

Fig. A1.11 Grain size effect on creep crack growth in Alloy 718 at 650°C.

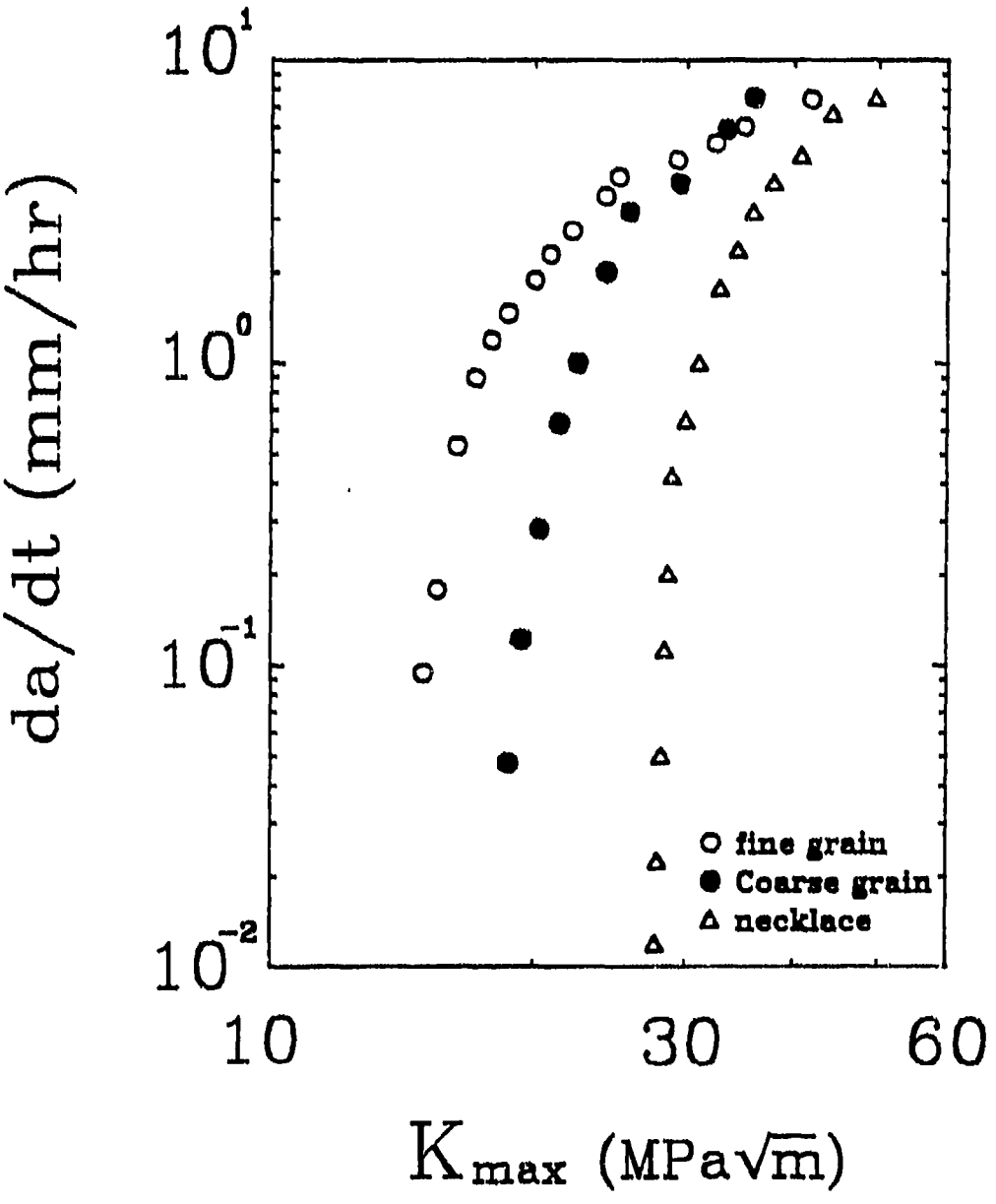

Fig. A1.12 Creep crack growth rate as a function of microstructure.

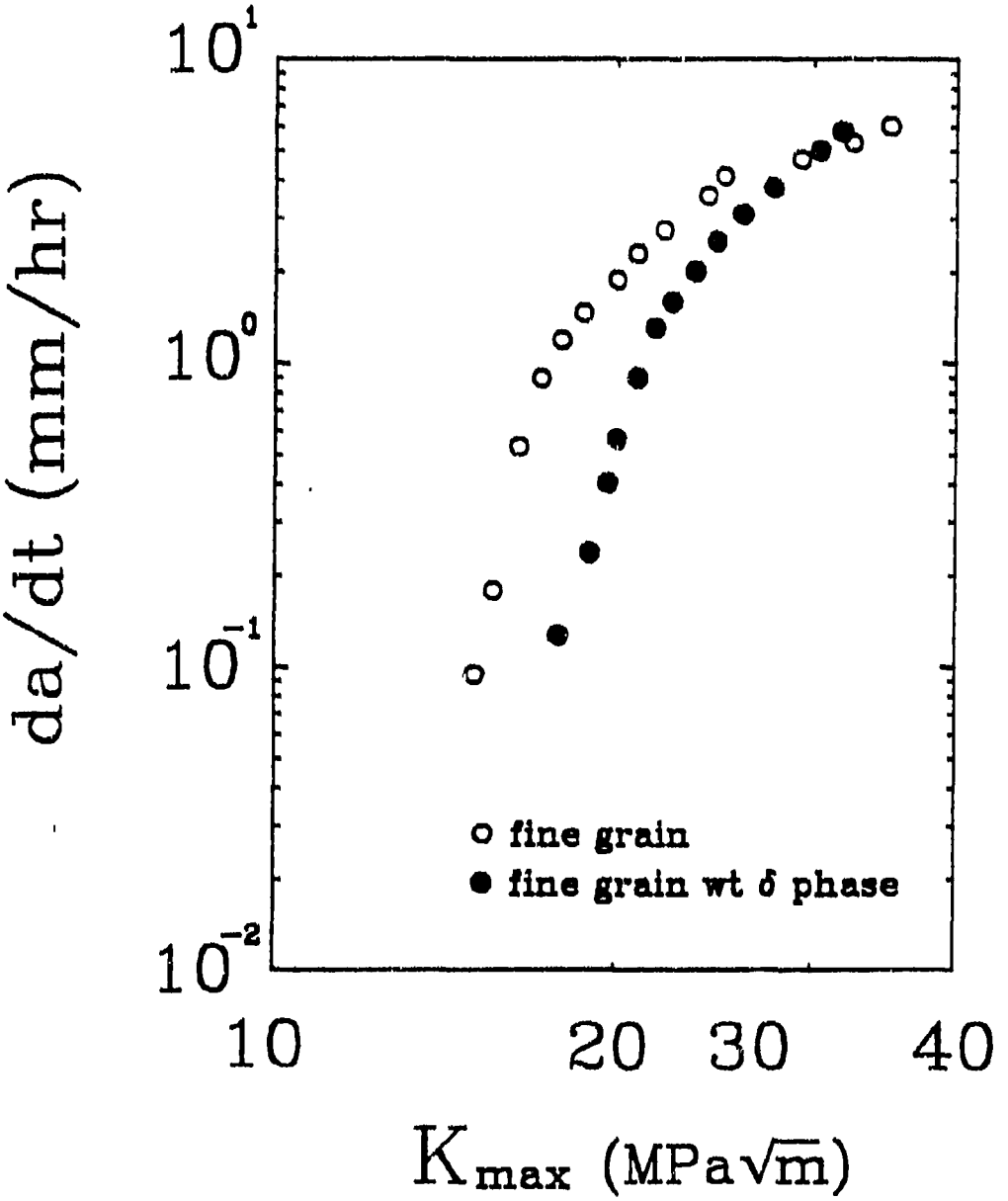

Fig. A1.13 Effects of presence of intergranular δ phase on creep crack growth rate at 650°C.

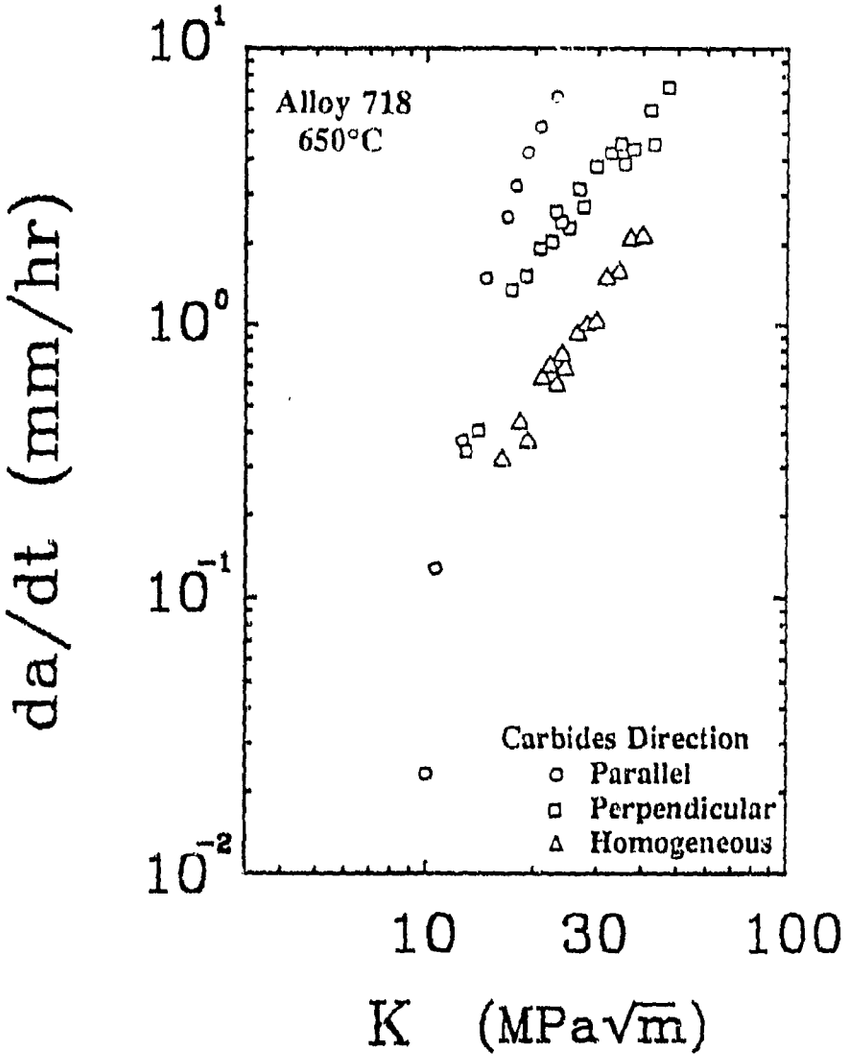

Fig. A1.14 Effects of carbide distribution on creep crack growth rate at 650°C.

and life of Alloy 718. Over 700 fatigue tests on several heats of Alloy 718 [149] were performed in Idaho National Engineering Lab at various temperatures and the loading frequencies are from 1 Hz to 167 Hz. The results are shown in Fig. A1.15.

Clavel et al [14] and Sanders et al [148] have examined the property of low cycle fatigue in Alloy 718. The variation in the fatigue life N_f with the plastic strain $\Delta\varepsilon_p$ or plastic strain amplitude $\Delta\varepsilon_p/2$ at various temperatures are illustrated in Figs. A1.16 and A1.17. It should be noticed that two distinct regions of life are existed.

Sanders et al [148] discussed the possible reason for the presence of a break in the curve. They thought that the nature of deformation process can be strongly affected by plastic strain amplitude, temperature and frequency. They postulated that the cyclic plastic behavior below 538°C is dominated by deformation twinning, and above 538°C the predominate mode of deformation is slip. Thus, the specimens tested above 538°C will have different strain-life response than those tested below that temperature.

I.2.5 Fracture Toughness

The fracture toughness is one of important mechanical properties for design concern. The room temperature and elevated temperature J_{Ic} and R-curve of conventional and modified Alloy 718 are illustrated in Figs. A1.18, A1.19 and A1.20 and tabulated in Table A1.9 [147].

These results indicated that fracture resistance for the MHT lots was consistently superior to that for their CHT counterparts, and the further work of Mills [147] found that fracture toughness for the CHT material was independent of temperature, whereas

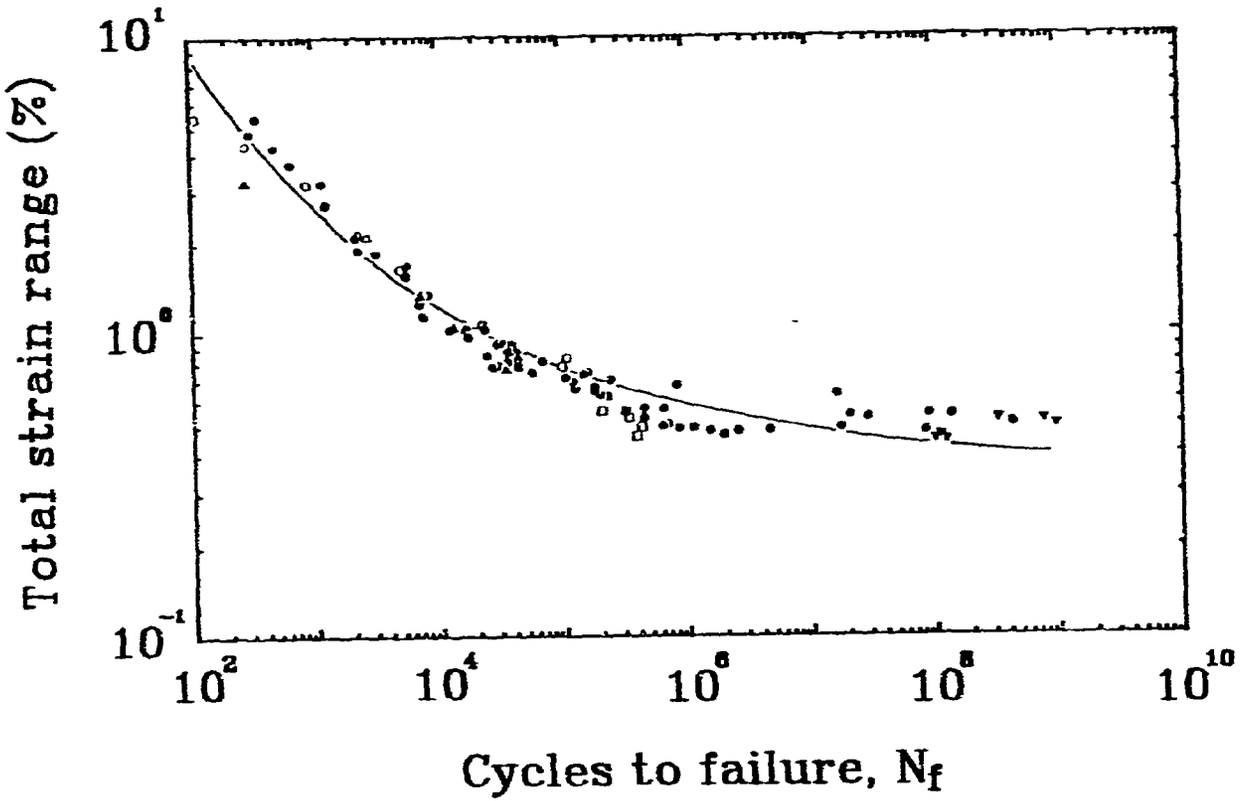

Fig. A1.15 Fatigue data of Alloy 718 at 24°C.

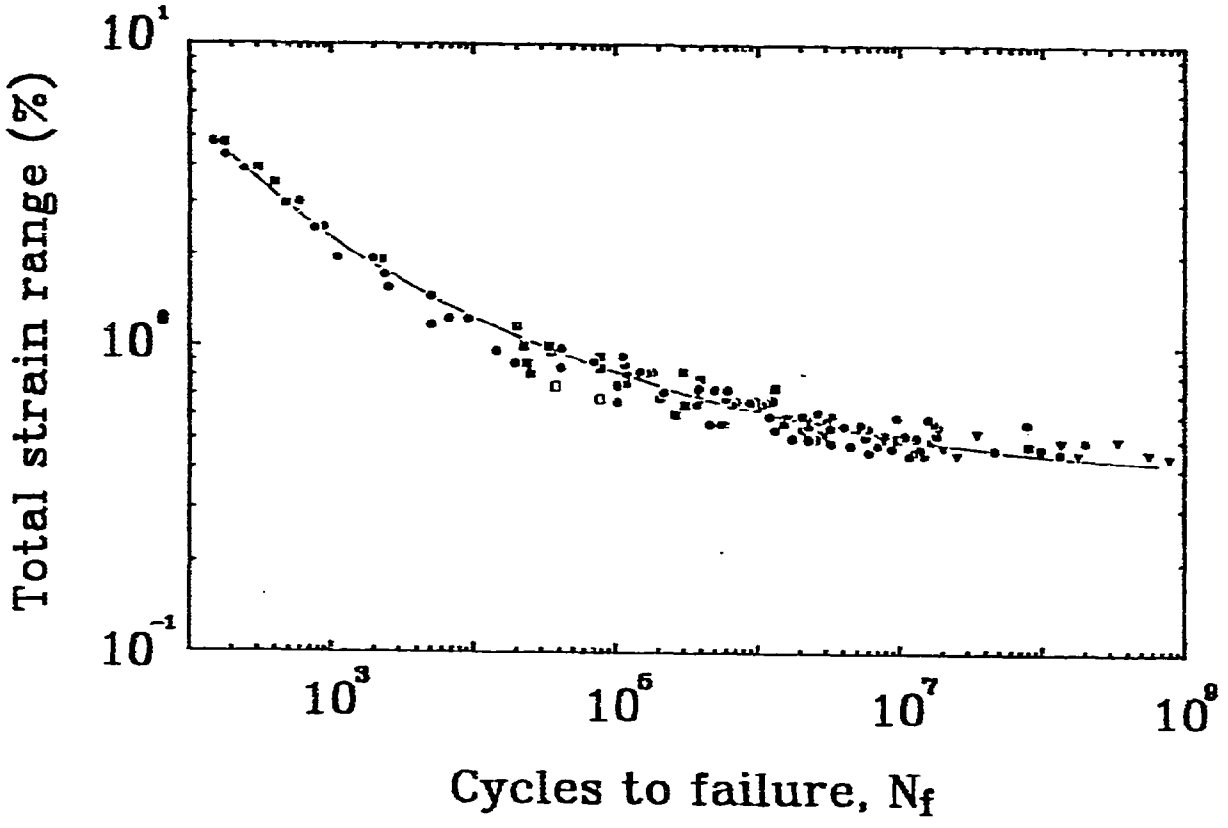

Fig. A1.15 Fatigue data of Alloy 718 at 427°C (cont.).

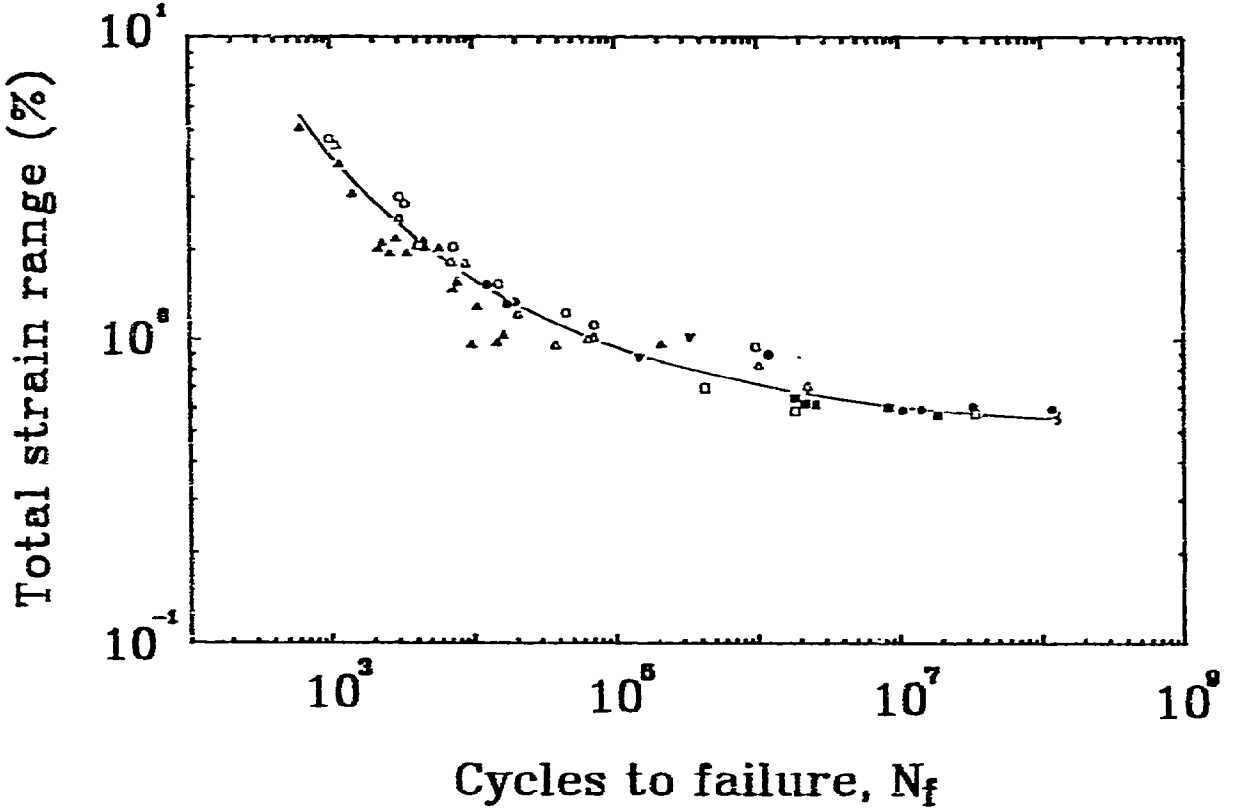

Fig. A1.15 Fatigue data of Alloy 718 at 538°C (cont.).

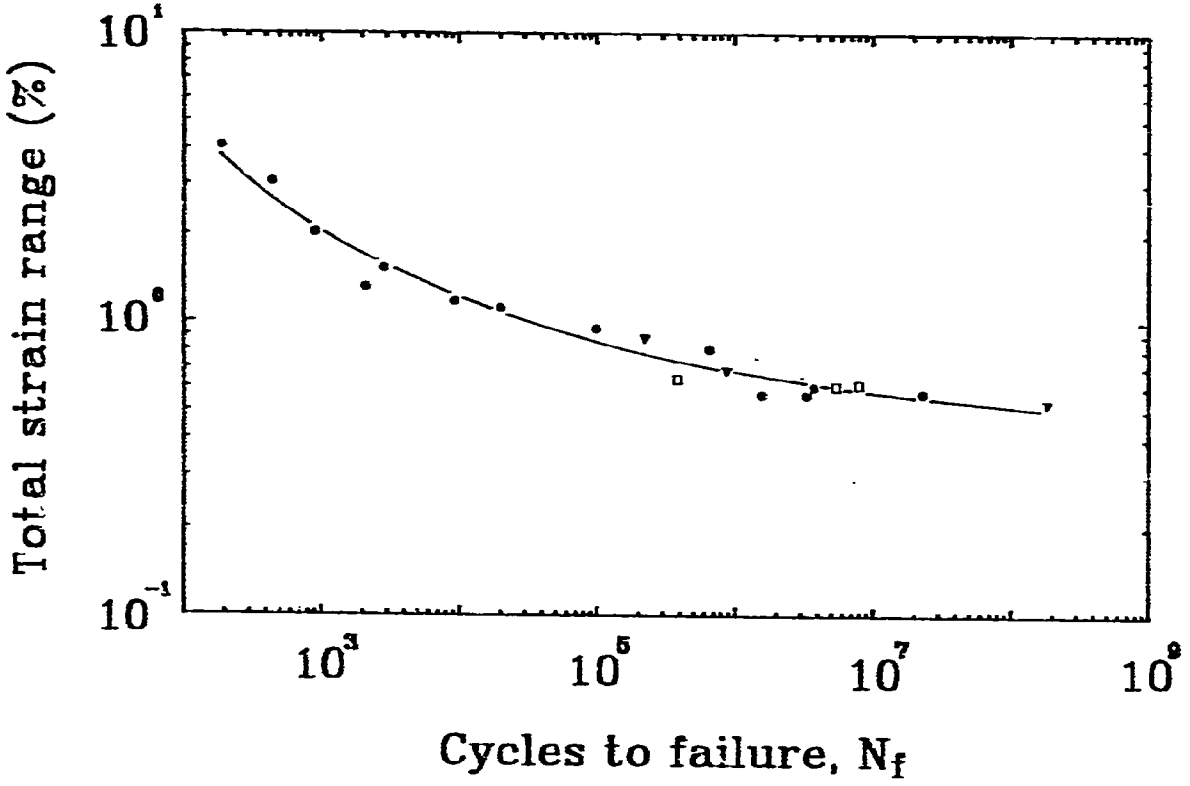

Fig. A1.15 Fatigue data of Alloy 718 at 593°C (cont.).

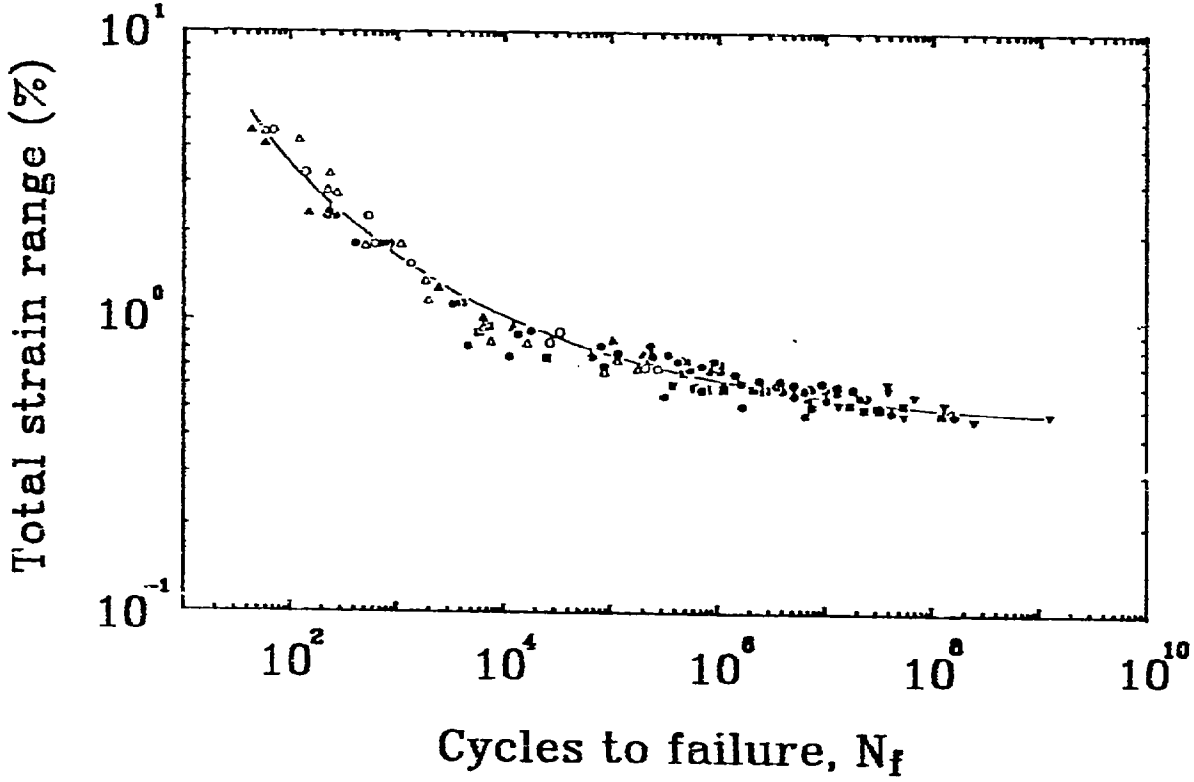

Fig. A1.15 Fatigue data of Alloy 718 at 649°C (cont.).

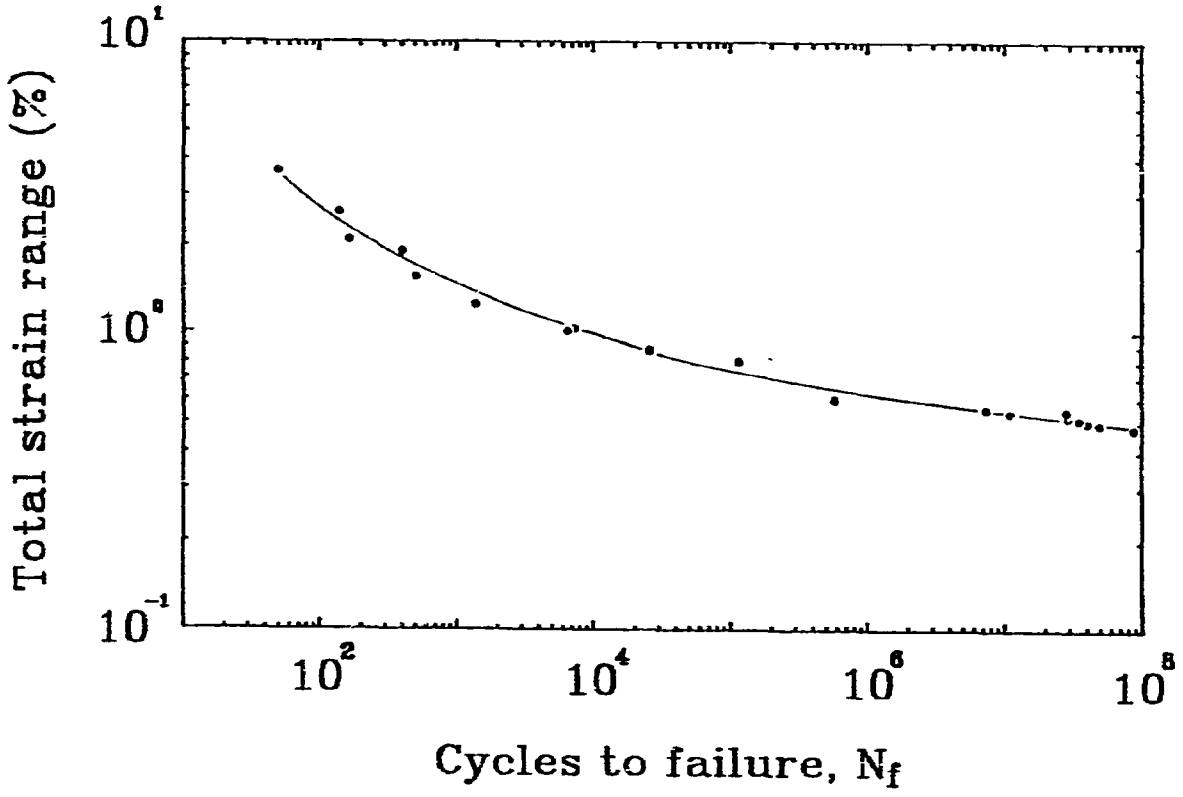

Fig. A1.15 Fatigue data of Alloy 718 at 704°C (cont.).

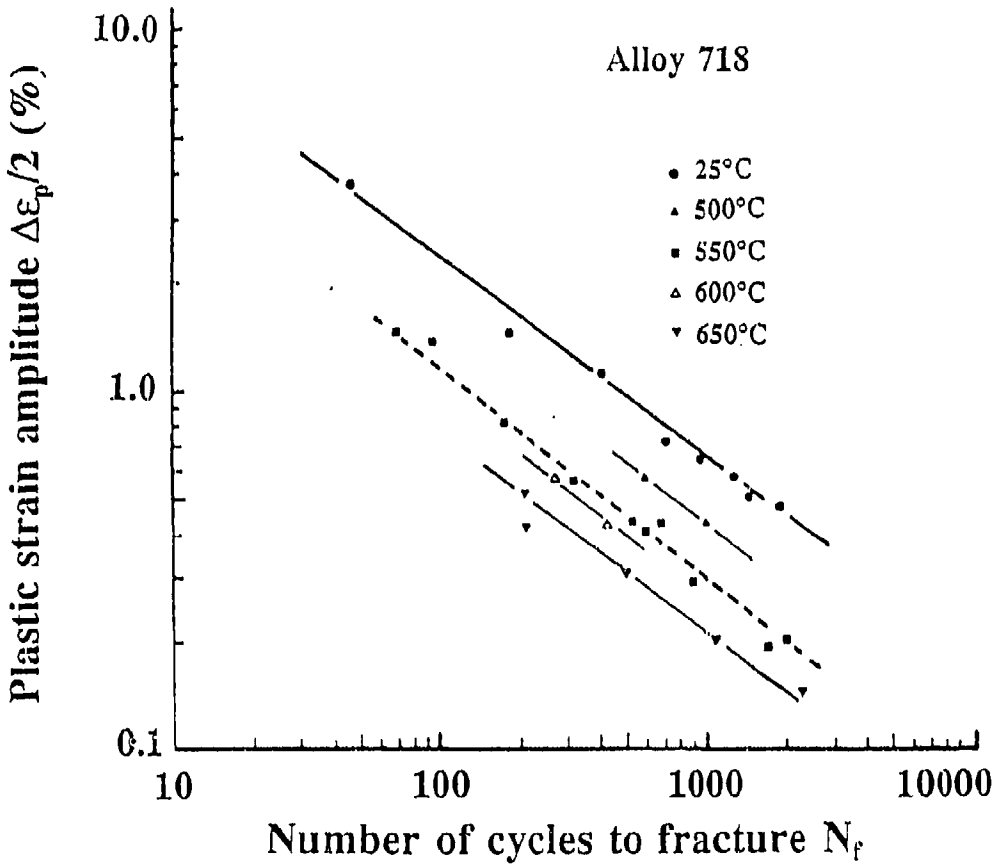

Fig. A1.16 Variation in fatigue life N_f with plastic strain amplitude $\Delta\varepsilon_p/2$ at various temperatures.

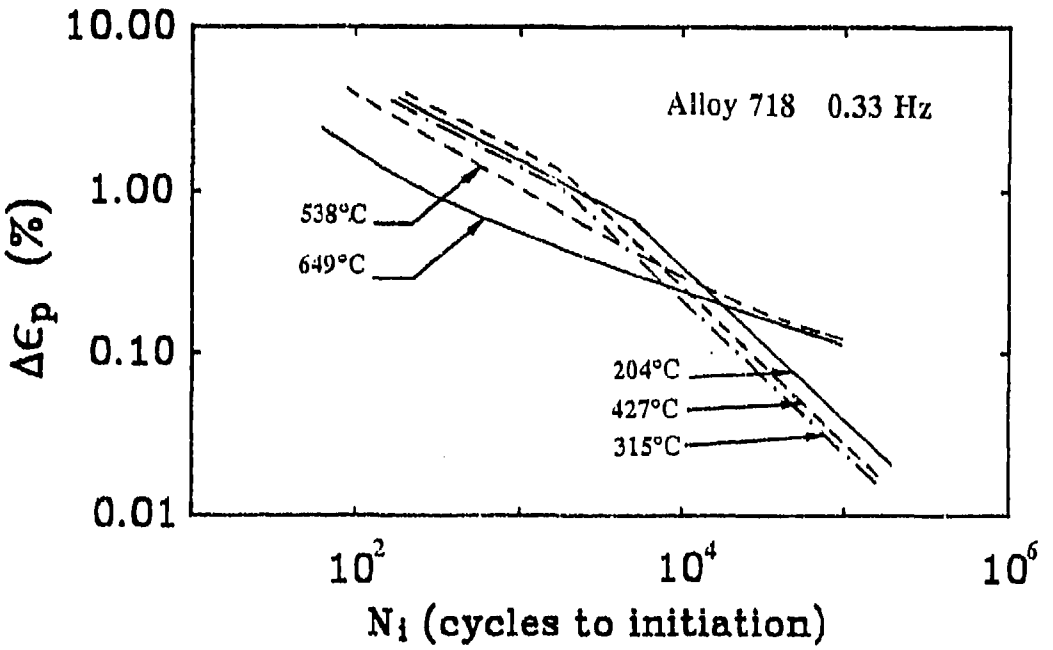

Fig. A1.17 Plastic strain range versus number of cycle to initiation for Alloy 718 at various temperatures.

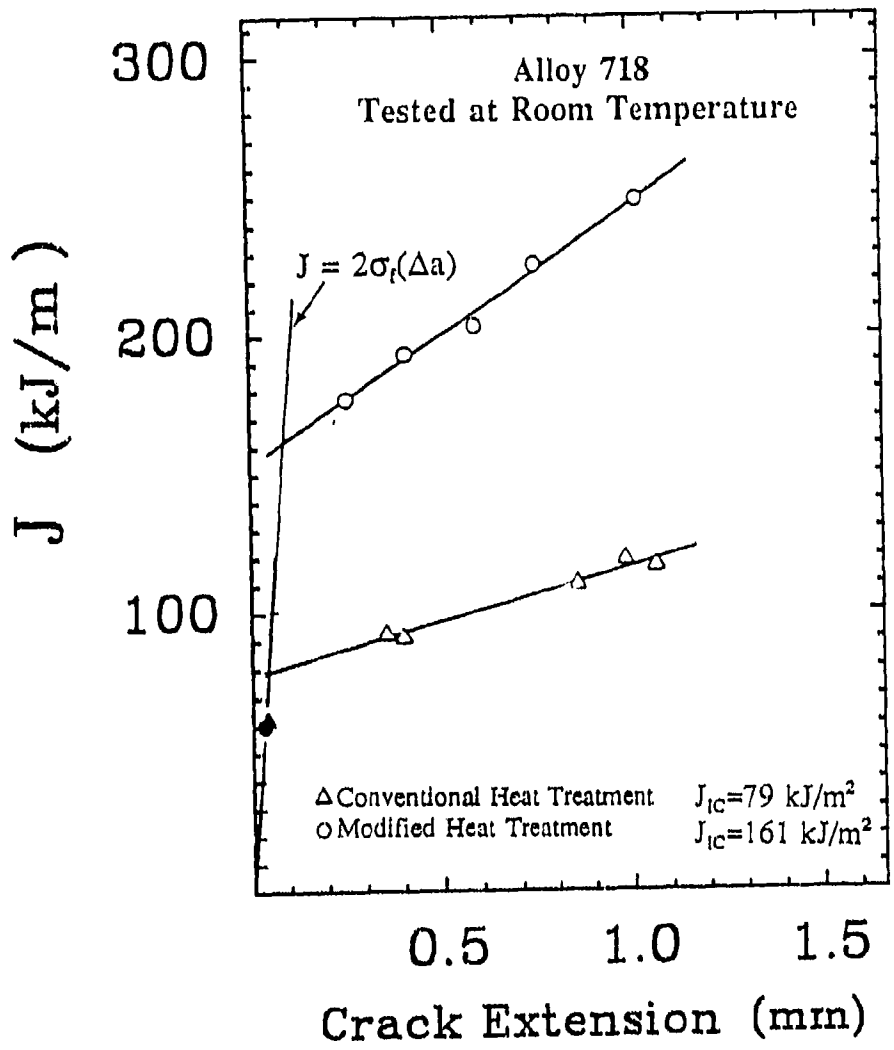

Fig. A1.18 R-curves for conventional and modified Alloy 718 tested at room temperature.

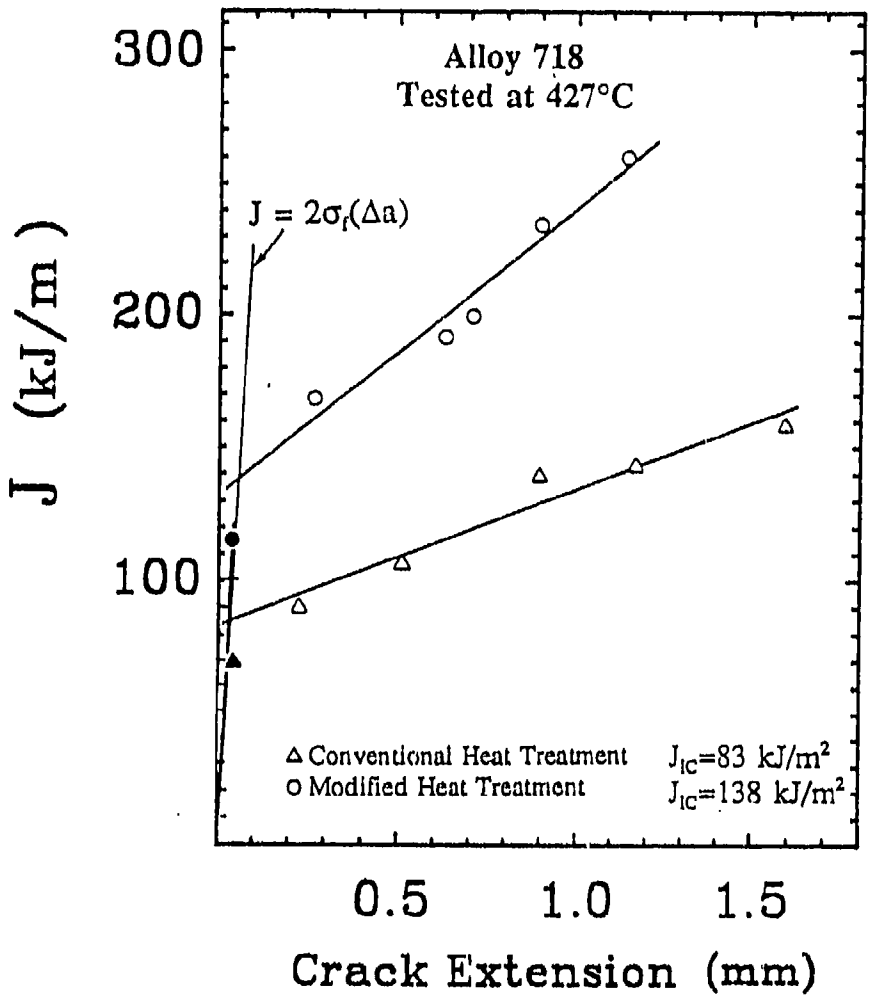

Fig. A1.19 R-curves for conventional and modified Alloy 718 tested at 427°C.

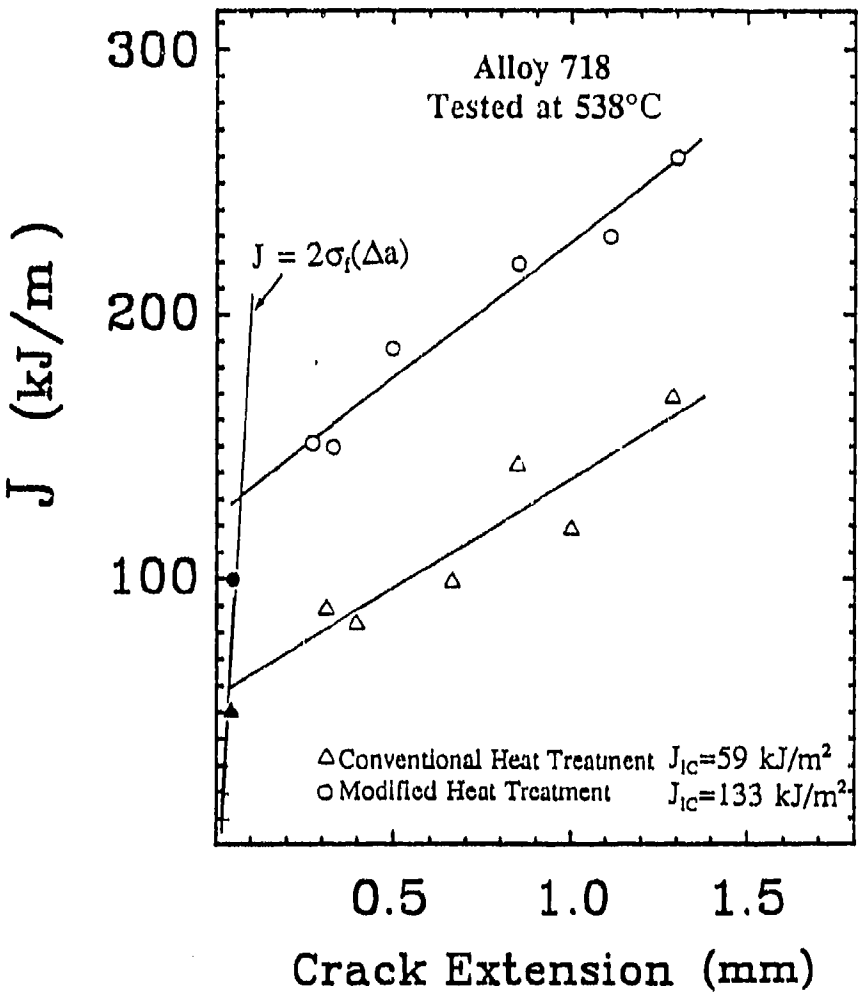

Fig. A1.20 R-curves for conventional and modified Alloy 718 tested at 538°C.

Heat Treatment	Temperature (°C)	J_{Ic} (KJ/m^2)	K_{Ic} (MPa$\sqrt{m}$)
CHT	24	79	131
CHT	427	83	126
CHT	538	59	105
MHT	24	161	188
MHT	427	138	163
MHT	538	133	156

Table A1.9 Fracture Properties of Alloy 718

toughness values for the MHT materials decreased by 20% as temperature increased from 24°C to 538°C. Fractographic examinations revealed [147,153] that primary microvoids nucleated at broken carbonitrides during the initial stages of plastic strainning, regardless of heat treatment. The inferior toughness for the CHT alloy was associated with the premature formation of a second population of dimples that were nucleated by coarse δ particles. The MHT alloy dissolved the coarse δ particles which suppressed secondary microvoid formation and thereby enhanced the fracture resistance. Mills [147] also studied the effect of aging on the fracture toughness. He found that aging at 566°C for 33,000 hours caused a 30% reduction in J_{Ic} at 24°C and 538°C for both the CHT and MHT materials.

I.2.5 Stress Rupture and Time-Dependent Notch Sensitivity

The stress rupture and time-dependent notch sensitivity are important properties of this material thus have been investigated by many researchers [16,47,154-159]. The normal stress versus time of failure at different temperatures are shown in Fig. A1.21. It was found [143] that exposure at 575°C for 10,000 hr then creep tested at 705°C with a stress of 415 MPa exhibited a longer life than the unexposed material. However, the material exposed at 650°C showed a significant decrease in the life when tested under the same conditions. Similar results also obtained from the work of Molins et al [129].

The time-dependent notch sensitivity is the susceptibility for premature crack initiation to occur at elevated temperatures, in the vicinity of a notch or stress raiser, as a function of time at a constant external stress below the yield stress as compared to an

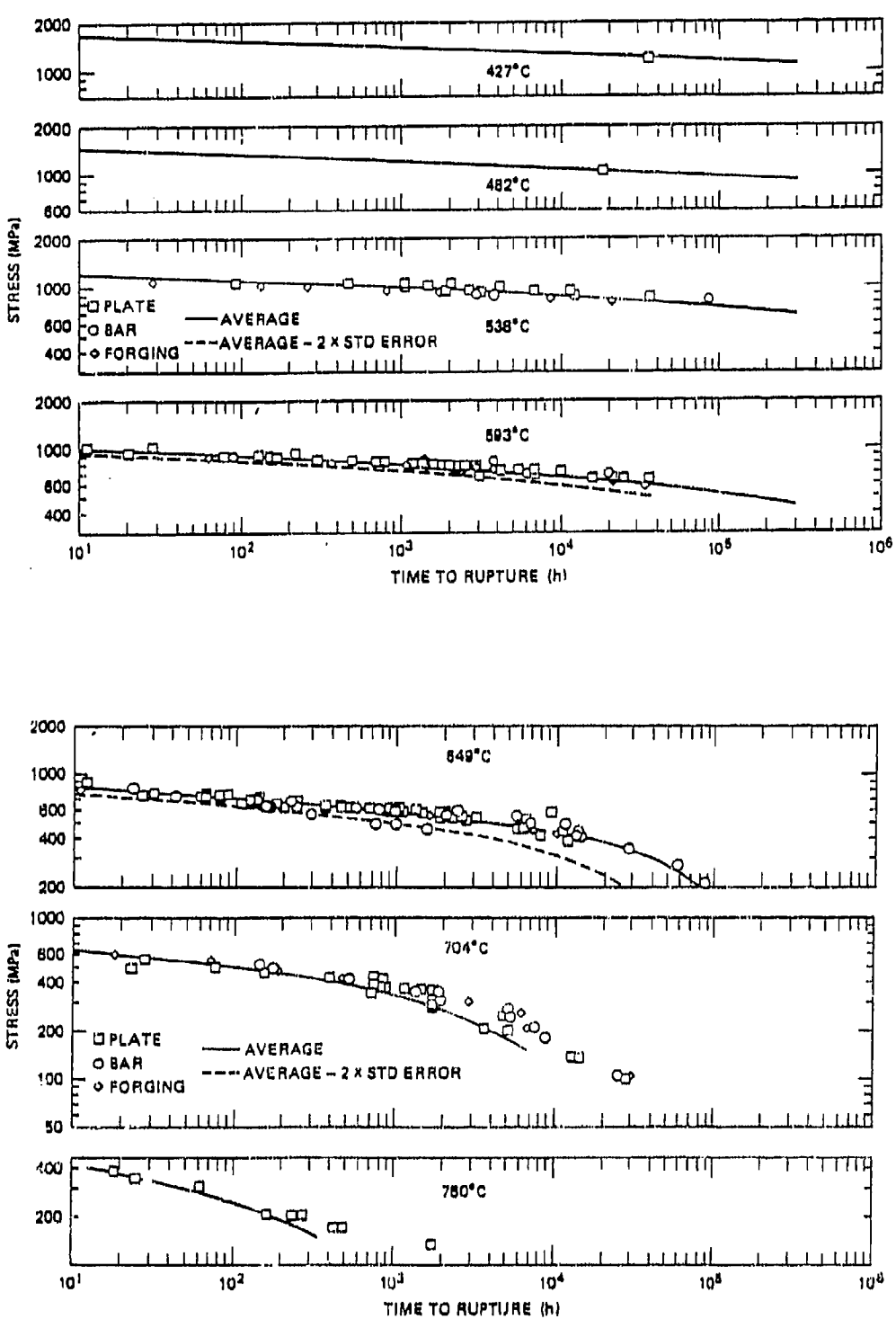

Fig. A1.21 Creep-rupture data for Alloy 718 at various temperatures.

identical unnotched specimen. The occurrence of time-dependent notch sensitivity was due to more rapid initiation of intergranular cracks in notched than in smooth specimens. This was associated with the local deformation at the base of the notches accompanying the relaxation of the stress concentrations.

Wilson [16] extensively studied the time-dependent notch sensitivity of Alloy 718. In his work, the results for the material heat treated 10 hr at 1066°C plus 48 hr at 732°C provide an example of severe time-dependent notch sensitivity (shown in Fig. A1.22). At the shorter times at the lower test temperatures, the rupture strengths for notched specimens were somewhat lower than those for smooth specimens. At varying time periods, the notched specimen rupture curves exhibited drastic increases in steepness so that the rupture strengths for notched specimens decreased with time to values considerably below those obtained in tensile tests, i.e. the material exhibited time-dependent notch sensitivity. The results for the material heat treated 10hr at 927°C plus 48 hr at 732°C are in contrast to the foregoing behavior and are typical of the heat treated material not susceptible to time-dependent notch sensitivity (shown in Fig. A1.23).

Wilson [16] found that variations in notch sensitivity were correlated with changes in the dislocation motion mechanism. the γ'/γ'' particles smaller than a critical size were sheared by dislocations. This gave rise to localized deformation and time-dependent notch sensitive behavior. Lager particles were bypassed by dislocations. under these conditions, the deformation was homogeneous and no time-dependent notch sensitivity was observed. He further pointed out that decreasing the solution temperature or increasing the time and/or temperature of the aging treatment decreased the susceptibility

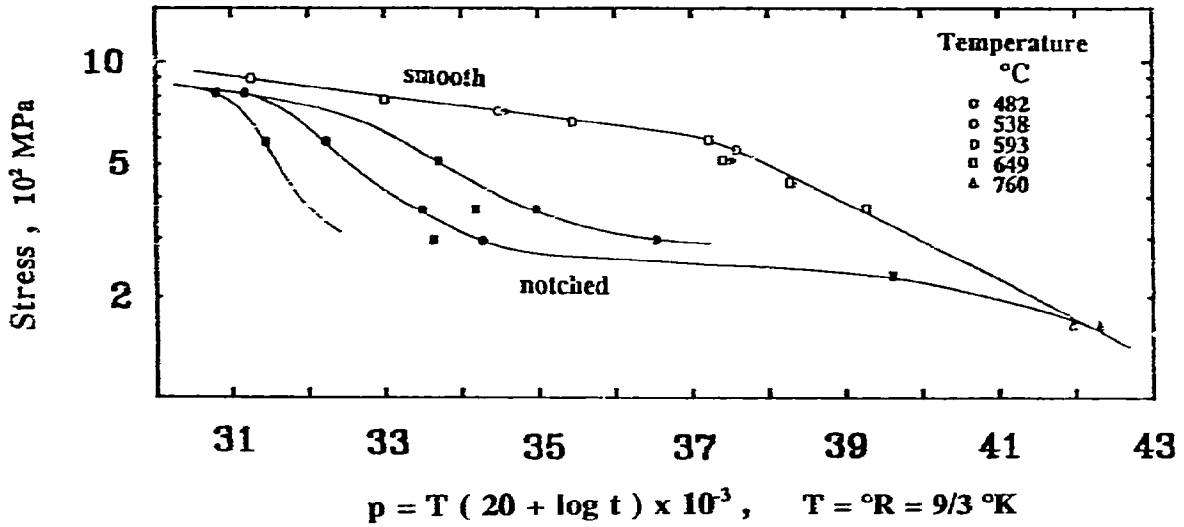

Fig. A1.22 Larson-Miller paramters curves showing time-dependent sensitivity.

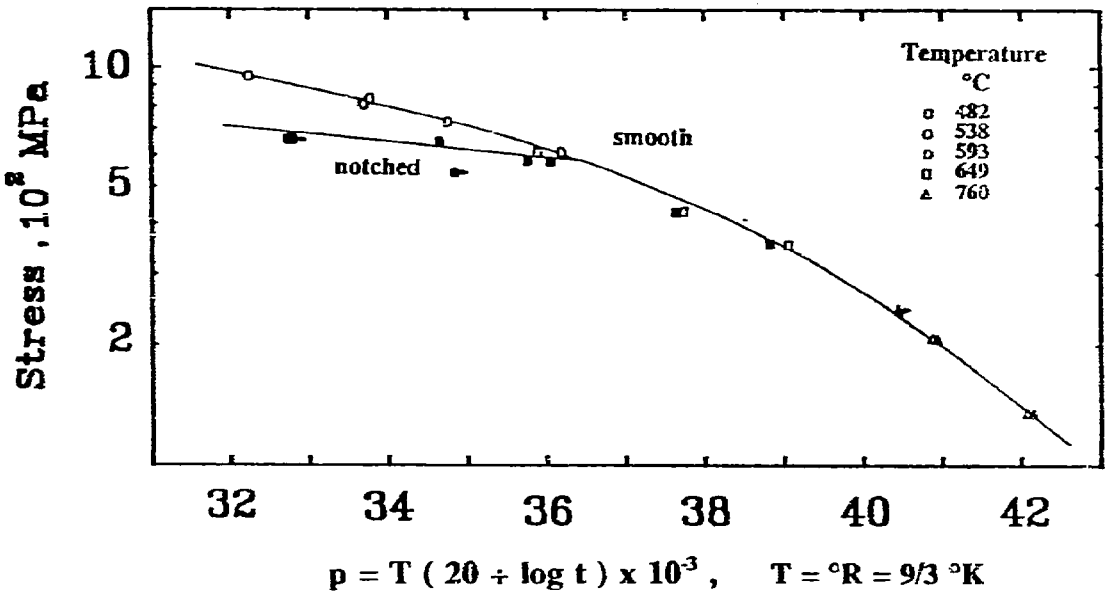

Fig. A1.23 Larson-Miller paramters curves for the rupture strengths of smooth and notched specimens. No time-dependent sensitivity was evident.

to the time-dependent notch sensitivity.

Feldstein and Mendoza [158] obtained similar results, but they thought that time-dependent notch sensitivity is due to the way dislocations break from their precipitate barrier in reference to a average critical distance between the precipitates. When the average distance between precipitates is less than or equal to the critical distance, dislocations will shear through the coherent particles thus will create localized plastic deformation. When this is combined at identical locations with high temperature creep deformation a crack will nucleate prematurely, and the notch sensitivity will occur. On the other hand, when the average distance between precipitates is greater than the critical distance, dislocations will pass between the precipitates without cracking them and the notch sensitivity does not occur.

I.3 Deformation Behavior of Alloy 718

I.3.1 Mode of deformation in Alloy 718

Wilson [16] has examined the deformation behavior of Alloy 718, and he observed that the precipitate particle size (γ'/γ'') governs the mechanism of dislocation motion in this material. When γ'/γ'' particles are smaller than a critical size, they are sheared by dislocation and this gives rise to a localized deformation. For the particles larger than a critical size, they are bypassed by dislocation. Under this condition, the deformation is homogeneous. He found that the critical size is associated to several factors, such as the fraction of γ'/γ'' precipitate, ageing time and temperature. Decreasing the amount of γ'/γ'' precipitate lowers the critical size, while longer ageing time or higher ageing

temperature will increase the critical size. Also, the critical size decreased with decreasing solution temperature. Fournier and Pineau [15] conducted similar investigation. In their work, the microstructure induced by cyclic deformation was examined. They noticed that shear of γ" precipitates occurs during the course of cyclic straining. The shearing process leads to faults in the precipitates. Plastic deformation proceeds very heterogeneously by the propagation of intense deformation bands which were identified as mechanical twins. They also explained that the cyclic softening in Alloy 718 is attributed primarily to the shear of precipitates which locally alters their crystallographic structure from a BCT metastable structure (γ" phase) to a orthorhombic stable structure (δ phase) and secondly to the reduction of the mean particle size in intense deformation bands.

Using TEM investigations by Sanders, Frishmuth and Embley [148] confirmed the presence of microtwins which formed during the deformation process. Principally, twinning was confined to the lower temperatures 204, 316 and 427°C. The density of microtwins appeared to increase with increasing plastic strain range as reported by Fournier and Pineau [15]. At higher temperatures (538°C and 649°C), the primary mode of deformation was thought to be by slip. When slip bands occurs, incoherent particles were often associated with these bands, suggesting that dislocations were generated at the interface between these particles and the matrix. Occasionally, however, a favorably oriented grain may twin at the higher temperatures. If after the twinning event occurs, successive deformation leads to slip, which is the predominate mode of deformation, the twin will become damaged. The damage of the twin does not occur uniformly since the

growth of a deformation twin generates lattice defects which are not uniformly distributed in the vicinity of the twin interface.

Investigations of Alloy 718 by Fournier and Pineau [15] have provided considerable information relative to the effect of frequency as well as temperature and plastic strain amplitude on the deformation mechanism. In their work, microtwins were observed at room temperature and 550°C as well. They noticed that more intense deformation bands formed by twinning were accumulated at high temperatures (550°C) than at low temperatures. However, deformation by twinning was promoted by a decrease in frequency at high temperatures. The results from Sanders et al [148] supported this conclusion since very little twinning was observed at a frequency of 0.33 Hz. This range of behavior from no twinning to intense deformation bands was exactly what has been observed in the work of Clavel and Pineau [14]. At high stress intensity factor range ΔK, no twinning was observed for frequencies of 0.67 Hz and above, whereas the intense deformation bands were noted for frequencies of 0.05 Hz and below. They concluded that the deformation mode at 538 and 649°C was characterized as slip bands, however, the deformation mechanism shifts form slip band deformation at high frequency (0.33 Hz) to increasing twin band formation at low frequency (0.05 Hz).

I.3.2 Deformation Mechanisms of γ'' Phase

The deformation mechanisms as well as the deformation microstructures pertaining to γ'' strengthened alloys have been investigated extensively [15,134,136,148,160,161]. For γ'' DO_{22}-ordered structure, the close-packed $(112)_\gamma$ planes are governed by the

stacking rule that all Nb atoms shall be in contact with all Ni triangular interstices in neighboring layer, so that each Nb atom is coordinated with Ni atoms only. In order to conform with this rule, the superlattice must span two three-layer stacking cycles, i.e. these planes are stacked in a six-layer sequence, ABCDEFABCDEF, to make the DO_{22}-ordered structure. Electron microscopy observations for deformed Alloy 718 specimens revealed that the γ'' precipitates were sheared by dislocations and that the cutting mechanisms lead faults within γ'' particles. These faults are frequently observed as bands lying along close-packed $(112)_\gamma$ planes. Several researchers [15,16,136,160,162] have suggested that these faults are formed by a dislocation reaction at the γ'' precipitates interface as, for example

$$\frac{a}{2}[110] \rightarrow \frac{a}{6}[211] + \frac{a}{6}[12\bar{1}]$$

and the passage of the second partial dislocation through the DO_{22}-ordered structure. This shearing mechanism changes that six-layer stacking sequence of the γ'' particles and gives the lower energy stacking sequence ABCDEFABABCDEF which is associated with the stable δ phase. It is worth noting that the observation of faults inside the precipitates by dark field technique using the extra reflection and the diffusion streak associated with twins in the matrix is in agreement with the above analysis for γ'' faulting. Kirman and Warrington [136] believed that this reaction may be an important factor in the deformation of γ'' dispersions.

This shearing mechanism by partial dislocations can promote deformation by twinning [15]. The above dislocation reaction leaves partial dislocation loops around

precipitates which can eventually coalesce under the influence of internal stresses to propagate micro-twins in the matrix. Furthermore, a noteworthy feature of the microstructure of the solution treated as well as deformed alloy was that dislocations were invariably arranged in planar arrays. Apparently cross slip of dislocations, leading to tangling and cell formation, was almost absent [162]. Such situation would arise if the stacking fault energy (SFE) of the alloy was sufficiently low to inhibit cross slip [163]. The low SFE structure also favors the formation of mechanical twinning in FCC metals [164,165]. Though pure nickel has a high SFE (about 240 mJ/m^2 [166]), it is known that alloying additions of elements like Cr, Mo, Al and Ti can bring down the value of the SFE substantially [165,167,168]. From the knowledge of the various elements present in this alloy, the SFE was roughly estimated by Sundararaman et al [162] to be 75 mJ/m^2 and by Fournier and Pineau to be $50mJ/m^2$, which is lower than that of pure nickel. Although these values should be regarded as approximate ones, they point to the fact that Alloy 718 is one of the intermediate SFE nickel base alloys. A common feature of these alloys is that dislocations in these materials are arranged in planar arrays [165], and deformation by twinning has effectively been observed for such values of the SFE in the case where high tensile stresses were applied [164]. Moreover, Stacking faults were quite frequently observed within γ'' precipitates in deformed as well as undeformed specimens. This suggested that the SFE of the γ'' phase in Alloy 718 is quite low. However, no further work has been done for determining the value of the SFE in the γ'' phase.

It is interesting to note that a great majority of deformation twins remained confined within the γ'' particles and did not propagate into the matrix [162]. This

observation was suggestive of the fact that the value of the critical resolved shear stress for twinning in the γ matrix was higher than that in the γ'' precipitates. As pointed out earlier, the SFE of the γ phase was higher than that of the γ'' phase and possibly this was the reason why the propagation of deformation twins through the γ phase was relatively difficult.

Sundararaman and associates [162] have discussed the mode of dislocation-precipitate interaction with reference to the room temperature deformation behavior of Alloy 718. They observed that matrix dislocations often appeared in pairs and the pair of dislocations were mainly associated with γ'' particles, which suggested that these dislocations are superdislocations that glided through the ordered precipitates. When a pair of 1/2[$\bar{1}$10] dislocations pass through γ'' particles and emerge in the matrix, no order faults are produced. Thus the paired dislocations observed, they believed, was corresponding to this situation. They found that the γ'' particle size is the parameter which controls a slip-to-twin transition, i.e. the deformation through the γ'' precipitates occurs by the passage of a group of dislocation which restores order in them for particle mean radius smaller than 100Å, while for precipitates radii larger than 100Å, precipitate shearing occurs by deformation twinning of precipitates. In their study, the bypassing mechanism was not observed for the range of γ'' particle size (up to 600Å). Contrast to the work of Sundararaman et al, Wilson [16] has observed that dislocations were entangled with γ'' particles when specimen tested at 760°C, and this indicated that dislocations bypassed the precipitates. The discrepancy of their results might related to the thermal activation by allowing dislocations to cross slip and climb out of their original

slip planes [169].

I.4 Strengthening Mechanisms in Alloy 718

Oblak et al [134] and Chaturvedi et al [170] have studied the strengthening mechanisms in Alloy 718. Oblak et al [134] have calculated the critical resolved shear stresses based on the order strengthening model and coherency strengthening model, respectively. By comparing these results, they found three major reasons why the coherency strengthening appears to be predominant rather than the order strengthening as follows:

a) the increase in critical resolved shear stress predicted by the coherency strengthening model exceeds that expected for order strengthening and closely matches the experimental results;

b) the temperature dependence of the critical resolved shear stress follows that of the shear modulus as predicted by the coherency strengthening model;

c) if the order strengthening mechanism were predominant, it would suggest that the alloy should deform at relatively low stressed by the motion of dislocation quadruplets. However, this is inconsistent with the observation of dislocation pairs rather than quadruplets in the material.

Thus, they suggested that the strength of Alloy 718 depends primarily upon the coherency strengthening arising from the tetragonally-distorted DO_{22} γ'' precipitate.

It worth mentioning that, after calculating the antiphase boundary energy (APBE) of the γ' phase, they found the value of this APBE was surprisingly low, which strongly suggested that the contribution of the γ' phase to the strength of Alloy 718 is minimal and can be ignored.

The work of Chaturvedi and Han [170] confirmed that the major strengthening is provided by the coherency hardening mechanism by the γ' precipitate, and they considered the strengthening contribution by the γ' precipitate particles, although relatively small amount, either by the coherency strengthening mechanism or by the order hardening mechanism.

APPENDIX II

METHODS OF EXPERIMENT

II.1 Specimens Specifications

The compact tension (CT) specimens have been used in this research program. The specimen specifications are following ASTM standard (E647-88a) and are shown in Fig. A2.1.

Fig. A2.2 shows the microstructural features of testing materials and the average grain size is about 130 μm.

II.2 Apparatus

An automated test system based on a microcomputer was used in conducting the experiments. All tests in air was carried out on a MTS mode 810 servo-hydraulic test station with a 250 KN load cell and a MTS model 880 servo-hydraulic test station with a 100 KN load cell was employed when tested in vacuum chamber. Inside the vacuum chamber, the elevated temperature is reached by using a 10 KHz induction heating system. During crack growth tests, the degree of vacuum is monotored with a residual gas analyzer and the testing vacuum is better than 5×10^{-8} torr total pressure which consists primarily of nitrogen and oxygen with partial pressure less than 10^{-9} torr. The vacuum testing system is shown in Fig. A2.3.

The digital PDP 11/34 microcomputer through the MTS 433 processor interface

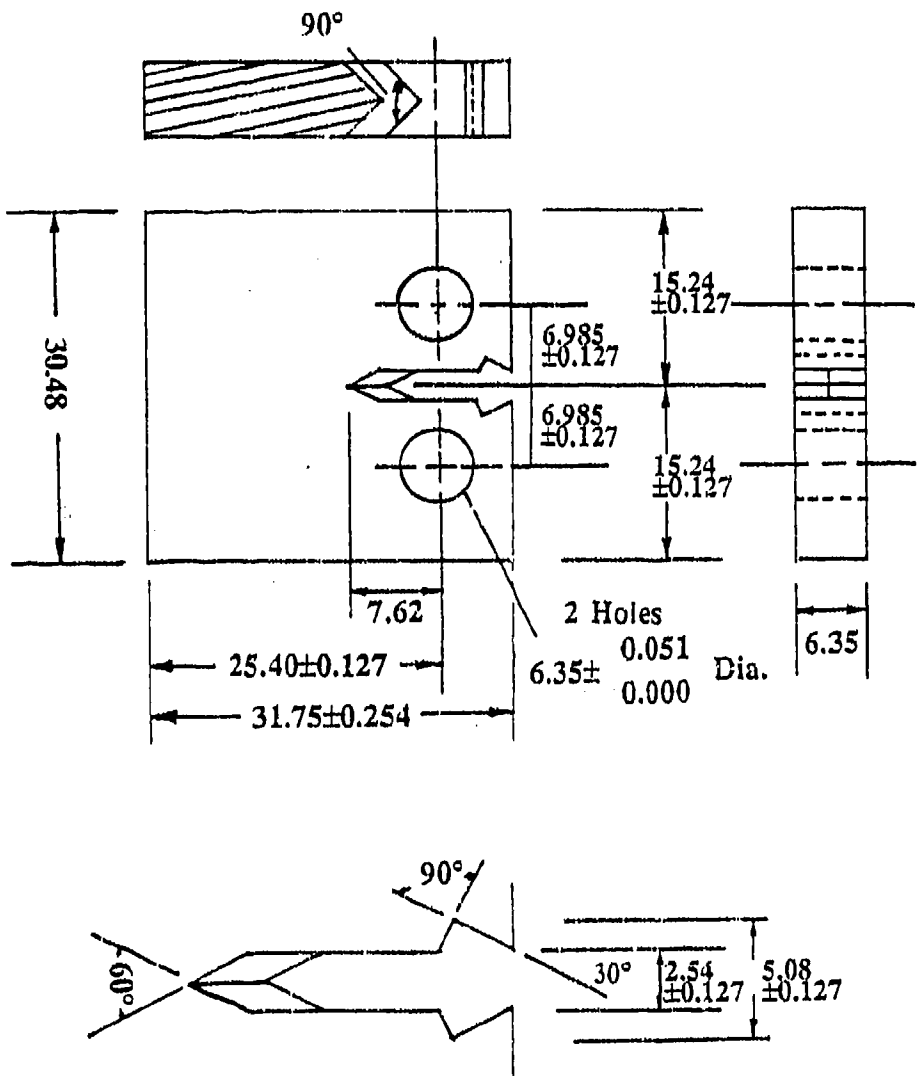

Fig. A2.1 Test specimen geometry for fatigue crack growth testing.

Fig. A2.2 The microstructure of the testing material.

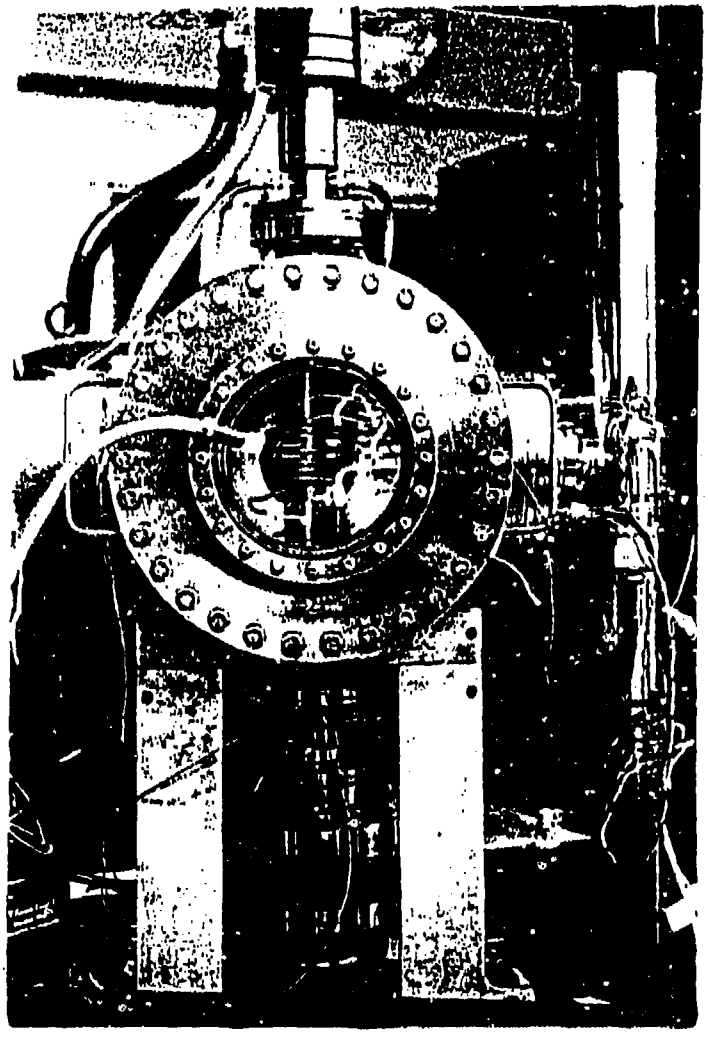

Fig. A2.3 The vacuum testing system.

was used in real time for feedback control of the test parameters and to acquire data. An IBM PC-AT computer was utilized to reduce data. The specimens were heated with a resistance two-zone furnace when tested in air and with a 10 KHz induction heating unit when tested in vacuum. Chromel/Alumel thermocouple was used to measure the temperature, and the temperature at a point on the specimen was controlled at 650°C ± 2°C by a CN1204 temperature controller.

II.3 Techniques of Measurement of Crack Length

II.3.1 The Elastic Compliance Method

For this method, crack length is determined indirectly from elastic compliance measurements using crack mouth opening displacement (CMOD) data obtained by a extensometer having mechanical extension (shown in Fig. A2.4). During a fatigue crack growth test, CMOD and load data are acquired simultaneously for the unloading part of the histeries loop by the computer, then a straight line is fitted according to the least-square error minimization procedure to this data set, the load data of unloading part is chosen from $45\%P_{max}$ to $95\%P_{max}$ in order to obtain good linear relationship (shown in Fig. A2.5). Thus, the elastic compliance, C, can be obtain as a slop of this straight line:

$$C = \frac{CMOD}{P} \qquad (2.1)$$

By using the initial crack length a_0 and elastic compliance C, the apparent Young's modulus E can be estimated as [171]:

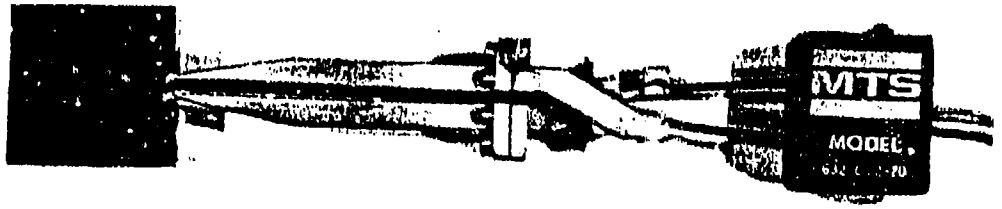

Fig. A2.4 Extensometer with mechanical extension used in the experiments.

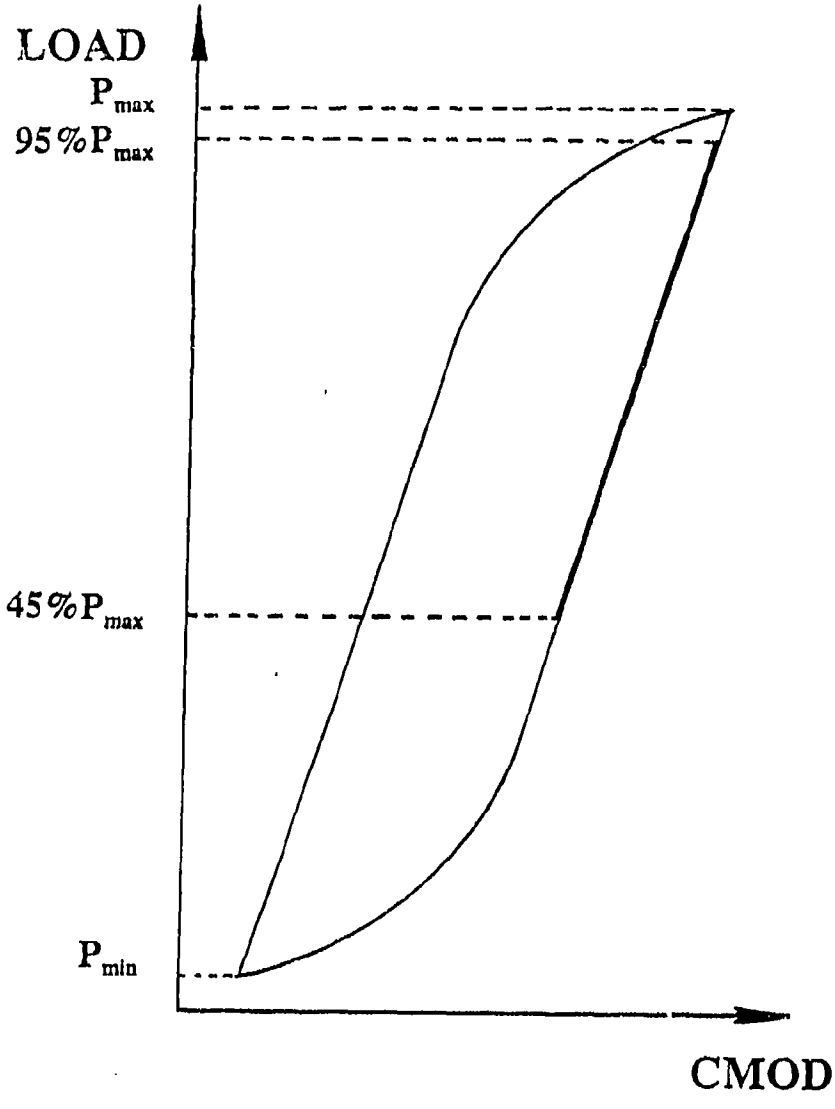

Fig. A2.5 The configuration for obtaining the elastic compliance.

$$E = \frac{1}{BC}\left(1 + \frac{0.25}{b}\right)\left(\frac{1+b}{1-b}\right)^2(1.61369 + 12.6778b - 14.2311b^2 - 16.6102b^3 + 35.0499b^4 - 14.4943b^5) \quad (2.2)$$

where B is the thickness of the specimen, b is the ratio of a_0/w. Now, the current crack length, a, can be calculated by the following expression [171]:

$$a = W(1.001 - 4.6695U + 18.46U^2 - 236.82U^3 + 1214.9U^4 - 2143.6U^5) \quad (2.3)$$

where

$$U = \left(\sqrt{BEC} + 1\right)^{-1}$$

Thus, by continually measuring the current elastic compliance, C, the current crack length, a, can be determined according to eq. (A2.3).

II.2.2 The D. C. Potential-Drop Method

The D. C. potential-drop method for measuring crack growth is relied on the increase in electrical resistance of the specimen when its cross-sectional area is reduced [172]. The basis of this method is to pass a known direct current generated by a stable power supply through a test specimen and to monitor the change in potential drop between one active probe pair which span a crack as the crack growth occurs. These probes will react to changes in crack length, temperature, current and deformations. A reference probe pair is located at a position remote to the crack. This probe pair will react in the same manner to all variables except crack length. As the crack grows, the increase in electrical resistance of the specimen will result in the potential drop to rise,

thus the measurements of the potential drop across the crack region can be related by experimentally determined calibration curve to crack length. The D. C. current applied for CT12.5 is 5 A while for CT31.5 is 12 A. Fig. A2.6 shows a schematic of D. C. potential drop system.

An thermal electrometric force (EMF) due to thermocouple action may be generated at the junction of the potential probe and the specimen. If the junction characteristics of the both potential probes are identical, the net EMF across the probes will be zero. However, in practice there is always a contribution of EMF to the output voltage which should be accounted for. In order to eliminate the effect of EMF, the corrected voltage V_c was used which is as follows

$$V_c = V - V_0 \tag{2.4}$$

where V is the voltage measurement when current is on, while V_0 is the voltage measurement when current is of, both are measured when current is stabilized. The current configuration during cycles is shown in Fig. A2.7. Furthermore, to minimize the effects of the variations of alloy resistivity, temperature and applied current, the normalization of V_{c1} and V_{c2} was utilized here:

$$\frac{V_{c1}}{V_{c2}} = \frac{V_1 - V_{01}}{V_2 - V_{02}} \tag{2.5}$$

where V_{c1} is the corrected voltage for active probe pair, and V_{c2} is the corrected voltage for reference probe pair. Thus, the ratio V_{c1}/V_{c2} versus the number of cycle, N, is recorded on the computer disk, and this set of data can be converted to crack length

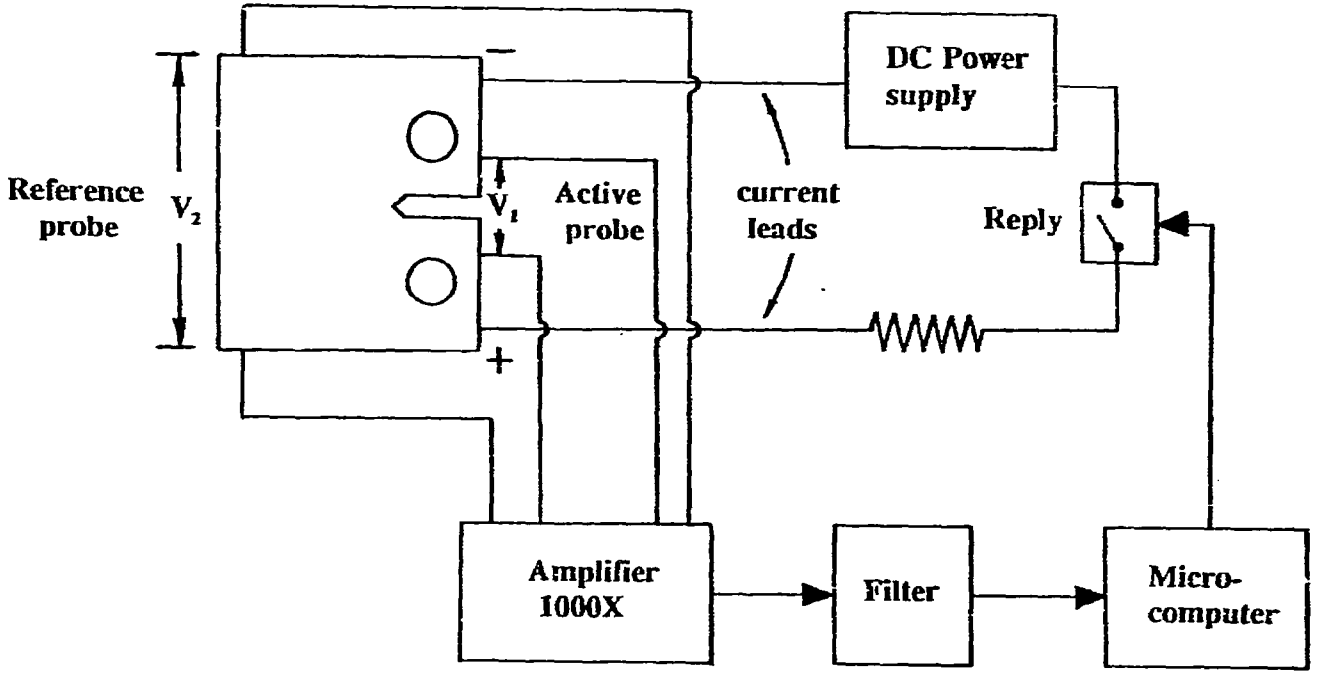

Fig. A2.6 Schematic of the D.C. potential drop system.

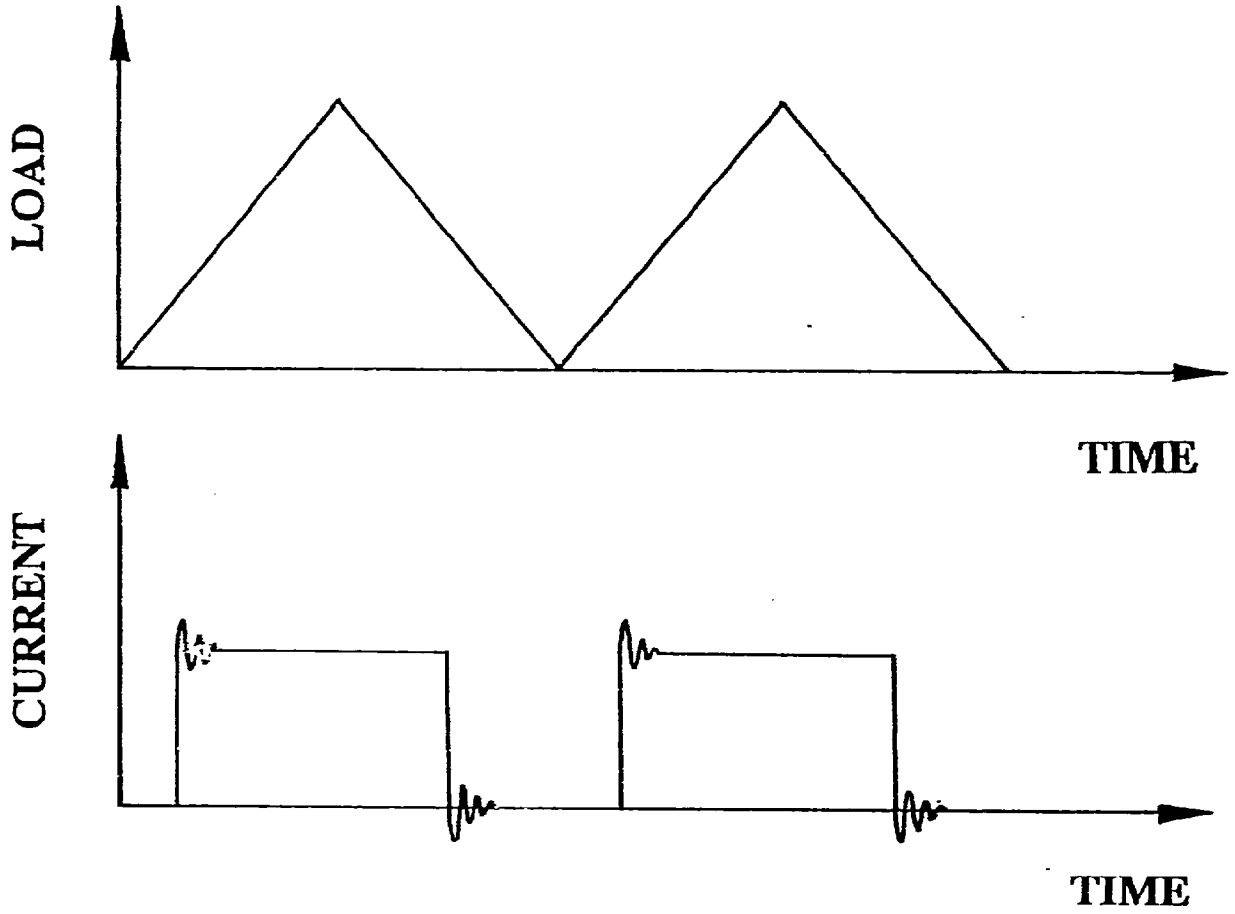

Fig. A2.7 The electric current profile of the D.C potential drop method during cyclic testing.

versus N by experimentally determined calibrated relationship between the ratio V_{c1}/V_{c2} and crack length a.

II.2.3 The Method of Obtaining da/dN and ΔK

From D. C. potential drop method, a data set of N versus V_{c1}/V_{c2} is obtained, so is has to be converted to a data set of N versus a, this can be done by using calibration curve experimentally determined from high temperature test (650°C), for CT12.5 this calibrated relationship is as follows:

$$\frac{a}{W} = 1.0986 - 0.03799\left(\frac{V_{c1}}{V_{c2}}\right) - 0.02092\left(\frac{V_{c1}}{V_{v2}}\right)^2 - 0.001976\left(\frac{V_{c1}}{V_{c2}}\right)^3 + 0.0004657\left(\frac{V_{c1}}{V_{c2}}\right)^4 \qquad (2.6)$$

It should be mentioned that since initial crack length, temperature, crack front configuration are not exactly the same for calibration test and real tests, thus for relationship of (a/W) versus (V_{c1}/V_{c2}), there exits a deviation from calibration test curve and real test curve, schematically shown in Fig. A2.8. In general, they are related as follows:

$$g(v) = f(v) + h(v) \qquad (2.7)$$

where $v = V_{c1}/V_{c2}$, g(v) represents the real test curve, f(v) represents the calibration test curve, and h(v) is a certain function of v, for the sake of convenience h(v) usually is taken as polynomial form, i.e.

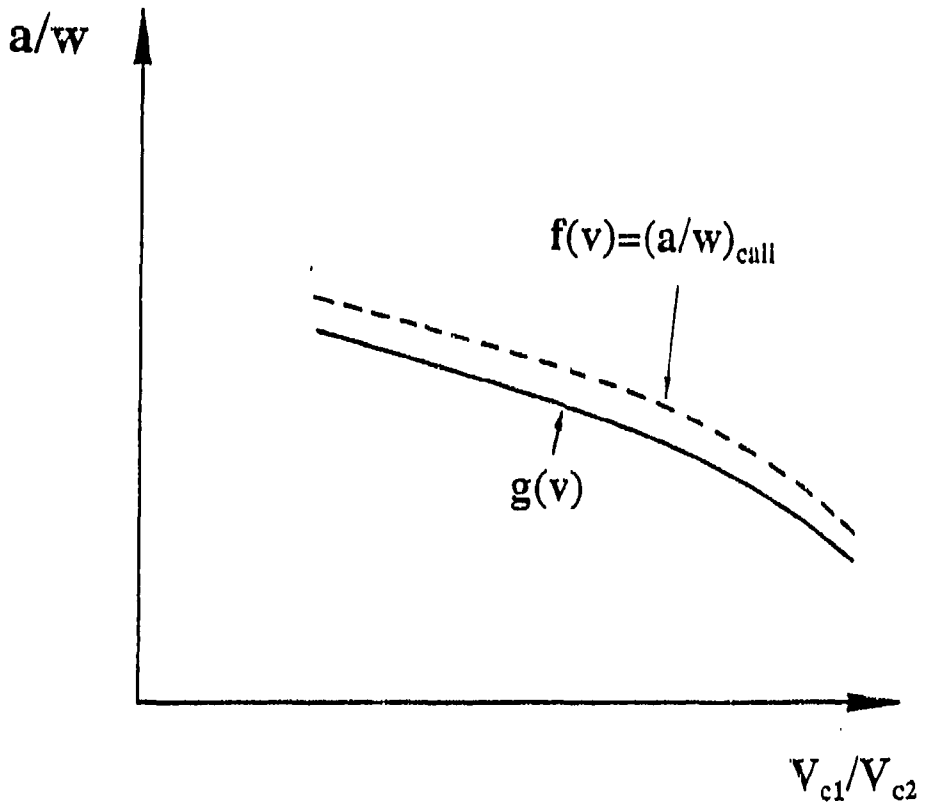

Fig. A2.8 Schematic illustration of correcting the calibration curve associated with initial and final measurements.

$$g(v) = f(v) + A_1 + A_2 v + A_3 v^2 + \cdots \tag{2.8}$$

For any tests, it is certain that the initial reading (a_0, v_0) and the final reading (a_f, v_f) can be measured, thus for simplicity, h(v) is often chosen as a linear form:

$$h(v) = A_1 + A_2 v \tag{2.9}$$

so we have

$$\begin{cases} g(v_0) = f(v_0) + A_1 + A_2 v_0 = \left(\dfrac{a_0}{W}\right) \\ g(v_f) = f(v_f) + A_1 + A_2 v_f = \left(\dfrac{a_f}{W}\right) \end{cases} \tag{2.10}$$

by solving eq. (A2.11) simultaneously, A_1 and A_2 can be obtained, and the relationship g(v), i.e.

$$g(v) = f(v) + A_1 + A_2 v \tag{2.11}$$

can be used to convert V_1/V_2 to crack length a. More readings, except initial and final readings, obtained during test will certainly benefit to increase the accuracy of this converting process. The typical curve of crack length versus number of cycles is shown in Fig. A2.9.

For data set (N,a), the total number of data points usually is around serval hundreds. However, based on experience of analyzing potential drop data sets [173], it is desirable to reduce the total number of data points to about 100. The so-called block averaging approach was used in the study, and the computer program is listed in

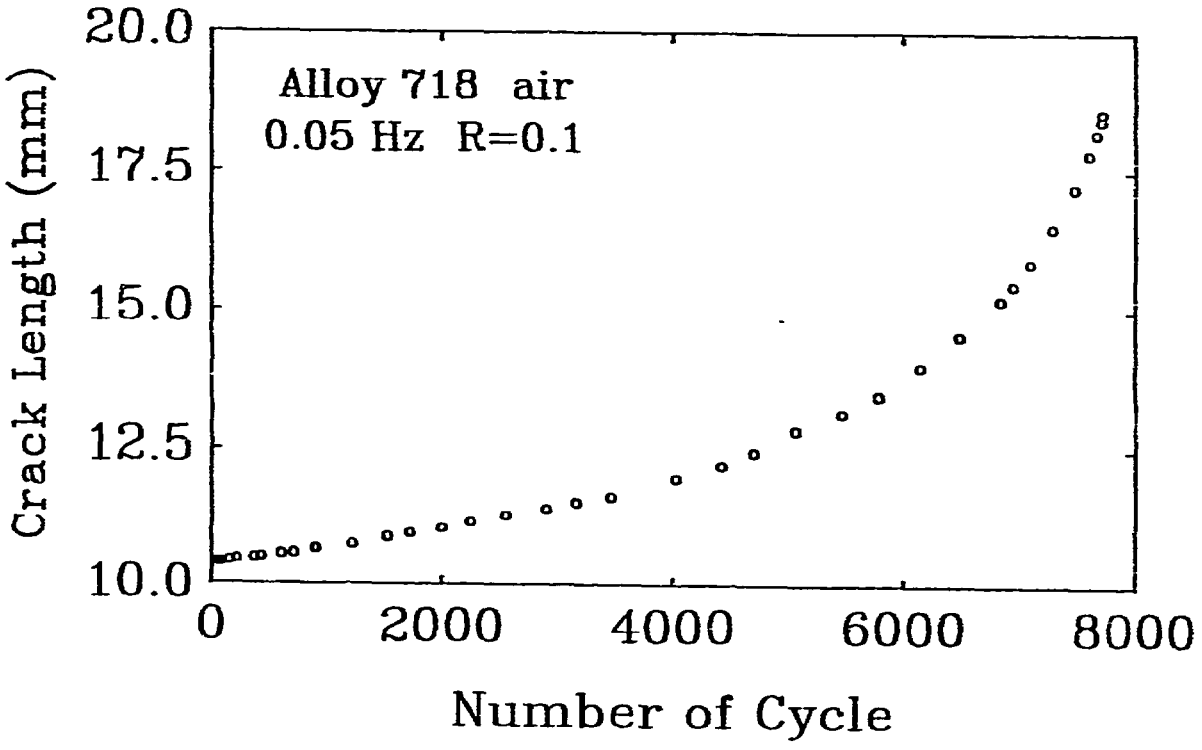

Fig. A2.9 The curve of crack length versus number of cycle obtained from D.C. potential drop method.

Appendix IV.

From constant ΔK tests, the data set is already in the form of N versus a. Thus in this case the data set just need to be smoothed, and then the linear regression analysis for this data set can be applied to obtain the slope which is the crack growth rate da/dN.

The seven point incremental polynomial technique [174] has been used to obtain fatigue crack growth rate da/dN, and the stress intensity factor range ΔK is calculated according to the following expression [174]:

$$\Delta K = \frac{\Delta P}{B\sqrt{W}} \frac{(2+\alpha)}{(1-\alpha)^{1.5}} (0.886 + 4.64\alpha - 13.32\alpha^2 + 14.72\alpha^3 - 5.5\alpha^4), \text{ for } \alpha \geq 0.2 \quad (2.12)$$

where $\alpha = a/W$.

Finally, in order to maitain crack growth in the plane strain condition, for CT specimen the following requirement should be fulfilled [174]:

$$W - a \geq \frac{4}{\pi} \frac{K_{max}^2}{\sigma_{Yc}^2} \quad (2.13)$$

or

$$\Delta K \leq \frac{\sigma_{Yc}(1-R)}{2} \sqrt{\pi (W-a)} \quad (2.14)$$

where σ_{Yc} is 0.2% offset cyclic yield strength, R is the load ratio.

APPENDIX III

DERIVATION OF THE EXPRESSION FOR CALCULATING OXIDATOIN CHARACTERISTIC PARAMETER β

During the grain boundary oxidation process, the chromium, iron and nickel oxides could form as follows:

$$2Cr + \frac{3}{2}O_2 = Cr_2O_3 \qquad \textbf{(A3.1)}$$

$$Fe = \frac{1}{2}O_2 = FeO \qquad \textbf{(A3.2)}$$

Denoting m_{O2}^{Cr}, m_{O2}^{Fe} and m_{O2}^{Ni} as the amount of oxygen required to form oxides Cr_2O_3, FeO and NiO, respectively. We assume that

$$m_{O_2} = m_{O_2}^{Cr} + m_{O_2}^{Fe} + m_{O_2}^{Ni} \qquad \textbf{(A3.4)}$$

From eqs.(A3.2) and (A3.3), the linkage between m_{O2}^{Cr}, m_{O2}^{Fe} and m_{O2}^{Ni} can be established as follows. According to eq.(A3.2) we know that 1 mole of Fe comsumes 1/2 mole of O_2 to form FeO, i.e. x_{Fe} moles of Fe need x_{O2}^{Fe} moles of O_2 to form FeO:

$$x_{Fe} = 2\,x_{O_2}^{Fe} \tag{A3.5}$$

the value of moles for a substance is the ratio of the amount of the subatance to the atomic or molecular weight of the substance. Thus according to this definition, we have

$$x_{Fe} = \frac{m_{Fe}}{M_{Fe}}$$

where m_{Fe} is the amount of iron required to form the iron oxide FeO, and M_{Fe} is the atomic weight of iron. Therefore, we have

$$\frac{m_{Fe}}{M_{Fe}} = 2\,\frac{m_{O_2}^{Fe}}{M_{O_2}}$$

or

$$\begin{aligned} m_{Fe} &= \frac{2M_{Fe}}{M_{O_2}}\, m_{O_2}^{Fe} \\ &= 3.491\, m_{O_2}^{Fe} \end{aligned} \tag{A3.6}$$

Similarly, from eq.(A3.3) we can get

$$\begin{aligned} m_{Ni} &= \frac{2M_{Ni}}{M_{O_2}}\, m_{O_2}^{Ni} \\ &= 3.6694\, m_{O_2}^{Ni} \end{aligned} \tag{A3.7}$$

Now, if eqs.(A3.6) and (A3.7) are combined together, we can obtain

$$\frac{m_{Fe}}{m_{Ni}} = 0.9513 \frac{m_{O_2}^{Fe}}{m_{O_2}^{Ni}} \qquad \textbf{(A3.8)}$$

For the sake of convenience, we denote

$$\gamma = \frac{m_{Fe}}{m_{Ni}}$$

then eq.(A3.8) could be written as

$$0.9513\, m_{O_2}^{Fe} - \gamma\, m_{O_2}^{Ni} = 0 \qquad \textbf{(A3.9)}$$

By solving eqs.(A3.4) and (A3.9) simultaneously, one can obtain:

$$m_{O_2}^{Fe} = \gamma \frac{m_{O_2} - m_{O_2}^{Cr}}{0.9513 + \gamma} \qquad \textbf{(A3.10)}$$

and

$$m_{O_2}^{Ni} = 0.9513 \frac{m_{O_2} - m_{O_2}^{Cr}}{0.9513 + \gamma} \qquad \textbf{(A3.11)}$$

From eq.(A3.1), the relationship between m_{O2}^{Cr} and m_{Cr} could be determined as

$$m_{O_2}^{Cr} = 0.4615\, m_{Cr} \qquad \textbf{(A3.12)}$$

Substituting eq.(A3.12) into eqs.(A3.10) and (A3.11), we have

$$m_{O_2}^{Fe} = \gamma \frac{m_{O_2} - 0.4615\, m_{cr}}{0.9513 + \gamma} \qquad \textbf{(A3.13)}$$

and

$$m_{O_2}^{Ni} = 0.9513 \frac{m_{O_2} - 0.4615\, m_{Cr}}{0.9513 + \gamma} \qquad \textbf{(A3.14)}$$

For the same reason as in eq.(A3.6), we have

$$\frac{m_{FeO}}{M_{FeO}} = 2 \frac{m_{O_2}^{Fe}}{M_{O_2}}$$

or

$$m_{FeO} = 2 \frac{M_{FeO}}{M_{O_2}} m_{O_2}^{Fe} = 4.49\, m_{O_2}^{Fe} \qquad \textbf{(A3.15)}$$

Now, combining eqs.(A3.14) and (A3.15), one obtains

$$m_{FeO} = 4.49\, \gamma \frac{m_{O_2} - 0.4615\, m_{Cr}}{0.9513 + \gamma} \qquad \textbf{(A3.16)}$$

In the same way, we can get

$$m_{NiO} = 4.442\, \gamma \frac{m_{O_2} - 0.4615\, m_{Cr}}{0.9513 + \gamma} \qquad \textbf{(A3.17)}$$

and

$$m_{Cr_2O_3} = 1.462\, m_{Cr} \qquad \textbf{(A3.18)}$$

Since parameter β is defined as

$$\beta = \frac{m_{Cr_2O_3}}{m_{OX}}$$

$$= \frac{m_{Cr_2O_3}}{m_{Cr_2O_3} + m_{FeO} + m_{NiO}} \qquad \textbf{(A3.19)}$$

by substituting eqs.(A3.16), (A3.17) and (A3.18) into (A3.19), the expression of parameter β in terms of m_{O2}, m_{Cr} and γ can be obtained as follows:

$$\beta = \frac{C_1 m_{Cr}}{C_2 m_{O_2} - C_3 m_{Cr}} \qquad \textbf{(A3.20)}$$

where

$$C_1 = 1.462(0.951 + \gamma), \quad C_2 = 4.442 + 4.498\gamma, \quad C_3 = 0.659 + 0.610\gamma$$

APPENDIX IV

COMPUTER CODE FOR PREDICTING da/dN BASED ON THE PROPOSED MODEL

```
C  ***********************************************************************
C     MODEL.FOR IS A PORGRAM THAT SIMULATES THE FATIGUE CRACK
C     GROWTH RATE BASED ON THE PROPOSED MODEL
C     ***********************************************************************

      DIMENSION DK(50),RES(50),GA1(50),GB1(50),GC1(50),GD1(50)
      COMMON/AA1/ ETA,ETA1,BTA
      COMMON/AA2/ DTK,R0,D1,R,TH
      COMMON/AA3/ DLP,DS
      COMMON/AA4/GA,GB,GC,GD
C     INPUT r*,d,hold-time,frequency,DELTA-K,Ratio-R
      OPEN(20,FILE='DA1.DAT',STATUS='OLD')
      READ(20,*)R0,DD,TH,FQ,R,STEP
C     INPUT COEFFICIENTS OF GRAIN BOUNDARY DUCTILITY
C     INPUT A SET OF STRESS INTENSITY FACTOR RANGES DELTA-K
      OPEN(22,FILE='DA2.DAT',STATUS='OLD')
      OPEN(24,FILE='DA3.DAT',STATUS='OLD')
      DO 9 I=1,50
      READ(22,*,END=11) GA1(I),GB1(I),GC1(I),GD1(I)
      READ(24,*,END=11) DK(I)
9     CONTINUE
11    NPTS=I-1
      RR0=R0
      DO 12 JY=1,NPTS
      WRITE(6,300) NPTS,JY
300   FORMAT(1X,'NPTS=',I2,2X,'JY=',I2)
      DTK=DK(JY)
      GA=GA1(JY)
      GB=GB1(JY)
      GC=GC1(JY)
      GD=GD1(JY)
      R0=RR0+(JY-1)*STEP
      RI0=R0
```

```
      I1=1
      JJ=0
      WRITE(6,2)
2     FORMAT(4X,'r*(uM)  d(uM)  Th(sec.)  fq(Hz) DTK(MPam1/2)  R')
      WRITE(6,21)R0,DD,TH,FQ,DTK,R
21    FORMAT(6F9.3)
      DLP=8.314*923.0
      RR=1./FQ-5.0
      IF(RR.GT.0.0) THEN
         GO TO 3
          ELSE
         TR=TH
          GO TO 105
      END IF
C     CALCULATION OF THE CYCLE EFFECTIVE OXIDATION TIME t*
3     TR=TH+(1/FQ*IFIX(RR/ABS(RR)))
      ETA1=DD/SQRT(TR*1.2E-6)
      WRITE(6,501)ETA1
501   FORMAT(2X,F12.6)
105   ETA=R0/SQRT(TR*1.2E-6)
       WRITE(6,34) I1
34     FORMAT(5X,'The Number of Iteration I1 :',I3)
      CALL ENGY
      CALL SIMP2(2,1.0,DS,1.E-6,CR)
      CALL SIMP2(1,1.0,D1,1.E-6,O2)
      CO2I=ETA*O2*0.28209479
     CCRI=ETA1*CR*0.28209479
C     THE AMOUNT OF OXYGEN
     CO2=CO2I*97.181
C     THE AMOUNT OF CHROMIUM
     CCR=CCRI*1.4988E6
      WRITE(6,10) CO2,CCR
      UV=3.1273*CO2-0.4433*CCR
      IF(UV.EQ.0.) THEN
      WRITE(6,71)
71    FORMAT(3X,'The model does not apply for this case')
      STOP
      ELSE
      CONTINUE
      END IF
      BTA=CCR/UV
      WRITE(6,99)BTA
99    FORMAT(5X,'BTA=',F10.6)
      CALL CMO(DR,CP)
```

```
      IF(ABS(CP).LT.3.5E-2.AND.ABS(CP).GT.1.E-2) THEN
        DRR=ABS(DR)
      END IF
      WRITE(6,51) DRR
51    FORMAT(5X,'DRR=',E20.10)
        ADR=ABS(DR)/FLOAT(3*I1)
       IF(CP.GT.0.0) THEN
       R01=R01+ADR
       ELSE
       R01=R01-ADR
      END IF
       IF(ABS(CP).LT.5.E-3) THEN
        GOTO 202
      END IF
      WRITE(6,42)R01
42    FORMAT(3X,'R0=',E20.10)
      IF(I1.GT.15) THEN
        GOTO 202
      END IF
       R0=R01*1.E6
        I1=I1+1
       GOTO 105
202   CONTINUE
       IF(JJ.EQ.1) THEN
        GOTO 25
      END IF
      RL=R01
      WRITE(6,37) RL
37    FORMAT(5X,'RL=',E20.10)
      WRITE(6,28)
28    FORMAT(10X,'Iteration from the other side')
      DP=RL*1.E6-RI0
      WRITE(6,63) DP
63    FORMAT(5X,'DP=',E20.10)
       IF(DP.GT.0.0) THEN
      R0=RL+DRR
       ELSE
        R0=RL-DRR
      END IF
      WRITE(6,64) R0
64    FORMAT(5X,'inial value r0 for  other side1:'E20.10)
       R0=R0*1.E6
      I1=1
      JJ=1
```

```
      GOTO 105
25    RK=R01
C     THE FINAL RESULT r*
      R02=(RL+RK)*0.5*1E-6
102   WRITE(6,35) R02
35    FORMAT(3X,'da/dN=',E20.10)
      RES(JY)=R02
10    FORMAT(2X,'CO2=',E20.10,1X,'CCR=',E20.10)
12    CONTINUE
      OPEN(25,FILE='RESULT.DAT',STATUS='NEW')
      WRITE(25,31)
31    FORMAT(4X,'Fatigue Crack Growth Rate--da/dN (mm/cyc)')
      WRITE(25,32) (RES(J),J=1,NPTS)
32    FORMAT(8X,E20.10)
      STOP
      END
C
C
      SUBROUTINE SIMP2(J,A,B,EPS,SUM)
      DIMENSION F(2,30),FM(2,30),E(2,30),KRTN(30)
      SUM=0.0
      T=1.0
      ABSA=1.0
      EST=1.0
      DA=B-A
      FA=FCT(A,J)
      FB=FCT(B,J)
      RA1=0.5*(A+B)
      FP=4.0*FCT(RA1,J)
      X=A
      L=0
1     K=i
      L=L+1
      T=T*1.7
      DX=DA/3.0
      SX=DX/6.0
      RA2=X+0.5*DX
      FM1=4.0*FCT(RA2,J)
      RA3=X+DX
      F1=FCT(RA3,J)
      FM(1,L)=FP
      RA4=X+2.0*DX
      RA5=X+2.5*DX
      F(1,L)=FCT(RA4,J)
```

```
      FM(2,L)=4.0*FCT(RA5,J)
      F(2,L)=FB
      E1=SX*(FA+FM1+F1)
      E(1,L)=SX*(F1+FP+F(1,L))
      E(2,L)=SX*(F(1,L)+FM(2,L)+FB)
      S=E1+E(1,L)+E(2,L)
      ABSA=ABSA-ABS(EST)+ABS(E1)+ABS(E(1,L))
     * +ABS(E(2,L))
      IF(EST.EQ.1.0) GO TO 5
      IF(T*ABS(EST-S).LE.EPS*ABSA) GO TO 2
      IF(L.LT.30) GO TO 5
2     SUM=SUM+S
3     L=L-1
      T=T/1.7
      K=KRTN(L)
      DX=DX*3.0
      IF(K.EQ.3) IF(L-1) 6,6,3
      EST=E(K,L)
      EP=FM(K,L)
      FA=FB
      FB=F(K,L)
      K=K+1
      X=X+DA
4     DA=DX
      KRTN(L)=K
      GO TO 1
5     EST=E1
      FP=FM1
      FB=F1
      GO TO 4
6     RETURN
      END
C
C
      FUNCTION FCT(X,J)
      COMMON/AA1/ ETA,ETA1,BTA
      IF(J.EQ.2) GO TO 10
      FCT=EXP(-0.25*ETA*ETA/X)/(X*SQRT(X))
      RETURN
10    FCT=EXP(-0.25*ETA1*ETA1/X)/(X*SQRT(X))
      RETURN
      END
C
C     CALCULATION OF INELASTIC STRAIN ENERGY Wp,GRAIN
```

```
C     BOUNDARY DIFFUSIVITY Dg AND DISLOCATION DIFFUSIVITY Dd
C
      SUBROUTINE ENGY
      COMMON/AA2/ DTK,R0,D1,R,TH
      COMMON/AA3/ DLP,DS
      R01=R0*1E-6
      DWP=0.0
      IF(TH.EQ.0.0) GOTO 4
C     CONVERTING DELTA-K TO Kmin
      EK=R*DTK/(1.-R)
      DWC=EK*EK/R01
C     CREEP PART OF Wp
      DWP=DWC*2.881542E-7
4     DWF=DTK*DTK/R01
C     FATIGUE PART OF Wp
      DWP1=DWF*2.9762E-9
C     TOTAL INELASTIC STRAIN ENERGY
      DWP2=DWP+DWP1
      WRITE(6,7) DWP2
7     FORMAT(3X,'inelastic strain energy density Wp ',E20.10)
      G1=(5.61144*DWP2+2.17105)**2
      G2=-14.98601349-25.8863*EXP(0.520202/G1)
C     GRAIN BOUNDARY DIFFUSIVITY Dg
      DG=EXP(G2)*1.477361802E6
C     THE RATIO OF Dg/Dm
      D1=DG/1.2E-18
      WRITE(6,3)D1,DG
3     FORMAT(3X,'The Ratio of Dg/Dm:',2E20.10)
C     DIFFUSIVITY Dd FOR Cr
      WE1=(35.7822*DWP2-37.572)**2
      WE2=32.007*EXP(0.371187/WE1)
      DDL=EXP(-16.69870073-WE2)*1.45000365779E7
      DS=DDL/1.2E-18
      WRITE(6,6)DS,DDL
6     FORMAT(3X,'The Ratio of Dd/Dm:',2E20.10)
      RETURN
      END
C
C     CALCULATION OF INELASTIC STRAIN AND GRAIN BOUNDARY
C     DUCTILITY
C
      SUBROUTINE CMO(DR,CP)
      COMMON/AA2/DTK,R0,D1,R,TH
      COMMON/AA1/ETA,ETA1,BTA
```

```
      COMMON/AA4/GA,GB,GC,GD
C     CONVERTING SECONDS TO HOURS
      TH1=TH/3600.
      RP0=R0*1E-6
C     GRAIN BOUNDARY DUCTILITY
      EC=GA*ATAN(-GB*BTA*BTA+GC)+GD
      WRITE(6,89)EC
89    FORMAT(5X,'EC=',E20.10)
C     TOTAL INELASTIC STRAIN
      EMC=0.0
      IF(TH.EQ.0.0) GOTO 57
      AK=DTK*R/(1.-R)
      EM1=TH1**0.09090909091
      EM2=AK**1.8181818182
      EM3=RP0**(-0.90909091)
      EMC=(EM1*EM2*EM3)*8.34E-9
57    EMF=((DTK*DTK/RP0)**0.909091)*6.202E-11
      EM=EMC+EMF
      WRITE(6,10)EM
10    FORMAT(3X,'EM=',E18.10)
      CP=(EM-EC)/EC
      AM=0.0
      IF(TH.EQ.0.0) GOTO 58
      AM=EM1*EM2*8.34E-9
58    BM1=DTK**1.818182
      BM=BM1*6.202E-11
      R1=((AM+BM)/EC)**1.1
C     THE DIFFERENCE BETWEEN r* AND r-trying
      DR=RP0-R1
      RETURN
      END
```

APPENDIX V

COMPUTER CODES FOR DATA REDUCTION

```
C     ************************************************************************
C     CT122.BAS IS A PROGRAM THAT CONVERTS A SET OF DATA N VS
C     V1/V2 TO A SET OF DATA N VS A FOR CT12.5 SPECIMEN BASED ON
C     TWO MEASURED PINTS
C     ************************************************************************

10    PRINT "ENTER THE NAME OF THE INPUT FILE":INPUT S$
20    PRINT "ENTER THE NAME OF THE OUTPUT FILE":INPUT T$
30    PRINT "ENTER V1/V2 (BEGINNING) AND A/W":INPUT V1,AW1
60    PRINT "ENTER V1/V2 (FINAL) AND A/W":INPUT V2,AW2
70    PRINT"ENTER THE WIDTH OF SPECIMEN":INPUT W
80    OPEN S$+"DAT" FOR INPUT AS #1
90    OPEN T$+"DAT" FOR INPUT AS #2
100   C1=1.007:C2=-0.0357:C3=-0.015898
110   AWC1=(C1+C2*V1+C3*V1^2):AWC2=(C1+C2*V2+C3*V2^2)
120   A=((AW21-AW1)-(AWC2-AW2))/(V2-V1)
130   B=(AW1-AWC1)-A*V1:G1=C1+B:G2=C2+A:G3=C3
140   INPUT #1, N,V
150   A=W*(G1+G2*V+G3*V^2)
160   PRINT #2, USING "#######";N,
170   PRINT #2, USING "####.#####";A
180   IF EOF(1)=0 GOTO 140
190   CLOSE #1:CLOSE #2:END
```

```
C     ************************************************************************
C     CT124.BAS IS A PROGRAM THAT CONVERTS A SET OF DATA N VS
C     V1/V2 TO A SET OF DATA N VS A FOR CT12.5 SPECIMEN BASED ON
C     FOUR MEASURED PINTS
C     ************************************************************************

10    PRINT "ENTER THE NAME OF THE INPUT FILE":INPUT S$
20    PRINT "ENTER THE NAME OF THE OUTPUT FILE":INPUT T$
30    PRINT "ENTER V1/V2 (BEGINNING) AND A/W":INPUT V1,AW1
```

```
40    PRINT "ENTER V1/V2 (SECOND) AND A/W":INPUT V2,AW2
50    PRINT "ENTER V1/V2 (THIRD) AND A/W":INPUT V3,AW3
60    PRINT "ENTER V1/V2 (FINAL) AND A/W":INPUT V4,AW4
70    PRINT"ENTER THE WIDTH OF SPECIMEN":INPUT W
80    OPEN S$+"DAT" FOR INPUT AS #1
90    OPEN T$+"DAT" FOR INPUT AS #2
100   C1=1.007:C2=-0.0357:C3=-0.015898
110   AWC1=(C1+C2*V1+C3*V1^2):AWC2=(C1+C2*V2+C3*V2^2)
120   AWC3=(C1+C2*V3+C3*V3^2):AWC4=(C1+C2*V4+C3*V4^2)
130   U1=AW1-AWC1:U2=AW2-AWC2:U3=AW3-AWC3:U4=AW4-AWC4
140   S1=V1-V2:Q1=V1^2-V2^2:F1=U1-U2
150   S2=V3-V4:Q2=V3^2-V4^2:F2=U3-U4
160   S3=V1-V3:Q3=V1^2-V3^2:F3=U1-U3
170   E1=S2*Q1-S1*Q2:Y1=S2*F1-S1*F2
180   E2=S1*Q3-S3*Q1:Y2=S1*F3-S3*F1
190   C=V1/E1
240   B=(S2*F1-S2*Q1*C)/(S1*S2)
250   A=U1-B*V1-C*V1^2
260   G1=C1+A:G2=C2+B:G3=C3+C
270   INPUT #1, N,V
280   A=W*(G1+G2*V+G3*V^2)
290   PRINT #2, USING "#######";N,
300   PRINT #2, USING "####.#####";A
310   IF EOF(1)=0 GOTO 270
320   CLOSE #1:CLOSE #2:END
```

```
C     ************************************************************
C     SMOOTH.BAS IS A PROGRAM THAT SMOOTHS THE DATA POINTS
C     BASED ON SEVEN POINT MOVING AVERAGE METHOD
C     ************************************************************

10    DIM X(3000),Y(3000),Y1(3000)
20    I=0
30    PRINT "ENTER THE NAME OF THE INPUT DATA FILE":INPUT S$
40    PRINT "ENTER THE NAME OF THE OUTPUT DATA FILE":INPUT Z$
50    OPEN Z$+".DAT" FOR OUTPUT AS #2
60    OPEN S$+".DAT" FOR INPUT AS #1
70    INPUT #1, N,A
80    X(I)=N:Y(I)=A:I=I+1
90    IF EOF(1)=0 GOTO 70
100   CLOSE #1:M=I-1:M1=M-3:PRINT M
```

```
110   FOR J=3 TO M1
120   Y1(J)=(Y(J-3)+Y(J-2)+Y(J-1)+Y(J)+Y(J+1)+Y(J+2)+Y(J+3))/7
130   NEXT J
140   Y1(0)=(13*Y(0)+10*Y(1)+7*Y(2)+4*Y(3)+Y(4)-2*Y(5)-5*Y(6))/28
150   Y1(1)=(5*Y(0)+4*Y(1)+3*Y(2)+2*Y(3)+Y(4)-Y(6))/14
160   Y1(2)=(7*Y(0)+6*Y(1)+5*Y(2)+4*Y(3)+3*Y(4)+2*Y(5)+Y(6))/28
170   B1=(Y(M-6)+2*Y(M-5)+3*Y(M-4)+4*Y(M-3)+5*Y(M-2))
180   Y1(M-2)=(B1+6*Y(M-1)+7*Y(M))/28
190   B2=(-Y(M-6)-2*Y(M-5)+Y(M-4)+4*Y(M-3)+7*Y(M-2))
200   Y1(M-1)=(B2+5*Y(M))/14
210   B3=(-5*Y(M-6)-2*Y(M-5)+Y(M-4)+4*Y(M-3)+7*Y(M-2))
220   Y1(M)=(B3+10*Y(M-1)+13*Y(M))/28
230   FOR J1=0 TO M
240   PRINT #2, USING "#######";X(J1),
250   PRINT #2, USING "###.#####";Y1(J1)
260   NEXT J1:CLOSE #2:END
```

```
C     ************************************************************************
C     BLOCK.BAS IS A PROGRAM THAT REDUCES THE NUMBER OF DATA
C     POINTS DOWN TO A APPROPRIATE NUMBER
C     ************************************************************************

10    PRINT "ENTER THE NAME OF THE INPUT FILE":INPUT Z$
20    PRINT "ENTER THE NAME OF THE OUTPUT FILE":INPUT S$
30    OPEN S$ FOR OUTPUT AS #1
40    I=0:V1=0:I1=O
50    OPEN Z$ FOR INPUT AS #3
60    INPUT #3, N,V:I1=I1+1
70    IF EOF(3)=0 GOTO 60
80    CLOSE #3:PRINT "TOTAL DATA POINTS",I1
90    PRINT "THE SMALLEST BLOCK SIZE IS":INPUT B2
100   PRINT "THE INCREMENT OF EACH BLOCK IS":INPUT D1
110   S1=(1-2*B2/D1):S2=S1^2:S3=8*I1/D1:P1=(S1+SQR(S2+S3))/2
120   OPEN Z$ FOR INPUT AS #3
130   I3=FIX(P1):BB=0
140   IF I3<0 GOTO 160
150   B1=FIX(B2+(I3-1)*D1)
160   INPUT #3, N,V
170   I=I+1:V1=V1+V
180   IF I=1 THEN M=N
190   IF EOF(3)=-1 GOTO 220
```

```
200    IF I=B1 GOTO 220
210    GOTO 160:V1=V1/B1:GOTO 230
220    V1=V1/I
230    M1=N:N1=FIX(M+M1)/2)
240    PRINT #1, USING "######";N1,
250    PRINT #1, USING "####.######";V1
260    I=0:V1=0:I3=I3-1:IF I3<0 THEN B1=1
270    BB=BB+B1:IF BB>I1 GOTO 290
280    IF EOF(3)=0 GOTO 140
290    CLOSE #1:CLOSE #3:END
```

```
C      ************************************************************************
C      DADNDK.FOR IS A PORGRAM THAT TAKES N VS A DATA AND
C      COMPUTES DA/DN USING THE SEVEN POINT INCREMETNAL
C      POLYNOMIAL TECHNIQUE THAT IS RECOMMENDED BY THE ASTM
C      STANDARD E647-88.
C      ************************************************************************

      DIMENSION A(900), N(900), BB(3), DADN(900), DELK(900), ID(7)
      DIMENSION AA(10), NN(10)
      REAL N
      REAL NN
      INTEGER QQ
      CHARACTER NAME*12
    1 FORMAT (A)
      WRITE(*,*) 'ENTER THE NAME OF THE DATA FILE CONTAINING
        *N/A DATA'
      READ(*,1) NAME
      OPEN(1,FILE=NAME)
      READ (1,*,END=10) (N(I),A(I),I=1,10000)
   10 CONTINUE
      WRITE(*,*) 'ENTER THE MINIMUM LOAD AND THE MAXIMUM LOAD'
      READ(*,*) PMIN,PMAX
      WRITE(*,*) 'ENTER THE THICKNESS AND THE WIDTH OF THE SPECIMEN'
      READ(*,*) B,W
      K=0
      R=PMIN/PMAX
      PP=PMAX-PMIN
      NPTS=I-1
      DO 11 I=1,NPTS
   11 CONTINUE
```

```
      WRITE(*,*) 'ENTER THE NAME OF THE OUTPUT DATA FILE'
      READ(*,1) NAME1
      OPEN(2,FILE=NAME1,STATUS='NEW')
      WRITE(*,*) 'OBS.NO. CYCLES  A(MEAS)  A(REG) M.C.C. DK  DA/DN'
      DO 110 I=1,3
      D12=(A(I+1)-A(I))/(N(I+1)-N(I))
      A1=(A(I+1)+A(I))*0.5
      T1=A1/W
         TP=(2.0+T1)/(1.0-T1)**(1.5)
         FT1=TP*(0.886+4.64*T1-13.32*T1**2+14.72*T1**3-5.6*T1**4)
      DELK1=(31.624*(FT1*PP))/(B*SQRT(W))
C     WRITE(2,78) I,N(I),A(I),DELK1,D12
      WRITE(2,79) DELK1,D12
      WRITE(*,78) I,N(I),A(I),DELK1,D12
  110 CONTINUE
      NPTS=NPTS-6
      DO 100 I=1,NPTS
      L=0
      K=K+1
      K1=K+6
      DO 60 J=K,K1
      L=L+1
      AA(L)=A(J)
      NN(L)=N(J)
   60 CONTINUE
      C1=0.5*(NN(1)+NN(7))
      C2=0.5*(NN(7)-NN(1))
      SX=0
      SX2=0
      SX3=0
      SX4=0
      SY=0
      SYX=0
      SYX2=0
      DO 70 J=1,7
      X=(NN(J)-C1)/C2
      YY=AA(J)
      SX=SX+X
      SX2=SX2+X*X
      SX3=SX3+X*X*X
      SX4=SX4+X*X*X*X
      SY=SY+YY
      SYX=SYX+X*YY
      SYX2=SYX2+YY*X*X
```

```
 70 CONTINUE
    DEN=7.0*(SX2*SX4-SX3**2)-SX*(SX*SX4-SX2*SX3)+SX2*(SX*SX3-SX2**2)
    T2=SY*(SX2*SX4-SX3**2)-SYX*(SX*SX4-SX2*SX3)+SYX2*(SX*SX3-SX2**2)
    BB(1)=T2/DEN
       T3=7.0*(SYX*SX4-SYX2*SX3)-SX*(SY*SX4-SYX2*SX2)+SX2*(SY*SX3
      *-SYX*SX2)
    BB(2)=T3/DEN
       T4=7.0*(SX2*SYX2-SX3*SYX)-SX*(SX*SYX2-SX3*SY)+SX2*(SX*SYX
      *-SX2*SY)
    BB(3)=T4/DEN
    YB=SY/7.0
    RSS=0
    TSS=0
    DO 75 J=1,7
    X=(NN(J)-C1)/C2
    YHAT=BB(1)+BB(2)*X+BB(3)*X**2
    RSS=RSS+(AA(J)-YHAT)**2
    TSS=TSS+(AA(J)-YB)**2
 75 CONTINUE
 76 FORMAT(I4,2X,F9.0,2X,F8.2,2X,F8.2,2X,F8.4,2X,F8.2,2X,E15.5)
 78 FORMAT(I4,2X,F9.0,2X,F8.2,2X,8X,2X,8X,2X,F8.2,2X,E15.5)
 79 FORMAT(F8.2,2X,E15.5)
    R2=1.0-RSS/TSS
    DADN(I)=BB(2)/C2+2.0*BB(3)*(NN(4)-C1)/C2**2
    X=(NN(4)-C1)/C2
    AR=BB(1)+BB(2)*X+BB(3)*X**2
    QQ=I+3
    T=AR/W
       TP=(2.0+T)/(1.0-T)**(1.5)
       FT=TP*(0.886+4.64*T-13.32*T**2+14.72*T**3-5.6*T**4)
    DELK(I)=(31.624*(FT*PP))/(B*SQRT(W))
C    WRITE(2,76) QQ,N(QQ),A(QQ),AR,R2,DELK(I),DADN(I)
    WRITE(2,79) DELK(I),DADN(I)
    WRITE(*,76) QQ,N(QQ),A(QQ),AR,R2,DELK(I),DADN(I)
100 CONTINUE
    J=NPTS+4
    K=NPTS+6
    DO 120 I=J,K
    D12=(A(I+1)-A(I))/(N(I+1)-N(I))
    A2=(A(I+1)+A(I))*0.5
    T2=A2/W
       TP=(2.0+T2)/(1.0-T2)**(1.5)
       FT=TP*(0.886+4.64*T2-13.32*T2**2+14.72*T2**3-5.6*T2**4)
    DELK2=(31.624*(FT2*PP))/(B*SQRT(W))
```

```
C     WRITE(2,78) I,N(I),A(I),DELK2,D12
      WRITE(2,79) DELK2,D12
      WRITE(*,78) I,N(I),A(I),DELK2,D12
  120 CONTINUE
      STOP
      END
```

BIBLIOGRAPHY

[1] T. Weerasooriya et al., "Research on Mechanical Properties for Engine Life Prediction", AFWAL-TR-88-4062, Wright-Patterson AFB, OH, May 1988

[2] P. Shahinian and K. Sadananda, "Creep-Fatigue-Environment Interaction on Crack Propagation in Alloy 718", in Engineering Aspects of Creep, Institute of Mechanical Engineers, London, **Vol. 2**, 1980, Paper C239/80

[3] L. A. James, "The Effect of Temperature upon the Fatigue-Crack Growth Behavior of Two Nickel-Base Alloy", Journal of Engineering Materials and Technology, **Vol.95**, 1973, pp.254-256

[4] M. Clavel and A. Pineau, " Frequency and Wave-Form Effects on the Fatigue Crack Growth Behavior of Alloy 718 at 298K and 823K", Metallurgical Transactions, **Vol. 9A**, 1978, pp.471-480

[5] S. Floreen and R. H. Kane, "An Investigation of the Creep-Fatigue-Environment Interaction in a Ni-Base Superalloys", Fatigue of Engineering Materials and Structures, **Vol. 2**, 1980, pp.401-412

[6] T. Weerasooriya and S. Venkataraman, "Frequency and Environment Effect on Crack Growth in Inconel 718," in Effects of Load and Thermal Histories, eds. by P. K. Liaw and T. Nicholas, the Metallurgical Society of AIME, Warrendal, PA, 1987, pp.101-108

[7] T. Weerasooriya, "Effect of Frequency on Fatigue Crack Growth Rate of Inconel 718 at High Temperature", in Fracture Mechanics: Nineteenth Symposium, ASTM STP 969, ed. by T. A. Cruse, American Society for Testing and Materials, Philadelphia, PA, 1988, pp.907-923

[8] L. A. James, "Fatigue Crack Propagation in Alloy 718: A review", in Superalloy 718: Metallurgy and Applications, ed. by E. A. Loria, Pittsburgh, PA, American Society for Metals, 1989, pp.499-515

[9] J. P. Pedron and A. Pineau, "The Effect of Microstructure and Environment on the Crack Growth Behavior of Inconel 718 Alloy at 650°C under Fatigue, Creep and Combined Loading", Materials Science and Engineering, **Vol. 56**, 1982, pp.143-156

[10] L. A. James, "The Effect of Grain Size upon the Fatigue-Crack Propagation

Behavior of Alloy 718 under Hold-Time Cycling at Elevated Temperature", Engineering Fracture Mechanics, **Vol. 25**, 1986, pp.305-314

[11] C. Bathias and R. M. Pelloux. "Fatigue Crack Propagation in Martensitic and Austenitic Steels", Metallurgical Transactions, **Vol. 4**, 1973, pp.1265-1273

[12] H. H. Smith and D. J. Michel, "Fatigue Crack Propagation and Deformation Mode in Alloy 718 at Elevated Temperatures", in Ductility and Toughness Considerations in Elevated Temperature Service, MPC-8, ed. by G. V. Smith, American Society of Mechanical Engineering, New York, 1978, pp.225-246

[13] M. Clavel and A. Pineau, "Intergranular Fracture Associated with Heterogeneous Deformation Modes during Low Cycle Fatigue in a Ni-Base Superalloy", Scripta Metallurgy, **Vol. 16**, 1982, pp.361-364

[14] M. Clavel and A. Pineau, "Fatigue Behavior of Two Nickel-Base Alloys, Part I: Experimental Results on Low Cycle Fatigue, Fatigue Crack Propagation and Substructures", Materials Science and Engineering, **Vol. 55**, 1982, pp.157-171

[15] D. Fournier and A. Pineau, "Low Cycle Fatigue Behavior of Inconel 718 at 298K and 823K", Metallurgical Transactions, Vol. 8A, 1977, pp.1095-1105

[16] D. J. Wilson, "Relationship of Mechanical Characteristics and Microstructural Features to the Time-Dependent Edge-Notch Sensitivity of Inconel 718 Sheet", Journal of Engineering Materials and Technology, **Vol. 113**, 1973, pp.112-123

[17] H. Ghonem, D. Zheng, E. Andrieu and A. Pineau, "Experimental Observations and Quantitative Modelling of Oxidation-Assisted Crack Growth Behavior in Alloy 718 at 650°C", Annual report, AFOSR-89-0285, 1990

[18] N. E. Ashbaugh, "Waveshape Effects Upon Crack Growth in Inconel 718," presented at 15th National Symposium on Fracture Mechanics, University of Maryland, Clooege Park, MD, July 8, 1982

[19] P. Shahinian and K. Sadananda, "Crack Growth under Creep and Fatigue Conditions", in Creep-Fatigue-Environment Interactions, eds. by R. M. Pelloux and N. S. Stoloff, the Metallurgical Society of AIME, Warrendal, PA, 1981, pp.86-111

[20] P. Shahianian and K. Sadananda, "Crack Growth Behavior under Creep-Fatigue Conditions in Alloy 718," in Creep Fatigue Interaction, MPC3, American Society of Mechanical Engineering, Philadelphia, PA, 1976, pp.365-390

[21] H. H. Smith and D. J. Michel, "Effect of Environment on Fatigue Crack Propagation Behavior of Ally 718 at Elevated Temperatures", Metallurgical

Transactions, **Vol. 17A**, 1986, pp.370-374

[22] P. Shahianian and K. Sadananda, "Effects of Stress Ratio and Hold-Time on Fatigue Crack Growth in Alloy 718", Journal of Engineering Materials and Technology, **Vol. 101**, 1979, pp.224-230

[23] T. Nicholas and T. Weerasooriya, "Hold-Time Effects in Elevated Temperature Fatigue Crack Propagation," in Fracture Mechanics: Seventeenth Volume, ASTM STP 905, American Society for Testing and Materials, Philadelphia, PA, 1986, pp.155-168

[24] J. P. Pedron and A. Pineau, "Effect of Hold Times on the Elevated Temperature Fatigue Crack Growth Behavior of Inconel 718 Alloy," in Advances in Fracture Research, **Vol. 5**, 1981, pp.2385-2392

[25] A. Diboine and A. Pineau, "Creep Crack Initiation and Growth in Inconel 718 at 650°C," Fatigue and Fracture of Engineering Materials and Structure, **Vol. 10**, 1987, pp.141-151

[26] K. Sadananda and P. Shahinian, "Effects of Environment on High Temperature Crack Growth Behavior of Several Nickel-Base Alloys", in Corrosion of Nickel-Base Alloys, ed. by R. C. Scarberry, ASM Publication, Cincinnati, Ohio, 1985, pp.101-115

[27] P. Shahinian, "Effect of Environment on Creep-Rupture Properties of Some Commercial Alloys", Transactions of the American Society for Metals, **Vol. 49**, 1957, pp.862-882

[28] R. H. VanStone, O. C. Gooden and D. D. Krueger, "Advanced Cumulative Damage Modeling", AFWAL-TR-88-4146, Materials Laboratory, Wright-Patterson AFB, OH, 1988.

[29] K. Sadananda and P. Shahinian, "Crack Growth Behavior in Alloy 718 at 425°C", Journal of Engineering Materials and Technology, **Vol. 100**, 1978, pp.381-387

[30] H. Ghonem and D. Zheng, "Characterization of Environment-Dependent Fatigue Crack Growth in Alloy 718 at 650°C", in Superalloy 718, 625 and Various Derivations, ed. by E. A. Loria, the Minerals, Metals & Materials Society, Warrendal, PA, 1991, pp.477-490

[31] S. Venkataraman and T. Nicholas, "Mechanisms of Elevated Temperature Fatigue Crack Growth in Inconel 718 as a Function of Stress Ratio," in Effects of Load and Thermal Histories, eds. by P. K. Liaw and T. Nicholas, the Metallurgical Society, Inc., 1987, pp.81-99

[32] A. Coles, R. E. Johnson and H. G. Popp, "Utility of Surface-Flawed Tensile Bars in Cyclic Life Studies", Journal of Engineering Materials and Technology, Vol. 98, 1976, pp.305-315

[33] H. F. Merrick and S. Floreen, "The Effects of Microstructure on Elevated Temperature Crack Growth in Nickel-Base Alloys", Metallurgical Transactions, Vol.9A, 1978, pp.231-236

[34] S. Floreen and R. Raj, "Environmental Effects in Nickel-Base Alloys", in Flow and Fracture at Elevated Temperatures, ed. by R. Raj, American Society for Metals, Metals Park, Ohio, 1985, pp. 383-402

[35] E. Andrieu, R. Cozar and A. Pineau, "Effect of Environment and Microstructure on the High Temperature Behavior of Alloy 718", in Superalloys Metallurgy & Applications, ed. by E. A Loria, Pittsburgh, PA, American Society for Metals, 1989, pp.241-247

[36] R. Thamburaj, T. Terada, A. K. Koul, W. Wallace and M. C. de Malherbe, "The Influence of Microsructure and Environment upon Elevated Temperature Crack Growth Rates in Inconel 718", in Proceedings of the International Conference on Creep, Tokyo, Japan, 1986, pp.275-282

[37] H. H. Smith and D. J. Michel, "Effects of Thermal and Thermomechanical Treatments on the Mechanical Properties of Centrfugally Cast Alloy 718", Materials Science and Engineering, Vol. 102A, 1988, pp.161-168

[38] S. Floreen, "High Temperature Crack Growth Structure-Property Relationships in Nickel Base Superalloys", in Creep-Fatigue-Environment Interactions, eds. by R. M. Pelloux and N. S. Stoloff, The Metallurgical Society of AIME, Warrendal, PA, 1982, pp.112-128

[39] R. Thamburaj, W. Wallace, T. L. Prakash and Y. N. Chari, "Influence of Processing Variables on Prior Particle Boundary Precipitation and Mechanical Behavior in PM Superalloy APK1", Powder Metallurgy, Vol. 27, 1984, pp.169-180

[40] M. Clavel, C. Levaillant and A. Pineau, "Influence of Micromechanisms of Cyclic Deformation at Elevated Temperature on Fatigue Behavior", in Creep-Fatigue-Environment Interactions, ed by R. M. Pelloux and N. S. Stoloff, AIME Publication, 1980, pp.24-45

[41] S. D. Antolovich and N. Jayaraman, "Metallurgical Instabilities during the High Temperature Low Cycle Fatigue of Nickel-Base Superalloys", Materials Science and Engineering, Vol. 57, 1982, L9-L12

[42] R. B. Scarlin, "Some Effects of Microstructure and Environment on Fatigue Crack Propagation", in Fatigue Mechanism, ASTM STP 675, ed. by J. T. Fong, American Society for Testing and Materials, Philadelphia, PA, 1979, pp.396-419

[43] J. M. Davidson and J. K. Tien, "Environmental Effects on the Creep Behavior of a Nickel-Base Superalloy", Metallurgical Transactions, **Vol. 12A**, 1981, pp.865-876

[44] J. Bressers and M. Roth, "The Effect of Time-Dependent Processes on the HTLCF Endurance of PM Astroloy", in Proceedings of International Conference on Advances in Life Prediction Methods, 1983, Albany, NY, American Society of Mechanical Engineering

[45] K. Sadananda and P. Shahinian, "High Temperature Time-Dependent Crack Growth", in Micro and Macro Mechanics of Crack Growth, eds. by K. Sadananda, B. B. Rath and D. J. Michel, The Metallurgical Society of AIME, 1981, pp.119-130

[46] K. Sadananda and P. Shahinian, "Creep Crack Growth behavior and Theoretical Modelling", Metal Science, **Vol. 15**, 1981, pp.425-432

[47] J. W. Brooks and P. J. Bridges, "Long Term Stability of Inconel Alloy 718 for Turbine Disc Applications", in Hihj temperature Alloys for Gas Turbines and Other Applications 1986, eds. by W. Betz, R, Brunetaud, D. Coutsouradis, H. Fischmeister, T. B. Gibbons, I. Kvernes, Y. Lindblom, J. B. Marriott and D. B. Meadowcroft, Reidel Publishing Company, Dordrecht, 1986, pp.1431-1440

[48] A. Pineau, "Intergranular Creep-Fatigue Crack Growth in Ni-Base Alloys", in Flow and Fracture at Elevated Temperature, ed. by R. Raj, American Society for Metals, 1985, pp.317-348

[49] H. Ghonem and D. Zheng, "Intergranular Oxygen Diffusion Depth during Environment-Dependent Fatigue Crack Growth in Alloy 718", to be published in Materials Science and Engineering, 1991

[50] E. Andrieu, "Influence de L'environmnt sur la Propagation des Fissures dans und Superalliage Base Nickel: L'Inconel 718", Ph.D. Thesis, Ecole des Mines de Paris, 1987

[51] K. U. Snowden, "The Effect of Atmosphere on the Fatigue of Lead", Acta Metallurgica, **Vol. 12**, 1964, pp.295-303

[52] S. Floreen, "Effects of Environment on Intermediate Temperature Crack Growth in Superalloys", in Micro and Macro Mechanics of Crack Growth, eds. by K. Sadananda, B. B. Rath and D. J. Michel, The Metallurgical Society of AIME,

1981, pp.177-184

[53] K. U. Snowden and J. N. Greenwood, "Surface Deformation Differences between Lead Fatigue in Air and in Partial Vacuum", Trans. of the Metallurgical Society of AIME, **Vol. 212**, 1958, pp.626-627

[54] K. U. Snowden, "The Distribution of Deformation in Lead Fatigue in Vacuo", Philosophical Magazine, **Vol. 6**, 1961, pp.321-327

[55] J. L. Yueu, P. Roy and W. D. Nix, "Effect of Oxidation Kinetics on the near Threshold Fatigue Crack Growth Behavior of A Nickel Base Superalloy," Metallurgical Transactions, **Vol. 15A**, 1984, pp.1769-1775

[56] L. F. Coffin, Jr., "Cyclic-Strain-Induced Oxidation of high-Temperature Alloys", Trans. of the ASM, **Vol. 56**, 1963, pp.339-350

[57] P. K. Wright, "Oxidation-Fatigue Interactions in a Single-Crystal Superalloy," in Low Cycle Fatigue, ASTM STP 942, eds. by H. D. Solomon, G. R. Halford and B. N. Leis, American Society for Testing and Materials, Philadelphia, PA, 1988, pp.558-575

[58] R. P. Skelton and J. Bucklow, "Cyclic Oxidation and Crack Growth during High Strain Fatigue of Low Alloy Steel", Met. Sci., **Vol. 12**, 1978, pp. 64-70

[59] J. R. Haigh, R. P. Skelton and C. E. Richards, "Oxidation-Assisted Crack Growth during High Cycle Fatigue of A 1%Cr-Mo-V Steel at 550°C," Materals Science and Engineering, **Vol. 26**, 1976, pp.167-174

[60] T. E. Strangman, "Thermal Fatigue Oxidation Resistant Overlay Coatings for Superalloys," Ph.D. Dissertation, University of Connecticut, Storrs, CT, USA, 1978

[61] P. Marshall, "The Influence of Environment on Fatigue and Creep/Fatigue," in Fatigue at High Temperature, International Spring Meeting, Societe Francaise de Metallurgie, Paris, France, 1986, pp.109-145

[62] G. Ward, B. S. Hochkenbull and P. Hancock, "The Effect of Cyclic Stressing on the Oxidation of A Low-Carbon Steel", Matallurgical Transactions, **Vol. 5**, 1974, pp.1451-1455

[63] J. W. Swanson and H. L. Marcus, "Oxygen Transport during Fatigue Crack Growth", Matallurgical Transactions, **Vol. 9A**, 1978, pp.291-293

[64] F. E. Fujita, "Oxidation and Dislocation Mechanisms in Fatigue Crack Formation," in Fracture of Solids, eds. by D. C. Drucker and J. J. Gilman, Interscience

Publisher, New York, 1963, pp.657-670

[65] K. D. Challenger, R. P. Skilton and J. S. Kamen, "The Effect of Oxidation on Fatigue Crack Growth in 2.25Cr-1Mo Steel at 525°C: A Metallographic Examination", Materials Science and Engineering, **Vol. 91**, 1987, pp.1-6

[66] J. Rechet and L. Remy, "Fatigue Oxidation Interaction in a Superalloy — Application to Life Prediction in High Temperature Low Cycle Fatigue," Metallurgical Transactions, **Vol. 14A**, 1983, pp.141-149

[67] M. Reger and L. Remy, "Fatigue Oxidation Interaction in IN100 Superalloy," Metallurgical Transactions, **Vol. 19A**, 1988, pp.2259-2268

[68] S. J. Balsone, T. Nicholas and M. Khobaib, "Effects of Stress History on the Magnitude of the Environmental Attack in Rene' 80," in Environmentally Assisted Cracking: Science and Engineering, ASTM STP 1049, eds. by W. B. Lisagor, T. W. Croofer and B. N. Leis, American Society for Testing and Materials, Philadelphia, PA, 1990, pp.303-318

[69] T. Nicholas, T. Weerasooriya and N. E. Ashbaugh, "A Model for Creep/Fatigue Interaction in Alloy 718", in Fracture Mechanics: Sixteenth Symposium, ASTM STP 868, eds. by M. F. Kannien and A. T. Hopper, American Society for Testing and Materials, Philadelphia, PA, 1985, pp.167-180

[70] R. P. Wei and J. D. Landes, "Correlation between Sustained-Load and Fatigue Crack Growth in High-Strength Steels", Materials Research and Standards, **Vol.9**, 1969, pp.25-28,44 and 46

[71] T. Nicholas, "Fatigue Crack Growth Modeling at Elevated Temperature Using Fracture Mechanics", in Elevated Temperature Crack Growth, eds. by S. Mall and T. Nicholas, American Society of Mechanical Engineers, New York, NY, 1990, pp.107-112

[72] M. R. Winstone, K. M. Nikbin and G. A. Webster, "Modes of Failure under Creep/Fatigue Loading of A Nickel-Based Superalloy", Journal of Materials Science, **Vol. 20**, 1985, pp.2471-2476

[73] A. Saxena, "A Model for Predicting the Environment Enhanced Fatigue Crack Growth Behavior at High Temperature", in Thermal and Environmental Effects in Fatigue: Research-Design Interface, eds. by E. J. Carl, J. H. Stephen, Jr. and E. M. Michael, American Society of Mechanical Engineering, New York, NY, 1983, pp.171-184

[74] M R. Achter, "The Adsorption Model for Environmental Effects in Fatigue Crack

Propagation", Scripta Metallurgica, Vol. 2, 1968, pp.525-528

[75] R. P. Wei, "On Understanding Environment-Enhanced Fatigue Crack Growth — A Fundamental Approach", in Fatigue Mechanisms, ed. by J. T. Fong, ASTM STP 675, American Society for Testing and Materials, Philadelphia, PA, 1979, pp.816-840

[76] T. W. Weir, G. W. Simmons, R. G. Hart and R. P. Wei, "A Model for Surface Reaction and Transport Controlled Fatigue Crack Growth", Scripta Metallurgica, Vol. 14, 1980, pp.357-364

[77] J. J. McGowan and H. W. Liu, "A Kinetic Model of High Temperature Fatigue Crack Growth", in Fatigue Environment and Temperature Effects, eds. by J. B. Jhon and W. Volker, Plenum Press, New York, NY, 1983, pp.377-390

[78] S. D. Antolovich and E. Rosa, "Low Cycle Fatigue of Rene 77 at Elevated Temperatures", Materials Science Engineering, Vol. 47, 1981, pp.47-57

[79] G. R. Romanoski, S.D. Antolovich and R. M. Pelloux, "A Model for Life Predictions of Nickel-Base Superalloy in High Tmperature Lw Ccle Ftigue", in Low Cycle Fatigue, ASTM STP 942, eds. by H. D. Solomon, G. R. Halford and B. N. Leis, American Society for Testing and Materials, Philadelphia, PA, 1988, pp.456-469

[80] L. F. Coffin, Jr., "Overview of Temperature and Environmental Effects on Fatigue of Structural Metals", in Fatigue: Environment and Temperature Effects, eds. by J. J. Burke and V. Weiss, Plenum Press, New York, NY, 1980, pp.1-40

[81] H. Ghonem and R. Foerch, "Frequency Effects on Fatigue Crack Growth Behavior in A near-α Titanium Alloy", in Elevated Temperature Crack Growth, eds. by S. Mall and T. Nicholas, American Society of Mechanical Engineering, New York, NY, 1990, pp.93-105

[82] E. Andrieu, H. Ghonem and A. Pineau A, "Two Stage Crack Tip Oxidation Mechanism in Alloy 718", in Elevated Temperature Crack Growth, eds. by S. Mall and T. Nicholas, American Society of Mechanical Engineers, New York, NY, 1990, pp.25-29

[83] H. Ghonem and D. Zheng, "Oxidation-Assisted Fatigue Crack Growth Behavior in Alloy 718 — Part I: Quantitative Modelling", Fatigue & Fracture Engineering Materials & Structures, Vol. 14 , 1991, pp.749-760

[84] P. G. Shewmon, Diffusion in solids, McGraw-Hill Book Company, Inc., New York,1963

[85] H. H. Smith, P. Shahinian and M. R. Achter, "Fatigue Crack Growth Rates in Types 316 Stainless Steel at Elevated Temperature as A Function of Oxygen Pressure", Transactions of the Metallurgical Society of AIME, **Vol. 245**, 1969, pp. 947-953

[86] R. H. Bricknell and D. A. Woodford, "The Embrittlement of Nickel Following High Temperature Air Exposure", Metallurgical Transactions, **Vol. 12A**, 1981, pp.425-433

[87] C. J. McMahon and L. F. Coffin, "Mechanisms of Damage and Fracture in High-Temperature Low Cycle Fatigue of A Cast Nickel-Based Superalloy", Metallurgical Transactions, **Vol. 1**, 1970, pp.3443-3451

[88] L. F. Coffin, "Fatigue at High Temperature", in Fatigue at Elevated Temperatures, ASTM STP 520, American Society of Testing Materials, Philadelphia, PA, 1973, pp.5-34

[89] C. J. McMahon, Jr., "On the Mechanism of Premature in-Service Failure of Nickel-Base Superalloy Gas Turbine Blades", Materilas Science Engineering, **Vol. 13**, 1974, pp.295-297

[90] D. A. Woodford and R. H. Bricknell, "Environmental Embrittlement of High Temperature Alloy by Oxygen", in Treatise on Materials Science and Technoloyg, **Vol. 25**, Academic Press, Inc. 1983, pp.157-199

[91] H. Teranishi and A. J. McEvily, "Effect of Oxidation on Hold Time Fatigue Behavior of 2.25 Cr-1 Mo Steel", Metallurgical Transactions, **Vol. 10A**, 1979, pp.1806-1808

[92] D. J. Michel and H. H. Smith, "Fatigue Crack Propagation in Neutron Irradiated Type 304 and Type 308 Stainless Steel Plate and Weld Materials", Journal of Nuclear Materials, **Vol. 71**, 1977, pp.173-177

[93] R. L. Stegman, and P. Shahinian, "Effect of Temperature on the Fatigue of Nickel at Varying Oxygen Pressures", in Fatugue at High Temperature, ASTM STP 459, ASTM, Philadelphia, PA, 1969, pp.42-58

[94] H. H. Smith and P. Shahinian, "Environmental Effects on Fatigue Crack Growth Rates in Silver", J. Int. Metals, **Vol. 99**, 1971, pp.243-247

[96] T. Ericsson, "Review of Oxidation Effects on Cyclic Life at Elevated Temperature", Canadian Metallurgical Quarterly, **Vol. 18**, 1979, pp.177-195

[95] M. R. Achter, G. J. Danek and H. H. Smith, "Effect on Fatigue of Gaseous

Environments under Varying Temperature and Pressure", Transactions of the Metallurgical Society of AIME, **Vol. 227**, 1963, pp.1296-1301

[97] P. Kofstad, High Temperature Corrosion, Elsevier Applied Science Publisher LTD, 1988.

[98] J. R. Haigh, R. P. Skelton and C. E. Richards, "Oxidation-Assisted Crack Growth during High Cycle Fatigue of A 1%Cr-Mo-V Steel at 550°C", Materials Science Engineering, **Vol. 26**, 1976, pp.167-174

[99] L. Remy, F. Rezai-Aria, R. Danzer and W. Hoffelner, "Evaluation of Life Prediction Methods in High Temperature Fatigue", in Low Cycle Fatigue, ASTM STP 942, eds. by H. D. Solomon, G. R. Halford and B. N. Leis, American Society for Testing and Materials, Philadelphia, PA, 1988, pp.1115-1132

[100] B. Tomkins, "Fatigue Crack Propagation — An Analysis", Philosophical Magazine, **Vol. 18**, 1968, pp.1041-1066

[101] A. Pineau, "Elevated Temperature Life Prediction Methods", in Advances in Fatigue Science and Technology, eds. by C. M. Brauw and L. G. Rosa, Kluwer Academic Publishers, **Vol. 159**, 1989, pp.314-338

[102] A. Diboine, "Etude de la Propagation des Fissures En Fatigue-Fluage-Oxydation A 650°C Dans un Superalliage Base Nickel L'Inconel 718", Ph.D. dissertation of L'Ecole, Nationale Superieure des Mines de Paris, France, 1986

[103] D. A. Utah, "Crack Growth Modelling in an Advance Powder Metallurgy Alloy", AFWAL-TR-80-4098, Accession No. ADAO 93992, 1980

[104] C. G. Annis, Jr., R. M. Wallace and D. L. Sims, "An Interpolative Model For Elevated Temperature Fatigue Crack Propagation", AFML-TR-76-176, part I, Accession No. ADAO38070, 1976

[105] A. Dboine, "Etude de la Propagation des Fissures en Fatigue-Fluage-oxydation A 650°C Dans un Superalliage Base Nickel L'Inconel 718", Ph.D. Dissertation of L'Ecole Nationale Superieure des Mines de Paris, France, 1986

[106] J. C. Fisher, "Calculation of Diffusion Penetration Curves for Surface And Grain Boundary Diffusion", Journal of Applied Physics, **Vol. 22**, 1951, pp.74-77

[107] N. L. Peterson, "Grain-Boundary Diffusion in Metals", International Metals Review, **Vol. 28**, 1983, pp.65-91

[108] A. Atkinso, "Diffusion Along Grain Boundary and Dislocations in Oxides, Alkali

Halides and Carbides", Solid State Ionics, Vol. 12, 1984, pp.309-320

[109] N. L. Peterson, "Grain-Boundary Diffusion-Structural Effects, Models, and Mechanisms", in Grain-Boundary Structure and Kinetic, ASME Publication, Metals Park, Ohio, 1979, pp.209-238

[110] R. T. P. Whipple, "Concentration Contours in Grain Boundary Diffusion", Philosophical Magazine, Vol. 45, 1954, pp.1225-1236

[111] G. Martin and B. Perraillon, "Measurements of Grain Boundary Diffusion", Transactions of Faraday Society, Vol. 57, 1979, pp.239-295

[112] L. G. Harrison, "Influence of Dislocation on Diffusion Kinetics in Solid with Particular Reference to the Alkali Halides", Transactions Faraday Society, Vol. 57, 1961, pp.1191-1199

[113] G. Glinka, "Relations between the Strain Energy Density Distrabution and Elastic-Plastic Fields near Cracks and Notches and Fatigue Life Calculation", in Fracture Mechanics: Sixteenth Symposium, ASTM STP 868, eds. by M. F. Kannien and A. T. Hopper, American Society for Testing and Materials, Philadelphia, PA, 1988, pp.1022-1047

[114] J. L. Chaboche, "Constitutive Equations in Creep-Fatigue Damage", in Engineering Approches to High Temperature Design, eds. by B. Wilshire and D. R. J. Owen, Vol. 2, Pineridge Press, Swansea, U. K., 1983, pp.177-235,

[115] T. G. Tanaka, "A Unified Numerical Method for Integrating Stiff Time Dependent Constitutive Eequations for Elastic/Visco-Plastic Deformation of Metal and Alloys", Ph.D. Dissertation of Stanford University. USA, 1982

[116] J. L. Chaboche and G. Cailletaud, "On the Calculation of Structures in Cyclic Plasticity or Viscoplasticity", Computer & Structures, Vol. 23, 1986, pp.23-31

[117] V. Moreno and E. H. Jordan, "Prediction of Material Thermo-Mechanical Response with A Unified Viscoplastic Constitutive Model", International Journal of Plasticity, Vol. 2, 1986, pp.233-245

[118] E. Krempl, "The Role of Servocontrolled Testing in the Development of the Theory of Viscoplasticity Based on Total Strain and Overstress", in Mechanical Testing for Deformation Model Development, ASTM STP 765, American Society for Testing and Materials, Philadelphia, PA, 1982, pp.5-28

[119] H. Riedel and J. R. Rice, "Tensile Cracks in Creeping Solids", in Fracture Mechanics: Twelfth Conference, ASTM STP 700, American Society for Testing

and Materials, Philadelphia, PA, 1980, pp.112-130

[120] Source Book on Industrial Alloy and Engineering Data, Compiled by Publications Department, American Society for Metals, Metals Park, Ohio, 1978

[121] D. M. R. Taplin, N. Y. Tang and H. H. E. Leipholz, "On Fatigue-Creep-Environment Interaction and Feasibility of Fatigue Maps", in Advances in Fracture Research, eds. by S. R. Valluri, D. M. R. Taplin, P. R. Rao, J. F. Knott and R. Dubey, Pergaman Press, New York, Vol. 1, pp.127-142, 1986

[122] H. L. Eiselstein, "Metallurgy of a Columbium-Hardened Nickel-Chromium-Iron Alloy", in Advances in the Technology of Stainless Steels and Related Alloys, ASTM STP 369, American Society for Testing and Materials, Philadelphia, PA, 1965, pp.62-79

[123] I. Kirman and D. H. Warrington, "Precipitation in Nickel-Based Alloys Containing both Niobium and Titanium", Institute of Metals, 1971, Vol. 99, pp.197-199

[124] R. Cozar and A. Pineau, "Morphology of γ' and γ'' Precipitates and Thermal Stability of Inconel 718 Type Alloys", Metall. Trans., Vol. 4, 1973, pp.47-59

[125] Properties and Selection: Nonferrous Alloys and Specila-Purpose Materials (Metals Handbook), Vol. 2, 10th edition, ASM International, the Materials Information Society, 1990

[126] C. P. Sullivan and M. J. Donachie, Jr., "Some Effects of Microstructure on the Mechanical Properties of Nickel-Base Superalloys", Metals Engineering Quarterly, February, 1967, pp.250-259

[127] D. D. Keiser and H. L. Brown, A Review of the Physical Metallurgy of Alloy 718", ANCR-1292, Idaho National Engineering Laboratory, Idaho Falls, Idaho, February. 1976

[128] J. F. Radavich, "Long Term Stability of A Wrought Alloy 718 Disk", in Spueralloys 718 —— Metallurgy and Applications, ed. by A. Loria, the Minerals, Metals & Materials Society, Warrendal, PA, 1989, pp.257-268

[129] R. Molins, E. Andrieu and A. Pineau, "Overaging, Deformation and Rupture Micromechanisms of Alloy 718 in Relation to Notch Creep Rupture Strength", in Spueralloys 718, 625 and Various Derivatives, ed. by E. A. Loria, the Minerals, Metals & Materials Society, Warrendal, PA, 1991, pp.589-602

[130] J. F. Radavich, "Aspects of Phase Reactions and Microstructure in Alloy 178 during Long Term Thermal Exposure Condition", presentation at International

Conference on Spueralloys 718, 625 and Various Derivatives, Pittsburgh, PA, 1991

[131] A. Oradei-Basile and J. F. Radavich, "A Current T-T-T Diagram for Wrought Alloy 718", in Superalloys 718, 625 and Various Derivatives, ed. by A. Loria, the Minerals, Metals & Materials Society, Warrendal, PA, 1991, pp.325-335

[132] R. F. Decker, "Strengthening Mechanisms in Nickel-Base Superalloys", in Steel Strengthening Mechanisms Symposium, Zurich, Swizerland, 1969, pp.147-170

[133] A. Lingenfelter, "Welding of Inconel Alloy 718: A Historical Overview", in Spueralloys 718 — Metallurgy and Applications, ed. by E. A. Loria, the Minerals, Metals & Materials Society, 1989, pp.673-683

[134] J. M. Oblak, D. F. Paulonis and D. S. Duvall, "Coherency Strengthening in Ni-Base Alloys Hardened by DO_{22} γ' Precipitates", Metallurgical Transactions, **Vol.5**, 1974, pp.143-153

[135] D. F. Paulonis, J. M. Oblab and D. S. Duvall, "Precipitation in Nickel-Base Alloy 718", Trans. of the ASM, **Vol. 62**, 1969, pp.611-622

[136] I. Kirman and D. H. Warrington, "The Precipitation of Ni_3Nb Phases in a Ni-Fe-Cr-Nb Alloy", Metallurgical Transactions, **Vol. 1**, 1970, pp.2667-2675

[137] E. L. Raymond, "Effect of Grain Boundary Denudation of Gamma Prime on Notch Rupture Ductility of Inconel Nickel-Chromium Alloys X750 and 718", Trans. AIME, **Vol. 239**, 1967,pp.1415-1422

[138] P. S. Kotval, "Identification of the Strengthening Phase in 'Inconel' Alloy 718", Trans. AIME, **Vol. 242**, 1968, pp.1764-1765

[139] J. F. Radavich, "The Physical Metallurgy of Cast and Wrought Alloy 718", in Superally 718 — Metallurgy and Applications, ed. by E. A. Loria, The Minerals, Metals & Materials Society, Warrendal, PA, 1989, pp.229-240

[140] W. J. Boesch and H. B. Canada, "Precipitation Reaction and Stability of Ni_3Cb in Inconel Alloy 718", Journal of Metals, October, 1986, pp.34-38

[141] M. Clavel, D. Fournier and A. Pineau, "Plastic Zone Sizes in Fatigued Specimens of Inco 718", Metall. Trans., **Vol. 6A**, 1975, pp.2305-2307

[142] N. A. Wilkinson, "Forging of 718 — The Importance of T.M.P.", in Superally 718 — Metallurgy and Applications, ed. by E. A. Loria, The Minerals, Metals & Materials Society, Warrendal, PA, 1989, pp.119-133

[143] S. D. Antolovich, "The Effect of Metallurgical Instabilities on the Behavior of IN718", in Superally 718 — Metallurgy and Applications, ed. by E. A. Loria, The Minerals, Metals & Materials Society, Warrendal, PA, 1989, pp.647-653

[144] M. G. Burke and M. K. Miller, "Precipitation in Alloy 718: A Combined AEM and APFIM Investigation", in Spueralloys 718, 625 and Various Derivatives, ed. by E. A. Loria, the Minerals, Metals & Materials Society, Warrendal, PA, 1991, pp.337-350

[145] E. F. Wachtel and H. J. Rack, "Phase Stability and Aging Response of TiC Reinforced Alloy 718", in Superally 718 — Metallurgy and Applications, ed. by E. A. Loria, The Minerals, Metals & Materials Society, Warrendal, PA, 1989, pp.599-610

[146] M. Kaufman and A. E. Palty, "The Phase Structure of Inconel 718 and 702 Alloys", Transactions of the Metallurgical Society of AIME, **Vol. 221**, 1961, pp.1253-1261

[147] W. J. Mills, "The Effect of Heat Treatment on the Room Temperature and Elevated Temperature Fracture Toughness Response of Alloy 718", Journal of Engineering Materials and Technology, **Vol. 102**, 1980, pp.118-126

[148] T. H. Sanders, Jr., R. E. Frishmuth and G. T. Embley, "Temperature Dependent Deformation Mechanisms of Alloy 718 in Low Cycle Fatigue", Metallurgy Transactions, **Vol. 12A**, 1981, pp.1003-1010

[149] G. E. Korth, "Effects of Various Parameters on the Fatigue Life of Alloy 718", in Spueralloys 718, 625 and Various Derivatives, ed. by E. A. Loria, the Minerals, Metals & Materials Society, Warrendal, PA, 1991, pp.457-476

[150] G. E. Korth and C. L. Trybus, "Tensile Properties and Microstructure of Alloy 718 Thermally Aged to 50,000 h", in Spueralloys 718, 625 and Various Derivatives, ed. by E. A. Loria, the Minerals, Metals & Materials Society, Warrendal, PA, 1991, pp.437-446

[151] K. Sadananda and P. Shahinian, "Creep Crack Growth in Alloy 718", Metallurgical Transactions, **Vol. 8A**, 1977, pp.439-449

[152] C. D. Liu, Y. F. Han, M. G. Yan and M. C. Chaturvedi, "Creep Crack Growth Behavior of Alloy 718", in Spueralloys 718, 625 and Various Derivatives, ed. by E. A. Loria, the Minerals, Metals & Materials Society, Warrendal, PA, 1991, pp.537-548

[153] W. J. Mills and L. D. Blackburn, "Fracture Toughness Variations in Alloy 718",

Journal of Engineering Materials and Technology, Vol. 112, 1988, pp.286-293

[154] J. K. Tien, J. P. Collier and G. Vignoul, "The Role of Niobium and Other Refractory Elements", in Superally 718 — Metallurgy and Applications,ed. by E.A. Loria, The Minerals, Metals & Materials Society, Warrendal, PA, 1989, pp.553-567

[155] S. M. Jones, J. Radavich and S. Tian, "Effectof Composition on Segregation Microstructures and Mechanical Properties of Cast Alloy 718", in Superally 718 — Metallurgy and Applications, ed. by E. A. Loria, The Minerals, Metals & Materials Society, Warrendal, PA, 1989, pp.589-598

[156] C. B. Brinkman, M. K. Booker and J. L. Ding, "Creep and Creep-Rupture Behavior of Alloy 718", in Spueralloys 718, 625 and Various Derivatives, ed. by E. A. Loria, the Minerals, Metals & Materials Society, Warrendal, PA, 1991, pp.519-536

[157] R. W. Hayes, "Creep Deformation of Inconel 718 in the 650°C to 760°C Temperature Range", in Spueralloys 718, 625 and Various Derivatives, ed. by E. A. Loria, the Minerals, Metals & Materials Society, Warrendal, PA, 1991, pp.549-562

[158] H. Feldstein and O. Mendoza, "Analysis and Elimination of time Defendent Notch Sensitivity in Alloy 718", in Superally 718 — Metallurgy and Applications, ed. by E. A. Loria, The Minerals, Metals & Materials Society, Warrendal, PA, 1989, pp.655-671

[159] J. A. Muller and M. J. Donachie, "The Effect of Solutions and Intermediate Heat Treatments on the Notch-Rupture Behavior of Inconel 718", Metallurgical Transactions, Vol. 6A, 1975, pp.2221-2227

[160] H. F. Merrick, "Effect of Heat treatment on the Structure and Properties of Extruded P/M Alloy 718", Metallurgical Transactions, Vol. 7A, 1976, pp.505-514

[161] M. C. Chaturvedi and Ya-fang Han, "Strengthening Mechanisms in Inconel 718 Superalloy", Metal Science, Vol. 17, 1983, pp.145-149

[162] M. Sundararaman, P. Mukhopadhyay and S. Banerjee, "Deformation Behavior of γ" Strengthened Inconel 718", Acta Metallurgy, Vol. 36, 1988, pp.847-864

[163] B. I. Verkin and N. M. Grinberg, "The Effect of Vacuum on the Fatigue Behavior of Metals and Alloys", Materials Science and Engineering, Vol. 41, 1979, pp.149-181

[164] L. Remy and A. Pineau, "Twinning and Strain-Induced F.C.C. → H. C. P. Transformation on the Mechanical Properties of Co-Ni-Cr-Mo Alloys", Materials Science and Engineering, **Vol. 26**, 1976, pp.123-132

[165] P. S. Kotval, "Carbide Precipitation on Imperfections in Superalloy Matrices", Trans. of the Metallurgical Society of AIME, **Vol. 242**, 1968, pp.1651-1656

[166] P. S. Dobson, P. J. Goodhew and R. E. Smallman, "Climb Kinetics of Dislocation Loops in Aluminium", Phil. Mag., **Vol. 16**, 1967, pp.9-22

[167] B. E. P. Beeston and L. K. France, "Stacking-Fault Energies of Some Binary Nickel Alloys Fundamental to Nimonic Series", Institute of Metals, **Vol. 96**, 1967, pp.105-107

[168] L. Delehouzee and A. Deruyttere, "The Stacking Fault Density in Solid Solutions Based on Silver, Nickel, Aluminium and Lead", Acta Metallurgy, **Vol. 15**, 1967, pp.727-734

[169] M. Gell and G. R. Leverant, "Mechanisms of High-Temperature Fatigue", Fatigue at Elevated Temperature, ASTM STP 520, eds. A. E. Carden, A. J. McEvily and C. H. Wells, American Society for Testing and Materials, Philadelphia, PA, 1973, pp.37-67

[170] M. C. Chaturvedi and Ya-fang Han, "Strengthening Mechanisms in Inconel 718 Superalloy", Metal Science, **Vol. 17**, 1983, pp.145-149

[171] A. Saxena and S. J. Hudak, Jr., "Review and Extension of Compliance Information for Common Crack Growth Specimens", International Journal of Fracture, **Vol. 14**, 1978, pp.453-468

[172] M. D. Halliday and C. J. Beevers, "The D. C. Electrical Potential Method for Crack Length Measurement", in The Measurement of Crack Length and Shape During Fracture and Fatigue, ed. by C. J. Beevers, EMAS Ltd., West Midlands, UK, 1980, pp.85-112

[173] R. H. VanStone and T. L. Richardson, "Potential-Drop Monitoring of Cracks in Surface-Flawed Specimens", Automated Test Methods for Fracture and Fatigue Crack Growth, ASTM STP 877, eds. by W. H. Cullen, R. W. Landgraf, L. R. Kaisand and J. H. Underwood, American Society for Testing and Materials, Philadelphia, PA, 1985, pp.148-166

[174] Annual Book of ASTM Standards, section 3, Metals Test Methods and Analytical Procedure, **Vol. 03.01**, American Society for Testing and Materials, Philadelphia, PA, 1989, pp.646-666

PUBLICATIONS RELATED TO THE RESEARCH PROGRAM

1. H. Ghonem and D. Zheng, "Quantitative modelling of oxidation-assisted crack growth behavior in Alloy 718", annual report prepared for United Technologies Corporation, Pratt & Whitney Group and Department of Air Force, Air Force Office of Scientific Research, January, 1990

2. E. Andrieu, H. Ghonem and A. Pineau, "Two-stage crack tip oxidation mechanism in Alloy 718", Elevated Temperature Crack Growth, 1990 ASME Winter Annual Meeting, pp.25-30

3. H. Ghonem and D. Zheng, "Oxidation-assisted fatigue crack growth behavior in Alloy 718 — Part I: Quantitative modelling", Fatigue & Fracture of Engng. Materials & Structures, Vol. 14, 1991, pp.749-760

4. D. Zheng and H. Ghonem, "Oxidation-assisted fatigue crack growth behavior in Alloy 718 — Part II: Application", Fatigue & Fracture of Engng. Materials & Structures, Vol.14, 1991, pp.761-768

5. H. Ghonem and D. Zheng, "Environmentally-dominated fatigue crack growth model for alloy 718", Proceedings of 6th International Conference on Mechanical Behavior of Materials, ICM6, Vol. 4, 1991, pp.373-378

6. H. Ghonem and D. Zheng, "Characterization of environmentally-dependent fatigue crack growth in Alloy 718 at 650°C," Proceedings of International Symposium on Superalloy 718, 625 and Various Derivatives, Ed. by E. Loria, IME Publications, Pittsburgh, PA, 1991, pp.477-490

7. H. Ghonem and D. Zheng, "The depth of Intergranular oxygen diffusion during environment-dependent fatigue crack growth in Alloy 718," to be published in Materials Science and Engineering, 1991

8. E. Andrieu, H. Ghonem and A. Pineau, "Intergranular crack tip oxidation mechanism in a nickel-based superalloy", to be published in Materials Science and Engineering, 1991

9. H. Ghonem, D. Zheng and A. Rosenburger, "Crack tip oxidation shielding mechanism in Alloy 718", subnitted to Materials Science and Engineering, July, 1991

10. H. Ghonem, T. Nicholas and A. Pineau, "Analysis of elevated temperature crack

growth mechanisms in Alloy 718", to be presented in Symposium on High Temperature Effects, ASME Winter Annual Meeting, Atlanta,Ga, November, 1991

11. H. Ghonem, T. Nicholas and A. Pineau, "Effects of mechanical, environmental and material variables on elevated temperature fatigue crack growth in Alloy 718", submitted to Materials Science and Engineering, August, 1991

12. D. Zheng and H. Ghonem, "Influence of overaging on environmentally-assisted crack growth performance in Alloy 718," submitted to Materials Science and Engineering, October, 1991

13. D. Zheng and H. Ghonem, "Investigation of environment-dependent fatigue crack growth stage in a Ni-based superalloy", submitted to 1992 Summer Mechanics and Materials Conference, September, 1991

14. D. Zheng and H. Ghonem, "Effects of frequency interaction on fatigue crack growth mode in a nickel-based superalloy at elevated temperature", submitted to AeroMat'92, September, 1991

15. A. Rosenberger, D. Zheng and H. Ghonem, "Influonce of predeformation on crack tip oxidation shielding in nickel based superalloys", submitted to 2nd International Conference on Computer Aided Assessment and Control Localized Damage, October, 1991

16. A. Rosenberger, D. Zheng and H. Ghonem, "Study of the role of slip line density in intergranular crack growth in nickel-base superalloys", submitted to Symposium on Fracture and Damage at Elevated Temperatures, 1991

17. A. Rosenberger, E. Andrieu and H. Ghonem, "Elastic-plastic small crack growth in superalloys at elevated temperature", submitted to 7th National Symposium on Superalloys, October, 1991

18. A. Rosenberger and H. Ghonem, "Effect of compression excursion on elastic-plastic small crack growth in nickel based superalloys", submitted to 3rd International Conference on Low Cycle Fatigue and Elastic Plastic Behavior of Materials, April, 1991

19. H. Ghonem, and A. Rosenberger, "Study of elastic-plastic small crack growth in nickel based superalloys", submitted to Fatigue & Fracture of Engng. Materials & Structures, October, 1991